Institut für Biochemie und Biologie

Arbeitsgruppe Molekulare Enzymologie

Dissecting the role of the TusA protein for cell functionality and FtsZ ring assembly in *Escherichia coli*

Dissertation

zur Erlangung des akademischen Grades

"doctor rerum naturalium"

(Dr. rer. nat.)

in der Wissenschaftsdisziplin Biochemie

eingereicht an der

Mathematisch-Naturwissenschaftlichen Fakultät

der Universität Potsdam

von

Tugba Yildiz

(geb. Gülcenbay)

Potsdam, den 06.06.2023

Published online on the
Publication Server of the University of Potsdam:
https://doi.org/10.25932/publishup-61713
https://nbn-resolving.org/urn:nbn:de:kobv:517-opus4-617135

Veröffentlichung der Dissertation

Mit Genehmigung des Instituts für Biochemie und Biologie, vertreten durch die Leiterin der Arbeitsgruppe Prof. Dr. Silke Leimkühler, wurden Teilergebnisse aus dieser Arbeit in folgenden Beiträgen vorab veröffentlicht:

Publikation:

Yildiz T, Leimkühler S. (2021). TusA is a versatile protein that links translation efficiency to cell division in *Escherichia coli*. J Bacteriol. **203**(7):e00659-20. doi: 10.1128/JB.00659-20.

Tagungsbeiträge:

T. Yildiz and S. Leimkühler. „Analysis of the role of TusA for cell functionality in *E. coli*". Vortrag Bioanalysis PhD Workshop, 2017, Luckenwalde (Deutschland)

T. Yildiz and S. Leimkühler. „Dissecting the role of the TusA protein for cell functionality and FtsZ ring assembly in *Escherichia coli*". Posterbeitrag auf der Konferenz "Iron sulfur for life", sattelite meeting to MoTEC XI, 2019, Potsdam (Deutschland)

Summary

In this work, the role of the TusA protein was investigated for the cell functionality and FtsZ ring assembly in *Escherichia coli*. TusA is the tRNA-2-thiouridine synthase that acts as a sulfur transferase in tRNA thiolation for the formation of 2-thiouridine at the position 34 (wobble base) of $tRNA^{Lys}$, $tRNA^{Glu}$ and $tRNA^{Gln}$. It binds the persulfide form of sulfur and transfers it to further proteins during mnm^5s^2U tRNA modification at wobble position and for Moco biosynthesis. With this thiomodification of tRNA, the ribosome binding is more efficient and frameshifting is averted during the protein translation. Previous studies have revealed an essential role of TusA in bacterial cell physiology since deletion of the *tusA* gene resulted in retarded growth and filamentous cells during the exponential growth phase in a rich medium which suddenly disappeared during the stationary phase. This indicates a problem in the cell division process. Therefore the focus of this work was to investigate the role of TusA for cell functionality and FtsZ ring formation and thus the cell separation.

The reason behind the filamentous growth of the *tusA* mutant strain was investigated by growth and morphological analyses. Δ*tusA* cells showed a retarded growth during the exponential phase compared to the WT strain. Also, morphological analysis of Δ*tusA* cells confirmed the filamentous cell shape. The growth and cell division defects in Δ*tusA* indicated a defect in FtsZ protein as a key player of cell division. The microscopic investigation revealed that filamentous Δ*tusA* cells possessed multiple DNA parts arranged next to each other. This suggested that although the DNA replication occurred correctly, there was a defect in the step where FtsZ should act; probably FtsZ is unable to assemble to the ring structure or the assembled ring is not able to constrict. All tested mutant strains (Δ*tusD*, Δ*tusE* and Δ*mnmA*) involved in the mnm^5s^2U34 tRNA modification pathway shared the similar retarded growth and filamentous cell shape like Δ*tusA* strain. Thus, the cell division defect arises from a defect in mnm^5s^2U34 tRNA thiolation.

Since the FtsZ ring formation was supposed to be defective in filaments, a possible intracellular interaction of TusA and FtsZ was examined by fluorescent (EGFP and mCherry) fusion proteins expression and FRET. FtsZ expressing *tusA* mutant (DE3) cells showed a red mCherry signal at the cell poles, indicating that FtsZ is still in the assembling phase. Interestingly, the cellular region of EGFP-TusA fusion protein expressed in Δ*tusA* (DE3) was conspicuous; the EGFP signal was spread throughout the whole cell and, in addition, a slight accumulation of the EGFP-TusA fluorescence was detectable at the cell poles, the same part of the cell as for mCherry-FtsZ. Thus, this strongly suggested an interaction of TusA and FtsZ.

Furthermore, the cellular FtsZ and Fis concentrations, and their change during different growth phases were determined via immunoblotting. All tested deletion strains of mnm^5s^2U34 tRNA modification show high cellular FtsZ and Fis levels in the exponential phase, shifting to the later growth phases. This shift reflects the retarded growth, whereby the deletion strains reach later the exponential phase. Conclusively, the growth and cell division defect, and thus the formation of filaments, is most likely caused by changes in the cellular FtsZ and Fis concentrations.

Finally, the translation efficiencies of certain proteins (RpoS, Fur, Fis and mFis) in *tusA* mutant and in additional gene deletion strains were studied whether they were affected by using unmodified U34 tRNAs of Lys, Glu and Gln. The translation efficiency is decreased in mnm^5s^2U34 tRNA modification-impaired strains in addition to their existing growth and cell division defect due to the elimination of these three amino acids. Finally, these results confirm and reinforce the importance of Lys, Glu and Gln and the mnm^5s^2U34 tRNA thiolation for efficient protein translation. Thus, these findings verify that the translation of *fur*, *fis* and *rpoS* is regulated by mnm^5s^2U34 tRNA modifications, which is growth phase-dependent.

In total, this work showed the importance of the role of TusA for bacterial cell functionality and physiology. The deletion of the *tusA* gene disrupted a complex regulatory network within the cell, that most influenced by the decreased translation of Fis and RpoS, caused by the absence of mnm^5s^2U34 tRNA modifications. The disruption of RpoS and Fis cellular network influences in turn the cellular FtsZ level in the early exponential phase. Finally, the reduced FtsZ concentration leads to elongated, filamentous *E. coli* cells, which are unable to divide.

Table of Contents

List of Figures

List of Tables

List of Abbreviations

α	anti
Ab	antibody
Ala	alanine
Amp	ampicillin
ATP	adenosine triphosphate
bp	base pairs
BSA	bovine serum albumin
C	carbon
°C	degree Celsius
Cm	chloramphenicol
cm, nm	centimeter, nanometer
$cmnm^5$	5-carboxymethylaminomethyl
CMP	cytidine monophosphate
cPMP	cyclic pyranopterin monophosphate
CTP	cytidine triphosphate
C-terminal	carboxy-terminal
CyaY	bacterial frataxin
Cys	cysteine
DAPI	4,6-diamidino-2-phenylindole
DNA	deoxyribonucleic acid
dNTP	deoxynucleosidetriphosphate
E. coli	*Escherichia coli*
EDTA	ethylenediaminetetraacetic acid
e.g.	lat. exempli gratia, engl. for example
EGFP	enhanced green fluorescent protein
EtOH	ethanol
EYFP	enhanced yellow fluorescent protein
Fe	iron
FeS	iron sulfur
FRET	Förster resonance energy transfer
g, mg, µg, ng	gram, milligram, microgram, nanogram
Gln	glutamine
Glu	glutamate
GMP	guanosine monophosphate

GTP	guanosine triphosphate
x g	gravity
H	hydrogen
h, min, sec	hour(s), minute(s), second(s)
HCl	hydrochloric acid
IPTG	isopropyl-β-D-thiogalactopyranoside
isc	*iron sulfur cluster*
kb	kilo base
kDa	kilo Dalton
Kana	kanamycin
LB	Luria Broth
Lys	lysine
M, mM, µM	molar, milimolar, micromolar
MCD	molybdopterin cytosine dinucleotide
MeOH	methanol
MES	N-morpholinoethanesulfonic acid
MGD	molybdopterin guanine dinucleotide
mi^6A37	2-methylthio-N6 isopentenyladenosine at position 37
µl, ml, l	microliter, mililiter, liter
mnm^5s^2U34	5-methylaminomethyl-2-thiouridine
Mo	molybdenum
Moco	molybdenum cofactor
MPT	molybdopterin
N	nitrogen
NA	numeric aperture
NaCl	sodium chloride
NO	nucleoid occlusion
NaOH	sodium hydroxide
N-terminus	amino-terminus
O	oxygen
OD_{600}	optical density at 600 nm
o.n.	overnight
PAGE	polyacrylamide gel electrophoresis
PBS	phosphate buffered saline
PCR	polymerase chain reaction
PLP	pyridoxal-5'-phosphate

POD	peroxidase
RE	restriction enzyme
RNA	ribonucleic acid
rpm	rounds per minute
RT	room temperature
S	sulfur
s^2C32	2-thiocytidin at position 32
SDS	sodium dodecyl sulfate
Sm	spectinomycin
s^2U34	2-thiouridine at position 34
s^4U8	4-thiouridine at position 8
suf	*mobilization of sulfur*
TAE	Tris-acetate-EDTA
T_M	melting temperature
Tris	tris-(hydroxymethyl)-aminomethane
tRNA	transfer ribonucleic acid
tus	2-*thiouridine synthesis*
U	unit (of enzyme activity)
U	uridine
v/v	volume per volume
WT	wild-type
w/v	weight per volume

1 Introduction

1.1 Sulfur in bacteria

Sulfur is an essential element for all living organisms and it is incorporated into a variety of important biomolecules (Beinert, 2000a). Among these are molybdenum, biotin, thiamin, lipoic acid, Fe-S cluster, thionucleosides, cysteine and methionine (Kessler, 2006). Sulfur has two special properties: 1) chemical bonds with sulfur are formed and broken in easy manner, 2) sulfur can act as an electrophile (e.g. in disulfides) and as a nucleophile (e.g. as thiol) (Kessler, 2006). The source for the sulfur in sulfur-containing molecules originates from L-cysteine. With the help of certain enzymes, the sulfur atom of L-cysteine is mobilized and delivered for the biosynthesis of several biomolecules as thiamin, biotin, lipoic acid and cofactors such as iron-sulfur (Fe-S) clusters, molybdopterin (MPT) and thiomodifications of tRNA (Kessler, 2006). During this mobilization, L-cysteine desulfurase mobilize the sulfur as persulfide (R-S-SH). Since this persulfide form of sulfur is instable and highly reactive it is bound by conserved cysteine residues in transfer proteins (Kessler, 2006; Müller, 2006).

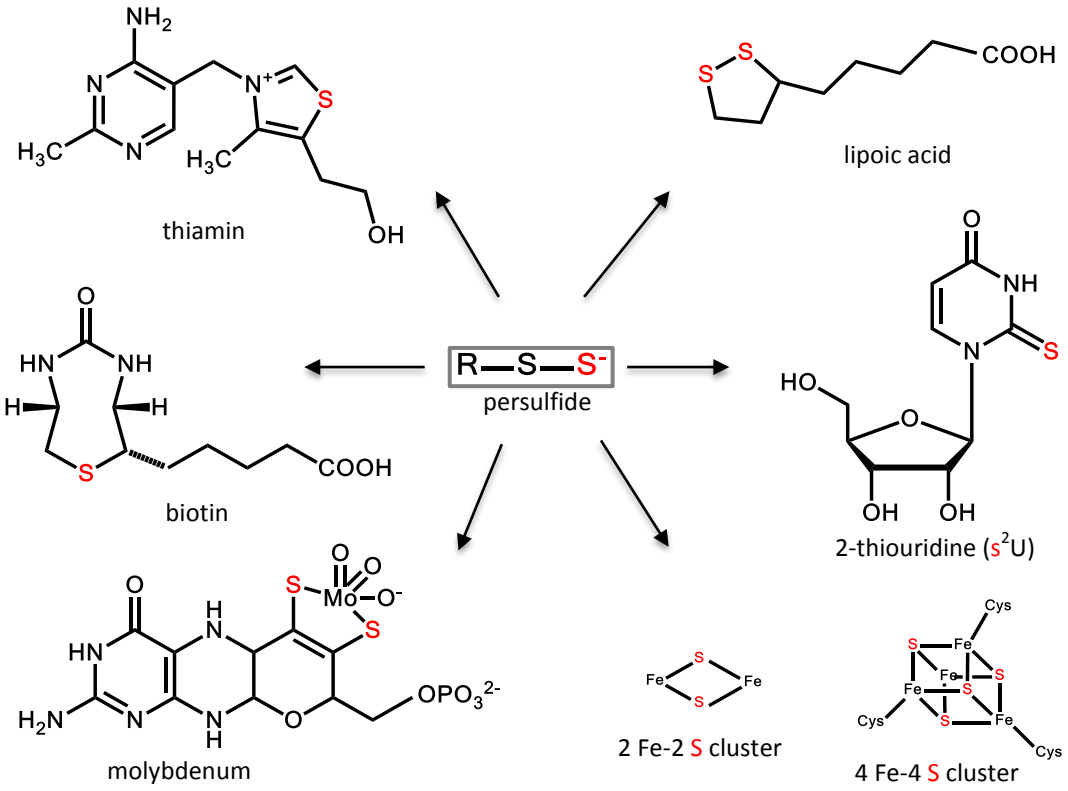

Figure 1: Biosynthesis of sulfur-containing biomolecules with active sulfur from L-cysteine.

Sulfur is mobilized by L-cysteine desulfurase via formation of persulfide. This persulfide serves as sulfur source and is used during synthesis of various biomolecules as vitamins (thiamin, biotin), cofactors (Fe-S cluster, lipoic acid, molybdenum cofactor) and ribonucleic acids (tRNA bases).

1.2 Role of the IscS protein in *E. coli*

An essential sulfur transfer protein is IscS, the house-keeping L-cysteine desulfurase (Zheng *et al.*, 1998). The role of the IscS protein is the mobilization of persulfide sulfur for tRNA thiolation pathway and Fe-S cluster biosynthesis in *E. coli* (Johnson *et al.*, 2005). Sulfur mobilization occurs in a pyridoxal-5-phosphate (PLP)-dependent reaction in which the IscS enzyme converts L-cysteine to L-alanine and sulfane sulfur. On IscS, the sulfane sulfur is bound to Cys-328 as persulfide (Agar *et al.*, 2000; Kato *et al.*, 2002; Shi *et al.*, 2010). IscS is encoded on the *isc* (iron sulfur cluster) operon (*iscRSUA-hscBAfdx-iscX*) with additional Isc proteins (IscR, IscU, IscA) (Mettert and Kiley, 2015). The expression of the *isc* operon is regulated by IscR (iron-sulfur cluster binding transcriptional repressor) (Zheng *et al.*, 1998; Roche *et al.*, 2013; Schwartz *et al.*, 2001). During the Fe-S cluster formation, after IscS mobilizes the sulfur via persulfide bonding, the scaffold protein IscU interacts directly with IscS to bind the persulfide sulfur (Kato *et al.*, 2002). This interaction leads to the transfer of sulfur to IscU enzyme (Shi *et al.*, 2010). In the presence of Fe^{2+}, a [2Fe-2S] cluster is initially formed on IscU as a scaffold protein, which is later converted from two [2Fe-2S] clusters to one [4Fe-4S] cluster on IscU (Marinoni *et al.*, 2012). It is likely that ferredoxin provides the electrons for the reductive coupling of two [2Fe-2S] clusters to form one [4Fe-4S] cluster on IscU (Chandramouli *et al.*, 2007). In a further step, the formed cluster is transferred to a target apoprotein with the support of IscA and/or the chaperones HscA and HscB (Ollagnier De Choudens *et al.*, 2004; Kim *et al.*, 2012; Hoff *et al.*, 2000; Silberg *et al.*, 2001). In particular, the two chaperones HscA and HscB catalyze exclusively the transfer of [2Fe-2S] clusters from IscU to apoproteins (Chandramouli and Johnson, 2006; Unciuleac *et al*., 2007; Shakamuri *et al.,* 2012). The IscA protein is responsible for the transfer of the [4Fe-4S] cluster directly from IscU to the apoprotein (Ollagnier de Choudens *et al.*, 2004). IscX is the last enzyme that is also encoded by the *isc* operon. It was reported that IscX and CyaY are both involved in the Fe-S cluster formation (Roche *et al.*, 2015). Both proteins can bind to IscS, but their precise role in Fe-S cluster biosynthesis is still unclear (Shi *et al.*, 2010). In addition, the iron donor for Fe-S clusters has not yet been determined, but CyaY or IscX are potential candidates to fill this role (Blanc *et al.*, 2015).

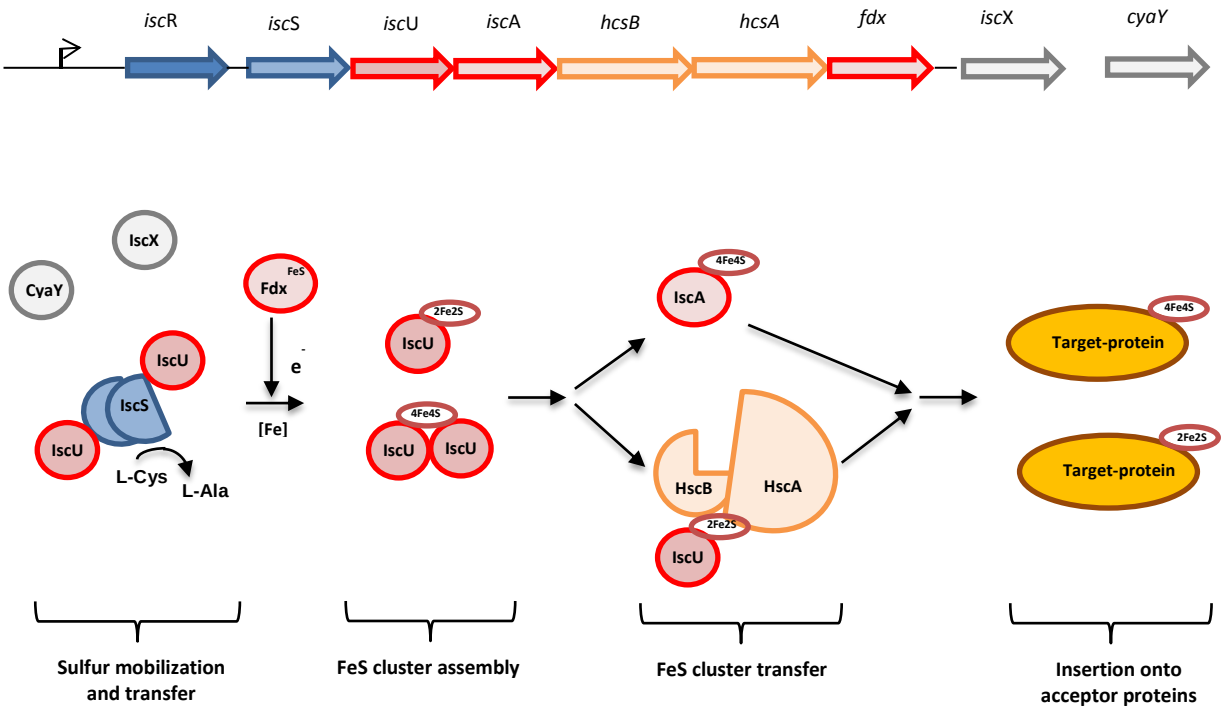

Figure 2: IscS acts in Fe-S cluster biosynthesis.

The biosynthesis of Fe-S clusters proceeds in four steps. It starts with the sulfur mobilization by cysteine desulfurase protein IscS via persulfide bond. This mobilized sulfur is subsequently transferred to the IscU protein through an IscS-IscU interaction. On the scaffold protein IscU, a [2Fe-2S] cluster is first built up with the addition of electrons and iron, which can then be converted into a [4Fe-4S] cluster. The required electrons are probably supplied by ferrodoxin (Fdx). The iron donor could be CyaY or IscX, but this remains to be clarified. The HscB-HscA chaperone system and/or the IscA protein support the transfer of formed Fe-S cluster to respective apoproteins.

Interestingly, IscS not only transfers the mobilized persulfide sulfur to IscU for the formation of Fe-S clusters, but also interacts with other proteins such as TusA and ThiI for tRNA thiolation, thiamin and Moco (molybdenum cofactor) biosynthesis (Hidese *et al.*, 2011; Shi *et al.,* 2010). During this transfer process, TusA and ThiI, both proteins are involved in tRNA thiolation pathway (TusA in 2-thioruidine (mnm^5s^2U34) and ThiI in 4-thiouridine (s^4U8)) (Ikeuchi *et al.*, 2006). But both of them have also additional separate roles, TusA plays a role in Moco biosynthesis (Dahl *et al.*, 2013) and ThiI in thiamin formation (Hidese *et al.*, 2011). So the described examples show that the persulfide sulfur can be delivered to acceptor proteins with the support of IscS in order to synthesize sulfur-containing biomolecules (Hidese *et al.*, 2011).

Under stress conditions the ISC-system is replaced by the SUF-system (sulfur mobilization) (Dai and Outten, 2012). Possible stress conditions include Fe deficiency or oxidative stress

(Outten *et al.*, 2004; Jang and Imlay, 2010). The *suf* operon encodes for SufA, SufB, SufC, SufD, SufS and SufE proteins of which SufS shows the L-cysteine desulfurase activity and is therefore a homolog to IscS (Mihara and Esaki, 2002). SufS forms the persulfide sulfur and transfers it then to SufE protein (Loiseau *et al.*, 2003). How the bacterial cell recognizes whether the Fe-amount is high or less depends on the Fur (ferric uptake regulator) protein. Fur binds the Fe in bacterial cell, if the Fe amount is enough. With this Fe-binding by Fur, the cell can adjust cellular Fe-metabolism accordingly (Bagg and Neilands, 1987). Since Fur cannot bind to the promotor region of Fur-regulated genes, the small RNA known as RyhB has a link to the Fur protein. Fur regulates, precisely it represses the synthesis of regulatory RyhB (Massé and Gottesman, 2002). RhyB itself can bind mRNA which should be degraded to shut down e.g. the Fe-S cluster biosynthesis under Fe-limiting conditions. For the mRNA-binding it needs the support of the RNA-chaperone Hfq which is important for the RyhB stability and activity (Masse *et al.*, 2003; Moll *et al.*, 2003). Furthermore Hfq acts as a global regulator which is involved in transcription of several genes. For this Hfq supports the binding between small RNA (sRNA) and target-mRNA and recruits further proteins to induce the degradation of the target-mRNA (Masse *et al.*, 2003).

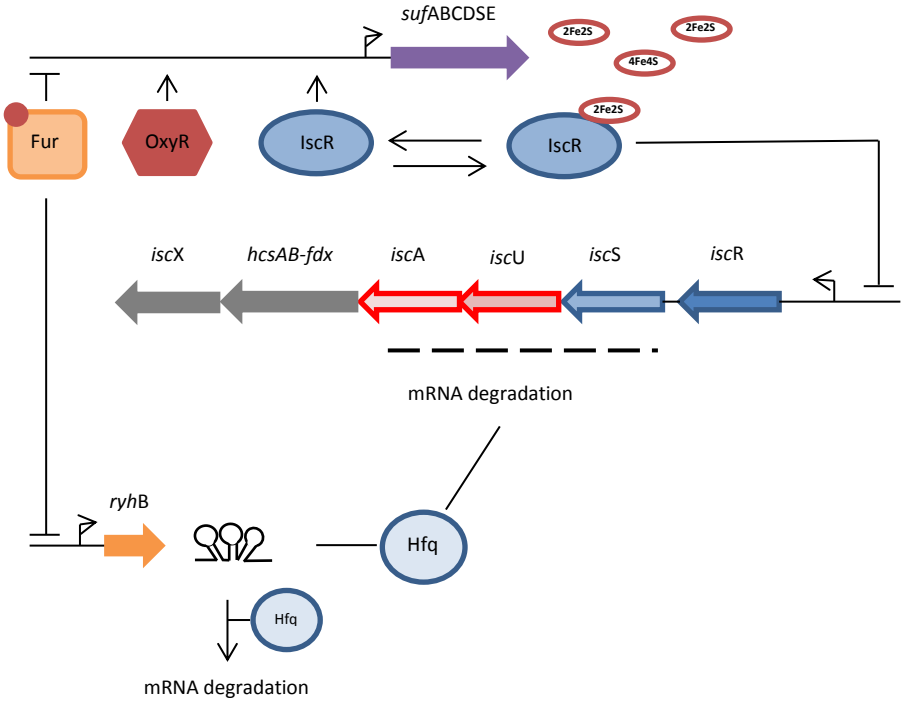

Figure 3: Under stress conditions Fe-S cluster biosynthesis through ISC system is replaced by SUF system

IscS, Fur, RhyB, Hfq and SUF-system proteins are related in Fe-S-cluster biosynthesis. IscS is the cysteine desulfurase protein which provides persulfide sulfur for tRNA thiolation and Fe-S cluster pathways. Its respective gene (light blue arrow) is encoded in *isc* operon. In stress conditions is this IscS protein replaced by SufS which is encoded in *suf* operon (purple arrow). The sensing of Fe-level within the cell is

regulated by the Fur protein. Under high Fe conditions, Fur binds Fe and represses further synthesis of Fe-S-cluster by inhibition of RyhB expression. RhyB is a small RNA which binds together with Hfq (RNA-binding protein) protein to isc*SUA* mRNA under Fe-limiting conditions to reduce Fe-cluster synthesis. Stress conditions like oxidative stress or requirement of Fe-S-cluster is mediated by OxyR and IscR proteins.

1.3 Role of the TusA protein in *E. coli*

Sulfur transferases are carrier proteins which mobilize sulfur as persulfide and transfer it to other proteins or biomolecules (Westley *et al.*, 1983). One of those proteins is the TusA protein which is a small protein of 81 amino acids (9 kDa) that was first identified in 1998 and initially named YhhP (Yamashino *et al.*, 1998). TusA is the tRNA-2-thiouridine synthetizing protein A and acts as a sulfur carrier in tRNA thiolation for the formation of 2-thiouridine at the position 34 (wobble base) of tRNAs for lysine (Lys), glutamate (Glu) and glutamine (Gln). In the first step of tRNA thiolation, the sulfur atom of L-cysteine is mobilized by IscS, a L-cysteine desulfurase protein which catalyzes the formation of L-alanine and a persulfide bound sulfur at IscS. Next, TusA receives the sulfur as a persulfide at his cysteine residue 19 (C19) by interacting with IscS and transferring the sulfur further to TusD (C78) of the TusBCD protein complex (Ikeuchi *et al.*, 2006). The persulfide sulfur is then transferred to TusE (C108) and MnmA proteins, the latter which finally modifies the uridine at the position 34. Since MnmA contains a P loop in its active site and acts as an ATP pyrophosphatase, the uridine C2 at position 34 of tRNA is activated in an ATP-dependent manner. The result of this pathway is the synthesis of mnm^{5}s^{2}U (5-methylaminomethyl-2-thiouridine) at the wobble position of the tRNA (Ikeuchi *et al.*, 2006). The importance of this thiomodification of uridine 34 is that it enables more efficient ribosome binding and averts frameshifting during translation of proteins (Ashraf *et al.*, 1999; Yokoyama *et al.*, 1985; Moukadiri *et al.*, 2013).

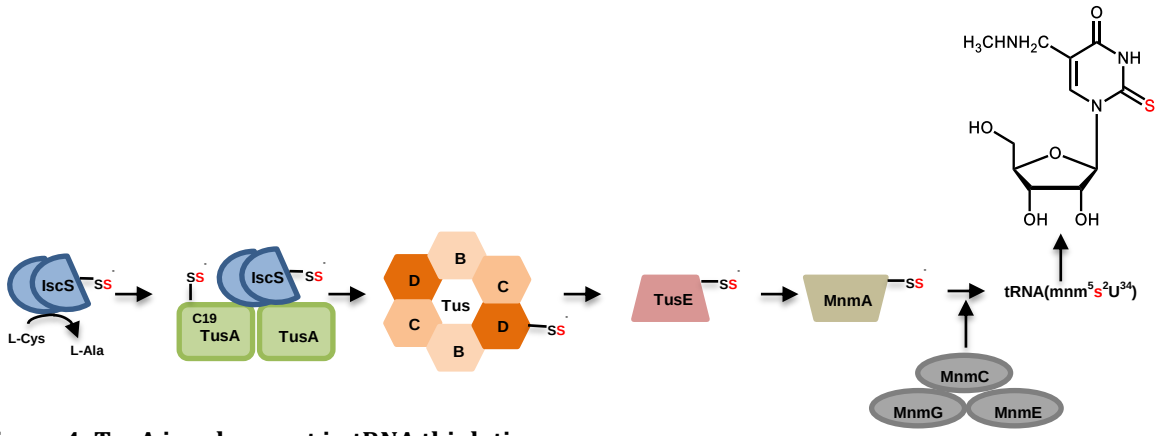

Figure 4: TusA involvement in tRNA thiolation.

TusA in synthesis of 2- thiouridine at wobble base 34 of tRNA: in the first step of tRNA thiolation the sulfur of L-cysteine is bound by IscS, a L-cysteine desulfurase protein which leads to the formation of L-alanine and a persulfide bound sulfur at IscS. TusA binds the persulfide sulfur by interacting with IscS and transfers it further to TusD of the TusBCD protein complex. Sulfur transport continues via TusE and MnmA proteins which then finally modifies the uridine at the position 34. The mnm^5s^2U34 synthesis is additionally supported by the enzyme complex MnmG-MnmE and MnmC.

Furthermore, the synthesis of mnm^5s^2U34 is supported by the MnmE-MnmG complex and the MnmC protein. After MnmA catalyzes the incorporation of sulfur in tRNA U34, the MnmE-MnmG enzyme complex performs additional modifications. Depending on the substrate (glycine or ammonium) MnmE (in complex with MnmG) produces $cmnm^5U$ (5-carboxymethylaminomethyluridine) or mnm^5U (5-methylaminomethyluridine). The bi-functional enzyme MnmC can convert $cmnm^5$ to nm^5U and nm^5U to the mature mnm^5U by adding a methyl group (Moukadiri *et al.*, 2013).

The role of mnm^5 group is together with the 2-thiomodification to support the C3´ endo form of the ribose (Kambampati and Lauhon, 2003). Since ribose in C2´ endo form would enter in steric conflict of 2´OH group with the 2- thio group, the ribose is structurally forced into the C3´ endo conformation by the substituents at position 2 and position 5 (Yokoyama *et al.*, 1979). This results in an enhanced conformational rigidity such that mnm^5s^2U modified bases pair preferentially with adenosine as the third base of the codon. The pairing of the wobble base with guanosine is reduced due to the increased rigidity (Yokoyama *et al.*, 1985). In addition, the 2-thiomodification of U34 leads to a stronger stacking interaction between the position 34 and 35, which contributes to the conformational rigidity of wobble base (Durant *et al.*, 2005). Furthermore, the more restricted flexibility prevents the misreading of codons which are ending in pyrimidines. So the modifications of U34 leads to increased rigidity in the anticodon loop (more precisely in the first position of the anticodon) to ensure more efficient translation (especially higher binding of tRNA to ribosomal A-site) and to prevent frameshifting (Yokoyama *et al.*, 1985; Rodriguez-Hernandez *et al.*, 2013).

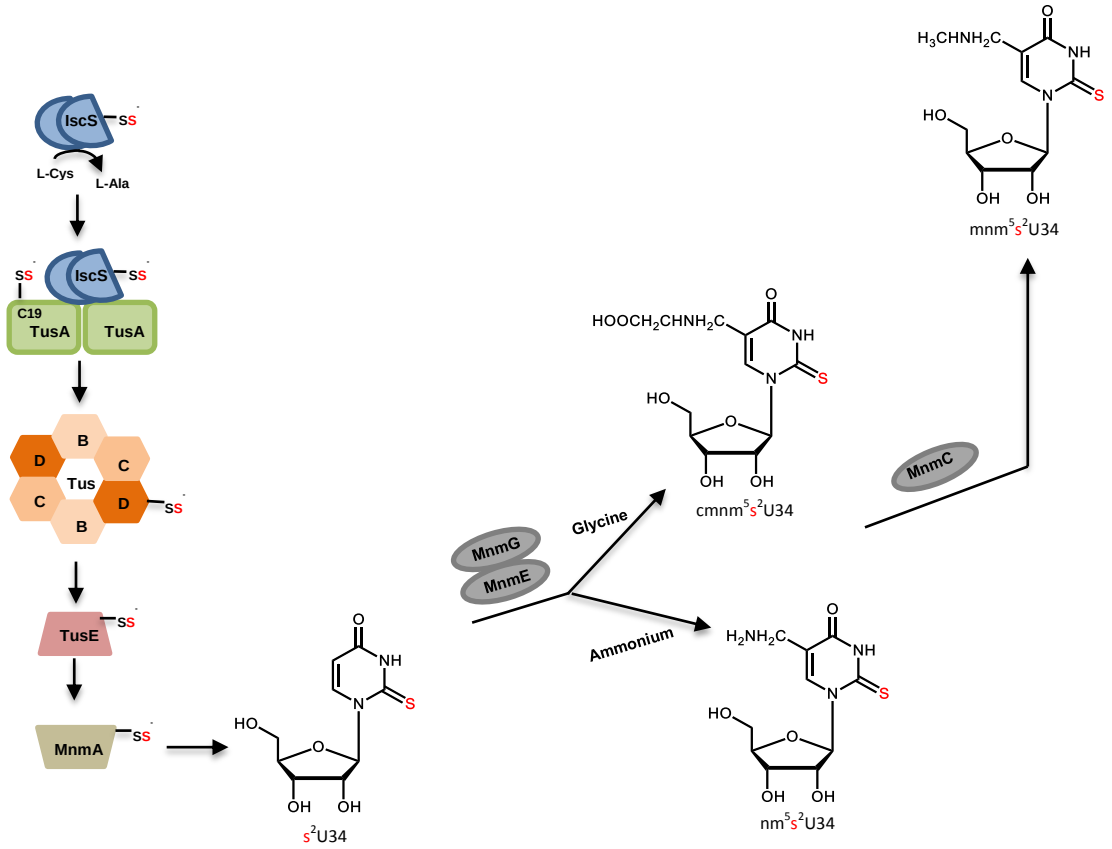

Figure 5: Biosynthesis of mnm^{5}s^{2}U34 in *E. coli*.

The synthesis of the side chain modification mnm^{5}of s^{2}U34 depends on the substrate. The MnmG-MnmE enzyme complex converts s^{2}U34 to cmnm^{5}s^{2}U34 if glycine is present as substrate and to nm^{5}s^{2}U34 if ammonium is present. In the next step MnmC produces mnm^{5}s^{2}U34 from both precursors cmnm^{5}s^{2}U34 and nm^{5}s^{2}U34. The sulfur for thiolation of U34 at C2 position originates from L-cysteine which is mobilized by IscS and further transferred by TusA, TusD, TusE and MnmA to U34 in tRNA.

In *E.coli*, there are three more tRNA thiomodifications. These include 4-thiouridine at position 8 (s^{4}U8), 2-thiocytidine at position 32 (s^{2}C32) and 2-methylthio-N6 isopentenyladenosine at position 37 (ms^{2}i^{6}A37) (Shigi, 2014). For the synthesis of these thionucelosides, IscS interacts with additional sulfur carrier proteins. IscS also interacts with ThiI which binds the persulfide sulfur and modifies the tRNA uridine at position 8 (4-thiouridine (s^{4}U8)) by sulfur incorporation. Moreover, ThiI is also responsible for sulfur transfer for thiamin synthesis (Kambampati and Lauhon, 2000). For the tRNA modifications s^{2}C32 and ms^{2}i^{6}A37 additional enzymes are involved, namely TtcA and MiaB.

The TtcA protein performs the sulfur transfer to C2 of cytidine at position 32 in tRNA (s^{2}C32). By comparison, MiaB catalyzes the formation of ms^{2}i^{6}A37 by adding of sulfur and methyl group at C2 of adenosine 37. The second modification i^6 at the same A37 is carried out by MiaA (before the MiaB catalyzed step). Therefore, MiaA is involved in the insertion of an isopentenyl group at the N-6 nitrogen of adenosine (Hernández *et al.*, 2007). Since TtcA and

MiaB are Fe-S cluster containing enzymes they receive the sulfur from IscU, a scaffold protein for Fe-S cluster formation that interacts directly with IscS (Shi *et al.*, 2010).

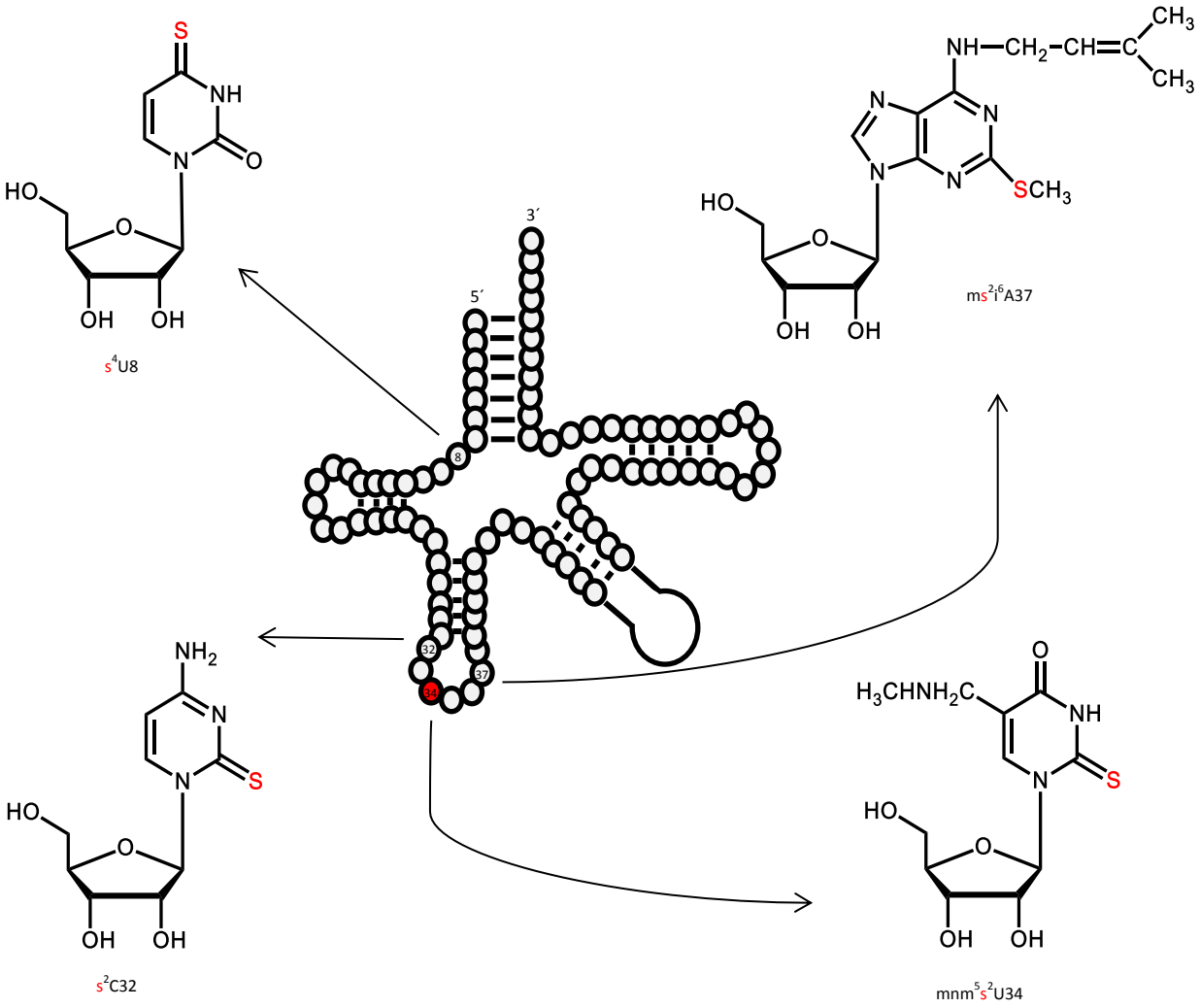

Figure 6: Overview of tRNA thiomodifications in *E. coli*.

Schematically shown is the structure of tRNA and the four different thionucelosides with their structure and position: from left to right (5´-3´in tRNA) 4-thiouridine at position 8 (s^4U8), 2-thiocytidine at position 32 (s^2C32), 5-methyaminomethyl-2-thiouridine at position 34 (mnm^5s^2U34) and 2-methylthio-N6-isopentenyladenosine (ms^2i^6A37).

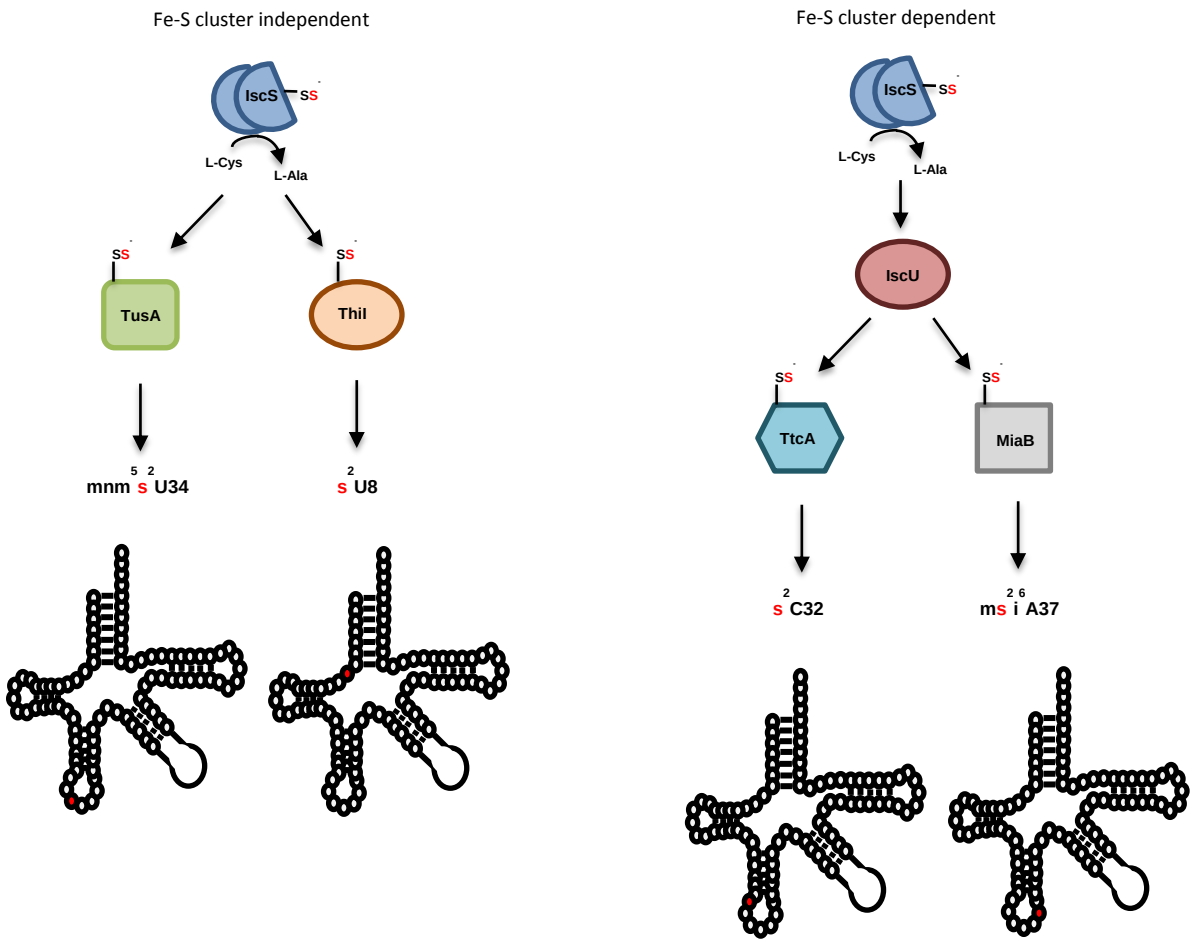

Figure 7: Biosynthesis of different thionucleosides in *E. coli*.

Biosynthesis of thionucelosides is divided into Fe-S cluster independent and dependent pathways. The Fe-S cluster independent pathways are catalyzed by TusA and ThiI protein. TusA accelerates the sulfur transfer for the formation of mnm^5s^2U34 and ThiI for s^4U8 synthesis. TtcA and MiaB require an Fe-S cluster which is assembled first on the IscU scaffold protein. TtcA transfers the sulfur to tRNA for the synthesis of s^2C32 and MiaB for ms^2i^6A37 formation. For both pathways the sulfur is provided by the IscS protein.

1.4 The role of TusA in Moco biosynthesis

An additionally important role of TusA is its involvement in molybdenum cofactor biosynthesis (Dahl *et al.*, 2013). In *E. coli* the Moco biosynthesis proceeds in several steps. First from 5´GTP the cyclic pyranopterin monophosphate (cPMP) is formed. In the second step TusA is involved. Similar to tRNA thiolation, TusA interacts with IscS, receives the persulfide sulfur and then forwards it to the MoaD of MPT synthase. This MPT synthase consists of two subunits of MoaE and two smaller MoaD like a heterotetramer, whereas the active MoaD possesses a C-terminal thiocarboxylate group (Gutzke *et al.*, 2001; Rudolph *et al.*, 2001). Subsequently, MPT synthase catalyzes the insertion of the sulfur into cPMP to

form the molybdopterin (MPT). In third step molybdate is incorporated into MPT which results in the formation of the molybdenum cofactor (Moco) (Dahl *et al.*, 2013; Leimkühler, 2014). After the formation of Moco, additional modifications can occur by binding of CMP or GMP at C4-phosphate of MPT. Resulting products are MPT cytosine dinucleotide (MCD) or MPT guanine dinucleotide (MGD) cofactor (Neumann *et al.*, 2009; Hilton and Rajagopalan, 1996).

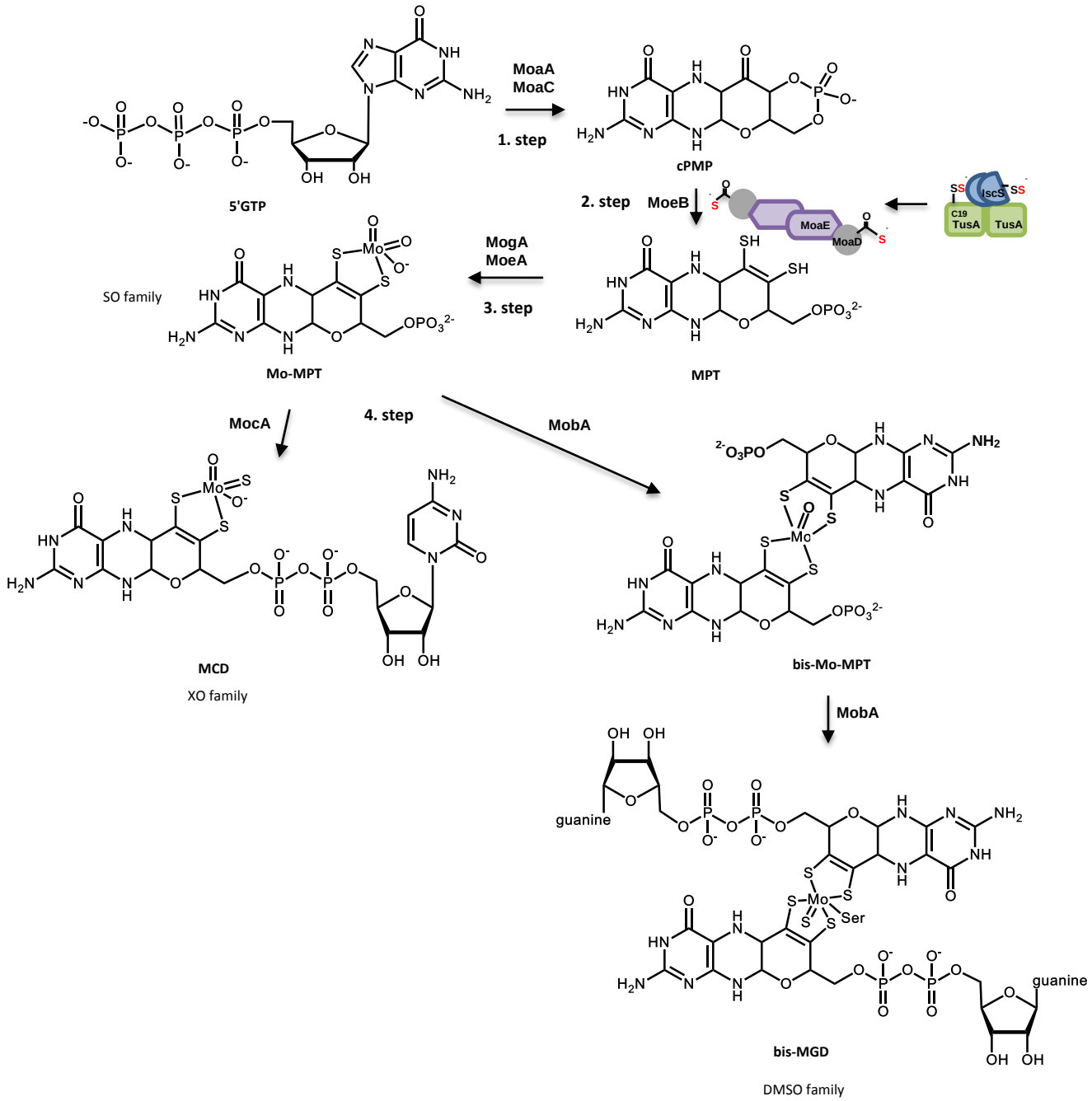

Figure 8: TusA involvement in Moco biosynthesis in *E. coli*.

Moco biosynthesis starts with the conversion of 5´GTP to cPMP by MoaA and MoaC enzymes. For the next step IscS mobilizes the sulfur from cysteine and interacts with TusA protein as in tRNA thiolation. This IscS-TusA complex transfers the sulfur to MPT synthase, precisely to the MoaD subunit which binds the sulfur as a thiocarboxylate group. It follows the insertion of sulfur into cPMP catalyzed by MPT synthase which leads to the formation of MPT. MoaD needs to be reactivated after every sulfur transfer step. This is catalyzed by MoeB. Subsequently molybdenum is incorporated into MPT by MogA and MoeA enzymes that produce Mo-MPT. Further modifications of Mo-MPT are either the insertion of CMP to Mo-MPT or GMP to bis-Mo-MPT with the formation of MCD or bis-MGD. During this the modification is catalyzed by MocA and to bis-MGD by MobA. The different cofactor forms are typical inserted into different enzymes, which are categorized into the enzyme families: Mo-MPT is bound directly to enzymes of the SO-family, MCD in enzymes of the XO-family of certain prokaryotes and bis-MGD is present in the DMSO reductase family enzymes.

1.5 Cell morphology of *tusA* deletion strains

The *tusA* gene was first identified in a screening study by Yamashino and his colleagues in 1998. They were looking for gene mutations which are influenced by the *katE* gene expression in a Δ*hns* background (Yamashino *et al.*, 1998). H-NS is one of the major components of the nucleoid in *E. coli* and its gene deletion leads to a distinct increase of σ^S (RpoS) during the exponential phase in the cell. σ^S is the stress induced sigma factor and is expressed more in stress situations. In turn, the deletion of *hns* appears as a stress condition that leads to an increased amount of σ^S and thus to an increased expression of genes that are dependent on σ^S (*katE* is one of these σ^S-dependent genes) (Yamashino *et al.*, 1998). In this assay they discovered the *tusA* gene which was designated *yhhp*. It impairs the stability of σ^S during the logarithmic growth phase which in turn leads to decreased *katE* expression in a Δ*hns* background (Yamashino *et al.*, 1998). Following Yamashino`s and colleagues initial report, other research groups confirmed the relationship between YhhP and bacterial cell growth (Ishii *et al.*, 2000; Katoh *et al.*, 2000). They assumed that YhhP has a fundamental role in bacterial cell physiology. Nine years later, an essential function for YhhP was discovered and the gene name was changed to *tusA*, the 2-thiouridine synthesizing protein. They demonstrated that its essential role is to transfer sulfur for the synthesis of 2-thiouridine nucleosides at tRNA position 34 for Lys, Gln, Glu (Ikeuchi *et al.*, 2006). Over the years, TusA functionality has not only been associated with sulfur transfer for mnm^5s^2U34 tRNA modification, but also with sulfur transfer for formation of the dithiolene group in Moco (Dahl *et al.*, 2013). The Cys-Pro-X-Pro motif was discovered at the N-terminus of TusA, which harbors the conserved cysteine as a catalytically active sulfur-binding residue. This residue can bind the sulfur of L-cysteine desulfurase, e.g. IscS, and transfers this sulfur to further sulfur acceptor proteins (Dahl *et al.*, 2013; Katoh *et al.*, 2000).

Another important function of TusA is that it plays a fundamental role in bacterial cell physiology (Yamashino *et al.*, 1998). *E. coli* cells usually grow as short rods. However, when the strain has a deletion in the *tusA* gene the cells grow slower than WT cells. They are long and grow as filaments during the exponential growth phase in rich medium. This indicates that the cells probably are not able to separate into two new cells during the growth process. Thus, the *tusA* deletion strain has a growth defect compared to the WT cells. This phenomenon suggests that TusA protein probably plays a role in the cytokinesis of *E. coli* cells. Such a phenotype occurs only during growth in rich medium and not in minimal medium (Yamashino *et al.*, 1998; Ishii *et al.*, 2000). More specifically, the absence of TusA protein due to the *tusA* gene deletion leads to a defect in FtsZ ring formation which results in non-dividing elongated cell (filaments) (Ishii *et al.*, 2000).

During the analysis of *tusA*-deficient cells a gene, named *dksA*, was discovered as a multisuppressor gene for the Δ*tusA* phenotype (Ishii *et al.*, 2000). The *dksA* gene can suppress the lethality of Δ*tusA* cells. It allows the Δ*tusA* cells to grow faster and to have a rod cell shape. Thus the insertion of multicopy suppressor genes like *ftsZ* or *dksA* leads to Δ*tusA* cells, which are able to grow in rich medium as rod-shaped cells similar to WT cells. But how the *tusA* deletion affects the FtsZ ring formation and thus the cell separation is not really clear (Ishii *et al.*, 2000). As mentioned, DksA acts as a suppressor in *tusA* mutant by complementing the Δ*tusA* growth defect (Ishii *et al.*, 2000). The DksA protein is involved in transcription of genes. It influences the transcript elongation by binding directly to RNA polymerase (Perederina *et al.*, 2004). Furthermore it regulates the translation of RpoS protein (Brown *et al.*, 2002), which is a further potential interaction partner of TusA (Yamashino *et al.*, 1998).

In the initial study by Yamashino and his colleagues, they postulated that TusA influences the stability of RpoS during exponential growth phase in a Δ*hns* background (Yamashino *et al.*, 1998). Later it was discovered that the *tusA* gene deletion diminishes additionally the translation and stability of RpoS protein (Aubee *et al.*, 2017). Under anaerobic conditions deletion of the *tusA* gene results in an increased *rpoS* gene expression (Dahl *et al.*, 2013). In general, RpoS is the RNA polymerase sigma factor (σ^S) which is induced under stress situations. It has the role as a master regulator for general stress response in bacteria to ensure an easier adjustment to stationary phase and starvation (Maciag *et al.*, 2011;

Hengge-Aronis, 1993). In addition, it affects the transcription of several genes, which are enhanced expressed in stationary phase (Yamashino *et al.*, 1998). Especially genes which are induced by RpoS are highly expressed during the transition of exponential to stationary phase (Maciag *et al.*, 2011). So the importance of RpoS protein for Δ*tusA* is not only the enhanced *rpoS* gene expression in Δ*tusA* cells, the TusA protein also influences the stability (Yamashino *et al.*, 1998) and directly the translation of RpoS (Aubee *et al.*, 2017).

But the more precise details about the effect of TusA on RpoS stability, the link to FtsZ and concerning to this to the filamentous growth is still unclear.

1.6 Role of the FtsZ protein in *E.coli*

Deletion of *tusA* gene revealed that FtsZ ring formation did not proceed as usual, although the FtsZ level was nearly the same like in WT cells. So it was assumed that an early step of FtsZ assembly did not work normally, or the formed FtsZ ring was not stable in Δ*tusA* cells (Ishii *et al.*, 2000). Insertion of extra *ftsZ* gene copies in Δ*tusA* cells shows a complementation of the growth defect of Δ*tusA* cells. The cell length of Δ*tusA* cells is reduced and cells grow like rods. So FtsZ acts as a multicopy suppressor of Δ*tusA* and the growth defect of Δ*tusA* cells is related to the defect FtsZ ring formation (Ishii *et al.*, 2000). But how the *tusA* deletion affects FtsZ ring formation and thus the cell separation is not clear (Ishii *et al.*, 2000).

FtsZ is the cell division protein, the prokaryotic tubulin homologue and is highly conserved. It is 40 kDa protein that forms a ring structure at the center of a cell. One cell can divide in two new cells through the switch of a lateral cell wall to a septum formation (Vaughan *et al.*, 2004; Margolin W., 2005).

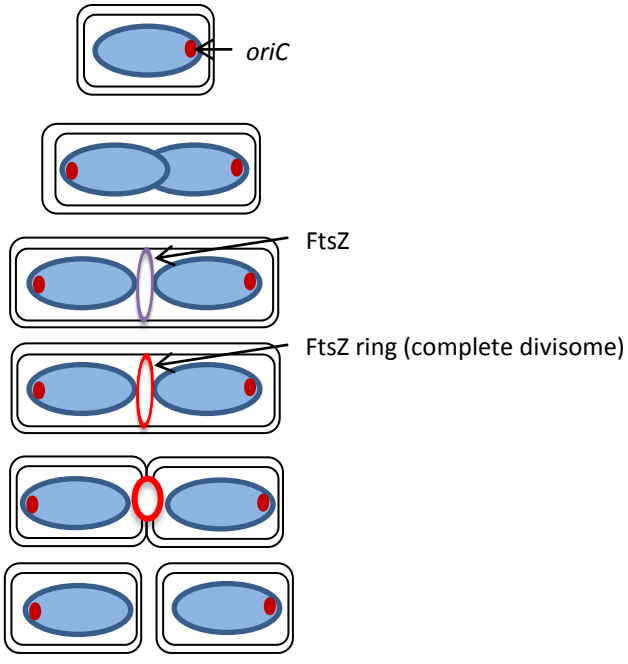

Figure 9: Cell division via FtsZ ring assembly in *E. coli*.

The chromosome replicates when the growth process is started. For cell division, the FtsZ protein assembles in the center of the cell and forms a ring-structure (purple ring). FtsZ assembles additional proteins to complete the cell division protein machinery (divisome) (red ring). Finally, a division septum is formed at the midcell, the Z ring contracts and this leads to the constriction of the outer membrane. Constriction results in two separated new daughter cells.

The general cell division process is visualized in Figure 9. A bacterial cell needs to divide during replication. After the replication of the chromosomes is finished, the daughter cells are split. FtsZ, one of the main proteins for cell division, assembles in the center of the cell to form a ring-structure (purple ring). Then FtsZ triggers the assembly of further proteins (at least ten) to complete the cell division protein machinery (divisome) (red ring). Finally a division septum is formed at the midcell, the Z ring contracts, and this leads to the constriction of the outer membrane. Then two separated new daughter cells are formed (Margolin W., 2005).

The FtsZ ring structure consists of several single protofilaments. Every FtsZ subunit can bind GTP and assembles in a head-to-tail fashion. This leads to the formation of single stranded protofilaments which can bind together over the sides of the subunits and form sheets or bundles (Haeusser *et al.*, 2015). Further, the FtsZ assembly into protofilaments is dynamic and regulated by GTP hydrolysis (Mukherjee and Lutkenhaus, 1994).

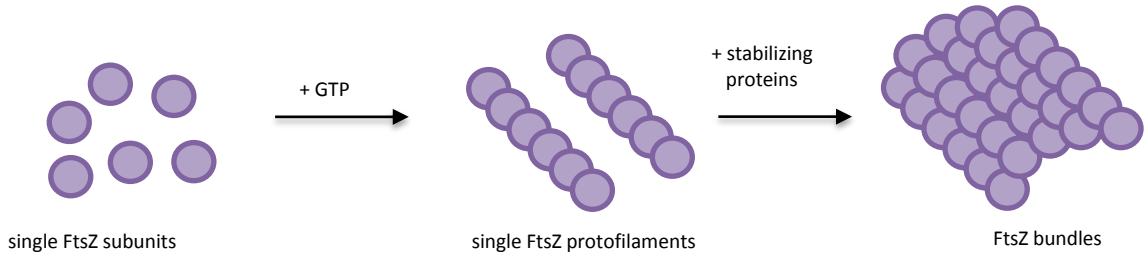

Figure 10: Scheme of FtsZ bundle synthesis.

Several single FtsZ subunits bind GTP which results in head-to-tail interaction of the subunits. They assemble into protofilaments. These protofilaments bind over their sides and form the FtsZ bundles which then end in the ring structure.

Several proteins support the assembly of FtsZ while they link the Z ring to the cell membrane (Figure 11). ZipA and FtsA proteins belong to these stabilizing enzymes whereby ZipA is a membrane-anchored protein and FtsA is a membrane-associated protein (Pichoff e*t al.*, 2015). To complete the cell divsion machinery (divisome), FtsZ recruits further proteins to the midcell (except FtsA and ZipA). This comprises the proteins FtsK, FtsQ/FtsL/FtsB, FtsW, FtsI, FtsN (Tsang and Bernhardt, 2015).

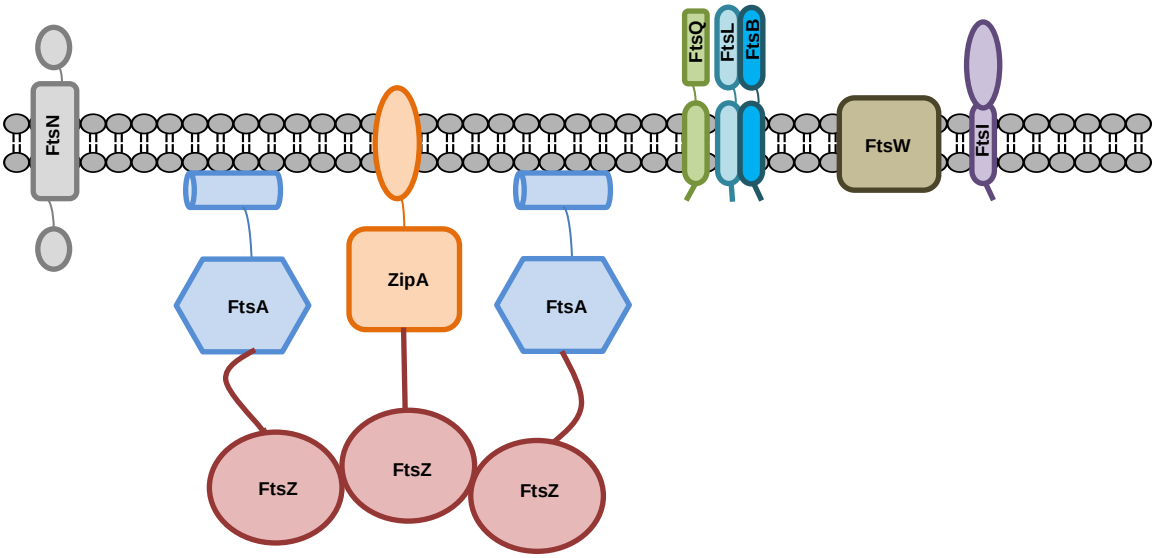

Figure 11: Protein components of complete division machinery in *E. coli*.

During the formation of the FtsZ ring at the midcell of an *E. coli* cell, a link of this FtsZ ring is built to the cell membrane via further proteins. Two proteins, one membrane-anchored ZipA and one membrane-associated FtsA, bind to FtsZ. This binding stabilizes the FtsZ ring at the center of the bacterial cell and anchors it to the cell membrane. To complete the cell division machinery, the divisome, further proteins are recruited to the midcell. The FtsN triggers the FtsQLB complex to induce the cell division. This FtsQLB complex protein complex stimulates the further FtsW and FtsI proteins to induce the septal peptidoglycan (PG) synthesis.

Important during this cell division process is that the FtsZ ring is formed at the right position. When the FtsZ system is impaired, then mini cells or unequal daughter cells result. To prevent this, two inhibitory systems, called nucleoid occlusion and the Min system, are present. Both systems are essential for exact positioning of the Z ring (Norris *et al.*, 2004; Margolin, W., 2006). During binary fission the cell grows by replication of the chromosomes. When chromosome replication and segregation are not completed, the nucleoid occlusion (NO) inhibits the FtsZ to assembly over the regions of the nucleoids (Norris *et al.*, 2004). By comparison, the Min system acts at the nucleoid-free cell poles of the bacterial cell. In *E. coli* the Min system consists of proteins MinC (Z ring inhibitor), MinD (ATPase, membrane-

associated) and MinE (improves MinD ATPase), with MinC as the the main actor to inhibit the FtsZ assembly (Sun and Margolin, 2004). During the cell growth, FtsZ ring assembly and Min system oscillate from one cell pole to the other until nucleoid segregation is completed and the FtsZ ring can assemble at the midcell. The cell poles are occupied by MinC so that FtsZ cannot assemble at the cell poles and is forced to form the Z ring at the nucleoid-free cell center (Addinall and Holland, 2002; Margolin, W., 2006).

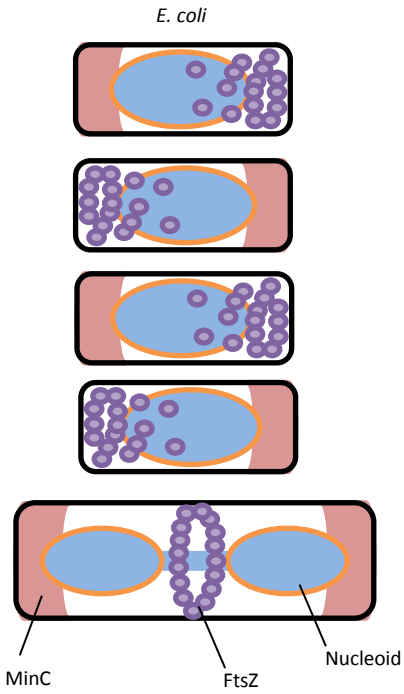

Figure 12: Correct positioning of the FtsZ ring at the midcell by nucleoid occlusion and the Min inhibitory systems.

The cell division process is regulated by inhibitory systems to allow constriction at the right position and produce equal new daughter cells. During the cell growth and chromosome (blue) replication, FtsZ (purple) assembles to a ring structure. It is important that FtsZ is positioned at the midcell and not at another position within the cell, e.g. at cell poles. Therefore the Min and nucleoid occlusion (NO) inhibitory systems block the cell areas where FtsZ is not allowed to form the Z ring structure. The nucleoid occlusion (NO, orange) system inhibits the region at the chromosomes and the MinC (pink) protein at the cell poles. As a result, the FtsZ and MinC proteins oscillate from one cell pole to the other until the chromosome segregation is completed and the FtsZ can assemble at the center of the cell to form a ring structure.

Deletion of *tusA* gene revealed that FtsZ ring formation did not proceed as usual although the FtsZ level is nearly the same like in WT cells. So it is assumed that an early step of FtsZ assembly was not working normally or the formed FtsZ ring was not stable in Δ*tusA* cells (Ishii *et al.*, 2000). Insertion of extra *ftsZ* gene copies in Δ*tusA* cells showed a

complementation of the growth defect of Δ*tusA* cells. The cell length of Δ*tusA* cells was reduced and cells grew like rods. So FtsZ acts as a multicopy suppressor of Δ*tusA* and the growth defect of Δ*tusA* cells is related to the defect FtsZ ring formation (Ishii *et al.*, 2000).

1.7 Deletion of TusA affects Fis and H-NS proteins in *E.coli*

As already mentioned, TusA was discovered in a screening assay to determine genes in Δ*hns* background which are regulated by RpoS during the exponential growth phase (Yamashino *et al.*, 1998). In addition, it was reported that the expression of *hns* is regulated by Fis protein. Fis is the **f**actor for **i**nversion **s**timulation which acts as a global regulator during transcription and is involved in transcription regulation of 21 % genes in *E. coli* (Travers and Muskhelishvili, 2005; Cho *et al.*, 2008). Fis is able to activate or repress the transcription of affected genes (Kahramanoglou *et al.*, 2010). In addition, Fis is a 98 aa (11 kDa) small protein which binds to the DNA together with H-NS for nucleoid structure organization (Cho *et al.*, 2008). Moreover, Fis is together with HNS, HU, IHF and DPS one of the major components of the bacterial nucleoid (Dame, 2005). The transcriptional regulatory role of the Fis protein refers to several genes which are involved in e.g. translation (rRNA and tRNA genes), stress response, and amino acid biosynthesis (Bradley *et al.*, 2007). However, the cellular Fis amount varies during the different growth phases. The Fis concentration is up to 60 000 copies per cell in exponential growth phase and therefore very high which decreases rapidly under 100 Fis molecules per cell (nearly undetectable) in the stationary phase. Thus the growth phase dependent intracellular levels of Fis emphasize his role in gene expression of growing cells in exponential phase (Ali Azam *et al.*, 1999; Schneider *et al.*, 1997).

As mentioned in the chapters before, TusA affects the stability and translation of RpoS (Yamashino *et al.*, 1998; Aubee *et al.*, 2017). The respective gene encodes for the alternative sigma factor σ^S which is embedded in the efficient transcription of genes for general stress response. Additionally it shows important function in nucleic acid synthesis, modification, and turnover (Maciag *et al.*, 2011). The abundance of RpoS changes during the different growth phases and is therefore growth phase-regulated. But the regulation is the opposite of that of Fis whereby the *rpoS* expression is regulated by a Fis-binding site in *rpoS* promoter (Brown *et al.*, 2002; Hirsch and Elliott, 2002; Hirsch and Elliott, 2005 (RpoS and Fis)). During the exponential growth phase, the Fis protein is produced in high amount in the bacterial

cell. Concomitant with this growth phase and relative amount of Fis produced, it binds to the *rpoS* promoter region and inhibits the transcription of *rpoS* (Hirsch and Elliott, 2005 (RpoS); McLeod *et al.*, 2000). As growth progresses and the cells enter stationary phase, the amount of Fis suddenly decreases so that it is almost undetectable (Hirsch and Elliott, 2005 (RpoS and Fis); Schneider *et al.*, 2000). In the same time *rpoS* shows the inverse phenomenon of Fis during the stationary growth phase, its transcription rises up to 10-fold (Hirsch and Elliott, 2005 (RpoS)).

Since TusA was originally identified in a Δ*hns* background when screening for genes affecting cellular RpoS levels during exponential phase (Yamashino *et al.*, 1998), and since Fis regulates the expression of *hns*, a possible relationship of Fis to TusA or changes of Fis content in Δ*tusA* does not seem unimportant. Moreover, it is noteworthy that the Fis protein is involved in cell division (Logan, 2006) and probably has a link to FtsZ. So Fis could have an effect on the cell division defect and therefore the filamentation observed in Δ*tusA* cells. Since filaments were not discovered only for the Δ*ftsZ* strain, but also for cells with a defect in Fis (Ishii *et al.*, 2000; Lioy *et al.*, 2018).

Previously, Ishii and colleagues reported that DksA can complement the growth defect and filamentous cell shape of Δ*tusA* mutant cells (Ishii *et al.*, 2000). This is not the only role identified for DksA; it also regulates the expression of *fis* and *rpoS* genes. DksA activates the *rpoS* expression and leads to an increased level of RpoS (Brown *et al.*, 2002). Conversely, to this, DksA impairs the transcription of Fis by reducing the lifetime of RNA polymerase-*fis*-promotor complex (Mallik *et al.*, 2006).

In addition to this Fis protein, there is a further DNA-binding protein, the H-NS, which is also responsible for the maintenance of nucleoid structure (Cho *et al.*, 2008). H-NS is the **h**istone-like **n**ucleoid **s**tructuring protein which is associated to the nucleoid and is responsible in the condensing and supercoiling of DNA (Dame *et al.* 2000; Dame, 2005). Additionally, H-NS is involved in gene regulation in regard to adaptation of environmental changes e.g. stress (Falconi *et al.*, 1996). Therefore, it is a part of the survival in stationary phase, which supports the bacterial cell growth during stationary phase (Chib and Mahadevan, 2012). But the more important function of H-NS as a global transcription repressor (Atlung and Ingmer, 1997) is due to chromosomal integration and not via its binding to a specific promotor (Dame, 2005; Paul *et al.*, 2004). In contrast to H-NS, the Fis protein shows a positive effect

during DNA transcription, it increases the transcription of genes (Travers and Muskhelishvili, 1998; Cho *et al.*, 2008). More specifically it bends the DNA around 40° and 90° which leads to stabilization of DNA looping (Finkel and Johnson, 1992). This DNA looping in turn adjusts the gene transcription and support the compaction of DNA structure (Skoko *et al.*, 2006; Travers and Muskhelishvili, 1998). The importance of these Fis and H-NS proteins is that their gene expression is affected if the TusA protein is deleted. Deletion of *tusA* gene results enhanced *fis* gene expression under anaerobic conditions and decreased *hns* expression under aerobic conditions (Dahl *et al.*, 2013).

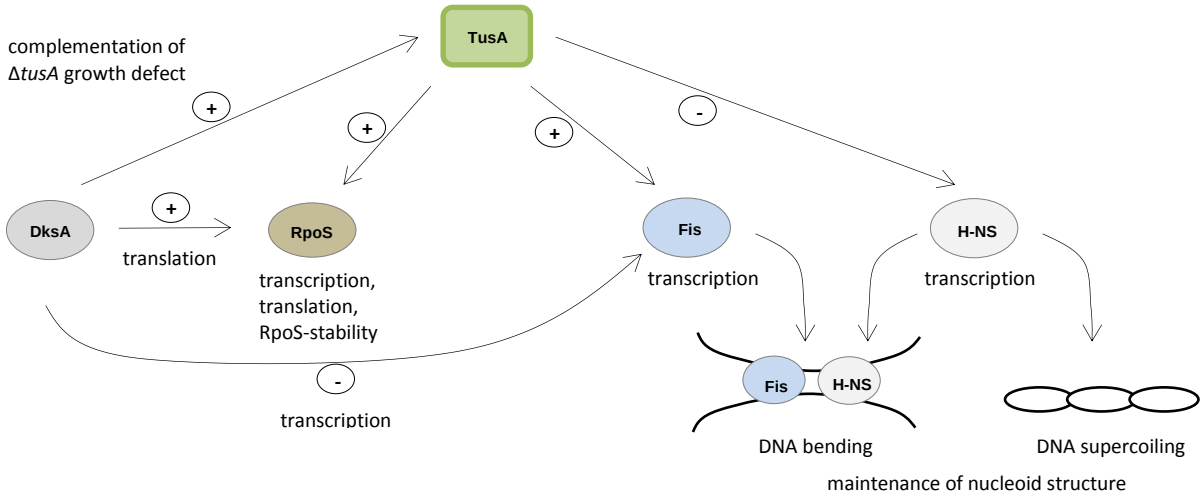

Figure 13: Role of TusA for DksA, RpoS, Fis and H-NS proteins.

Several proteins are affected by the deletion of TusA protein. The deletion of the *tusA* gene results in an increased *rpoS* and *fis* transcription whereas the transcription of *hns* is downregulated. Furthermore, TusA has an effect on RpoS translation and stability. Fis and H-NS are nucleoid-associated proteins (NAPs) which are binding to the DNA and organizing the nucleoid structure. Beside the TusA, also the DksA affects the *fis* transcription but in a negative way. Another effect of DksA is to regulate the translation of RpoS and to complement the growth defect of Δ*tusA*.

2 Aim of this work

The focus of this project was to investigate the role of TusA for FtsZ ring assembly and cell functionality in *E. coli*. It was known that Δ*tusA* cells have a growth defect and an abnormal cell separation, they were growing as filaments. So in these cells it was implied that the FtsZ ring formation is defective since the cells were not able to divide. One of the aims was to discover why a deletion of *tusA* results in filamentous growth.

To elucidate the role of TusA for cell division, following analyses were planned:

- recording the growth curves of *tusA*-depleted cells
- analysis of the cell morphology of *tusA*-depleted cells by fluorescence microscopy
- suppression of Δ*tusA* growth deficiency and the cell division defect by complementation of the Δ*tusA* strain with selected genes.

The IscS protein is involved in mnm^5s^2U34 tRNA modification but it has also many interaction partners outside the tRNA thiolation pathway (Figure 7). IscU, ThiI, TtcA and MiaB belong to these interaction partners. Gene deletion strains of these proteins could give a hint toward the source of the cell division defect. If the cells of these strains show no filamentation this would probably confirm that the cell division defect is related to mnm^5s^2U34 tRNA modification. These goals could be achieved by:

- recording the growth curves of mutant strains involved in the mnm^5s^2U34 tRNA modification pathway
- analysis of the cell morphology of deletions strains involved in mnm^5s^2U34 tRNA modification by fluorescence microscopy
- comparison of growth behaviour and morphological phenotype of mnm^5s^2U34 tRNA modification mutants strains with deletions strains outside the mnm^5s^2U34 tRNA modification pathway (e.g. Δ*iscU*, Δ*thiI*, Δ*ttcA*, Δ*miaB*)

Since *tusA*-deleted cells have a cell division problem and FtsZ is responsible for the formation of the division ring at midcell, it was important to:

- visualize an interaction between TusA and FtsZ or further interaction proteins in living cells via **f**luorescence **r**esonance **e**nergy **t**ransfer (FRET)
    - establish expression of fluorescent fusion protein constructs in Δ*tusA* and WT cells
    - localize fusion proteins in living cells
    - co-express of two different fluorescent proteins fused to possible interaction partners in one cell.

Further, it was planned to visualize the interaction of:

- IscS-IscU, IscS-CyaY and IscS-FtsZ where the IscS would be fused to EYFP and the possible interaction partners IscU, CyaY and FtsZ should be fused to mCherry or

- TusA-IscU, TusA-CyaY and TusA-FtsZ where the TusA would be fused to EGFP and the possible interaction partners IscU, CyaY and FtsZ should be fused to mCherry.

- The visualization would be determined by FRET.

Due to the fact that the pure Δ*tusA* strain has a cell division defect which leads to filaments and the main player of cell separation in *E. coli* is the FtsZ protein it was planned to investigate the role of TusA on FtsZ levels in detail:

- The cellular FtsZ amounts were planned to be determined at different growth phases by immunoblotting using a FtsZ antiserum.

Further it was planned to analyze the effect of TusA on cellular Fis levels:

- The cellular Fis concentration were planned to be determined at different growth phases by immunoblotting using a Fis antiserum.

It also appears to be important to analyze the effect of the absence of mnm^5s^2U34 tRNA modification on protein translation. Since TusA is missing due to *tusA* gene deletion, it could influence the translation of proteins by using the unmodified U34 tRNAs of lysine, glutamate and glutamine. Therefore it was planned to investigate the translation efficiencies of RpoS, Fur and Fis proteins.

- For this assay, produced EGFP fusion constructs with *rpoS*, *fur* or *fis* gene sequences will be fused each separately to a C-terminal EGFP gene sequence.

- The EGFP-fusion constructs should be transformed in Δ*tusA* and WT strains and after protein expression the EGFP fluorescence will be determined by flow cytometry.

- Probably further strains of mnm^5s^2U34 tRNA modification pathway as Δ*mnmA* and *iscS* could be considered to check whether all these strains have an affected protein translation.

- In addition, to show any positive effects of $tRNA^{Lys}$, $tRNA^{Glu}$, $tRNA^{Gln}$ a further control construct should be produced. For this purpose, all lysines, glutamates and glutamines in *fis* gene sequence were planned to mutate to alanine to eliminate the positive effect of mnm^5s^2U34 tRNA modification such as efficient ribosome binding and averting of frameshift during translation. The translation efficiency of (mutated) mFis-EGFP would be analyzed by flow cytometry as for the other EGFP fusion constructs.

3 Materials and Methods

3.1 Chemicals and enzymes

For this study, standard chemicals were used from the companies Sigma-Aldrich Corporation, Merck KGaA, Carl Roth GmbH & Co, VWR International GmbH and Duchefa Biochemie B.V. The restriction enzymes were used either from Fermentas or New England Biolabs (NEB) GmbH. Special chemicals, enzymes or devices are mentioned in the respective section.

3.2 Buffers and Solutions

Buffer and solutions were prepared using deionized water (Millipore water). The pH, unless mentioned, was adjusted using NaOH or HCl. Sterilization was done either by autoclaving (1 bar, 121 °C for 20 min) or by filtration (0.2 µm).

3.3 Media and additives

E. coli cells were cultivated in LB medium (10 g tryptone, 5 g yeast extract for 1 l) without NaCl (LB-0%). The LB medium was autoclaved and additives for the medium were filter sterilized. The special media additives are mentioned in the respective method. Antibiotics used were: 150 µg/ml ampicillin (Amp), 25 µg/ml kanamycin (Km), 50 µg/ml chloramphenicol (Cm) in 97% (v/v) ethanol and 100 µg/ml streptomycin (Sm).

3.4 Molecular biological methods

3.4.1 Cultivation of *E. coli* cells

Escherichia coli cultures were grown in M9 minimal medium (Miller 1972, modified by Müller 1997: per liter (pH 7,4) 0,5 g NaCl, 1 g NH_4Cl, 3 g KH_2PO_4, 6 g Na_2HPO_4, 100 mg of every amino acid (alanine, arginine, asparagine, aspartic acid, cysteine, glutamine, glutamic acid, glycine, histidine, isoleucine, leucine, lysine, methionine, phenylalanine, proline, serine, threonine, tryptophan, tyrosine, valine), after autoclaving addition of filter sterile 0,1% element solution (400 µM H_3BO_3, 30 µM $CoCl_2$, 10 µM $CuCl_2$, 10 µM $ZnCl_2$, 80 µM $MnCl_2$, 10 mM $FeCl_3$), 0,8% glycerol, 5 ml 0,1 M $CaCl_2$, 1 ml 1 M $MgCl_2$, 1 ml 12,6 g/l KNO_3, 15 ml 20% glucose) aerobically for pre-cultures overnight (*o.n.*) at 37 °C, 200 rpm if needed with the respective antibiotic. The main cultures were inoculated from these *o.n.* pre-cultures in Luria

Broth (LB) which were grown aerobically at 37 °C, 180 rpm. Antibiotics Amp/ Kana/ Cm/ Sm were only added to the medium if the cells contained a vector.

3.4.2 Lysogenization of *E. coli* strains

The gene of the T7-RNA polymerase was inserted into the genome of the *E. coli* strains via the λD3 Lysogenization Kit (Novagen) according to the manufacturer's instructions. This allows the expression of proteins whose gene sequence is inserted in a plasmid with T7 promotor.

3.4.3 Storage of *E. coli* cells

750 µl of *o.n. E. coli* culture was mixed with 750 µl sterile 87% (v/v) glycerol. The mixture was frozen in liquid nitrogen and stored at -80 °C.

3.4.4 Bacterial strains

All bacterial strains used in this work are listed in table 1.

Table 1: Bacterial strains used in this study.

strain	genotype	resistance	usage	reference
DH5α	F-, supE44, Δlac U169, (φ80*lacZ* ΔM15), hsdR17, endA1, gyrA96, thi-1, relA1, recA56	---	cloning, plasmid isolation, plasmid storage	Hanahan, 1983
BW25113	lacIq, rrnBT14 Δ*lacZ*WJ16, hsdR514, ΔaraBADAH33, ΔrhaBADLD78	---	wild-type strain / reference	Baba *et al.*, 2006
BW25113 (DE3)	lacIq, rrnBT14 Δ*lacZ*WJ16, hsdR514, ΔaraBADAH33, ΔrhaBADLD78(DE3)	---	wild-type strain / reference, protein expression	Bühning *et al.*, 2017
Δ*hns*	BW25113 *hns*: Km	Km	investigation of *hns* deletion	Baba *et al.*, 2006
Δ*iscS*	BW25113 *iscS*: Km	Km	investigation of *iscS* deletion	Baba *et al.*, 2006
Δ*iscS* (DE3)	BW25113 *iscS*: Km(DE3)	Km	protein expression in Δ*iscS strain*	this work
Δ*iscU*	BW25113 *iscU*: Km	Km	investigation of iscU deletion	Baba *et al.*, 2006
Δ*iscU* (DE3)	BW25113 *iscU*: Km(DE3)	Km	protein expression in Δ*iscU strain*	this work
Δ*moaD*	BW25113 *moaD*: Km	Km	investigation of *moaD* deletion	Baba *et al.*, 2006
Δ*mnmA*	BW25113 *mnmA*: Km	Km	investigation of *mnmA* deletion	Baba *et al.*, 2006
Δ*mnmA* (DE3)	BW25113 *mnmA*: Km(DE3)	Km	protein expression in Δ*mnmA strain*	this work
Δ*mnmC*	BW25113 *mnmC*: Km	Km	investigation of *mnmC* deletion	Baba *et al.*, 2006
Δ*mnmE*	BW25113 *mnmE*: Km	Km	investigation of *mnmE* deletion	Baba *et al.*, 2006

Δ*miaA*	BW25113 *miaA*: Km	Km	investigation of *miaA* deletion	Baba *et al.*, 2006
Δ*miaB*	BW25113 *miaB*: Km	Km	investigation of *miaB* deletion	Baba *et al.*, 2006
Δ*rpoS*	BW25113 *rpoS*: Km	Km	investigation of *rpoS* deletion	Baba *et al.*, 2006
Δ*sufS*	BW25113 *sufS*: Km	Km	investigation of *sufS* deletion	Baba *et al.*, 2006
Δ*tusA*	BW25113 *tusA*: Km	Km	investigation of *tusA* deletion	Baba *et al.*, 2006
Δ*tusA* (DE3)	BW25113 *tusA*: Km(DE3)	Km	protein expression in Δ*tusA strain*	Bühning *et al.*, 2017
Δ*tusD*	BW25113 *tusD*: Km	Km	investigation of *tusD* deletion	Baba *et al.*, 2006
Δ*tusE*	BW25113 *tusE*: Km	Km	investigation of *tusE* deletion	Baba *et al.*, 2006
Δ*thiI*	BW25113 *thiI*: Km	Km	investigation of *thiI* deletion	Baba *et al.*, 2006
Δ*ttcA*	BW25113 *ttcA*: Km	Km	investigation of *ttcA* deletion	Baba *et al.*, 2006

3.4.5 Competent *E. coli* cells

E. coli cells were made chemically competent so that they can absorb external DNA. Pre-culture (5 ml) of the respective *E. coli* strain was inoculated in LB *o.n.* at 37 °C, 200 rpm. If needed, respective antibiotic(s) were added. The next day to 50 ml sterile LB were added 1 ml sterile 1 M $MgSO_4$ and 100 µl *o.n. E. coli* culture. The cells were cultivated at 37 °C, 200 rpm until they reached the OD_{600} of 0.09. The cells were cooled on ice bath for 2 min by shaking and incubated for 28 min. 50 ml culture was divided in 2 falcons with each 25 ml culture and harvested at 720 x g, 0 °C for 12 min. Cell pellets were resuspended in 8 ml MES buffer (500 mM N-morpholinoethanesulfonic acid (MES), 30 mM $CaCl_2xH_2O$, 22 mM $MnCl_2xH_2O$, 10% glycerol, pH 6.3 set with KOH) each and incubated on ice for 10 min. They were again harvested and pellets resuspended in 4 ml MES buffer each. At the end, the cell suspension was pipetted as 100 µl aliquots in pre-cooled Eppendorf tubes. After freezing in liquid nitrogen these were stored at -80 °C.

3.4.6 Cloning

3.4.6.1 Isolation of genomic DNA

Genomic DNA was isolated from *E. coli* MG1655 and was used as template for PCR reactions to produce the desired gene. The *E. coli* strain was cultivated in 5 ml of LB at 37 °C, 220 rpm without antibiotics. 1.5 ml culture was centrifuged at 14000 x g for 1 min and the pellet was

washed in 1 ml sterile TES buffer (50 mM Tris, 50 mM NaCl, 5 mM EDTA, pH 8.0). After second centrifugation at 11000 x g for 10 min the cell pellet was resuspended in 800 µl TES buffer. Cells were lysed by adding of 20 µl 20% SDS, mixed by vortexing and incubation at RT for 30 min. 300 µl phenol was added to the cell suspension to denature the proteins, vortexed and centrifuged 12000 x g for 10 min. The upper phase was transferred in a new Eppendorf tube and this 'phenolization' step was repeated 4 times. 600 µl isopropanol was added to 600 µl of the upper aqueous phase, vortexed and incubated at -20 °C for 30 min to precipitate the DNA. Then the mixture was centrifuged at 15000 x g, 4 °C for 15 min and the pellet was washed with 500 µl 70% (v/v) ethanol for 5 min at RT, centrifuged and ethanol was decanted completely. The pellet was dried at 37 °C (30 min – 1 h). The dried pellet was resuspended in sterile 100 µl TE buffer (1 mM Tris, 1 mM EDTA, pH 8.0) at 37°C for 30 min. Concentration of total genomic DNA was determined at 260 nm and the DNA was stored at -20°C.

3.4.6.2 Oligonucleotides

Oligonucleotides (Primer) were synthetized at BioTeZ Berlin Buch GmbH (Berlin, Germany) and later at Eurofins Genomics GmbH (Ebersberg, Germany). All used oligonucleotides were listed in table 2.

Table 2: Oligonucleotides used in this study.

primer name	Sequence (5´-3´)	usage
FW NdeI-*ftsZ*	GCG CAT ATGTTTGAACCAATGGAAC	Cloning of *ftsZ* in pET15b
RV *ftsZ*-BamHI	CGC GGATCC TTAATCAGCTTGCTTACGC	
FW XhoI-*dksA*	GCGGCG CTCGAG ATGCAAGAAGGGCAAAACCG	Cloning of *dksA* in pET15b
RV *dksA*-BamHI	CGC GGATCC TTAGCCAGCCATCTG	
FW XbaI-*ftsZ*	GCG TCTAGA ATGTTTGAACCAATGGAACTTACC	Cloning of *ftsZ* in mCherry-pCDFDuet-1
RV *ftsZ*-NotI	CGC GCGGCCGC TTAATCAGCTTGCTTACGC	
FW *ftsZ* internal	CGCTACCAGCAGCATGGGATGGC	Sequencing of mCherry-*ftsZ* fusion in mCherry-plueScript
RV *ftsZ* internal	GCACCATGTGTTCAACAGCATTACC	
RV *ftsZ* internal 2	GCCAACTTCTGGATTAGCGCC	
FW XbaI-*cyaY*	GCG TCTAGA ATGAACGACAGTGAATTTCATCGC	Cloning of *cyaY* in mCherry-pCDFDuet-1
RV *cyaY*-NotI	CGC GCGGCCGC TTAGCGGAAACTGACTGTTTC	
RV *cyaY* internal	CAGCGGCTCCTGGCGGTTGATAATG	Sequencing of mCherry-*cyaY* fusion in mCherry-pCDFDuet-1

3.4.6.3 Polymerase chain reaction (PCR)

PCR reaction was used for amplification of specific genes of the genome. Each sample (50 µl) contained the following components:

- 1 µl 10 mM dNTP
- 1 µl 50 µM forward (FW) primer
- 1 µl 50 µM reverse (RV) primer
- 1 µl Herculase II (polymerase, Agilent Technologies)
- 10 µl 5 x Herculase buffer
- 1 µl 20 – 50 ng genomic DNA / Plasmid-DNA
- 35 µl sterile H_2O
-

The PCR program contained following steps:

1) 3 min 95 °C - denaturation
2) 45 sec 95 °C – denaturation
3) 45 sec (T_M – 5) °C - primer annealing
4) 45 sec 72 °C - elongation
5) 35 times repeat step 2,3,4
6) 10 min 72 °C - final synthesis
7) 4 °C - storage

The temperature for primer annealing (step 3) depends on the melting temperature (T_M) of the used primer pair. The elongation time (step 4) depends on the fragment length. Herculase II polymerase amplifies at a rate of 1000 bp/min.

3.4.6.4 Restriction digestion

The analytical digestion (10 µl) consisted of:

- 0.2 µg Plasmid-DNA
- 1 µl 10 x restriction enzyme (RE) buffer
- 0.25 µl (0.5 U) per RE
- x µl sterile H_2O (add 10 µl)

The digestion mixture was incubated at 37 °C for 1 h. If fast digest restriction enzymes (New England Biolabs (NEB) GmbH, Frankfurt am Main, Germany) were used, the incubation time was 15 min. The restriction enzymes were inactivated at 80 °C, 20 min, whenever possible.

The components for the preparative digestion (30 µl) were:

- 10 µg Plasmid-DNA/ PCR-Product
- 3 µl 10 x restriction enzyme buffer
- 1 µl (10 U) per restriction enzyme
- x µl sterile H_2O (add 30 µl)

The digestion mixture was incubated at 37 °C for 3 h or 15 min with fast digest enzymes.

3.4.6.5 Agarose gel electrophorese

To probe the PCR product or the digestion with restriction enzymes, the sample was mixed with 6 x DNA loading dye (10 mM Tris/HCl (pH 7.6), 0.15% orange G, 0.03% xylene cyanol FF, 60% glycerol, 60 mM EDTA) and the whole sample was loaded on 1% agarose gel which contains 1% (w/v) ethidium bromide. 1 kb DNA ladder (Fermentas) was also loaded next to the sample to determine the size of the DNA bands. The electrophoresis was performed in 1 x TAE buffer (40 mM Tris/HCl, 20 mM HAc, 1 mM EDTA, pH 8.0 (set with HAc) at 100 V for 30 min. Separated DNA bands were visualized via UV light and imaged by Geldoc (Biorad).

3.4.6.6 Isolation of DNA fragments from agarose gels

Separated DNA fragments were isolated from agarose gel for cloning. For this, agarose gel containing the DNA fragments were cut out from agarose gel and DNA was extracted from these pieces by using the NucleoSpin Gel and PCR clean-up Kit (Machery-Nagel) according to manufacturer's instructions. The DNA was eluted in pre-warmed (70 °C) 15 µl sterile H_2O. To enhance the amount of DNA elution step was done 3 times. After the first elution, the eluted 15 µl DNA was applied again on the column and the elution step was repeated for further 2 times.

3.4.6.7 Ligation of vector and insert

Ligation reaction was used to insert a gene sequence in a vector. PCR fragments were first ligated into pJET1.2 cloning vector (Fermentas) and from there into the desired expression vector. A ratio of 3:1 or 5:1 of insert-DNA to vector DNA was used for a successful ligation reaction.

Required components for the ligation (20 µl) in pJET1.2 were following:

- 1 µl pJET1.2
- 3 µl / 5 µl digested PCR product

- 2 µl 10 x ligase buffer
- 1 U T4-ligase
- x µl sterile H_2O (add 20 µl)

The mixture was incubated at 22 °C for 1 h and then transformed in DH5α cells.

The insert DNA was digested from pJET1.2 and ligated in the appropriate expression vector. For this following reagents were used for 20 µl:

- 2 µg digested vector DNA
- 6 µg / 10 µg digested insert DNA
- 2 µl 10 x ligase buffer
- 1 U T4-ligase
- x µl sterile H_2O (add 20 µl)

The mixture was incubated at 22 °C for 1 h and then transformed in DH5α cells.

3.4.6.8 Transformation of plasmid DNA

Competent *E. coli* cells were transformed with the complete ligation mixture (20 µl) or with 1 µl plasmid DNA. Therefor ligation mixtures or plasmid DNA were added to 100 µl competent *E. coli* and incubated on ice for 30 min. Then the cells were heat-shocked at 42 °C for 2 min which allows the cell to absorb the DNA. After this, cells were incubated on ice 1 min. 700 µl LB was mixed with the cells and they were shaken at 37 °C, 200 rpm for 1 h. Finally, 100 µl of the culture was spread on LB plate (if needed with antibiotic) and incubated at 37 °C, *o.n.*.

3.4.6.9 Isolation of plasmid DNA

A culture of 5 ml LB with antibiotic was inoculated with a single colony and cultivated *o.n.* at 37 °C, 200 rpm. The next day the plasmid-DNA was isolated with the usage of NucleoSpin Plasmid Kit (Machery-Nagel) according to the manufacturer`s instructions. Plasmid-DNA was eluted with pre-warmed (70 °C) 45 µl sterile H_2O (separated in 3 x 15 µl steps).

3.4.6.10 Determination of DNA concentration

If needed the DNA concentration was detected by measuring the absorbance of DNA at 260 nm in Biospec-nanodrop (Shimadzu).

3.4.6.11 Sequencing of plasmid DNA

To proof e.g. the inserted gene sequence the DNA sequence was sequenced at GATC Biotech (Konstanz) according to their specifications.

3.4.6.12 Plasmids

All the used plasmids are listed in the appendix in table 3.

Table 3: Plasmids used in this study.

plasmid name	inserted gene	vector	RE sites	resistance	usage	reference
pJD34	*tusA*	pET11b	NdeI/BamHI	Amp	Expression of TusA	Dahl *et al*., 2013
pET15b-*ftsZ*	*ftsZ*	pET15b	NdeI/BamHI	Amp	Expression of FtsZ	this work
pET15b-*dksA*	*dksA*	pET15b	XhoI/BamHI	Amp	Expression of DksA	this work
pACYC-*suf*	suf operon	pACYCDuet-1	NcoI/EcoRI	Cm	Expression of suf operon	Hänzelmann *et al*., 2004
pJD73	*rpoS*	pACYDuet-1	BamHI/SacI	Cm	Expression of RpoS	PhD work Dahl
mCherry-pCDF	mCherry	pCDFDuet-1	BamHI/NotI	Sm	Expression of mCherry	PhD work Bühning
mCherry-*ftsZ*-pCDF	*ftsZ*	pCDFDuet-1	XbaI/NotI	Sm	Expression of mCherry-FtsZ	this work
mCherry-*cyaY*-pCDF	*cyaY*	pCDFDuet-1	XbaI/NotI	Sm	Expression of mCherry-CyaY	this work
mCherry-*iscU*-pCDF	*iscU*	pCDFDuet-1	XbaI/NotI	Sm	Expression of mCherry-IscU	PhD work Bühning
EGFP-pACYC	EGFP	pACYCDuet-1	BamHI/NotI	Cm	Expression of EGFP	PhD work Bühning
EGFP-*tusA*-pACYC	*tusA*	pACYCDuet-1	XbaI/NotI	Cm	Expression of EGFP-TusA	PhD work Bühning
EYFP-pET28a	EYFP	pET28a	BamHI/NotI	Kana	Expression of EYFP	PhD work Bühning
EYFP-*iscS*-pET28a	*iscS*	pET28a	BamHI/NotI	Kana	Expression of EYFP-IscS	PhD work Bühning
fis-EGFP-pACYC	*fis*	pACYCDuet-1	NdeI/XhoI	Cm	Expression of Fis-EGFP	this work
mfis-EGFP-pACYC	*mfis*	pACYCDuet-1	NdeI/XhoI	Cm	Expression of mFis-EGFP	this work
fur-EGFP-pACYC	*fur*	pACYCDuet-1	NdeI/XhoI	Cm	Expression of Fur-EGFP	this work
rpoS-EGFP-pACYC	*rpoS*	pACYCDuet-1	NdeI/XhoI	Cm	Expression of RpoS-EGFP	this work

3.5 Biochemical methods

3.5.1 Overexpression of proteins

For overexpression of proteins, *E. coli* DE3 strains were transformed with the plasmid containing the respective gene of interest. Pre-cultures of the *E. coli* strains were inoculated in M9 minimal medium with the appropriate antibiotic(s), and they were grown *o.n.* at 37 °C, 200 rpm. The following day the cells were inoculated in 50 ml of LB with 0% NaCl to an OD_{600} of 0.05 and they were cultivated at 37 °C, 180 rpm for 5 h without antibiotics. Expression of fusion proteins was induced with 100 µM isopropyl-β-D-thiogalactopyranoside (IPTG) at time point 0 h for flow cytometry and with 15 µM IPTG for FRET for the last 2.5 h. After 5 h of growth cell cultures were transferred in 50 ml falcons (flow cytometry) or 2 ml samples of the cell culture were taken and stored at -20 °C (for FRET).

3.5.2 Cell lysis by sonification

After cultivation, the cells were lysed by sonification. Cell pellets were resuspended in 3.5 ml lysis buffer and lysed at 100% amplitude with 2 sec pulse / 2 sec pause for 2 min. During the sonification, cells were held on ice to avoid heat generation. Cell debris was separated from soluble proteins by centrifugation.

3.5.3 Determination of total protein concentration by Bradford

The total protein concentration in crude extracts was determined via Bradford. BSA Standard (2.5 µg – 20 µg) was measured to detect the total protein concentration in each sample. The lysates were diluted with 0.9% NaCl to an appropriate concentration within the BSA Standard range. 150 µl were mixed with 150 µl Coomassie Plus protein assay reagent (Fermentas) and incubated at RT for 10 min. Coomassie binds to basic amino acids (arginine, lysine and histidine) of proteins in an acidic environment. It forms a colored complex with an absorption maximum at 595 nm. Each sample was measured in triplicate.

3.6 Analytical methods

3.6.1 Growth analysis

Growth curves were recorded to determine the growth defect of the *tusA* deletion (Δ*tusA*) strain in comparison to BW25113 (WT). Further additionally tested strains have all the BW25113 background. Pre-cultures of the strains were inoculated in M9 minimal medium

(Miller 1972, modified by Müller 1997) with the appropriate antibiotics and they were grown over night (*o.n.*) at 37 °C, 200 rpm. Next day, the cells were inoculated in 50 ml of LB with 0% NaCl to an optical density of 0.05 at 600 nm (OD_{600}). For cell growth, the cells were cultivated at 37 °C, 180 rpm for 10 h in the absence of IPTG. Within the first six hours, OD_{600} was measured every 30 minutes. After six hours of growth, the measurements were done every hour. Cell samples (2 ml) of each strain were taken in the exponential (3 h and 5 h) and stationary (7 h and 10 h) phases for morphological analysis via microscopy. The main cultures were usually cultivated without antibiotics only if they were transformed before with a vector.

3.6.2 Morphology analysis (according to Hiraga *et al.*, 1989)

After taking cell samples (2 ml) during the respective growth curve, the cells were harvested by centrifugation at 11000 x g for 1 min. The pellet was resuspended in 1 x PBS (phosphate buffered saline pH 7.4) and centrifuged at 14000 x g, 1 min for washing the cells from LB medium. The washing step was repeated twice. The pellet was resuspended in 1 ml 1 x PBS and 5 µl of the cells were transferred on a glass slide cleaned with ethanol (EtOH). Cell drop was dried at RT or at 30 °C. For fixation of the cells on the glass slide, 1 drop of methanol (MeOH) was applied to the cells and incubated for 5 min, RT. The remaining MeOH was washed away by immersing the slide in tap water 6 times. After drying the slides for 5 min at RT, 20 µl of Poly-L-Lysine (5 µg/ml in 1x PBS) was pipetted on the cells to enhance the adhesion of cells to the glass slide and slides were dried by incubation at 30 °C. The DNA in the cells was labeled with 20 µl DAPI 1:1000 (5 µg/ml in 1x PBS) and incubated for 10 min at 8 °C in the dark (staining is better at colder temperatures). It has blue fluorescence with the excitation at 358 nm and the emission at 461 nm. Afterwards the DAPI solution was washed with 200 µl – 400 µl 1 x PBS and the cells were embedded with 20 µl Mowiol. Finally, the cells were covered with a cleaned coverslip (with EtOH) and stored at 4 °C until observation via fluorescence microscopy (Axiovert 200M, Zeiss). A PlanApo oil objective with 100 x magnification and 1.4 NA (numeric aperture) was used for microscopy. The imaging of the cells was done via AxioCam MRm Rev. 3 camera and Axiovision 4.7 Rel software. Later the scale bar was inserted in ImageJ 1.8 (National Institutes of Health).

3.6.3 Sodium dodecyl sulfate-polyacrylamide gel electrophoresis (SDS-PAGE)

SDS-PAGE enables to separate proteins according to their molecular weight (Laemmli, 1970). SDS binds to hydrophobic areas of proteins and leads to denaturation. Therefore the separation of the proteins depends only on their molecular weight in an electrical field and not anymore of their net charge. That means the higher the protein size the slower it moves through the SDS- acrylamide gel and vice versa. After determination of the total protein concentration 50 µg were loaded on 12% or 15% SDS-Gel. For this 75 µl protein was mixed with 25 µl 4 x SDS-PAGE loading dye (50% (v/v) glycerol, 3.5% (w/v) SDS, 15% (v/v) β-mercaptoethanol, 0.02% (w/v) bromphenol blue) to total volume of 100 µl. Proteins in this mixture were denaturated at 95 °C, 3 min and 50 µg were directly loaded on SDS- gel. Separation of the proteins was performed at 150 V, 70 min in SDS running buffer (25 mM Tris/HCl, 200 mM glycin, 0.1% (w/v) SDS). 10 µl of Prestained Protein Molecular Weight Marker 20 - 120 kDa (Fermentas) was used to determine of the protein size.

The acrylamide percentage of the gel affects also the speed of the protein movement. The higher acrylamide percentage the better is the separation at small protein size (lower gel area) and vice versa. For the analysis in this work were used 12% or 15% SDS-gels. SDS-Gel contains the following components (table 4).

Table 4: Composition of separating and stacking gels to analyze the soluble proteins in crude extract via SDS-PAGE.

	12%	**15%**	**5%**
	separating gel		**stacking gel**
H_2O	1.75 ml	1.25 ml	1.16 ml
30% (w/v) acrylamide / 0.8% (w/v) bisacrylamide	2 ml	2.50 ml	0.34 ml
4 x lower Tris (1,5 M Tris/HCl, pH 8.8)	1.25 ml	1.25 ml	---
4 x upper Tris (0,5 M Tris/HCl, pH 6.8)	---	---	0.50 ml
10% (w/v) APS	25 µl	25 µl	10 µl
TEMED	2.5 µl	2.5 µl	2.0 µl

3.6.4 Immunoblot

Immunoblot analysis was performed in order to detect and compare the cellular FtsZ, Fis and SufS protein contents in *E. coli* WT and deletion strains. Pre-cultures of the *E. coli* strains were inoculated in M9 minimal medium with the appropriate antibiotics and they were grown *o.n.* at 37 °C, 200 rpm. The next day, the cells were inoculated in 50 ml of LB with 0% NaCl to an OD_{600} of 0.05. For cell growth, the cells were cultivated at 37 °C, 180 rpm for 5 h (for FtsZ and SufS) or 10 h (for Fis). The cultivation was done without IPTG otherwise it is mentioned for the respective experiment. After 5 h or 10 h, the cells were harvested in 50 ml falcons at 8000 x g, 5 min, 4 °C. Cell pellets were washed 3 times with 25 ml 50 mM Tris/HCl (pH 7.5) and lysed in 3.5 ml 50 mM Tris/HCl, 150 mM NaCl, 0.5% (w/v) NP-40 (pH 8.0) through sonification. Subsequently, the cell debris was separated from the soluble protein fraction (supernatant) by centrifugation at 18000 x g, 15 min, 4 °C. Protein concentration of the supernatant was determined via Bradford. 50 µg protein of every supernatant sample (mixed with 4 x SDS loading dye) was loaded on SDS-Gel (12% or 15%) and separated through SDS-PAGE. Protein bands were then transferred on a PVDF membrane (for FtsZ, Fis) or nitrocellulose membrane (for SufS). Before the usage of PVDF membrane it had to be activated with methanol. For this PVDF membrane was incubated 1 min in 100% methanol, washed in H_20 and incubated for 10 min in cold transfer buffer (25 mM Tris/HCl, 200 mM glycin, 20% methanol). The nitrocellulose membrane was exclusively incubated in cold transfer buffer. The SDS-gels were also incubated for 10 min in cold transfer buffer to wash completely the remaining SDS. After this, SDS-gel and membrane were inserted between wet sponges and filter papers (incubated in cold transfer buffer) and installed in the transfer device (Biorad) according to the manufacturer's instructions. During the blot (90 V, 90 min, 4 °C) the proteins were transferred from SDS-gel to the membrane via electrical voltage (Mini Trans-Blot cell, Biorad). The membrane with the proteins was washed briefly once in 1 x TBST (50 mM Tris/HCl, 150 mM NaCl, 0.1% (w/v) Tween-20, pH 7.4) and blocked with 5% BSA ON, 4 °C. The following day the rest of the BSA was washed with 1 x TBST at RT, 5 min and primary antibody (Ab) was applied on the membrane for 1 h, RT. The incubation with α-FtsZ (rabbit, a gift of Mercedes Casanova (CNB-CSIC, Madrid)) Ab was performed 1:20000 diluted in 1 x TBST at RT, 1 h. The α-Fis (rabbit, a gift of Prof. Reid C. Johnson (University of California)) Ab was performed 1:10000 diluted at 4 °C, *o.n.*. Primary α-SufS (chicken, provided by Prof. Outten (University of South Carolina) Ab was used 1:2000 diluted 1 x TBST

at 4 °C, *o.n.*. As loading control α-GroEL (rabbit, abcam) Ab was applied 1:10000 diluted 1 x TBST at 4 °C, *o.n.*. After incubation with the primary Ab the membrane was washed 3 x with 1 x TBST for 10 min each to remove the unbound antibodies. The labeling of α-FtsZ and α-GroEL antibodies was done by α-rabbit horseradish peroxidase (POD)-conjugated secondary antibody (goat, Sigma) 1:10000 diluted for at RT, 1 h. For labeling of α-SufS Ab α-chicken POD-conjugated secondary antibody (goat, abcam) was used diluted 1:5000 at RT, 1 h. Finally, the unbound antibodies were again removed by washing the membrane 3 x with 1 x TBST for 10 min each. The protein bands were detectable via chemiluminescence. For visualization, the membrane was covered by a 2 ml mix of solution A (100 µl 250 mM luminol, 44 µl 90 mM p-cumaric acid, 8.85 ml H_2O, 1 ml 1 M Tris/HCl, pH 8.5) and solution B (6 µl 30% H_2O_2, 9 ml H_2O, 1 ml 1 M Tris/HCl, pH 8.5). The detection of the bands was carried out through the illumination in FUSION FX7 (Vilber) which suggested the optimal exposure time to see the bands. For determination of the size the Prestained Protein Molecular Weight Marker 20 - 120 kDa (Fermentas) was used. Fis is visible at 11 kDa, FtsZ at 40 kDa, SufS at 44 kDa and GroEL at 57 kDa.

3.6.5 *In vivo* interaction studies via fluorescence resonance energy transfer (FRET)

3.6.5.1 Overexpression of fluorescent fusion proteins

To detect a possible interaction of TusA and FtsZ, the expression of fusion proteins was analyzed via fluorescence resonance energy transfer (FRET). Three plasmids were cloned with different fluorophores (mCherry (red), EYFP (yellow), EGFP (green)) and used as controls. The EYFP (enhanced yellow fluorescent protein) was cloned in pET28a vector fused with the *iscS* gene and EGFP (enhanced green fluorescence protein) was cloned in pACYCDuet-1 vector with the *tusA* gene. mCherry was fused to the *iscU* gene. For this study a further mCherry fusion construct was produced, the mCherry fused to the *ftsZ* gene in pCDFDuet-1 vector. After cloning BW25113 (DE3) and Δ*tusA* (DE3) strains were transformed with one of these three constructs or the respective controls with the empty vectors (mCherry-pCDFDuet-1, EYFP-pET28a or EGFP-pACYCDuet-1) to analyze the expression of fusion proteins. To detect the FRET signal BW25113 (DE3) and Δ*tusA* (DE3) strains were transformed with mCherry+EGFP or mCherry+EYFP constructs (either with fusion protein or the empty control vectors). Subsequently, pre-cultures were grown in M9 minimal medium

(with antibiotics) and cultivated overnight at 37 °C, 200 rpm. On the following day, the main cultures were inoculated in LB-0% NaCl with the overnight cultures to an OD_{600} = 0.05 for expression of the fusion proteins (with and without antibiotics). The cells were cultivated for 2.5 h at 37 °C until they reached the exponential phase. After 2.5 h, the expression of the fusion protein, or in controls, the expression of the fluorophore was induced with 5 µM IPTG (low IPTG concentration to avoid any stress caused by IPTG on cells). Use of different IPTG concentration, if any, is mentioned in respective experiment. Then the cells were cultivated for a further 2.5 h at 25 °C. 2 ml cells of each sample were taken after 5 h of expression. The cell samples were centrifuged and pellets were resuspended in 1 ml 1 x PBS. For live cell imaging, 1% agarose slides were produced. Therefore agarose was cooked and 700 µl 1% agarose was pipetted on glass slides (disinfected before with EtOH) from right to left. A second glass slide was put on the first glass slide with the agarose on it. This process should be done preferably without forming air bubbles. Then they were stored in an empty box with wet tissue (so they cannot dry out) at 4 °C until usage. It is important not to use them immediately after they are newly produced. To make the agarose slides ready to use, the glass slide on the top was taken carefully and the agarose film was held with the thumb at one end without breaking the agarose film. The agarose film was cut into squares with the border of the second glass slide and 5 µl of the cells was pipetted in the center of the agarose square. The area containing cells was marked at the bottom to facilitate microscopic analysis. The cell suspension was dried for a few minutes and then the cover slip was placed on. The live cell imaging was carried out via a fluorescence microscope (Axiovert 200M, Zeiss) and they were stored during this time in the dark. The detection of fusion protein expression was performed with PlanApo 100 x/ NA 1.4 oil objective, AxioCam MRm Rev. 3 camera and Axiovision 4.7 Rel software. Later the scale bar was inserted in ImageJ 1.8 (National Institutes of Health). The method for preparing the fluorescent microscopy samples and microscopy analysis for live cell imaging was learned at the University of Bonn in collaboration with Dr. Fabian Grein.

3.6.5.2 Measuring of FRET signal

The same protocol of overexpression of fluorescent fusion proteins was applied until the cell cultivation to 5 h. Since the fluorescence intensities were stronger in BW25113 (DE3) samples than in Δ*tusA* (DE3) samples the induction for BW25113 (DE3) was performed with 5 µM IPTG and for Δ*tusA* (DE3) samples was kept the 15 µM IPTG concentration. Another

change was that the cells were not resuspended in 1 ml 1 x PBS and applied 5 µl of them on agarose pads. The cell number was enriched to have more cells in one area expressing both fusion proteins. Therefore 1 ml cells of each culture were taken and resuspended after washing in 75 µl 1 x PBS and applied 50 µl of these on agarose pads. The images were recorded via Apochromat 60 x/ NA 1.40 oil objective of an inverted fluorescence microscope (Eclipse Ti-E, Nikon) to have a bigger area with more cells expressing both fusion proteins. The observation area was displayed via iXon 897-X3 EM camera (Andor) and NIS-Elements AR 4.40 software (Nikon). The acceptor bleaching method was used to measure FRET signals. Therefor images of EGFP or EYFP (donor) were taken before (30x) and after (25x) bleaching of mCherry (acceptor) and simultaneously the fluorescence signals were also measured in these images for FRET. The main idea of FRET is that two proteins are interacting and because of this the fluorescence energy of the excited fluorophore (donor) is transferred to the second fluorophore (acceptor), which then shows higher fluorescence. In the acceptor bleaching method, the bleaching of mCherry, will result in higher EGFP fluorescence if there is an interaction between FtsZ and TusA. Excitation and emission wavelength for the used three fluorescent proteins are the following:

Table 5: Excitation and emission wavelengths of the fluorescent proteins used.

Fluorescent protein	Excitation λ (nm) (centered on (nm))	Emission λ (nm) (centered on (nm))
EGFP	473-491 (482)	500-550 (525)
EYFP	498-510 (504)	529-556 (542)
mCherry	556-614 (585)	618-675 (647)

The FRET measurement was carried out in collaboration with Dr. Gabriele Malengo at the Max Planck Institute (MPI) in Marburg. The FRET data analysis was done by Dr. Gabriele Malengo via ImageJ and Kaleidagraph.

3.6.6 Analysis of fusion protein translation via flow cytometry *in vivo*

To analyze the difference between WT and Δ*tusA* on the translation level, the expression of fusion proteins was measured by flow cytometry. For this *E. coli* WT (DE3) and protein deletion strains (DE3) were transformed with *fis*-EGFP-pACYCDuet-1 (for Fis-EGFP overexpression) / *fur*-EGFP-pACYCDuet-1 (for Fur-EGFP overexpression) / *rpoS*-EGFP-

pACYCDuet-1 (for RpoS-EGFP overexpression) / m*fis*-EGFP-pACYCDuet-1 (for mutated Fis-EGFP overexpression) and mCherry-pCDFDuet-1. Expression of mCherry serves as an internal control for translation. If the cell were not transformed with fusion protein construct they were transformed with corresponding empty EGFP-pACYCDuet-1 and mCherry-pCDFDuet-1 vector (as an additional control). For the mutated Fis all lysines, glutamates and glutamines were changed to alanine to eliminate the positive effects of tRNA thiolation (more efficient ribosome binding; prevention of frameshift). Pre-cultures of the *E. coli* strains were inoculated in M9 minimal medium with the appropriate antibiotic(s) and they were grown *o.n.* at 37 °C, 200 rpm. On the next day, the cells were inoculated in 50 ml of LB with 0% NaCl to an OD_{600} of 0.05 and the cells were cultivated at 37 °C, 180 rpm for 5 h without antibiotics. Expression of fusion proteins was induced with 100 µM IPTG at time point 0 h. After 5 h of growth cell cultures were transferred in 50 ml falcons and the OD_{600} was determined. By use of the OD_{600}, the cell count for each sample was set to 10^8 cells/ml for flow cytometry. Therefore, the volume of cells for 10^8 cells/ml was mixed in Eppendorf tube with 1 x PBS to a total volume of 500 µl and centrifuged at 11000, 2 min. This washing with 1 x PBS was repeated one more time. Finally, the cell pellets were resuspended in 1 x PBS with the calculated volume for 10^8 cells/ml and kept on ice until the measurement. The whole sample (500 µl) was transferred to a special plastic tube for flow cytometry. Each sample was detected for EGFP and mCherry fluorescence signal with FACS Melody (Bioscience). In total 10000 cells were measured for each sample with a flow rate of 1. The expressed EGFP in the cells was excited at 488 nm and the mCherry at 587 nm. The fluorescence signal of EGFP is detected at 507 nm in the GFP channel and of mCherry at 610 nm in the mCherry channel. The method of flow cytometry measurement was learned in the group of Dr. Katrin Messerschmidt at University of Potsdam and then carried out in collaboration and using with their equipment.

4 Results

4.1 Growth of BW25113 and Δ*tusA*

TusA is the sulfur transferase that transports the sulfur from IscS to the TusBCD complex during mnm^{5}s^{2}U34 tRNA thiolation of Lys, Gln, and Glu (Ikeuchi *et al.*, 2006). Previously, it was determined that a *tusA*-deficient strain shows an abnormal phenotype. The respective cells have a retarded growth and displayed filamentous cell shape in a low salt (0% NaCl) LB medium (Yamashino *et al.*, 1998, Ishii *et al.*, 2000). To analyze the growth defect of the Δ*tusA* deletion strain growth curves of BW25113 (WT) and Δ*tusA* strains were recorded (Figure 14). Additionally, the growth defect of Δ*tusA* strain was tried to overcome by increasing the salt concentration in LB medium (Figure 14, 3% NaCl) as it was reported in Ishii *et al.*, 2000.

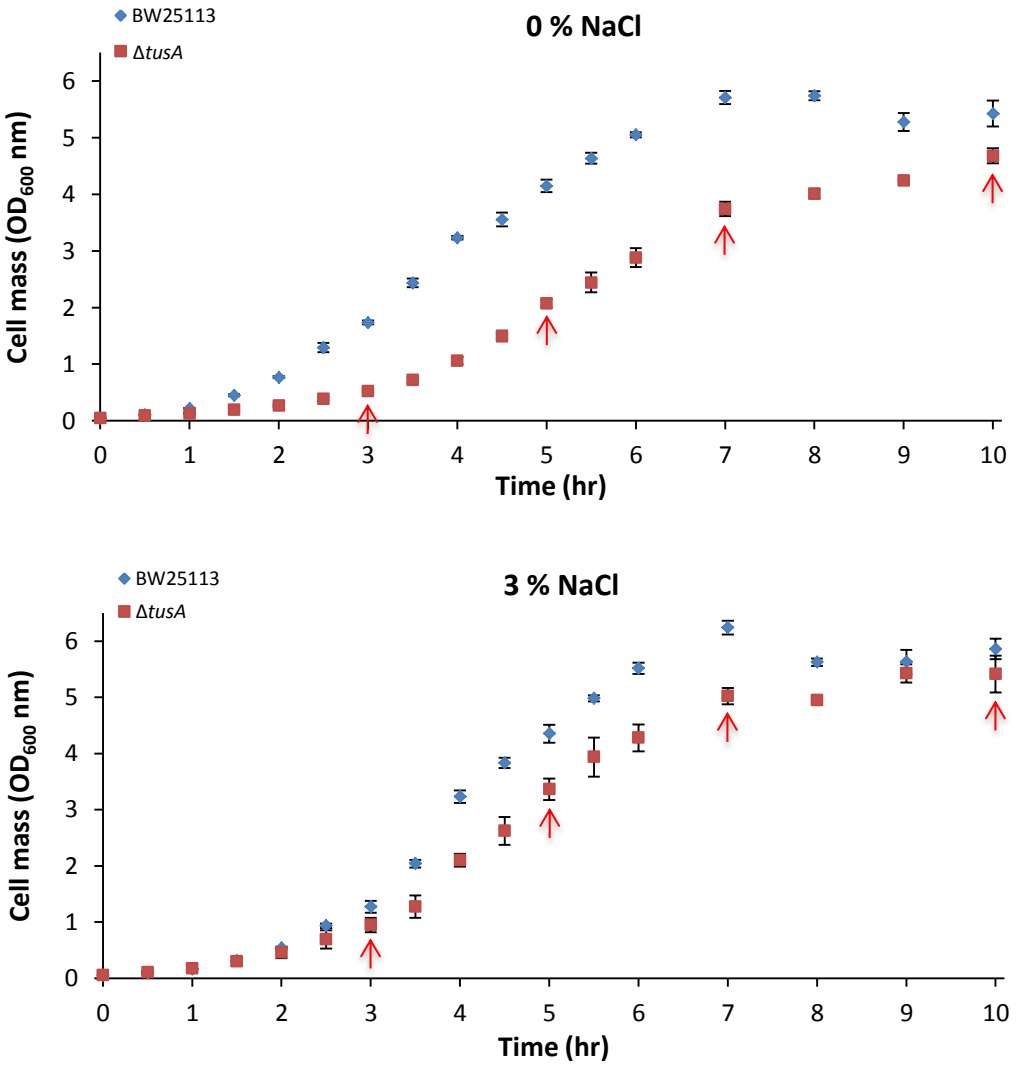

Figure 14: Growth curves of BW25113 (WT) and his *tusA* deleted strain (Δ*tusA*) at low (0%) and high salt (3%) conditions.

Cells of all strains were grown in 50 ml cultures of LB-0% NaCl (low salt condition- upper chart) and LB-3% NaCl (high salt condition –lower chart) at 37 °C, 180 rpm for 10 h. The increasing cell density was recorded in the first six hours every 30 min and later every hour by measuring the optical density at 600 nm (OD_{600}). The start OD_{600} was 0.05. Red arrows indicate the time at which 2 ml cells were collected for microscopy studies.

Figure 14 shows the growth difference of WT (BW25113) and the Δ*tusA* strains. The Δ*tusA* strain grew slower than the WT strain which indicated a growth defect for the Δ*tusA* strain (upper chart). This growth defect was detectable in the LB medium without sodium chloride in the exponential phase, in which the cell density for the Δ*tusA* strain was two times reduced as compared to the WT strain. Increasing the percentage of sodium chloride in the LB medium (lower chart) compensated for this growth defect, so that Δ*tusA* cells grew faster almost like WT cells.

The morphological difference between the Δ*tusA* and WT strains was investigated by phase contrast microscopy (Figure 15). Cell samples were collected during the growth in the exponential (3 h and 5 h) and stationary phase (7 h and 10 h). Cells were fixed and stained for immunofluorescence analysis (Figure 15).

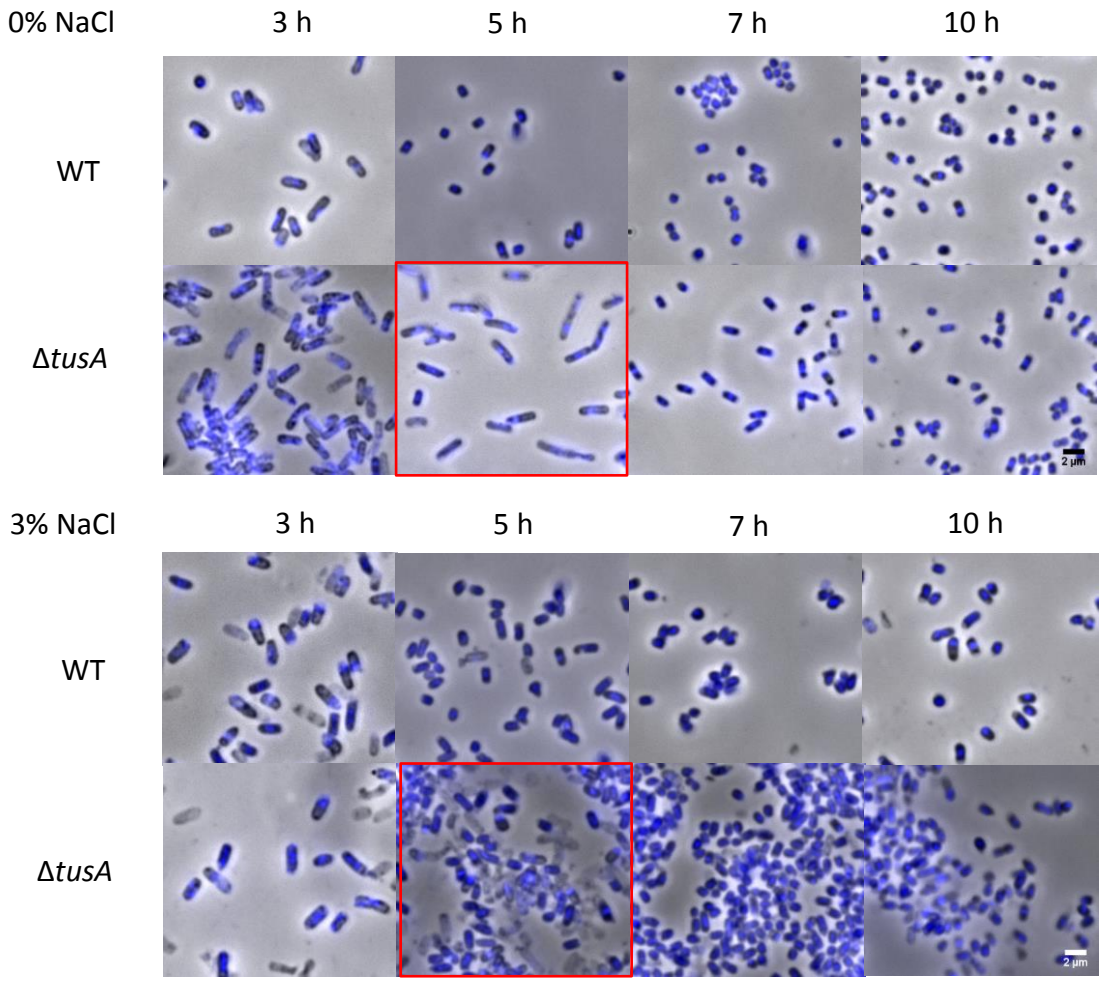

Figure 15: Cell morphology analysis of BW25113 (WT) and Δ*tusA* cells.

WT (upper panel) and Δ*tusA* (lower panel) cells were grown in LB-0% NaCl and LB-3% NaCl. 2 ml cells were analyzed at 3 h, 5 h, 7 h and 10 h after inoculation. DNA is stained with DAPI 1:1000 and has a blue fluorescence. The morphology of the cells was observed by fluorescence microscopy. Red squares highlight the different morphology between low (0%) and high (3%) salt conditions of Δ*tusA*. Scale bars: 2 µm.

WT cells showed during their whole growth rod-shaped cells. In contrast, Δ*tusA* cells formed filamentous-shaped cells in the exponential phase (Figure 15, upper LB-0% NaCl 3 h and 5 h). These Δ*tusA* filaments disappeared upon entering the stationary phase and showed the same rod shape as WT cells (LB-0% NaCl 7 h and 10 h). The increased amount of sodium chloride to 3% led to normal cell growth of Δ*tusA* (Figure 15, lower LB-3% NaCl 3 h). They showed growth like WT. These results indicated that the deletion of the *tusA* gene led to a growth defect which was represented by slow growth (growth defect) and filamentous cell shape. It has been proposed before, that the filamentous cell shape probably indicated a defect in cell division. For further assays, the conditions of 0% salt were selected, to determine the basis of the growth defect in the Δ*tusA* mutant.

4.2 Test of cultivation with and without IPTG

To check whether IPTG affected the cell growth and morphology of WT and Δ*tusA* strains complementation assays were performed with WT (DE3) and Δ*tusA* (DE3) cells transformed with the empty pET11b plasmid or with pET11b-*tusA*. The growth and cell morphology were tested in the presence and absence of IPTG and ampicillin.

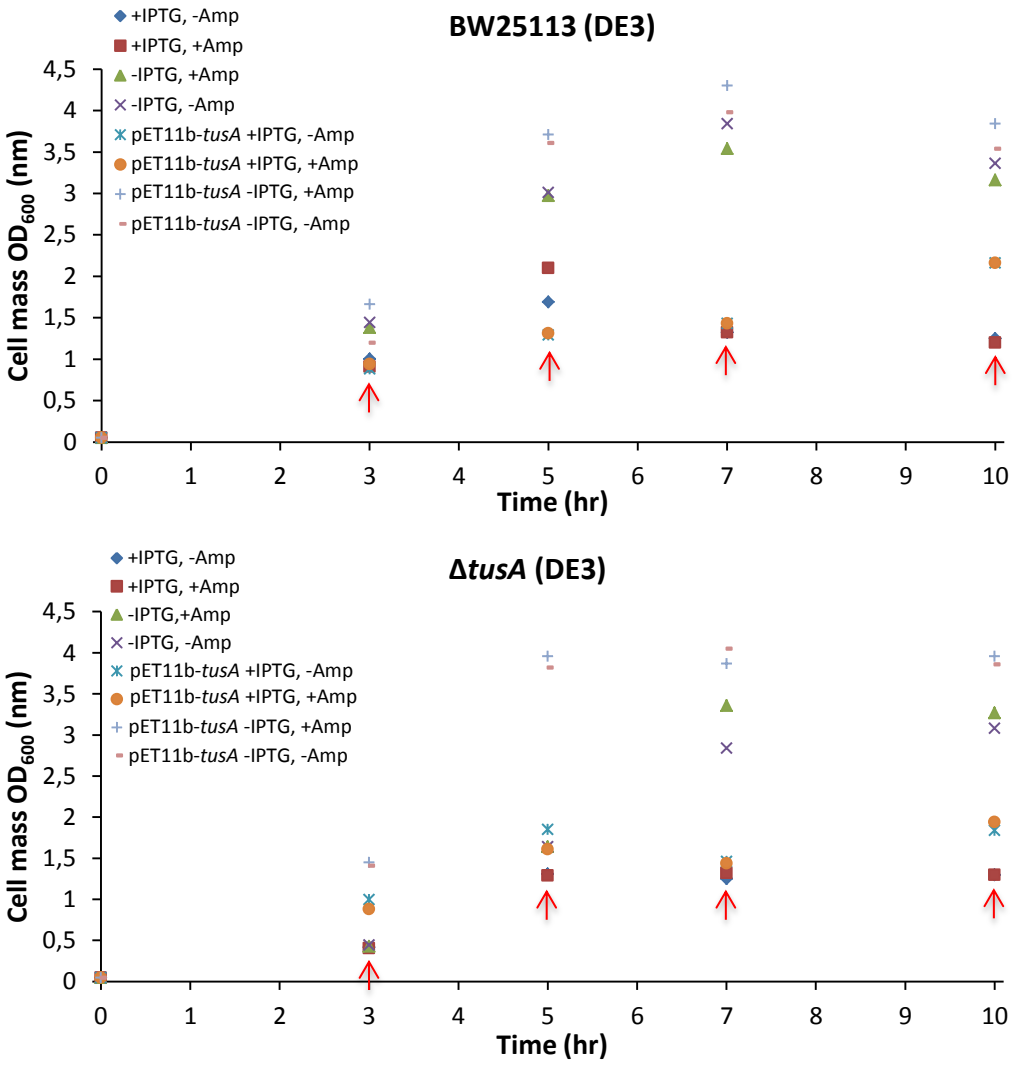

Figure 16: Effect of IPTG on the growth of BW25113 (DE3) and Δ*tusA* (DE3) with and without overexpression of TusA.

BW25113 (DE3) (upper chart) and Δ*tusA* (DE3) (lower chart) cells were transformed with pET11b-*tusA* for TusA overexpression or with the corresponding empty pET11b vector. Cells of both strains were grown in 50 ml cultures of LB-0% NaCl at 37 °C, 180 rpm for 10 h. They were cultivated in the presence and absence of 100 µM IPTG and 150 µg/ml ampicillin. Cell density was recorded by measuring OD_{600}. The start OD_{600} was 0.05. Red arrows indicate the time at which 2 ml cells were collected for microscopy studies.

Figure 16 shows, the recorded growth curves in the presence and absence of IPTG and ampicillin. Cells were grown in 50 ml cultures of LB-0% NaCl at 37 °C, 180 rpm for 10 h. They were cultivated in the presence and absence of 100 µM IPTG and 150 µg/ ml ampicillin. WT (DE3) cells with TusA expression and without IPTG showed the highest growth (Figure 16, upper chart). There was no significant difference in TusA expressing WT (DE3) cells which were cultivated with and without ampicillin. The growth of WT (DE3) cells without TusA expression was slightly lower than the highest growth but still higher than the IPTG-cultivated cells. The lowest growth was visible at WT (DE3) cells with and without TusA expression but in the presence of IPTG. The Δ*tusA* cells showed the same results as the WT (Figure 16, lower chart). The TusA-expressing cells in the absence of IPTG revealed a higher growth than cells in the presence of IPTG. Thus, IPTG had a negative stress effect on the cell growth of WT (DE3) and Δ*tusA* (DE3). The cell growth was significantly decreased. Ampicillin had no remarkable influence on cell growth.

4.3 Effect of IPTG on cell morphology of Δ*tusA*

During the test cultivation of WT (DE3) and Δ*tusA* (DE3) with and without IPTG, cell samples were collected in exponential and stationary phase for microscopy studies. The collected samples were used to detect the morphological difference of WT (DE3) and Δ*tusA* (DE3) for the mentioned conditions in Figure 16. The results are shown in the next four figures (Figure 17 – 20).

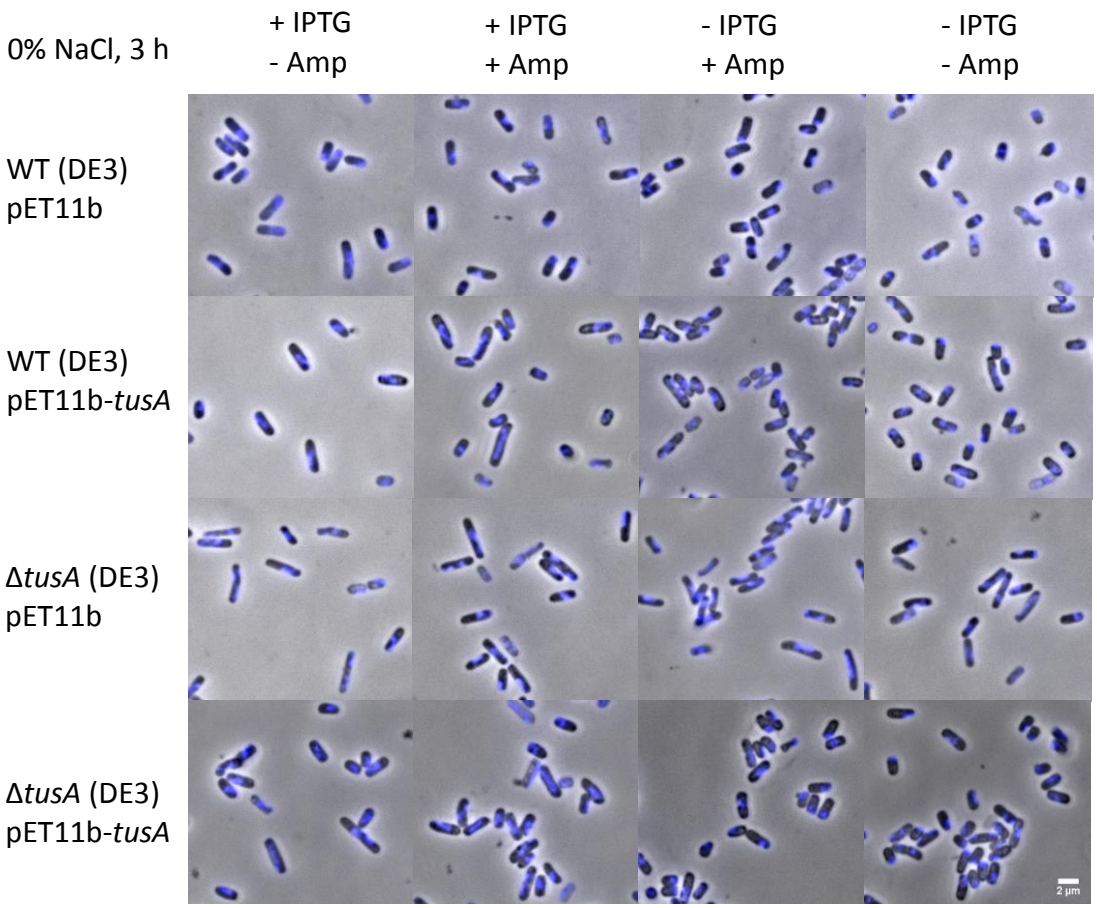

Figure 17: Effect of IPTG on cell morphology of BW25113 (DE3) and Δ*tusA* (DE3) with and without overexpression of TusA at 3 h.

WT (DE3) cells (first panel), with *tusA* overexpression (second panel), Δ*tusA* (DE3) cells (third panel), with *tusA* overexpression (fourth panel) were grown in LB-0% NaCl. Cell samples (2ml) were analyzed at 3 h after inoculation. Cells cultivated with 100 µM IPTG, no ampicillin (first column); with IPTG, with 150 µg/ml ampicillin (second column); no IPTG, with ampicillin (third column); no IPTG, no ampicillin (fourth column). DNA is stained with DAPI 1:1000 and has a blue fluorescence. Scale bars: 2 µm.

After 3 h of growth, no noticeable difference between the cells was visible (Figure 17). Δ*tusA* (DE3) cells showed the typical long, filamentous cell shape (Figure 17, third row) compared to WT (DE3) cells. WT (DE3) cells were short and rod-shaped (Figure 17, first row). A slight difference between Δ*tusA* (DE3) cells and Δ*tusA* (DE3) cells with TusA expression was visible. The TusA expressing Δ*tusA* (DE3) cells were slightly shorter than Δ*tusA* (DE3) cells in the absence of IPTG and in the presence of ampicillin.

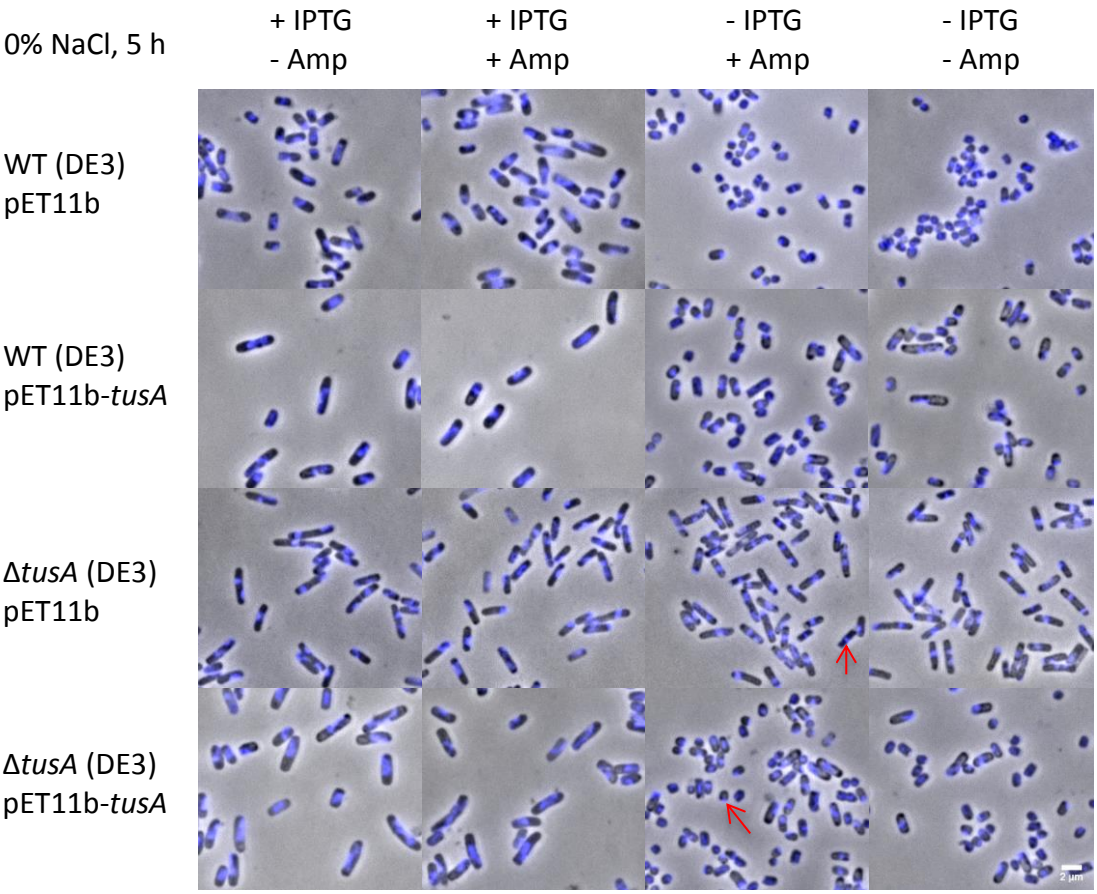

Figure 18: Effect of IPTG on cell morphology of BW25113 (DE3) and Δ*tusA* (DE3) with and without overexpression of TusA at 5 h.

WT (DE3) cells (first panel), with *tusA* overexpression (second panel), Δ*tusA* (DE3) cells (third panel), with *tusA* overexpression (fourth panel) were grown in LB-0% NaCl. Cell samples (2ml) were analyzed at 5 h after inoculation. Cells cultivated with 100 µM IPTG, no ampicillin (first column); with IPTG, with 150 µg/ml ampicillin (second column); no IPTG, with ampicillin (third column); no IPTG, no ampicillin (fourth column). DNA is stained with DAPI 1:1000 and has a blue fluorescence. Red arrows show the difference in cell length of Δ*tusA* (DE3). Scale bars: 2 µm.

The differences were more visible after 5 h of cell growth. WT (DE3) cells in the absence of IPTG and with or without ampicillin showed shorter cells than WT (DE3) cells with IPTG (Figure 18). This morphology indicated that the cells in the absence of IPTG grew better. TusA expressed WT (DE3) cells exhibited a kind of mixed phenotype. The majority of the cells were short, except some were slightly longer. Δ*tusA* (DE3) cells and TusA expressed Δ*tusA* (DE3) cells displayed a remarkable difference. After 5 h of growth, the TusA expressing Δ*tusA* (DE3) cells were short as WT (DE3) cells, whereas, Δ*tusA* (DE3) cells were longer (Figure 18, red arrows). This phenotype was present without IPTG conditions. This indicates the complementation of the *tusA* deletion by expression of TusA protein was successful in the

absence of IPTG. Since the filamentous Δ*tusA* (DE3) cells disappeared and they showed the same rod-shaped cell morphology as WT cells.

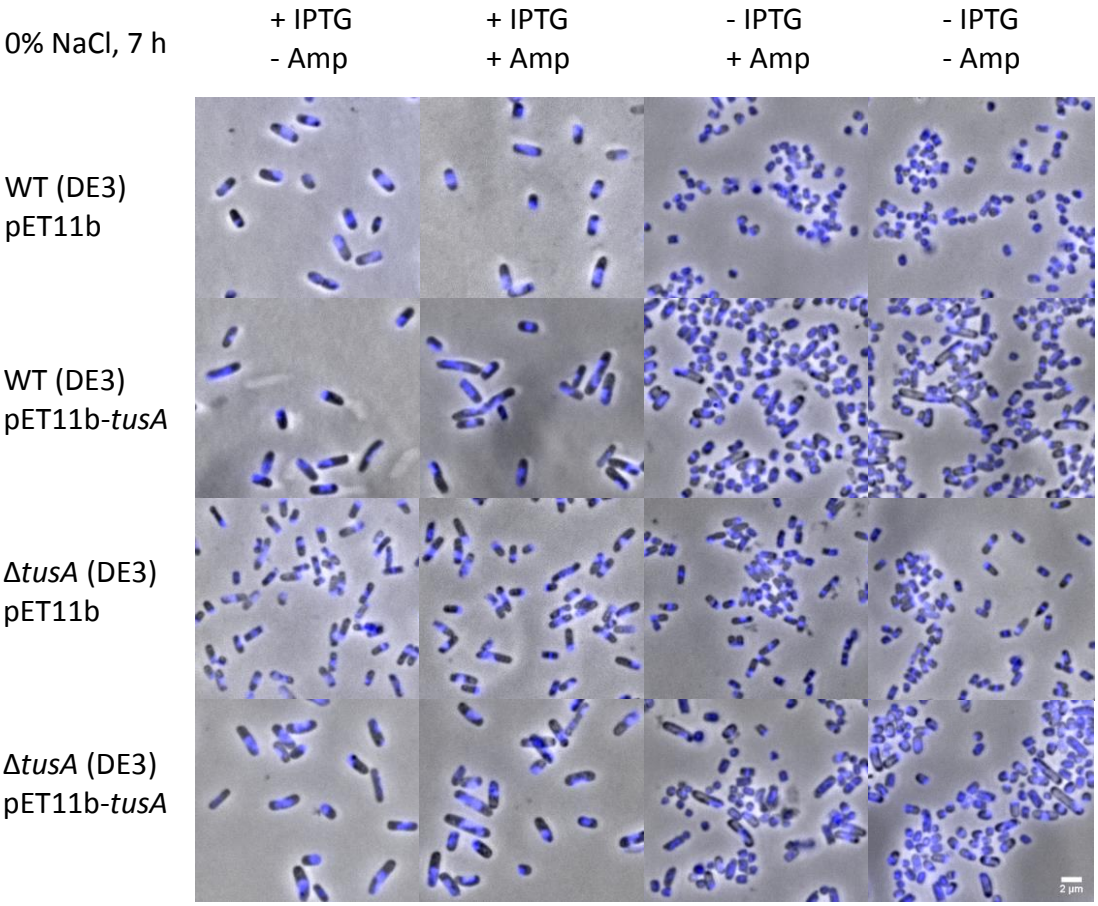

Figure 19: Effect of IPTG on cell morphology of BW25113 (DE3) and Δ*tusA* (DE3) with and without overexpression of TusA at 7 h.

WT (DE3) cells (first panel), with *tusA* overexpression (second panel), Δ*tusA* (DE3) cells (third panel), with *tusA* overexpression (fourth panel) were grown in LB-0% NaCl. Cell samples (2ml) were analyzed at 7 h after inoculation. Cells cultivated with 100 µM IPTG, no ampicillin (first column); with IPTG, with 150 µg/ml ampicillin (second column); no IPTG, with ampicillin (third column); no IPTG, no ampicillin (fourth column). DNA is stained with DAPI 1:1000 and has a blue fluorescence. Scale bars: 2 µm.

After 7 h of growth, the effect of IPTG on cell growth became further clearer (Figure 19). Δ*tusA* (DE3) cells got shorter in the stationary phase in the absence of IPTG (Figure 19, third row). In the presence of IPTG the Δ*tusA* (DE3) cells are longer, which indicates the growth is retarded (Figure 19, third row). A similar retarded effect of IPTG is also visible for the WT (DE3) cells (Figure 19, first row). The WT (DE3) cells are also longer in the presence of IPTG (so they grew slower) and are shorter in the absence of IPTG.

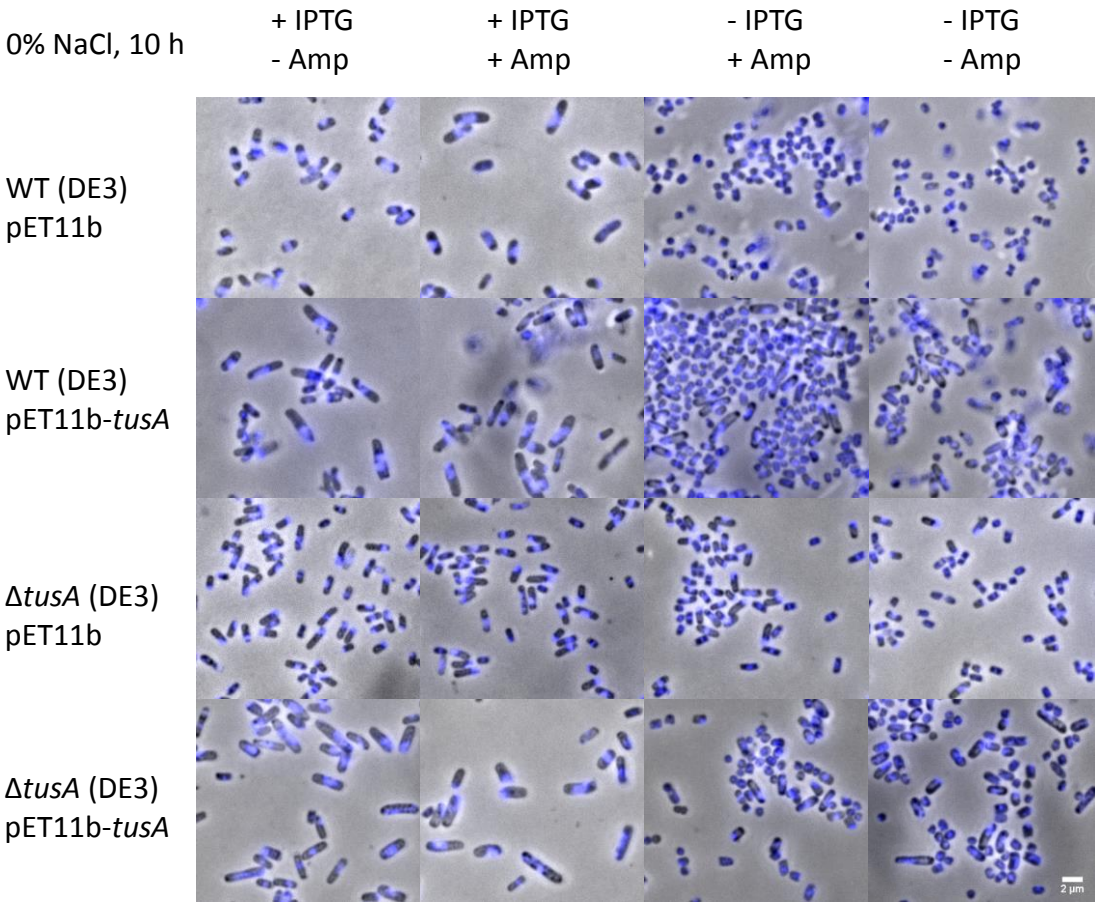

Figure 20: Effect of IPTG on cell morphology of BW25113 (DE3) and Δ*tusA* (DE3) with and without overexpression of TusA at 10 h.

WT (DE3) cells (first panel), with *tusA* overexpression (second panel), Δ*tusA* (DE3) cells (third panel), with *tusA* overexpression (fourth panel) were grown in LB-0% NaCl. Cell samples (2ml) were analyzed at 10 h after inoculation. Cells cultivated with 100 µM IPTG, no ampicillin (first column); with IPTG, with 150 µg/ml ampicillin (second column); no IPTG, with ampicillin (third column); no IPTG, no ampicillin (fourth column). DNA is stained with DAPI 1:1000 and has a blue fluorescence. Scale bars: 2 µm.

The negative impact of IPTG was very good visible in the case of Δ*tusA* (DE3) cells at 10 h (Figure 20). In the absence of IPTG, the Δ*tusA* (DE3) cells were short as WT (DE3) cells, whereas, the Δ*tusA* (DE3) cells got longer in the stationary phase in the presence of IPTG.

So with this approach, it was possible to show that IPTG had a negative impact on cell growth. Therefore IPTG was a stress factor for the cells and they grew slower and show aberrant cell morphology. Consequently, in all further experiments, no IPTG was added during the growth of the cells.

4.4 Fluorescence resonance energy transfer (FRET)

One of the aims of this work was to detect and visualize an interaction between TusA and FtsZ. Since *tusA*-deleted cells have a cell division problem (Ishii *et al.*, 2000) and FtsZ is responsible for the formation of the division ring at midcell (Margolin W., 2005). Therefore the probability for an interaction between these two proteins appeared likely.

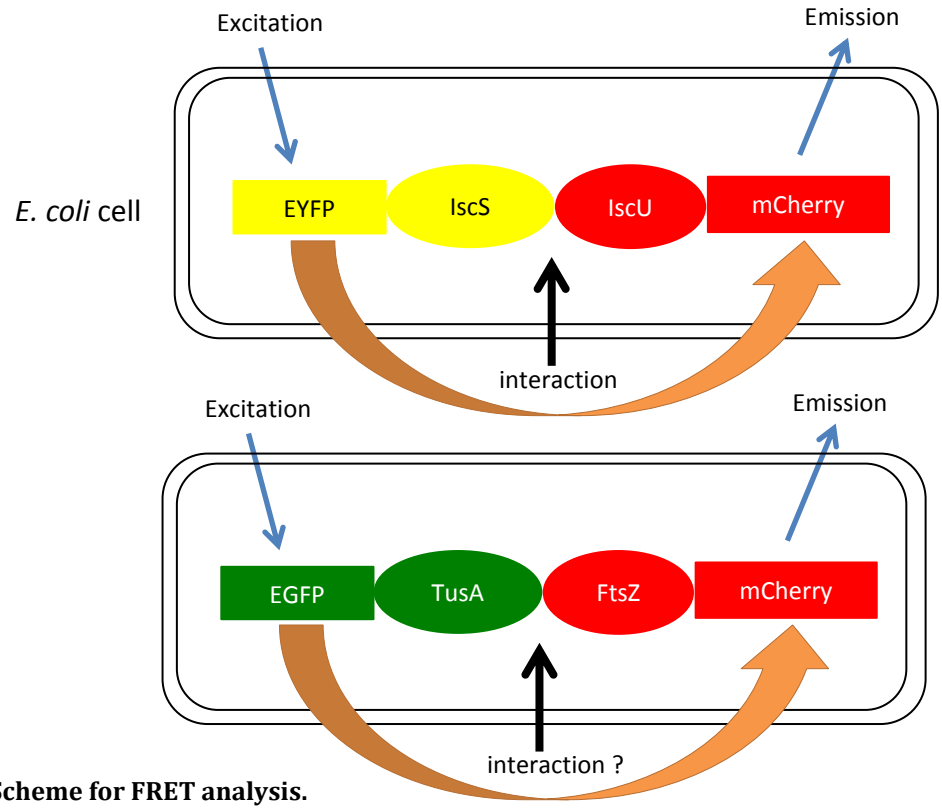

Figure 21: Scheme for FRET analysis.

Shown is a schematic representation of the FRET principle. One *E. coli* cell is transformed with EYFP-*iscS*-pET28a and mCherry-*iscU*-pCDFDuet-1 or with EGFP-*tusA*-pACYCDuet-1 and mCherry-*ftsZ*-pCDFDuet-1 plasmid. Cells were grown in LB-0% NaCl for 5 h at 37 °C and 180 rpm. The expression of the fusion protein was induced 2.5 h after growth initiation with IPTG and the cells were cultivated for a further 2.5 h. If the fusion proteins are interacting within the cell, e.g. EYFP-IscS and mCherry-IscU, the fluorescence energy of the excited dye is transferred to the second dye, which then shows higher fluorescence. Here, after the excitation of EYFP, the fluorescence energy will be transferred (orange arrow) to mCherry in case IscS and IscU are interacting. Thus mCherry will show a higher fluorescence signal. The aim was to investigate whether TusA and FtsZ proteins are interacting within the cell. Yellow is the fluorescence color of EYFP, red of mCherry and green of EGFP. Black rectangles are visualizing an *E. coli* cell.

The interaction between two proteins can be estimated using FRET, in which proteins should be close together with a distance of less than 10 nm (Simkova and Stanek, 2012). This leads to the fluorescence energy of the excited dye being transferred to the second dye, and

which shows higher fluorescence (Figure 21). The aim was to determine the interaction between TusA and FtsZ since *tusA* deleted cells grew as elongated cells (Figure 15). This indicated a cell division defect and since FtsZ is the main actor in this process it enhanced the possibility that TusA and FtsZ could interact. For the FRET principle, this means that if the TusA protein interacts with FtsZ the energy of the excited EGFP will be transferred to mCherry. Therefore mCherry accepts the energy of EGFP which makes it to an acceptor and EGFP to donor fluorophore. As a result, mCherry will show higher fluorescence intensity due to this energy transfer. A negative control, a positive control and the sample to be investigated were used for the assay. The empty vector only with the fluorophore (mCherry (red), EYFP (yellow), EGFP (green)) served as a negative control. Since it does not contain a fused protein, an interaction is not possible. The protein pair IscS-IscU was used as a positive control, as these two previously were reported to interact with each other. During the Fe-S cluster formation, after IscS mobilizes the sulfur via persulfide bonding, in which the scaffold protein IscU interacts directly with IscS to bind the persulfide sulfur. As a result, the sulfur is transferred from IscS to IscU (Kato *et al.*, 2002; Shi *et al.*, 2010). Accordingly, the protein pair TusA-FtsZ was the sample to be analyzed as explained above.

Three plasmids cloned with different fluorophores (mCherry (red), EYFP (yellow), EGFP (green)) were used for this interaction analysis (Figure 22).

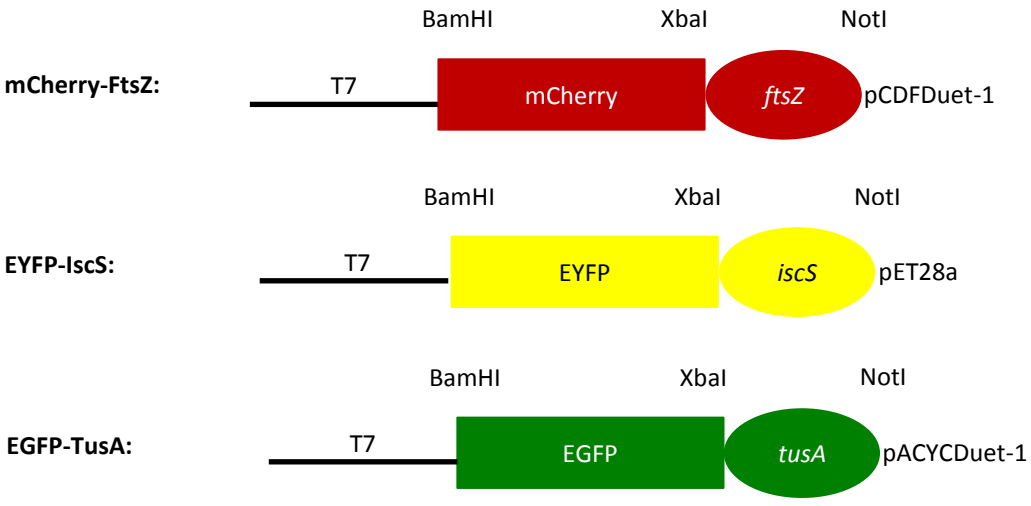

Figure 22: First fluorescent fusion protein constructs.

Three different fusion constructs were used for the expression of fluorophore-tagged proteins. MCherry-FtsZ was created by cloning mCherry fused to *ftsZ* in the pCDFDuet-1 vector. The *mCherry* gene contained the restriction sites BamHI, NotI and the *ftsZ* gene XbaI, NotI sites. EYFP-IscS and EGFP-TusA were also produced by using the same restriction sites. The only difference was that these two were cloned into other vectors, EYFP-*iscS* in pET28a and EGFP-*tusA* in pACYCDuet-1. The colors represent the fluorescence color of the respective fluorophores. MCherry shows a red fluorescence, EYFP a yellow and EGFP a green fluorescence.

The mCherry was fused with the *ftsZ* gene in the pCDFDuet-1 vector with the BamHI, XbaI and NotI restriction sites. EYFP was cloned in the pET28a vector fused with the *iscS* gene and EGFP in the pACYCDuet-1 vector with the *tusA* gene (Figure 22). For all three constructs were used the same restriction sites. Subsequently, the BW25113 (DE3) and Δ*tusA* (DE3) strains were transformed with one of these three constructs and the respective controls with the empty vectors (mCherry-pCDFDuet-1, EYFP-pET28a or EGFP-pACYCDuet-1). For the expression of fusion proteins, almost the same conditions as in the growth curve experiments were applied. The method for preparing the fluorescent microscopy samples was learned at the University of Bonn in collaboration with Dr. Fabian Grein. The following six images are the results for which the fusion proteins were expressed individually to test whether they were produced and detectable under the used growth condition (Figures 23 to 28).

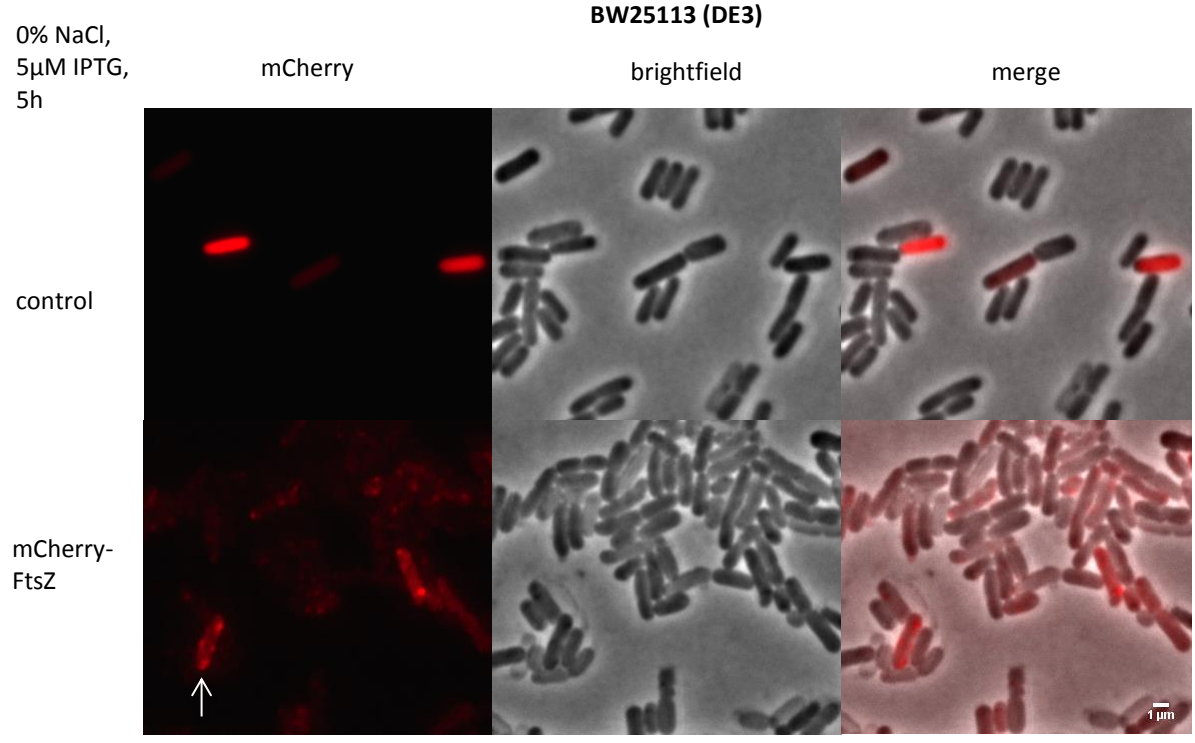

Figure 23: Expression of mCherry-FtsZ in BW25113 (DE3) strain.

BW25113 (DE3) cells (upper panel) were transformed with the control plasmid, which contained only the fluorophore on the plasmid (mCherry-pCDFDuet-1). The remaining BW25113 (DE3) cells (lower panel) are transformed with plasmid, which contained the fusion protein construct (mCherry-*ftsZ*-pCDFDuet-1). The cells were cultivated in LB-0% NaCl for 5 h. The expression of the fusion protein was induced 2.5 h after growth initiation with 5 µM IPTG. 2 ml cells of each sample were analyzed after 5 h of expression. MCherry shows red fluorescence. The first channel (left lane) displays the mCherry fluorescence channel (red), the second channel (middle lane) the cells in brightfield (grey) and the third channel (right lane) the merged image of both channels (red and grey). White arrows indicate the localization of mCherry-FtsZ at cell poles and cell centers. Scale bars: 1 µm.

The control cells for WT (DE3) mCherry showed whole fluorescent cells (Figure 23, upper panel), whereas, a clear localization of the fluorescence was visible for the FtsZ expressing WT (DE3) cells at midcell and cell poles. The two fluorescent points in the midcell indicated that the FtsZ ring is still in the assembling phase (Figure 23, lower panel mCherry-FtsZ, arrow).

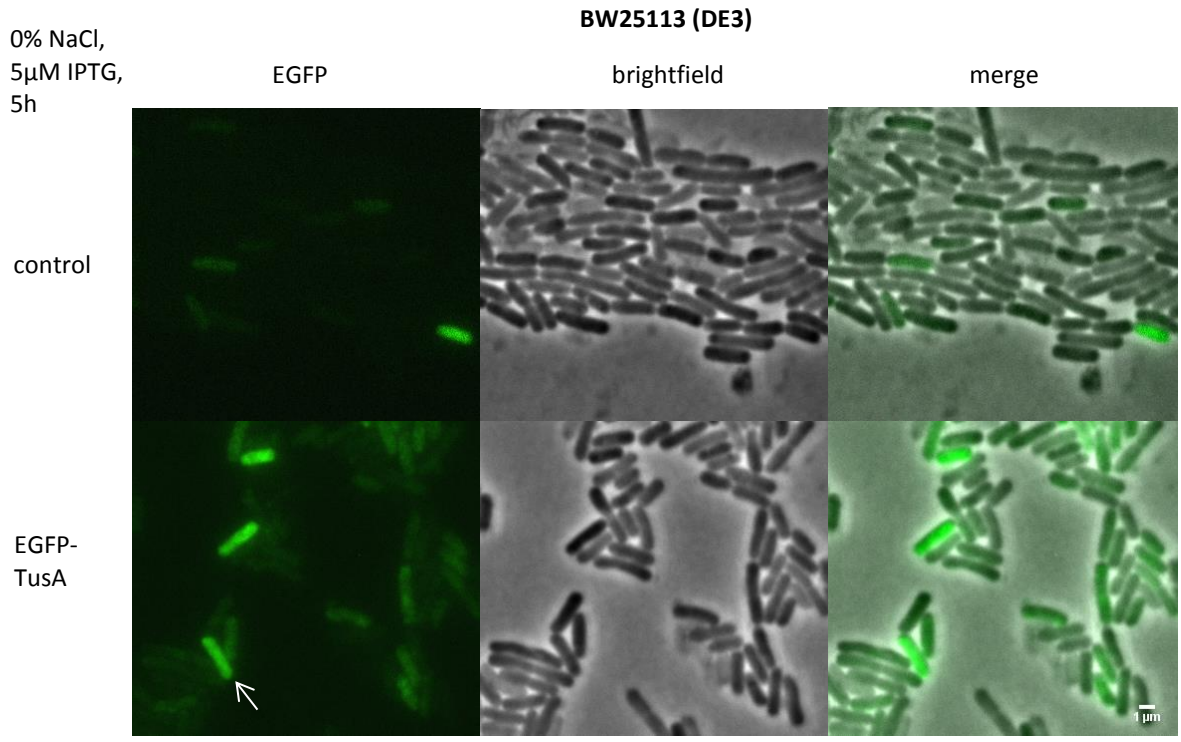

Figure 24: Expression of EGFP-TusA in BW25113 (DE3) strain.

BW25113 (DE3) cells (upper panel) were transformed with the control plasmid, which contained only the fluorophore on the plasmid (EGFP-pACYCDuet-1). The remaining BW25113 (DE3) cells (lower panel) are transformed with plasmid, which contained the fusion protein construct (EGFP-*tusA*-pACYDuet-1). The cells were cultivated in LB-0% NaCl for 5 h. The expression of the fusion protein was induced 2.5 h after growth initiation with 5 µM IPTG. 2 ml cells of each sample were analyzed after 5 h of expression. EGFP shows green fluorescence. The first channel (left lane) displays the EGFP fluorescence channel (green), the second channel (middle lane) the cells in brightfield (grey) and the third channel (right lane) the merged image of both channels (green and grey). White arrows indicate the localization of EGFP-TusA within the cell. Scale bars: 1 µm.

TusA-expressing cells exhibited a very strong signal spread over the whole cell (Figure 24 lower panel EGFP-TusA, arrow). The control cells show also some fluorescent cells (Figure 24 upper panel). The EGFP fluorescence in the control was less compared to the EGFP-TusA fusion protein which would indicate that for some reason the EGFP expression is higher in fusion with the TusA.

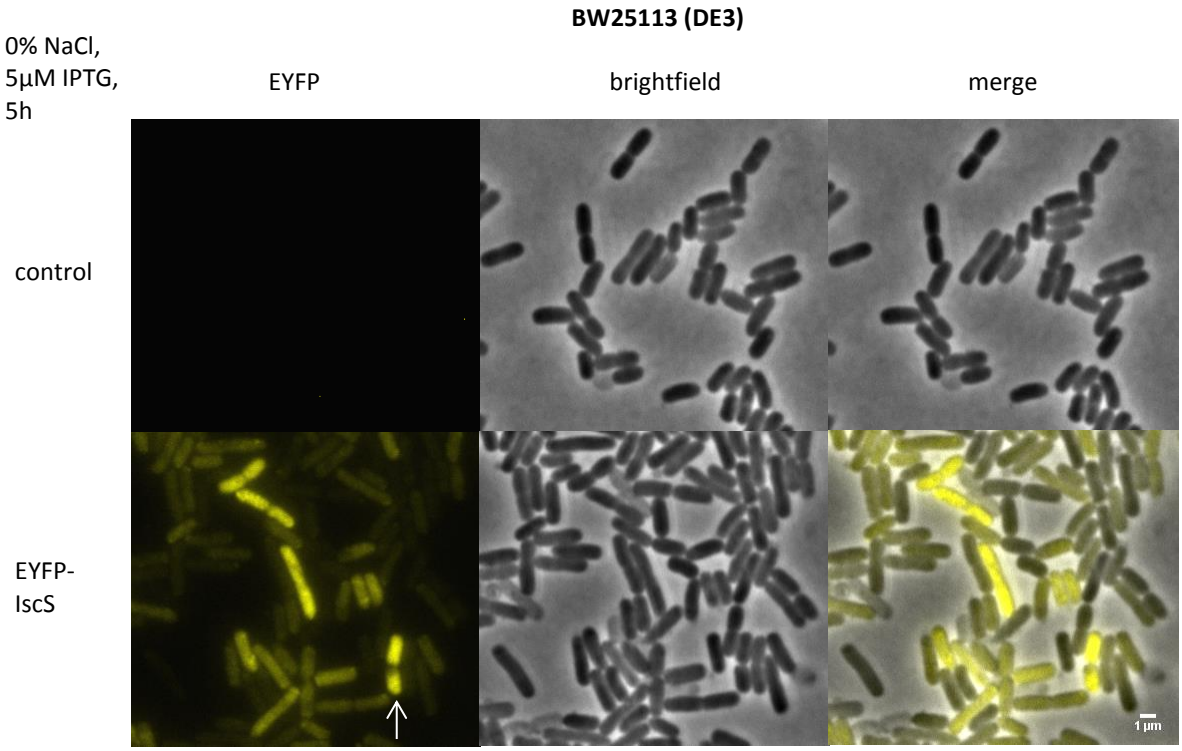

Figure 25: Expression of EYFP-IscS in BW25113 (DE3) strain.

BW25113 (DE3) cells (upper panel) were transformed with the control plasmid, which contained only the fluorophore on the plasmid (EYFP-pET28a). The remaining BW25113 (DE3) cells (lower panel) are transformed with plasmid, which contained the fusion protein construct (EYFP-*iscS*-pET28a). The cells were cultivated in LB-0% NaCl for 5 h. The expression of the fusion protein was induced 2.5 h after growth initiation with 5 µM IPTG. 2 ml cells of each sample were analyzed after 5 h of expression. EYFP shows yellow fluorescence. The first channel (left lane) shows the EYFP fluorescence channel (yellow), the second channel (middle lane) the cells in brightfield (grey) and the third channel (right lane) the merged image of both channels (yellow and grey). White arrows indicate the localization of EGFP-IscS within the cell. Scale bars: 1 µm.

IscS-expressed WT (DE3) cells demonstrated a very strong signal, which was spread over the whole cell (Figure 25 lower panel EYFP-IscS, arrow). For unknown reasons, there was no EYFP signal in WT (DE3) control cells detectable.

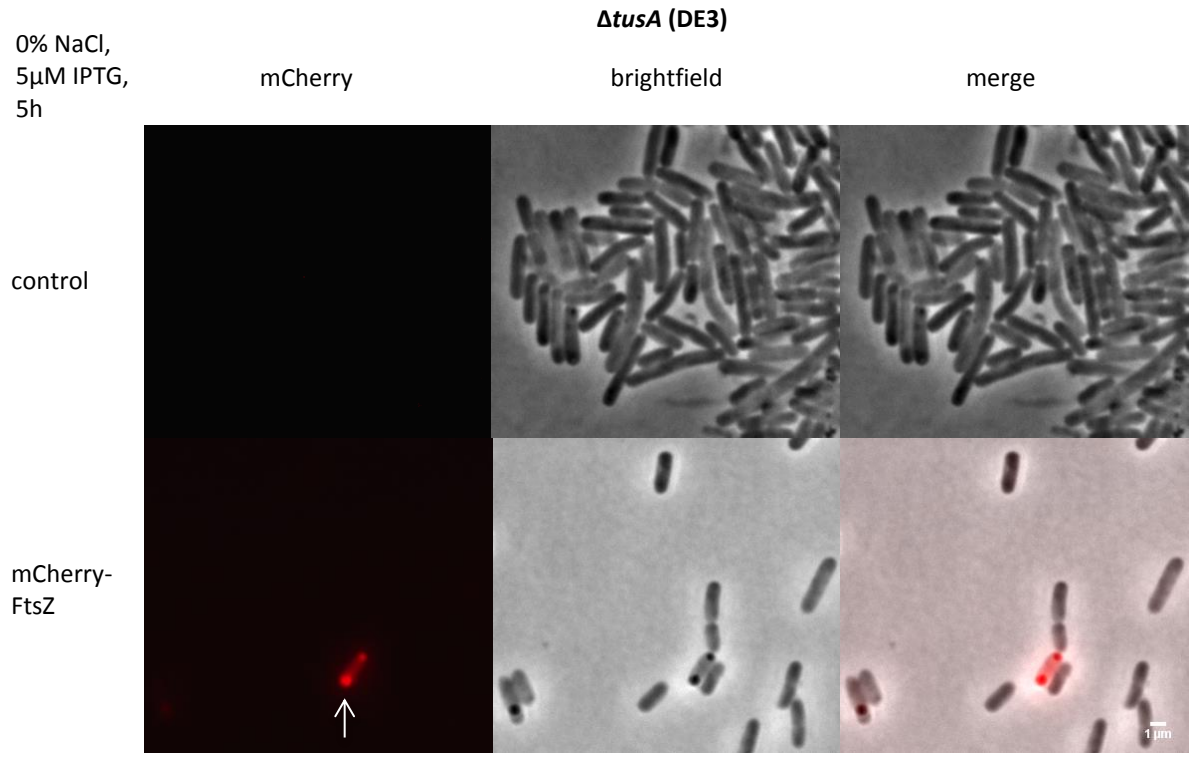

Figure 26: Expression of mCherry-FtsZ in Δ*tusA* (DE3) strain.

Δ*tusA* (DE3) cells (upper panel) were transformed with the control plasmid, which contained only the fluorophore on the plasmid (mCherry-pCDFDuet-1). The remaining Δ*tusA* (DE3) cells (lower panel) are transformed with plasmid, which contained the fusion protein construct (mCherry-*ftsZ*-pCDFDuet-1). The cells were cultivated in LB-0% NaCl for 5 h. The expression of the fusion protein was induced 2.5 h after growth initiation with 5 µM IPTG. 2 ml cells of each sample were analyzed after 5 h of expression. MCherry shows red fluorescence. The first channel (left lane) displays the mCherry fluorescence channel (red), the second channel (middle lane) the cells in brightfield (grey) and the third channel (right lane) the merged image of both channels (red and grey). White arrows indicate the localization of mCherry-FtsZ at cell poles. Scale bars: 1 µm.

FtsZ expressing *tusA* mutant (DE3) cells displayed a clear visible signal at the cell poles (Figure 26 lower panel mCherry-FtsZ, arrow). For the Δ*tusA* (DE3) control cell, the mCherry signal was invisible (Figure 26 upper panel).

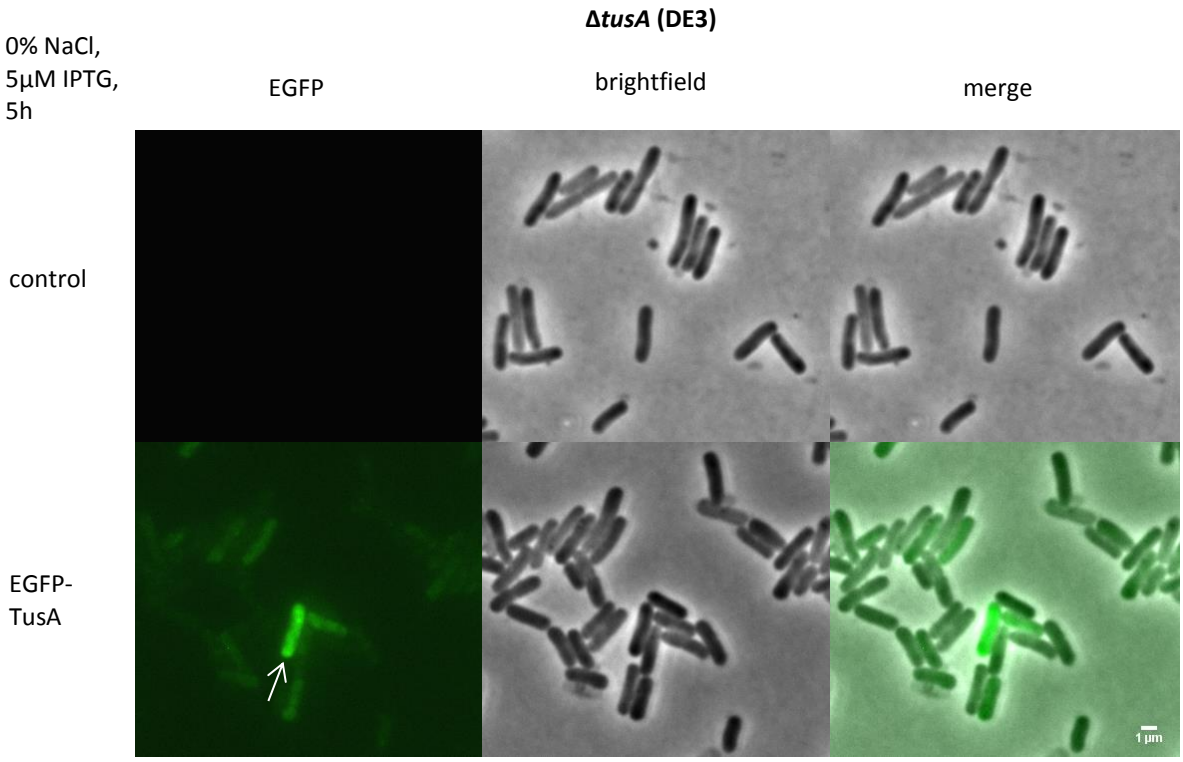

Figure 27: Expression of EGFP-TusA in Δ*tusA* (DE3) strain.

Δ*tusA* (DE3) cells (upper panel) were transformed with the control plasmid, which contained only the fluorophore on the plasmid (EGFP-pACYCDuet-1). The remaining Δ*tusA* (DE3) cells (lower panel) are transformed with plasmid, which contained the fusion protein construct (EGFP-*tusA*-pACYDuet-1). The cells were cultivated in LB-0% NaCl for 5 h. The expression of the fusion protein was induced 2.5 h after growth initiation with 5 µM IPTG. 2 ml cells of each sample were analyzed after 5 h of expression. EGFP shows green fluorescence. The first channel (left lane) displays the EGFP fluorescence channel (green), the second channel (middle lane) the cells in brightfield (grey) and the third channel (right lane) the merged image of both channels (green and grey). White arrows indicate the localization of EGFP-TusA within the cell whereby it shows a slight accumulation at cell poles. Scale bars: 1 µm.

No fluorescence of EGFP was detectable also for Δ*tusA* (DE3) control cells as mentioned for the mCherry sample (Figure 27 upper panel). However, a clear signal is visible with the Δ*tusA* (DE3) cells expressed with the fusion protein EGFP-TusA (Figure 27 lower panel EGFP-TusA, arrow). This EGFP-TusA fluorescence signal was spread over the whole cell, which was a bit accumulated at the cell poles.

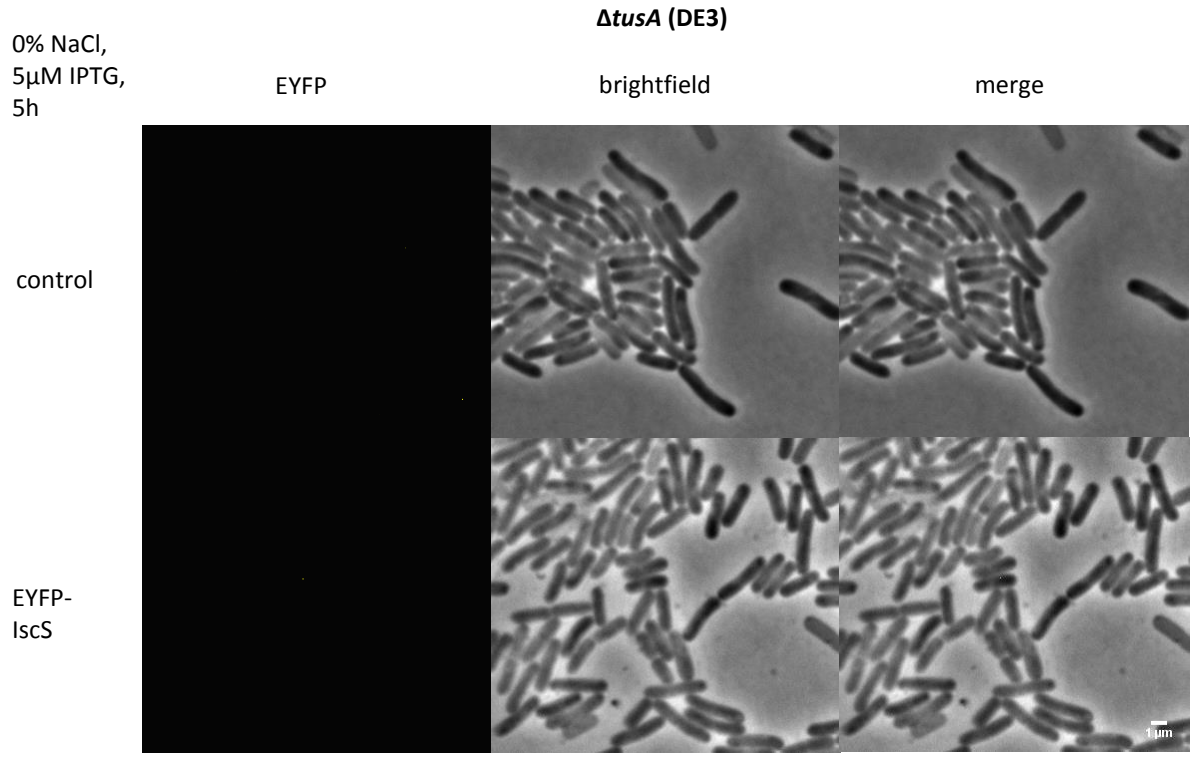

Figure 28: Expression of EYFP-IscS in Δ*tusA* (DE3) strain.

Δ*tusA* (DE3) cells (upper panel) were transformed with the control plasmid, which contained only the fluorophore on the plasmid (EYFP-pET28a). The remaining Δ*tusA* (DE3) cells (lower panel) are transformed with plasmid, which contained the fusion protein construct (EYFP-*iscS*-pET28a). The cells were cultivated in LB-0% NaCl for 5 h. The expression of the fusion protein was induced 2.5 h after growth initiation with 5 µM IPTG. 2 ml cells of each sample were analyzed after 5 h of expression. EYFP shows yellow fluorescence. The first channel (left lane) shows the EYFP fluorescence channel (yellow), the second channel (middle lane) the cells in brightfield (grey) and the third channel (right lane) the merged image of both channels (yellow and grey). The EYFP channel is black since there was no EYFP signal detectable. Scale bars: 1 µm.

In Figure 28, no signal was detectable for EYFP in the *tusA* mutant (DE3).

4.5 Co-expression of EGFP+mCherry or EYFP+mCherry protein fusions in single *E. coli* cell

The images from Figures 23 to 28 depicted no strong fluorescence intensities to measure FRET signals. Therefore, in a further assay, it was aimed to optimize the cultivation conditions to achieve higher fluorescence signals. Usually, the expressions of fluorescent fusion proteins were done under cultivation without antibiotics. The induction of fusion proteins was carried out with 5 µM IPTG. Since the samples did not contain many cells showing the two different fluorescences at the same time and additionally the fluorescence signals were not enough to measure FRET. The samples were then cultivated with antibiotics and expression of fusion protein constructs was induced with higher IPTG concentration (15 µM, Figures 30 - 37).

The following combination of fusion protein constructs was used for FRET analysis (Figure 29).

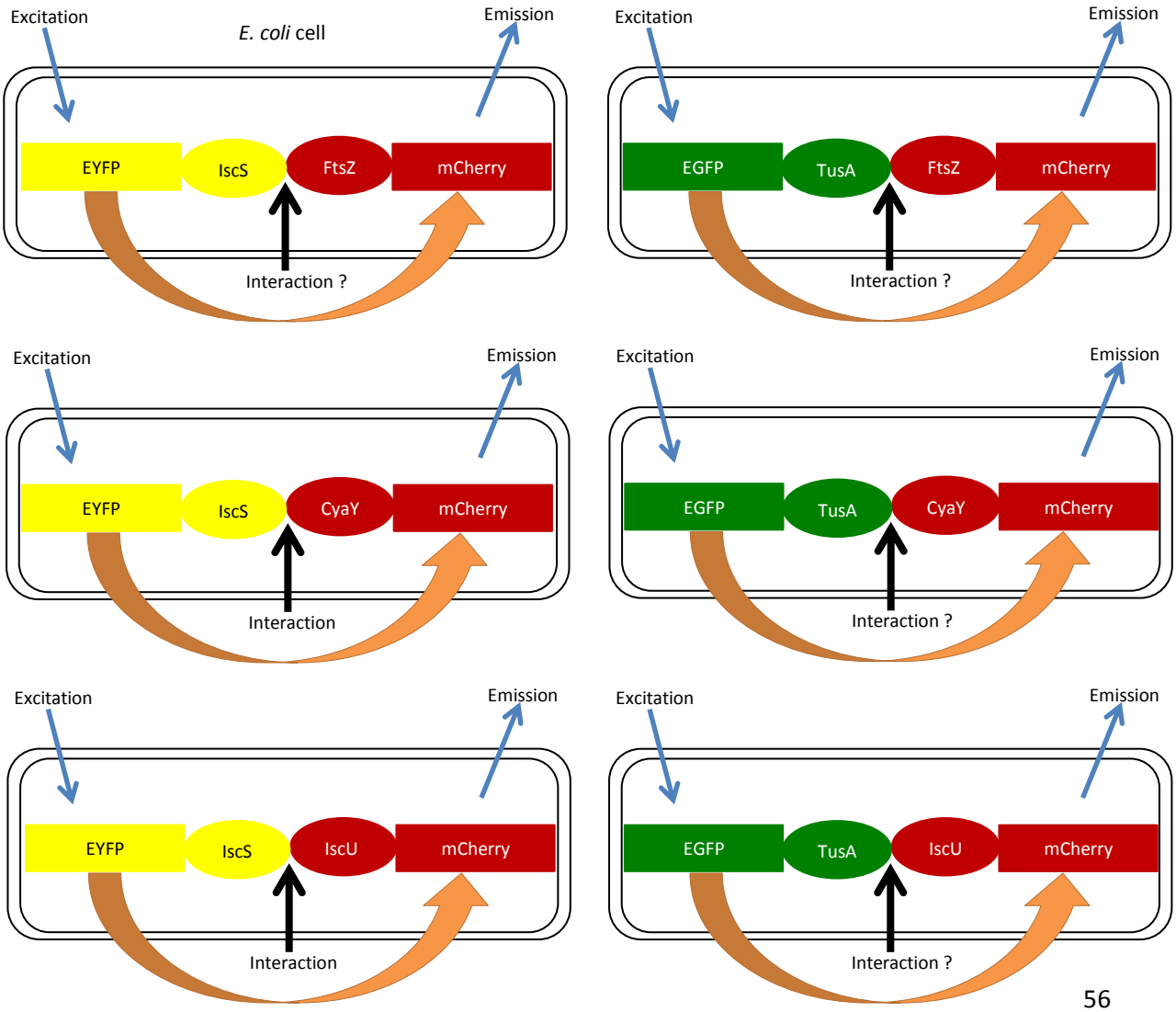

Figure 29: Fusion protein constructs with different fluorophores for FRET (FRET-pairs).

The image shows the FRET principle of the used fluorescent fusion proteins for interaction analysis. One *E. coli* cell is transformed with one of the mCherry fusion constructs (mCherry-*ftsZ*-/mCherry-*cyaY*/ mCherry-*iscU*-pCDFDuet-1) and with EYFP-*iscS*-pET28a or EGFP-*tusA*-pACYCDuet-1. Cells were grown in LB-0% NaCl for 5 h at 37 °C and 180 rpm. The expression of the fusion protein was induced 2.5 h after growth initiation with IPTG and the cells were cultivated for a further 2.5 h. These FRET-pairs allow the determination of a possible interaction between FtsZ/CyaY/IscU and IscS or TusA proteins. So if the fusion proteins are interacting within the cell, e.g. EYFP-IscS and mCherry-IscU, the fluorescence energy of the excited dye is transferred to the second dye, which then shows higher fluorescence. Here, after the excitation of EYFP, the fluorescence energy will be transferred (orange arrow) to mCherry in case IscS and IscU are interacting. The colors represent the different fluorescence colors of the respective fluorophores. MCherry shows a red fluorescence, EYFP a yellow and EGFP a green fluorescence. Black rectangles are visualizing an *E. coli* cell.

Figure 29 illustrates the used fusion proteins to detect FRET. One *E. coli* cell contained one mCherry construct with EGFP-TusA or EYFP-IscS. Therefore the possible interaction between mCherry-FtsZ, mCherry-CyaY and mCherry-IscU was investigated with EGFP-TusA or EYFP-IscS. These fusion proteins were expressed in WT (DE3) and Δ*tusA* (DE3) cells to determine the difference in expression and possible interaction between these two strains. MCherry-CyaY was also cloned with the same restriction sites as the other constructs in pCDFDuet-1. The idea is that the CyaY protein is competing for the binding to IscS with the TusA protein (Leimkühler, 2014) which led to the motivation to analyze also CyaY-IscS interaction. As already mentioned, IscU-IscS is the positive control for this approach since their interaction was reported before (Shi *et al.*, 2010). The method for preparing the fluorescent microscopy samples was learned at the University of Bonn in collaboration with Dr. Fabian Grein.

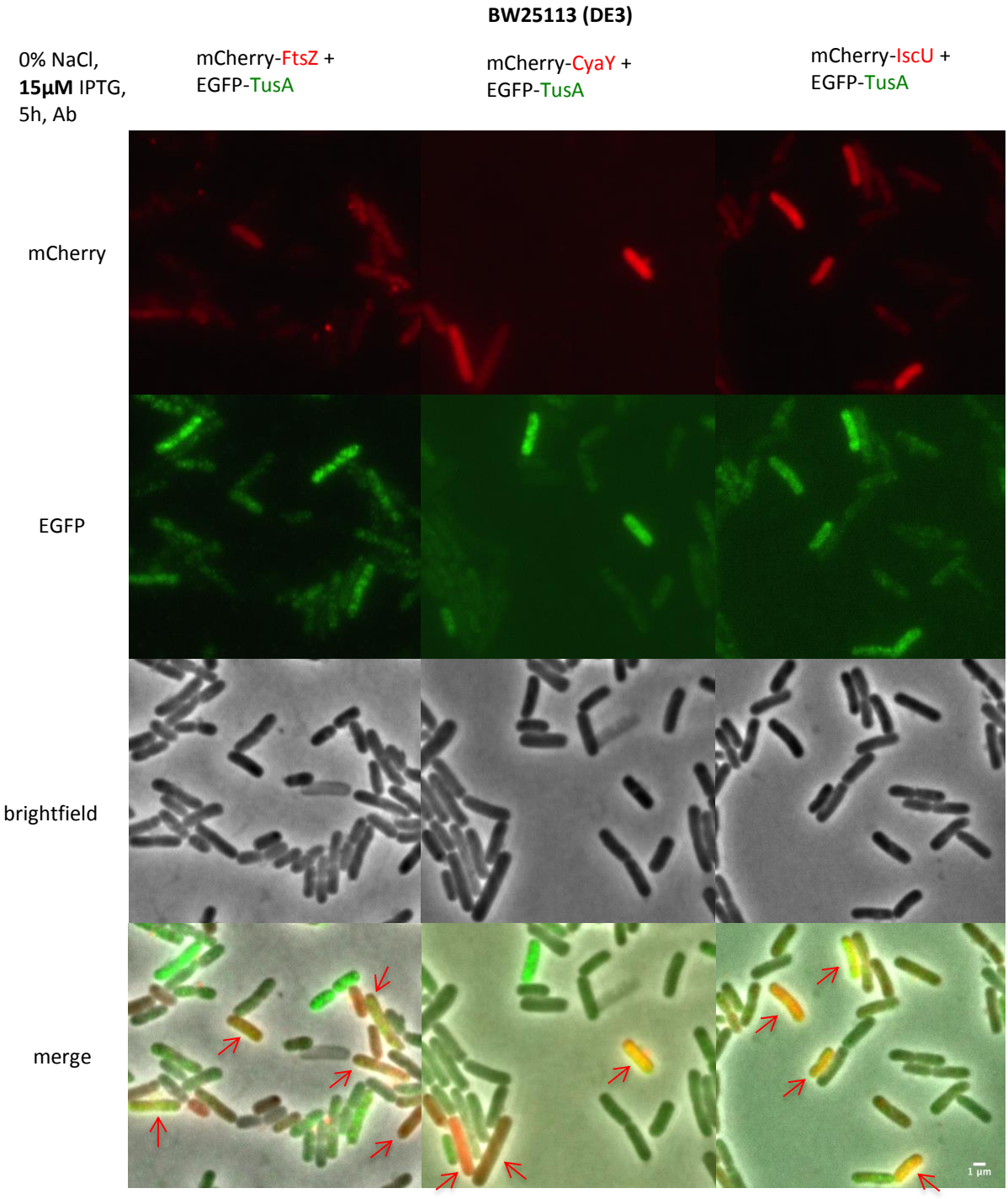

Figure 30: Co-expression of mCherry-FtsZ, mCherry-CyaY, mCherry-IscU with EGFP-TusA in BW25113 (DE3) strain.

BW25113 (DE3) cells are transformed with a plasmid, which contains the fusion protein construct (mCherry-*ftsZ/cyaY/iscU*-pCDFDuet-1) and EGFP-*tusA*-pACYCDuet-1 vector. The cells were cultivated with the respective antibiotics in LB-0% NaCl for 5 h. The expression of the fusion protein was induced 2.5 h after growth initiation with 15 µM IPTG. 2 ml cells of each sample were analyzed after 5 h of expression. The first channel (upper lane) shows the mCherry fluorescence channel (red), the second channel (second lane) the cells in EGFP fluorescence channel (green) and the third channel (third lane) the cells in

brightfield (grey) and the lowest lane the merged image of all channels (red, green, grey). Arrows (red) show such cells expressing both fusion proteins simultaneously. Scale bars: 1 µm.

For the WT (DE3) cells mCherry-FtsZ fluorescence was often detectable as accumulated points within the cell (Figure 30 left upper lane, mCherry channel). In contrast, the EGFP-TusA green signal was more spread over the whole cell (second lane, EGFP channel). The cultivation under the new conditions (with antibiotics and with 15 µM IPTG) resulted in higher fluorescence signals and more cells showed both red and green fluorescence. This is important for the FRET measurement (Figure 30, **red arrows** pointed out exemplary cells). This indicated that both proteins were expressed in the same cell. For FRET it was important to have several cells in one area expressing both proteins (to gain good statistics). Furthermore, the intensity of the fluorescence signal was a hint for the expression level of the fusion protein, since the higher signal indicates a high expression of this protein and vice-versa. MCherry-CyaY and mCherry-IscU signals were cytoplasmic (Figure 30, middle and right upper lane, mCherry channel) and not accumulated at a certain area as it was the case for mCherry-FtsZ. For mCherry-CyaY and mCherry-IscU was also the co-expression with EGFP-TusA was clearly visible (Figure 30, **red arrows**).

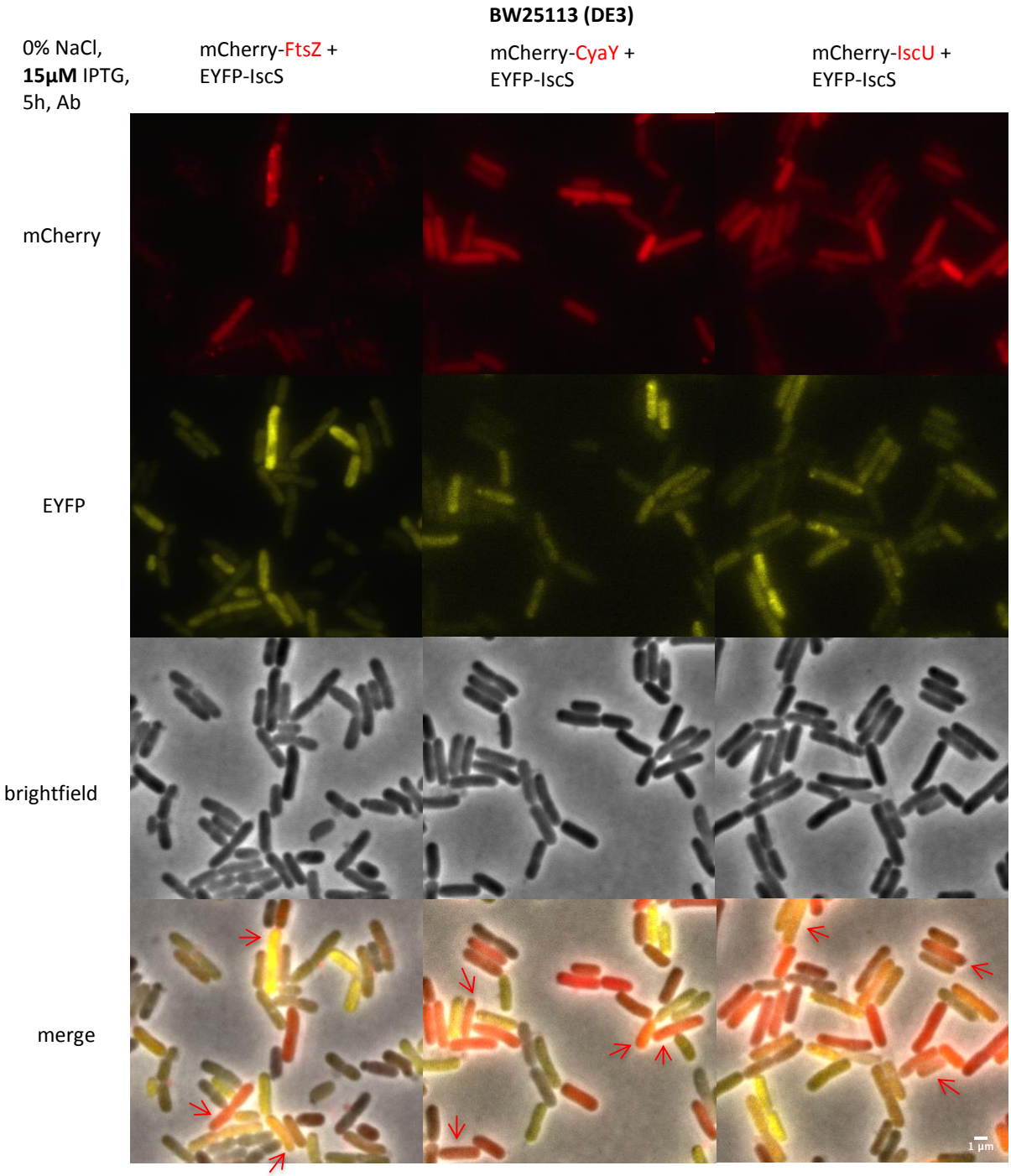

Figure 31: Co-expression of mCherry-FtsZ, mCherry-CyaY, mCherry-IscU with EYFP-IscS in BW25113 (DE3) strain.

BW25113 (DE3) cells are transformed with a plasmid, which contains the fusion protein construct (mCherry-*ftsZ/cyaY/iscU*-pCDFDuet-1) and EYFP-*iscS*-pET28a vector. The cells were cultivated with the respective antibiotics in LB-0% NaCl for 5 h. The expression of the fusion protein was induced 2.5 h after growth initiation with 15 µM IPTG. 2 ml cells of each sample were analyzed after 5 h of expression. The first channel (upper lane) shows the mCherry fluorescence channel (red), the second channel (second lane) the cells in EYFP fluorescence channel (green) and the third channel (third lane) the cells in brightfield (grey) and the lowest lane the merged image of all channels (red, yellow, grey). Arrows (red) show such cells expressing both fusion proteins simultaneously. Scale bars: 1 µm.

The co-expressions of the same fusion proteins with EYFP-IscS in WT (DE3) samples were higher (Figure 31) than with EGFP-TusA (Figure 30) which were indicated by the stronger and higher fluorescence signals.

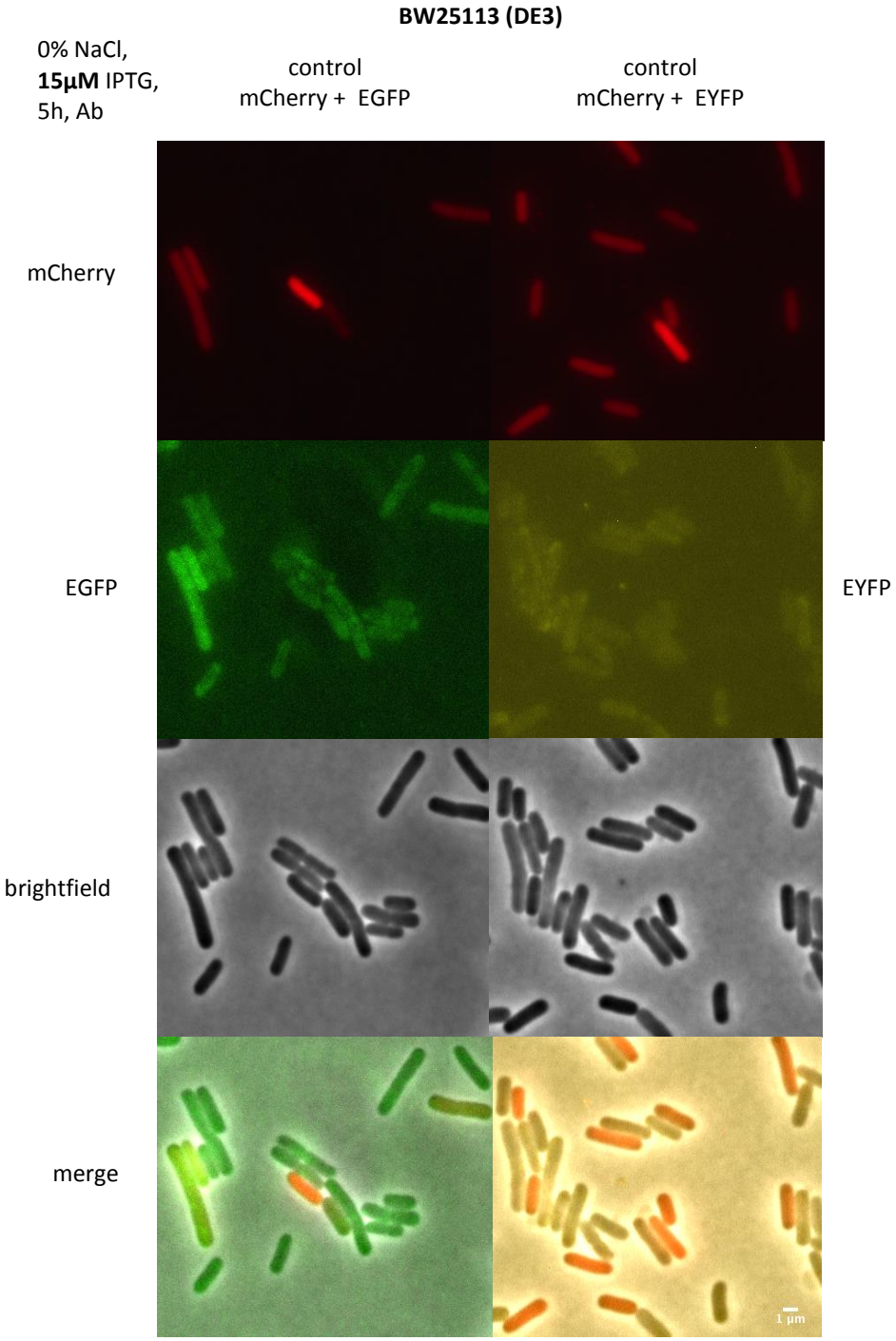

Figure 32: Co-expression of mCherry + EGFP and mCherry + EYFP in BW25113 (DE3) strain.

BW25113 (DE3) cells are transformed with a control plasmid, which contains only the fluorophore on the plasmid (mCherry-pCDFDuet-1/EGFP-pACYCDuet-1/EYFP-pET28a). The cells were cultivated with the respective antibiotics in LB-0% NaCl for 5 h. The expression of the fusion protein was induced 2.5 h after growth initiation with 15 µM IPTG. 2 ml cells of each sample were analyzed after 5 h of expression. The

first channel (upper lane) shows the mCherry fluorescence channel (red), the second channel (second lane) the cells in EGFP (left) or EYFP (right) fluorescence channel (green/yellow), the third channel (third lane) the cells in brightfield (grey) and the lowest lane the merged image of all channels (red, green/yellow, grey). Scale bars: 1 µm.

Figure 32 displays the control WT (DE3) cells which were expressing only the fluorophores, mCherry and EGFP or mCherry and EYFP. Among these three fluorophores, mCherry depicted the highest clear fluorescence signal followed by EGFP and EYFP whereas EYFP exhibited the lowest fluorescence signal.

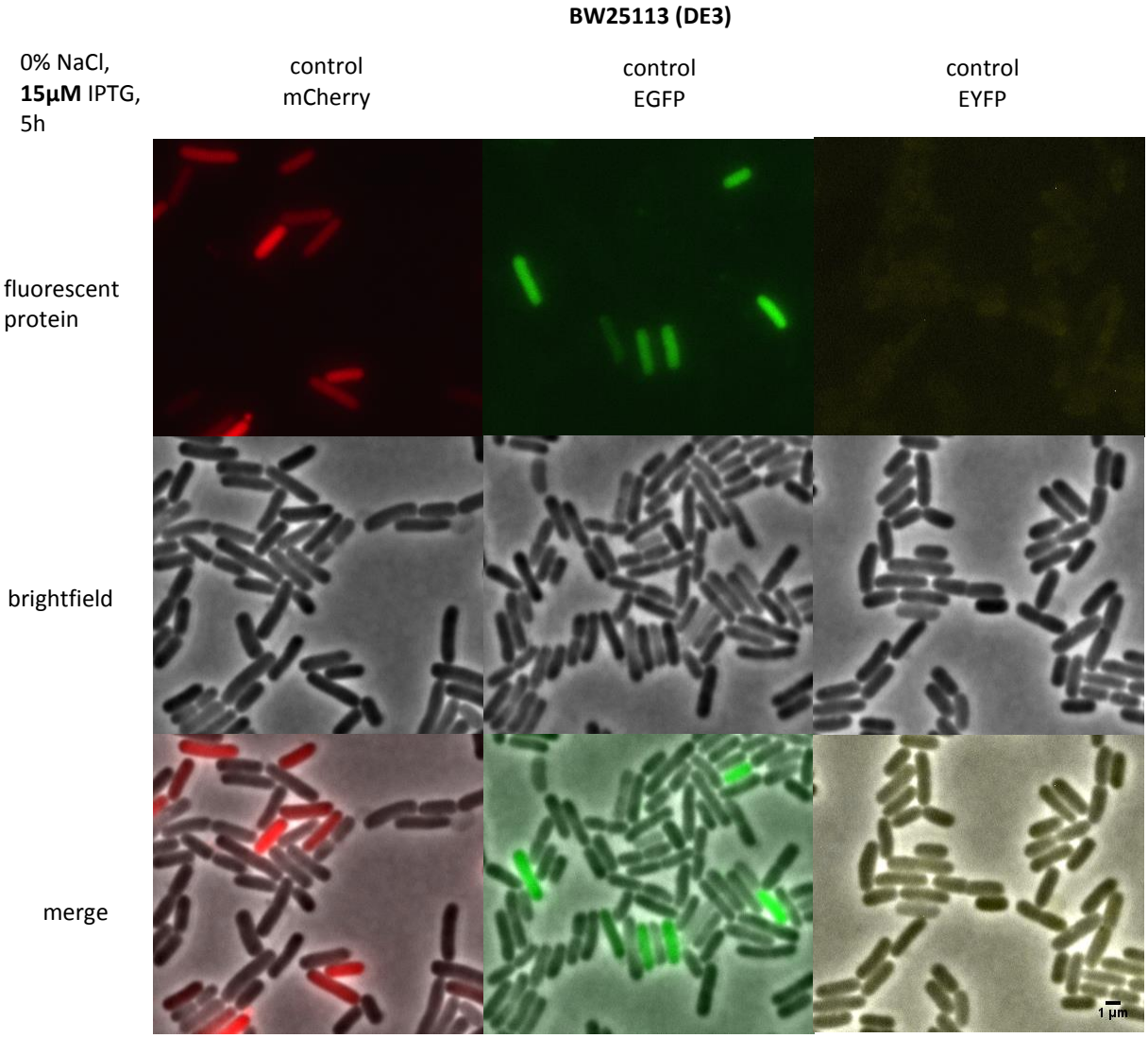

Figure 33: Expression of mCherry, EGFP or EYFP in BW25113 (DE3) strain.

BW25113 (DE3) cells are transformed with a control plasmid, which contains only the fluorophore on the plasmid (mCherry-pCDFDuet-1/EGFP-pACYCDuet-1/EYFP-pET28a). The cells were cultivated with the respective antibiotics in LB-0% NaCl for 5 h. The expression of the fusion protein was induced 2.5 h after growth initiation with 15 µM IPTG. 2 ml cells of each sample were analyzed after 5 h of expression. The first channel (left upper lane) shows the mCherry fluorescence channel (red), the second channel (middle upper lane) the cells in EGFP (green) and the third channel (right upper lane) EYFP fluorescence channel (yellow). The complete second lane displays the cells in the brightfield channel (grey). The merged images

are shown of each fluorescence channel plus brightfield (red + grey, green + grey, yellow + grey) in the lower lane. Scale bars: 1 µm.

Figure 33 shows the last control cells expressing only one fluorophore in the WT (DE3) strain. The result was similar to that in Figure 32. MCherry and EGFP fluorescent protein revealed higher fluorescence intensity than that of EYFP.

The expressions of the same fusion proteins were also analyzed in Δ*tusA* (DE3) to detect a difference in the expressions in the WT (DE3) strain.

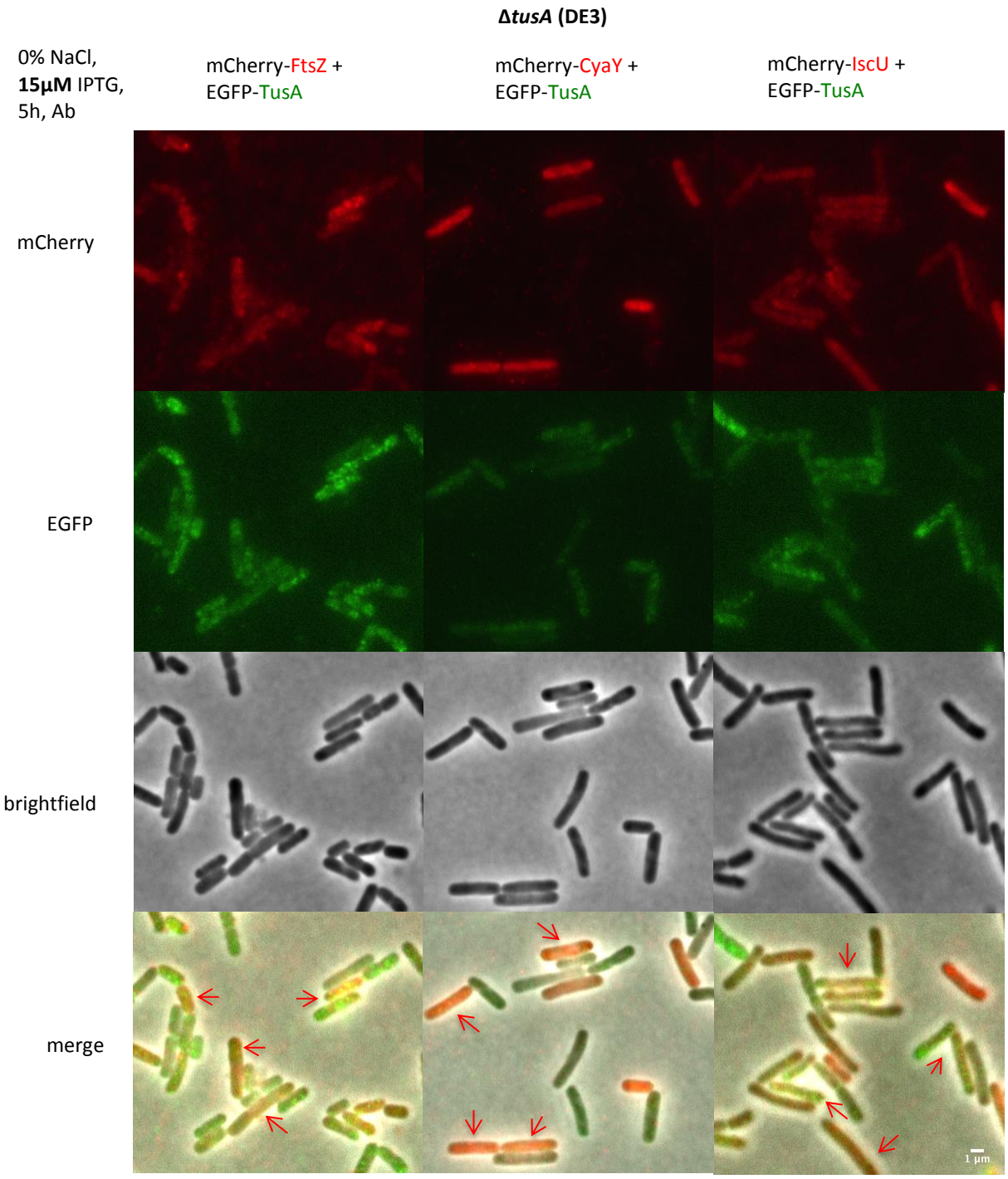

Figure 34: Co-expression of mCherry-FtsZ, mCherry-CyaY, mCherry-IscU with EGFP-TusA in Δ*tusA* (DE3) strain.

Δ*tusA* (DE3) cells are transformed with a plasmid, which contains the fusion protein construct (mCherry-*ftsZ/cyaY/iscU*-pCDFDuet-1) and EGFP-*tusA*-pACYCDuet-1 vector. The cells were cultivated with the respective antibiotics in LB-0% NaCl for 5 h. The expression of the fusion protein was induced 2.5 h after growth initiation with 15 µM IPTG. 2 ml cells of each sample were analyzed after 5 h of expression. The first channel (upper lane) shows the mCherry fluorescence channel (red), the second channel (second lane) the cells in EGFP fluorescence channel (green) and the third channel (third lane) the cells in brightfield (grey) and the lowest lane the merged image of all channels (red, green, grey). Arrows (red) show such cells expressing both fusion proteins simultaneously. Scale bars: 1 µm.

The *tusA* mutant (DE3) showed the opposite result of the WT (DE3) strain (Figure 34). In the mutant, the samples with EGFP-TusA depicted higher fluorescence intensities than the EYFP-IscS samples (Figure 35, EYFP-IscS samples). The signals were a bit less than the WT (DE3) signals, which were caused by the slow growth of the Δ*tusA* (DE3) strain. MCherry-FtsZ was detected as dots and the other fusion proteins are cytoplasmic (mCherry-CyaY, -IscU, EGFP-TusA). As already shown in WT (DE3), in Δ*tusA* (DE3) were also more cells showing both fluorescence signals, which indicated that they expressed both fusion proteins (Figure 34, red arrows).

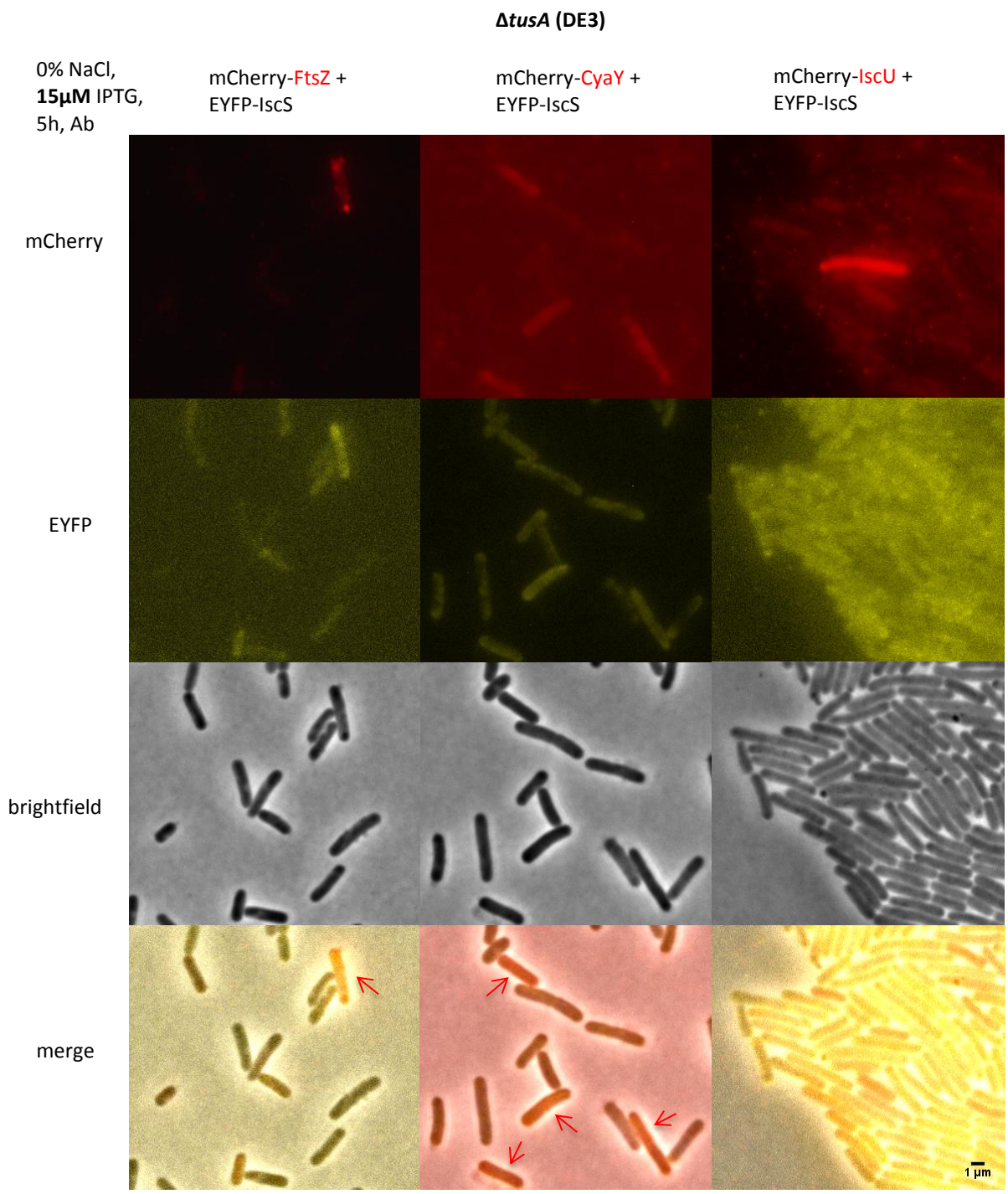

Figure 35: Co-expression of mCherry-FtsZ, mCherry-CyaY, mCherry-IscU with EYFP-IscS in Δ*tusA* (DE3) strain.

Δ*tusA* (DE3) cells are transformed with a plasmid, which contains the fusion protein construct (mCherry-*ftsZ/cyaY/iscU*-pCDFDuet-1) and EYFP-*iscS*-pET28a vector. The cells were cultivated with the respective antibiotics in LB-0% NaCl for 5 h. The expression of the fusion protein was induced 2.5 h after growth initiation with 15 µM IPTG. 2 ml cells of each sample were analyzed after 5 h of expression. The first channel (upper lane) shows the mCherry fluorescence channel (red), the second channel (second lane) the cells in EYFP fluorescence channel (green) and the third channel (third lane) the cells in brightfield (grey) and the lowest lane the merged image of all channels (red, yellow, grey). Arrows (red) show such cells expressing both fusion proteins simultaneously. Scale bars: 1 µm.

As mentioned above, the fluorescence signal of EYFP-IscS samples was less (Figure 35) compared to the Δ*tusA* (DE3) cells shown in Figure 34. For mCherry-FtsZ and mCherry-CyaY, it was successful to identify some cells expressing both fusion proteins (Figure 35, lowest lane, arrows). But for mCherry-IscU in combination with EYFP-IscS, it was not easy to detect the fluorescence. Only in areas of clustered cells was a low fluorescence signal detectable (Figure 35, second panel EYFP channel, mCherry-IscU + EYFP-IscS), whereas in separately presented cells, it was very difficult to detect the fluorescence.

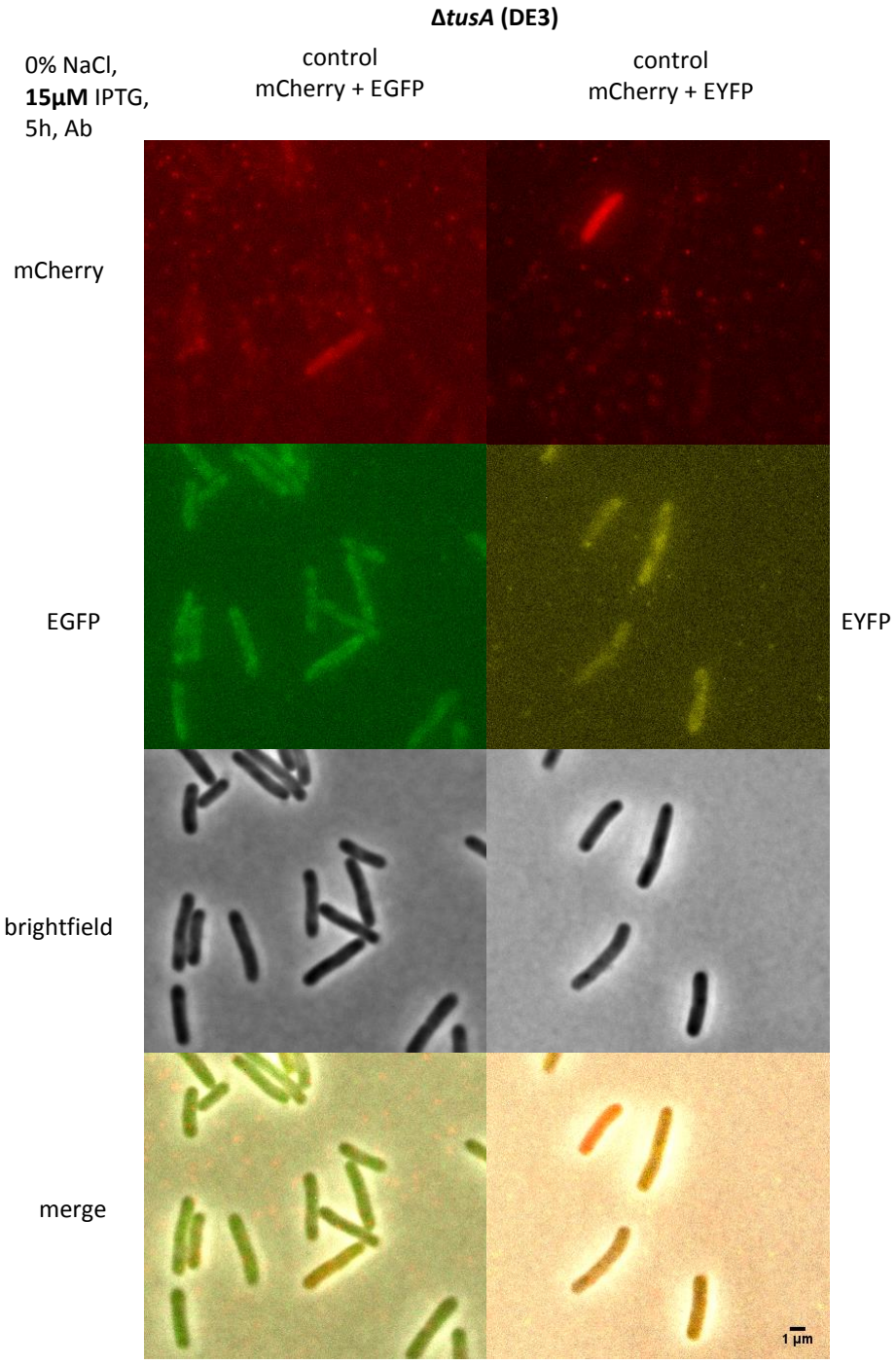

Figure 36: Co-expression of mCherry + EGFP and mCherry + EYFP in Δ*tusA* (DE3) strain.

Δ*tusA* (DE3) cells are transformed with a control plasmid, which contains only the fluorophore on the plasmid (mCherry-pCDFDuet-1/EGFP-pACYCDuet-1/EYFP-pET28a). The cells were cultivated with the respective antibiotics in LB-0% NaCl for 5 h. The expression of the fusion protein was induced 2.5 h after growth initiation with 15 µM IPTG. 2 ml cells of each sample were analyzed after 5 h of expression. The first channel (upper lane) shows the mCherry fluorescence channel (red), the second channel (second lane) the cells in EGFP (left) or EYFP (right) fluorescence channel (green/yellow), the third channel (third lane) the cells in brightfield (grey) and the lowest lane the merged image of all channels (red, green/yellow, grey). Scale bars: 1 µm.

Figure 36 shows the control cells with both fluorophores in the Δ*tusA* (DE3) cells. It was noticeable that the fluorescence signals of the control cells were not as strong as the fusion proteins in the same strain.

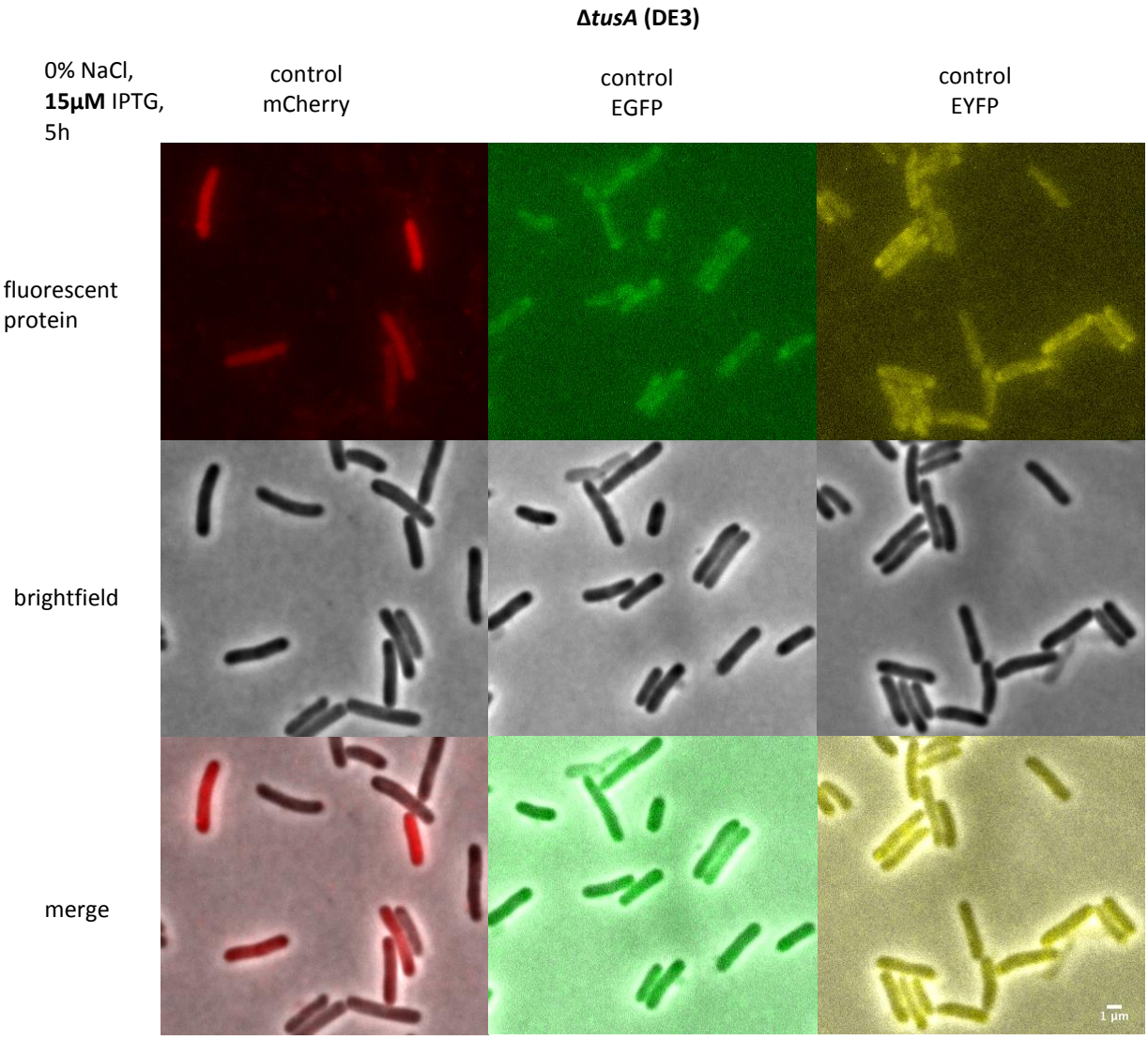

Figure 37: Expression of mCherry, EGFP or EYFP in Δ*tusA* (DE3) strain.

Δ*tusA* (DE3) cells are transformed with a control plasmid, which contains only the fluorophore on the plasmid (mCherry-pCDFDuet-1/EGFP-pACYCDuet-1/EYFP-pET28a). The cells were cultivated with the respective antibiotics in LB-0% NaCl for 5 h. The expression of the fusion protein was induced 2.5 h after

growth initiation with 15 µM IPTG. 2 ml cells of each sample were analyzed after 5 h of expression. The first channel (left upper lane) shows the mCherry fluorescence channel (red), the second channel (middle upper lane) the cells in EGFP (green) and the third channel (right upper lane) EYFP fluorescence channel (yellow). The complete second lane displays the cells in the brightfield channel (grey). The merged images are shown of each fluorescence channel plus brightfield (red + grey, green + grey, yellow + grey) in the lower lane. Scale bars: 1 µm.

The last picture of this assay visualizes the Δ*tusA* (DE3) cells which were expressing only one fluorophore (Figure 37). MCherry and EGFP fluorescence intensities stayed nearly at the same level as the expression of both control proteins in one cell in Δ*tusA* (DE3) (Figure 36). However, the only difference to the expression of mCherry and EYFP simultaneously was that the Δ*tusA* (DE3) cells expressing only EYFP exhibited slightly increased yellow fluorescence (Figure 37, right upper lane, EYFP channel).

4.6 FRET measurement

After optimizing the expression conditions for the fusion proteins, FRET measurements of the same protein pairs (FtsZ-/CyaY-/IscU-TusA and FtsZ-/CyaY-/IscU-IscS in WT (DE3) or Δ*tusA* (DE3)) were performed. The software settings were adjusted to the different fluorescence intensities via a test measurement. Since the fluorescence intensities were stronger in WT (DE3) samples than in Δ*tusA* (DE3) samples, the induction was performed with 5 µM IPTG for WT (DE3) cells and the 15 µM IPTG concentration was kept for Δ*tusA* (DE3) samples. Another change to the previous assays was that the cells were not resuspended in 1 ml 1 x PBS and 5 µl of them were not applied on agarose pads. To obtain more cells in one area expressing both fusion proteins the cell number was enriched. For this 1 ml cells of each culture were resuspended after washing in 75 µl 1 x PBS and 50 µl were applied on agarose pads. An exemplary result is imaged in Figure 38. The FRET measurement was carried out in collaboration with Dr. Gabriele Malengo at the MPI in Marburg.

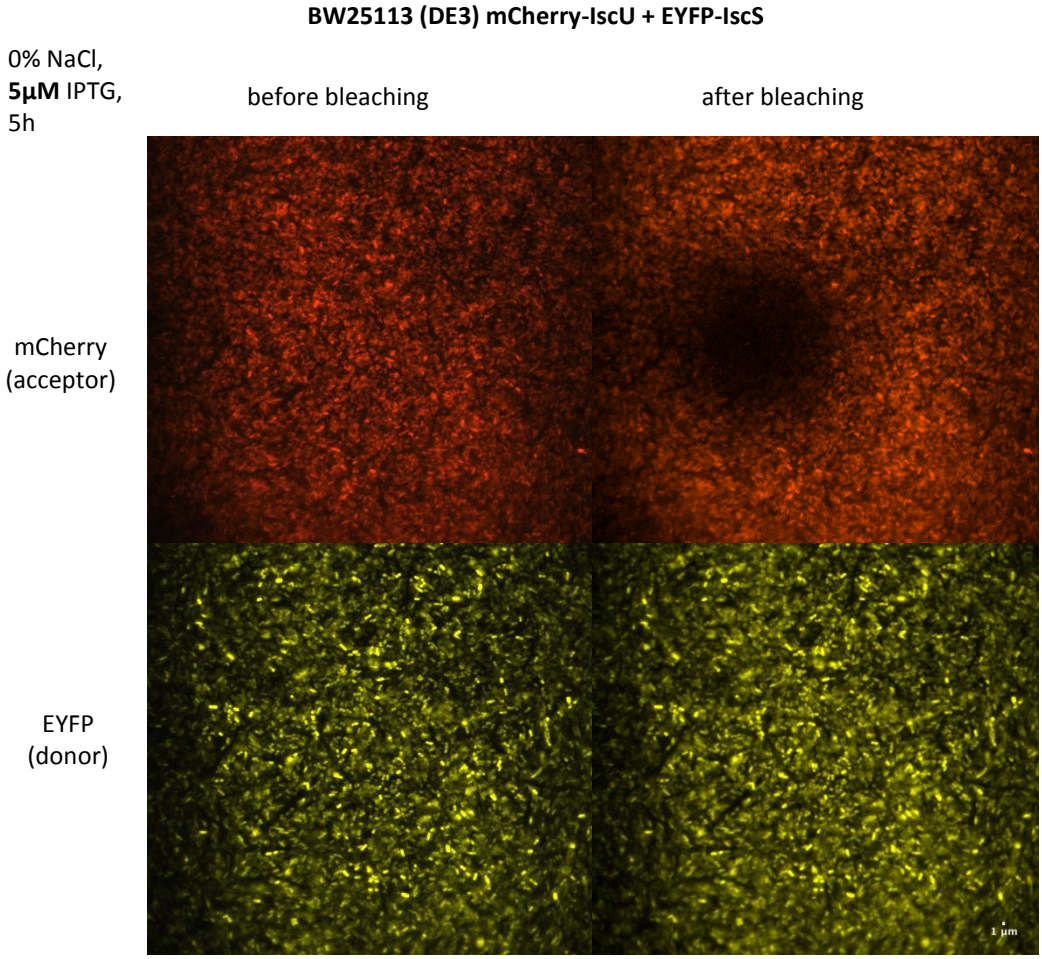

Figure 38: Co-expression of mCherry-IscU with EYFP-IscS in BW25113 (DE3) strain for FRET.

BW25113 (DE3) cells are transformed with a plasmid, which contains the fusion protein construct (mCherry-*iscU*-pCDFDuet-1) and EYFP-*iscS*-pET28a vector. The cells were cultivated with the respective antibiotics in LB-0% NaCl for 5 h. The expression of the fusion protein was induced 2.5 h after growth initiation with 5 µM IPTG. 1 ml cells of each sample were analyzed after 5 h of expression. MCherry shows red fluorescence (upper lane) before (left) and after bleaching (right). EYFP displays a yellow fluorescence (lower lane) before (left) and after bleaching (right). The images were recorded via a 60x oil objective to record a bigger area, which contains more cells expressing both fusion proteins. The acceptor bleaching method was applied to measure a FRET signal. MCherry is the acceptor and EYFP is the donor of this FRET-pair. After the bleaching of mCherry and a present interaction of IscU and IscS the fluorescence of EYFP should be increased at the bleaching area. Scale bars: 1 µm.

The FRET measurement for the co-expression of mCherry-IscU with EYFP-IscS in WT (DE3) is visualized in Figure 38. To measure the FRET signal, the acceptor bleaching method was applied. That meant if the acceptor was bleached in this area the fluorescence intensity of the donor will be increased in case of an interaction of both proteins. Therefore it is visible that the fluorescence of mCherry (acceptor) was bleached in one area (Figure 38, mCherry channel right), which is visible as a black hole. In the case of IscU and IscS protein interaction, the EYFP fluorescence will be increased exactly in this area where the mCherry fluorescence was bleached. However, the difference between the fluorescence intensity of EYFP before and after bleaching is not detectable to the naked eye (Figure 38, lower lane left and right).

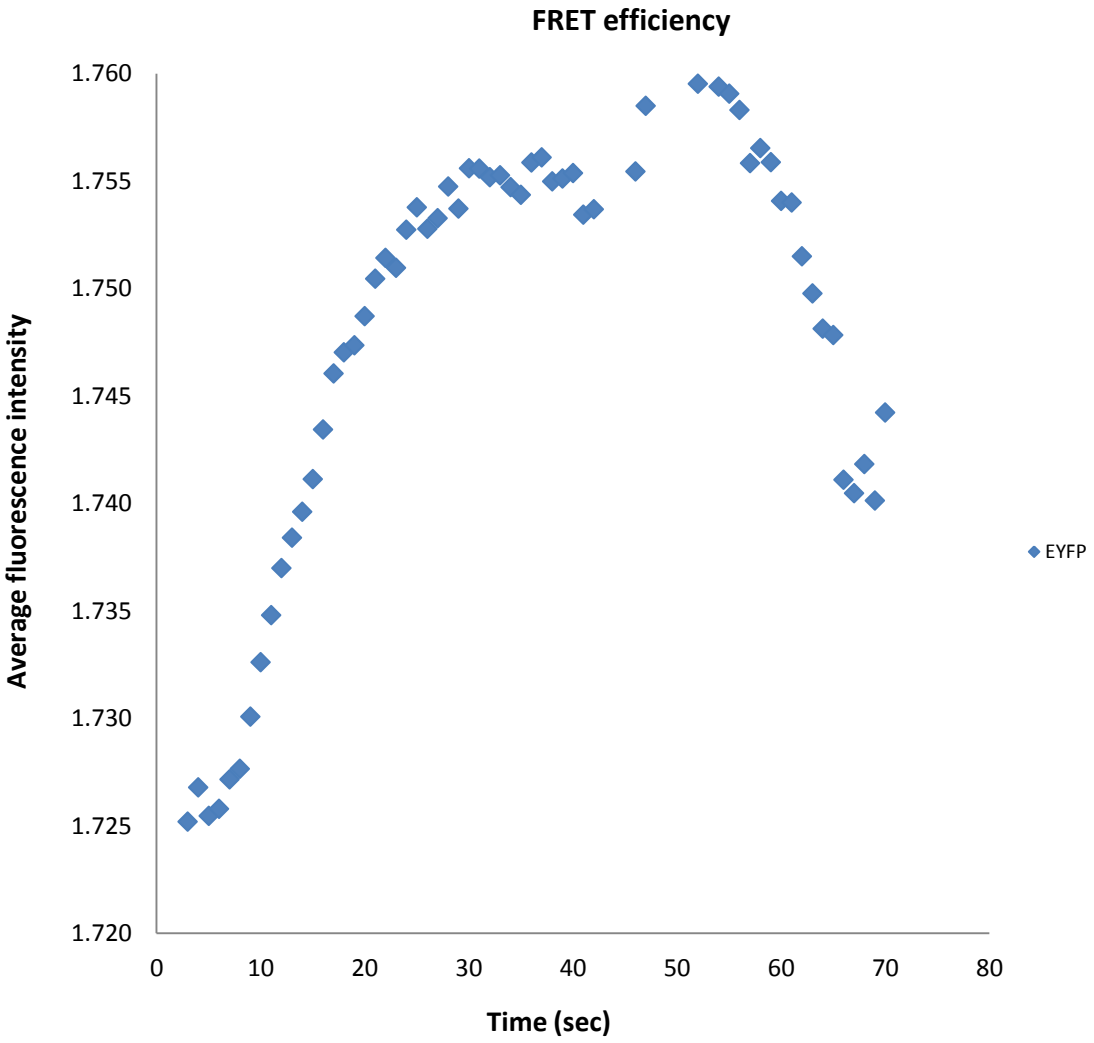

Figure 39: FRET efficiency for the interaction of mCherry-IscU with EYFP-IscS in BW25113 (DE3) strain.

BW25113 (DE3) cells are transformed with a plasmid, which contains the fusion protein construct (mCherry-*iscU*-pCDFDuet-1) and EYFP-*iscS*-pET28a vector. The cells were cultivated with the respective antibiotics in LB-0% NaCl for 5 h. The expression of the fusion protein was induced 2.5 h after growth initiation with 5 µM IPTG. The y-axis shows the fluorescence intensity which was measured via ImageJ software using the EYFP before and after microscope images (from Figure 35: Co-expression of mCherry-IscU with EYFP-IscS in BW25113 (DE3) strain for FRET). The x-axis visualizes the exposure time. The break of the signal represents the bleaching point. After mCherry acceptor bleaching the EYFP fluorescence intensity revealed a very slight increase which is less than 0.5% for FRET. The data analysis was performed by Dr. Gabriele Malengo at the MPI in Marburg.

The data analysis of the FRET measurement of mCherry-IscU with EYFP-IscS in WT (DE3) is imaged in Figure 39. The break of the signal represents the bleaching point. After bleaching of mCherry acceptor there is a low increase of the EYFP donor fluorescence detectable. The FRET efficiency is about 0.5% which is already very low for a positive control. The reason for to use of IscU-IscS as a positive control for FRET was that the *in vivo* and *in vitro* interaction of the IscU and IscS protein was reported previously (Raulfs *et al.*, 2008; Shi *et al.*, 2010).

But with this method, it was not possible to detect a significant FRET signal. Probably it was not really the right method to detect the interaction of proteins under *in vivo* conditions under the used conditions. Since if the FRET efficiency was already so low for the positive control and even in the WT (DE3) strain, so for Δ*tusA* strain it would be probably very hard to detect any signal. As already explained in part (Growth of BW25113 and Δ*tusA*) the Δ*tusA* strain grows slower than the WT, which also resulted in lower fluorescence intensities than in WT (DE3) samples.

4.7 Complementation of Δ*tusA* growth defect by FtsZ and DksA overexpression

In the report of Ishii *et al.* were identified two multicopy suppressors of Δ*tusA* in a complementation study, namely the *ftsZ* and *dksA* genes. They transformed Δ*tusA* with a plasmid library construct and analyzed the colony-forming ability of Δ*tusA* on LB-0.2% agar plates since Δ*tusA* was not able to form colonies in this LB-0.2% (rich-) medium. So within this assay, it was determined that the *dksA* and *ftsZ* genes both can suppress the lethality of Δ*tusA* cells. They allow the Δ*tusA* cells to form colonies on LB-0.2% agar plates, grow faster and have rod cell shape. Thus, the insertion of multicopy suppressor genes like *ftsZ* or *dksA* leads to Δ*tusA* cells, which are able to grow in a rich medium as rod-shaped cells similar to WT cells. However, the effect of *tusA* deletion on the FtsZ ring formation and thus the cell separation remains unclear (Ishii *et al.*, 2000). In addition, it is known that DksA is involved in the transcription of genes during transcript elongation by binding directly to RNA polymerase (Perederina *et al.*, 2004).

After gaining the knowledge that cultivation with IPTG caused stress, and led to retarded growth and aberrant cell morphology of the used strains (see chapter 4.2) further complementation assays were done without IPTG. It was aimed to complement the growth defect of Δ*tusA* strain by expressing the *ftsZ* gene from the pET15b plasmid via translation on the basal level. Therefore the WT (DE3) and Δ*tusA* (DE3) cells were transformed with pET15b-*ftsZ* or the empty pET15b plasmid (Figure 40).

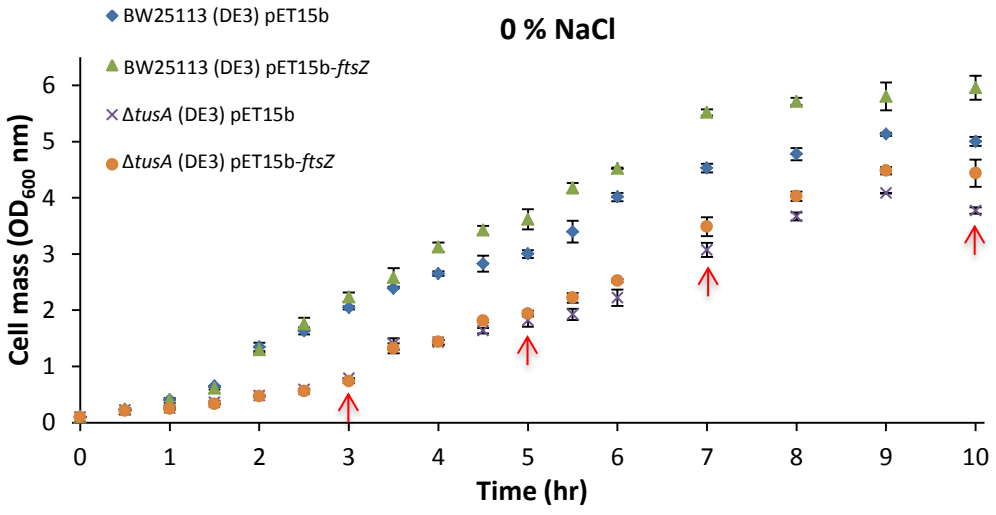

Figure 40: Complementation assay of Δ*tusA* (DE3) growth defect by overexpression of FtsZ.

BW25113 (DE3) and Δ*tusA* (DE3) strains were transformed with pET15b-*ftsZ* for FtsZ overexpression or with the corresponding empty pET15b vector. Cells were grown in 50 ml cultures of LB-0% NaCl at 37 °C, 180 rpm for 10 h. Cell density was recorded by measuring OD_{600}. The start OD_{600} was 0.05. Red arrows indicate the time at which 2 ml cells were collected for microscopy studies.

FtsZ-expressing WT (DE3) cells showed a slightly increased growth compared to control WT (DE3) cells (Figure 40). Δ*tusA* (DE3) cells with FtsZ overexpression had nearly the same growth as their respective control. So, concerning the growth FtsZ overexpression could not complement the Δ*tusA* growth defect.

The cell morphology was also analyzed via phase contrast microscopy to prove the effect of FtsZ overexpression on Δ*tusA* (DE3) cells.

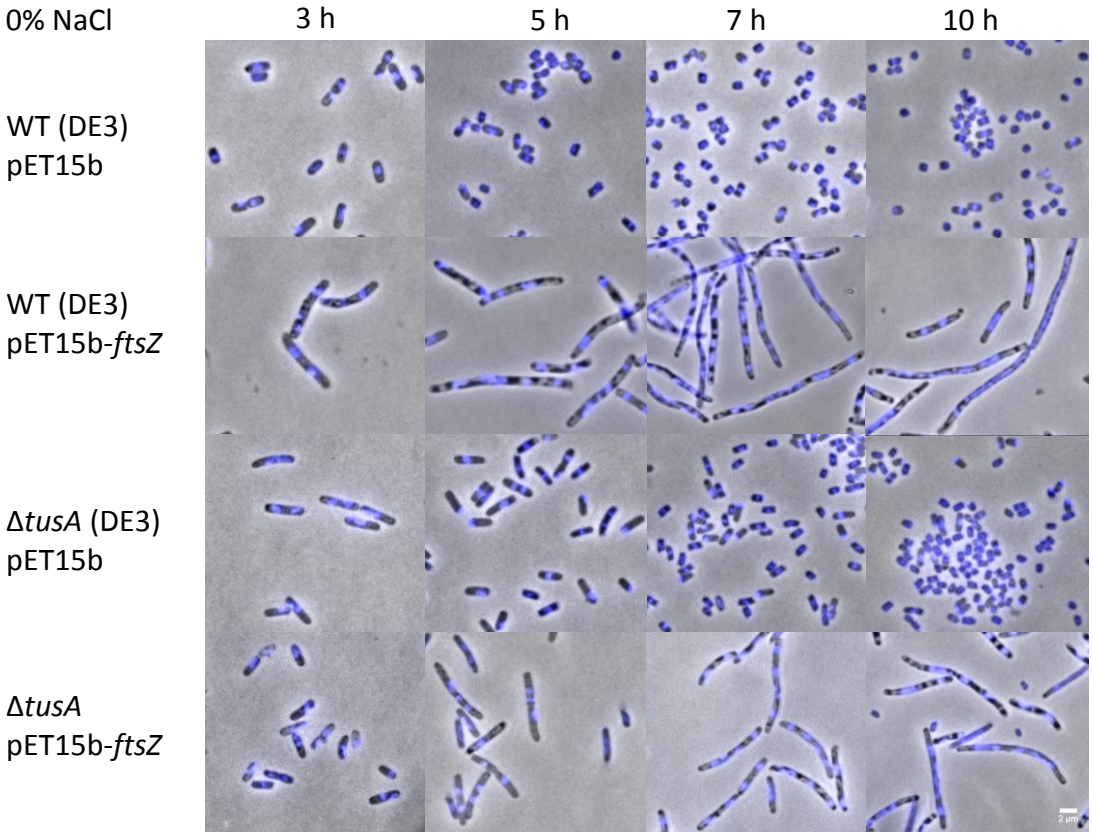

Figure 41: Impact of FtsZ overexpression on WT (DE3) and Δ*tusA* (DE3) cell morphology.

WT (DE3) and Δ*tusA* (DE3) were grown in LB-0% NaCl and samples (2ml) were analyzed at 3 h, 5 h, 7 h and 10 h after inoculation. WT (DE3) cells with empty pET15b (upper panel), with *ftsZ* overexpression (second panel), Δ*tusA* (DE3) with empty pET15b (third panel), and with *ftsZ* overexpression (lower panel). DNA is stained with DAPI 1:1000 and has a blue fluorescence. Scale bars: 2 µm.

Figure 41 represents the result of morphology observation. FtsZ overexpression resulted in longer WT (DE3) filaments compared to the control WT (DE3) cells which had the typical rod shape (around 1-2 µm). The cell length of the filaments further increased with the increasing growth time (Figure 41 second panel, 7 h and 10 h). A similar effect of FtsZ overexpression was visible on Δ*tusA* (DE3) cells. Filaments were detectable as FtsZ was overexpressed in Δ*tusA* (DE3) strain, whereas the cells were not as long as FtsZ expressing WT (DE3) cells. The filaments had many nuclei which were visible in the blue DAPI-stained DNA. But they were still in one cell which is covered by the cell membrane. So this assay revealed no complementation of growth and cell division defect of Δ*tusA* (DE3) strain by overexpression of the *ftsZ* gene (as it was reported in Ishii *et al.*, 2000).

Based on the reported findings of Ishii *et al.*, 2000 that *dksA* gene expression influences the Δ*tusA* growth and cell division the effect of DksA overexpression was tested on WT (DE3) and Δ*tusA* (DE3) cells. It was aimed to investigate whether overexpression of DksA leads to the complementation of Δ*tusA* growth and cell division (Figure 42).

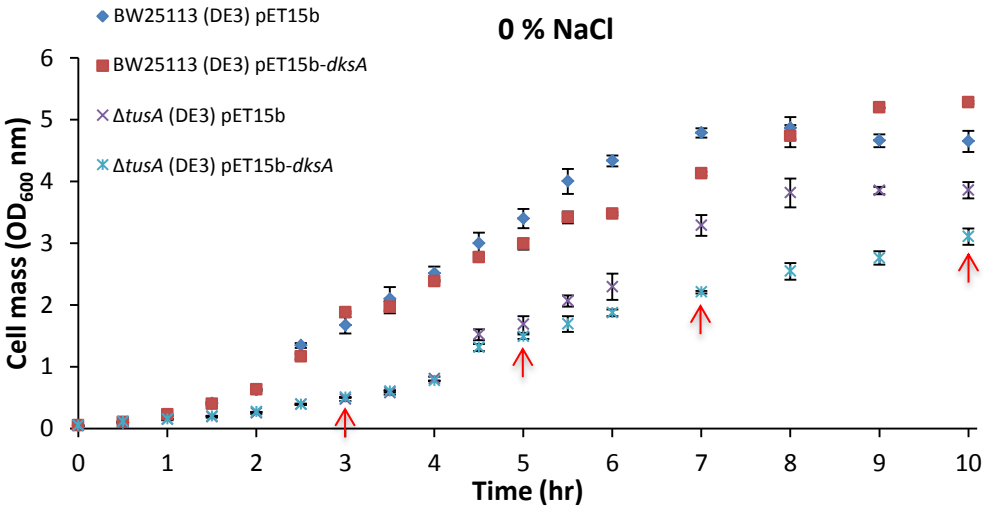

Figure 42: Complementation assay of Δ*tusA* (DE3) growth defect by overexpression of DksA.

BW25113 (DE3) and Δ*tusA* (DE3) strains were transformed with pET15b-*dksA* for DksA overexpression or with the corresponding empty pET15b vector. Cells were grown in 50 ml cultures of LB-0% NaCl at 37 °C, 180 rpm for 10 h. Cell density was recorded by measuring OD_{600}. The start OD_{600} was 0.05. Red arrows indicate the time at which 2 ml cells were collected for microscopy studies.

The DksA expression did not affect WT growth (Figure 42). Only DksA-expressing Δ*tusA* cells displayed a slightly decreased growth compared to their control.

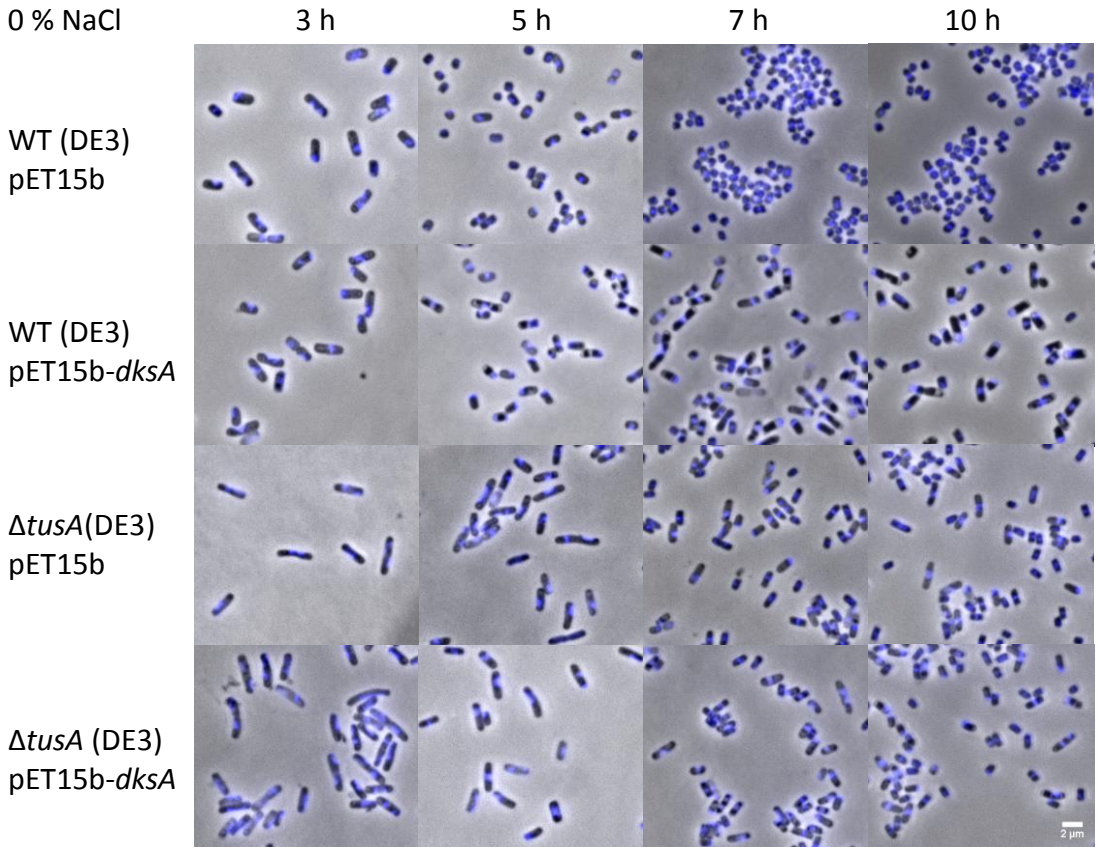

Figure 43: Impact of DksA overexpression on WT (DE3) and Δ*tusA* (DE3) cell morphology.

WT (DE3) and Δ*tusA* (DE3) were grown in LB-0% NaCl and samples (2ml) were analyzed at 3 h, 5 h, 7 h and 10 h after inoculation. WT (DE3) cells with empty pET15b (upper panel), with *dksA* overexpression (second panel), Δ*tusA* (DE3) with empty pET15b (third panel), and with *dksA* overexpression (lower panel). DNA is stained with DAPI 1:1000 and has a blue fluorescence. Scale bars: 2 µm.

The phase contrast analysis (Figure 43) revealed that DksA overexpression was not affecting the WT (DE3) cell morphology since the cells showed the same short cell morphology as the control WT (DE3) cells. The result was the same for Δ*tusA* (DE3) cells. When DksA was overexpressed, the cells were long and filamentous like the respective control Δ*tusA* (DE3) cells (Figure 43, third and lower panel). Therefore, the cell length shortening effect of DksA expression on Δ*tusA* cells was not visible as it was reported in the literature (Ishii *et al.*, 2000).

4.8 Growth of deletion strains in genes involved in mnm^{5}s^{2}U34 tRNA thiolation

The next approach was to check whether only the deletion of *tusA* led to the cell division defect or remaining proteins in tRNA thiolation were also responsible for this defect. A defect in tRNA thiolation had probably a negative effect on the FtsZ protein which resulted in no cell division. So to investigate whether the cell division defect derived only from *tusA* deletion or from a defect in tRNA thiolation, cell growth and morphology were analyzed of the protein deletion strains of IscS, TusD, TusE and MnmA of mnm^{5}s^{2}U34 tRNA thiolation.

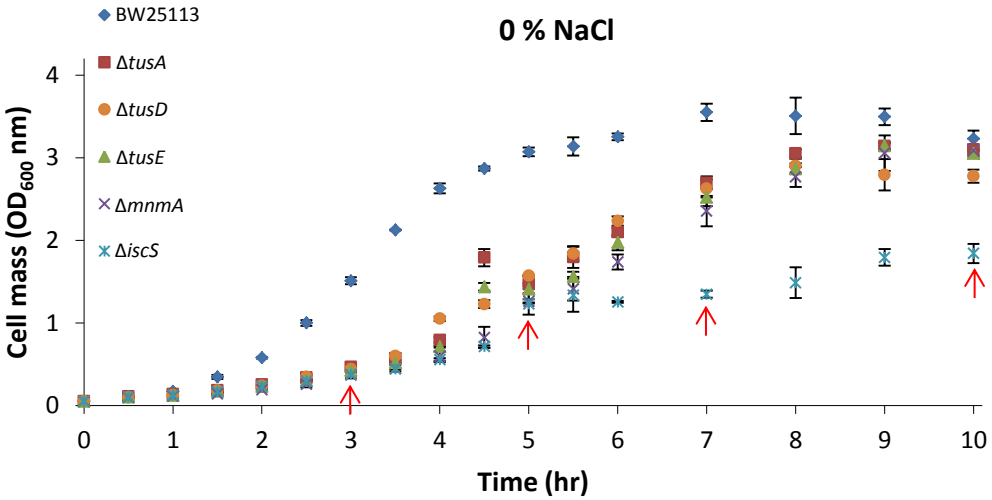

Figure 44: Growth curves of BW25113, Δ*tusA* and deletion strains in genes involved in mnm^{5}s^{2}U34 tRNA thiolation (Δ*tusD*, Δ*tusE*, Δ*mnmA*, Δ*iscS*).

Cells of all strains were grown in 50 ml cultures of LB-0% NaCl at 37 °C, 180 rpm for 10 h. The increasing cell density was recorded in the first six hours every 30 min and later every hour by measuring the optical density at 600 nm (OD_{600}). The start OD_{600} was 0.05. Red arrows indicate the time at which 2 ml cells were collected for microscopy studies.

The recorded growth curves show that the Δ*tusD,* Δ*tusE* and Δ*mnmA* cells have the same growth as the Δ*tusA* strain (Figure 44). Only Δ*iscS* cells showed an even more reduced growth phenotype than Δ*tusA* cells. Additionally, cell samples were collected in the exponential and stationary phase of every strain to investigate the cell morphological differences (Figure 45).

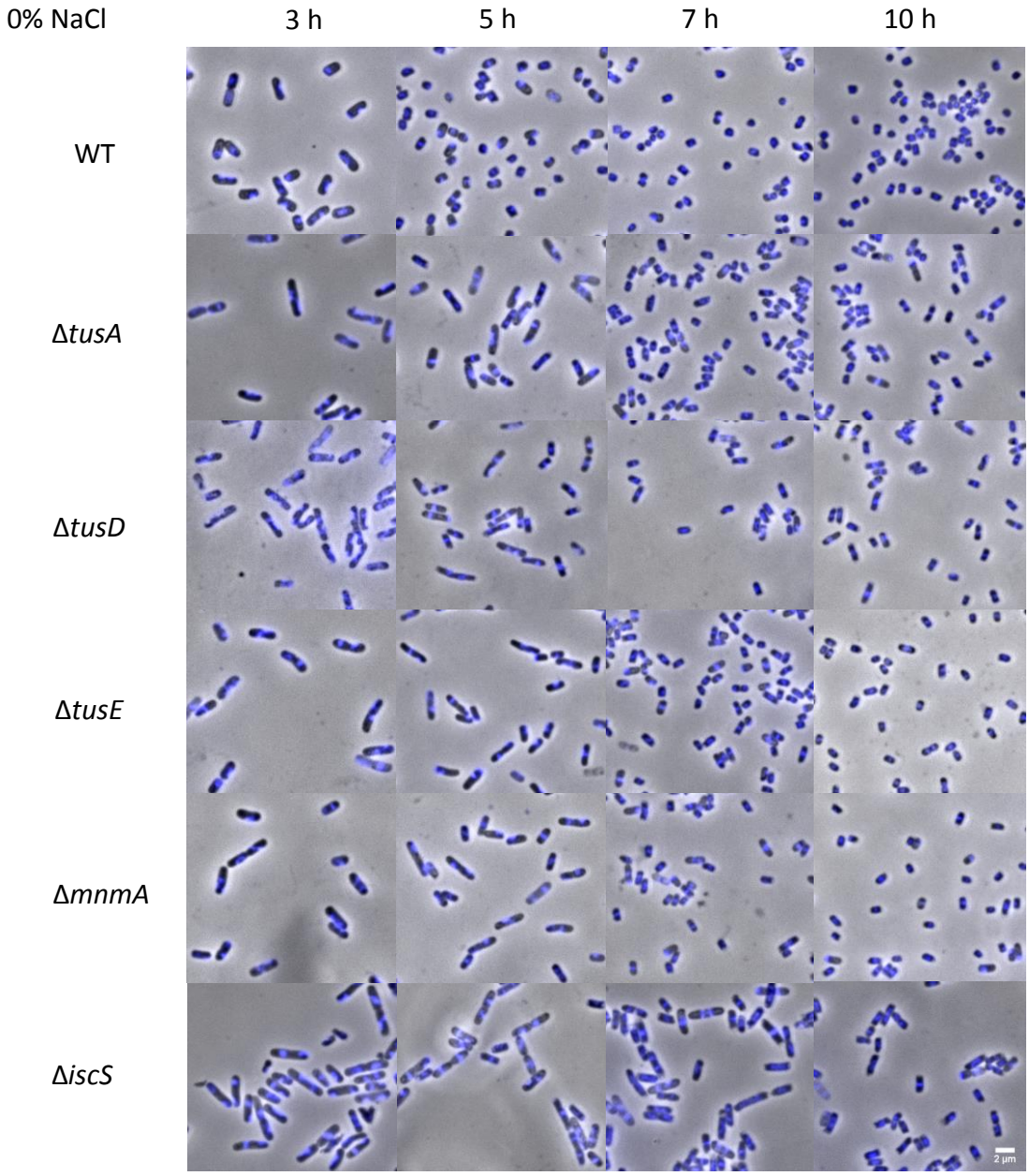

Figure 45: Cell morphology analysis of WT, Δ*tusA* and gene deletion strains of mnm^{5}s^{2}U34 tRNA thiolation.

WT (upper panel), Δ*tusA* (second panel), Δ*tusD* (third panel), Δ*tusE* (fourth panel), Δ*mnmA* (fifth panel) and Δ*iscS* (sixth panel) cells were grown in LB-0% NaCl and 2 ml cells were analyzed at 3 h, 5 h, 7 h and 10 h after inoculation. DNA is stained with DAPI 1:1000 and has a blue fluorescence. The morphology of the cells was observed by fluorescence microscopy. Scale bars: 2 µm.

All tested gene deletion strains of mnm^{5}s^{2}U34 tRNA thiolation exhibited similar cell morphology as Δ*tusA* cells (Figure 45). They were longer in the exponential phase (3 h and 5 h) and shorter in the stationary phase (7 h and 10 h). Only Δ*iscS* cells were slightly longer than Δ*tusA*, Δ*tusD*, Δ*tusE* and Δ*mnmA* cells in the stationary phase. But this was caused by

the slower growth of Δ*iscS* cells. These results show that the cell division defect might be derived from a defect in mnm^{5}s^{2}U34 tRNA thiolation.

So if the cell division defect derives from a defect in mnm^{5}s^{2}U34 tRNA thiolation then other mutated strains, which are not involved in mnm^{5}s^{2}U34 tRNA thiolation, should show normal short rod-shaped cells and not filaments. To examine this idea growth and morphology analysis were carried out for Δ*iscU*, Δ*moaD*, Δ*thiI*, Δ*miaB* and Δ*ttcA* strains. The IscU protein is involved in Fe-S cluster biosynthesis, MoaD in Moco biosynthesis, ThiI in thiamine biosynthesis, MiaB in ms^{2}i^{6}adenosine and TtcA in s^{2}cytidine modifications (Leimkühler, 2014). SufS is a cysteine desulfurase protein that mobilizes sulfur. It is a homologous protein of IscS and is expressed under stress conditions. Furthermore, it can complement the defective Fe-S cluster biosynthesis in the Δ*iscS* strain (Bühning *et al.*, 2017). Additionally to the other non-tRNA thiolation strains, Δ*sufS* was also tested to show if it shared similarities in growth behavior with Δ*tusA*.

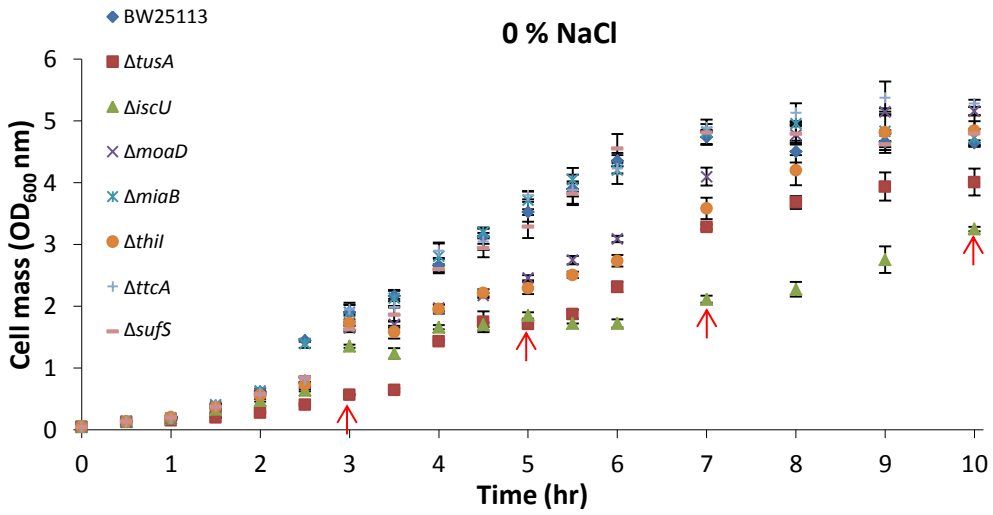

Figure 46: Growth curves of BW25113, Δ*tusA* and deletion strains in genes that are not involved in mnm^{5}s^{2}U34 tRNA thiolation (Δ*iscU*, Δ*moaD*, Δ*miaB*, Δ*thiI*, Δ*ttcA*, Δ*sufS*).

Cells of all strains were grown in 50 ml cultures of LB-0% NaCl at 37 °C, 180 rpm for 10 h. The increasing cell density was recorded in the first six hours every 30 min and later every hour by measuring the optical density at 600 nm (OD_{600}). The start OD_{600} was 0.05. Red arrows indicate the time at which 2 ml cells were collected for microscopy studies.

Figure 46 represents the result of the growth of the different mutant strains. Δ*miaB* and Δ*ttcA* cells behaved as WT cells. In addition, Δ*sufS* showed the same growth behavior as the WT strain. Δ*moaD* and Δ*thiI* cells showed a slightly decreased growth than WT cells but were

still higher than Δ*tusA* cells. The slowest growth was visible for Δi*scU* cells. Also, for these strains, cells were collected in exponential and stationary phases for phase contrast analysis.

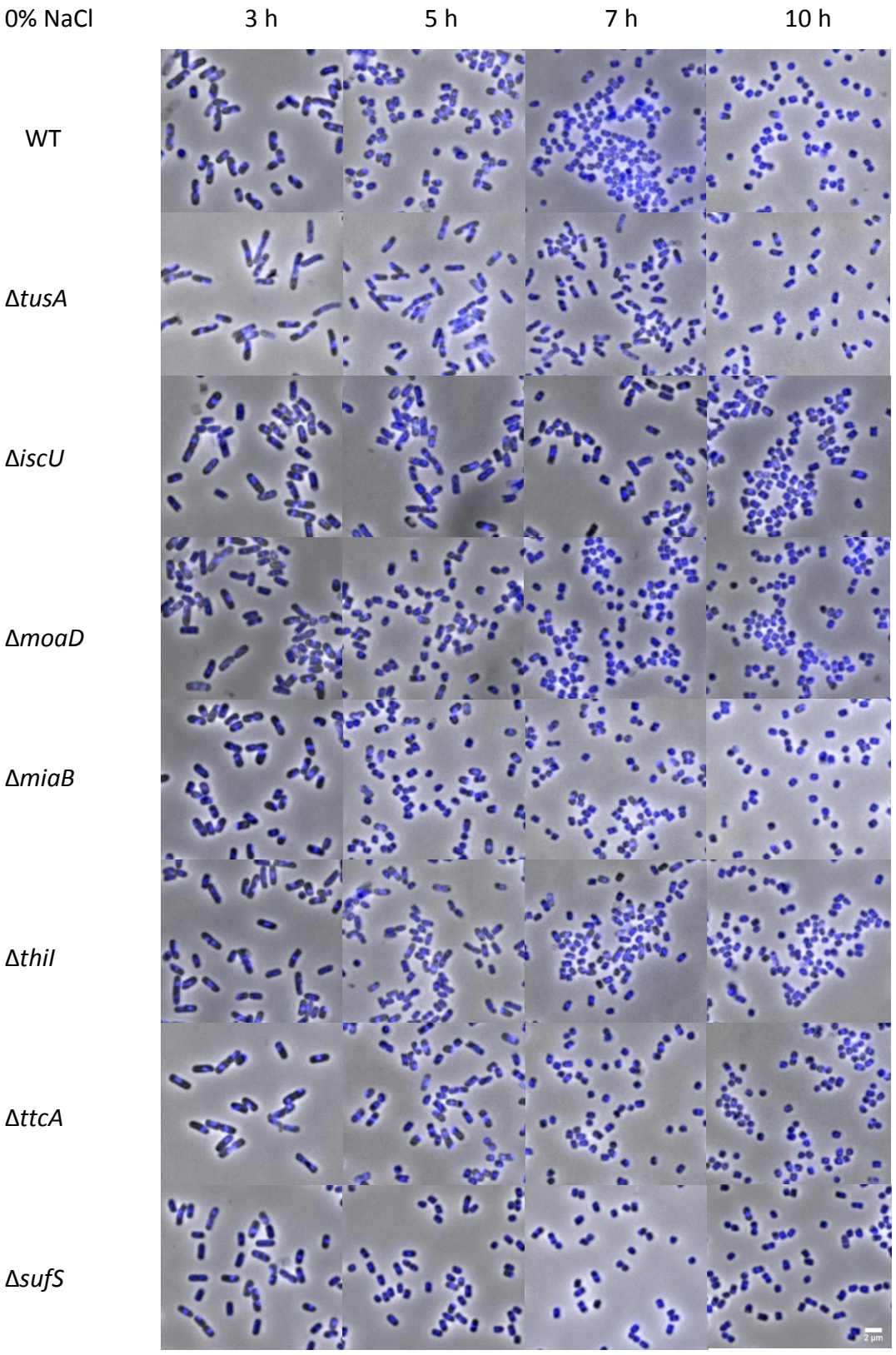

Figure 47: Cell morphology analysis of WT, Δ*tusA* and gene deletion strains that are not involved in mnm^{5}s^{2}U34 tRNA thiolation.

WT (first panel), Δ*tusA* (second panel), Δ*iscU* (third panel), Δ*moaD* (fourth panel), Δ*miaB* (fifth panel), Δ*thiI* (sixth panel), Δ*ttcA* (seventh panel) and Δ*sufS* (eight panel) cells were grown in LB-0% NaCl and 2ml cells were analyzed at 3 h, 5 h, 7 h and 10 h after inoculation. DNA is stained with DAPI 1:1000 and has a blue fluorescence. The morphology of the cells was observed by fluorescence microscopy. Scale bars: 2 µm.

For cells of every tested strain (except Δ*iscU*) similar rod-shaped cell morphology was detected as for WT cells (Figure 47). Only Δ*iscU* cells had a cell length, which was not as short as WT cells and not as long as Δ*tusA* cells. They became shorter like the WT cells at 10 h.

Mutant strains, which are not involved in mnm^5s^2U34 tRNA thiolation, exhibited normal typical short, rod-shaped cell morphology like WT cells (except Δ*iscU*) (Figure 47). They showed no filaments. This result indicated that only strains with gene deletions, which are involved in mnm^5s^2U34 tRNA thiolation, showed a growth defect and long, filamentous cells compared to WT (Figure 45). Thus the cell division defect was caused by a defect in mnm^5s^2U34 tRNA thiolation.

After the yielded results it was clear that the cell division defect in Δ*tusA* cells is based on a defect in mnm^5s^2U34 tRNA thiolation. The next approach was to show exactly where the defect in mnm^5s^2U34 tRNA thiolation lies. For this Δ*miaA*, Δ*mnmC* and Δ*mnmE* strains were tested besides WT and Δ*tusA* strains. MnmC and MnmE have other modifying functions than MnmA (Leimkühler *et al.*, 2017; Moukadiri *et al.*, 2013). During the tRNA thiolation MnmA transfers the sulfur to the tRNA uridine at position 34 and leads to the formation of 2-thiouridine. After this further modifications are done by MnmE and MnmC proteins. Depending on the substrate (glycine or ammonium) MnmE (in complex with MnmG) produces $cmnm^5U$ (5-carboxymethylaminomethyluridine) or mnm^5U (5-methylaminomethyluridine). The bi-functional enzyme MnmC can convert $cmnm^5$ to nm^5U and nm^5U to the mature mnm^5U by adding a methyl group (Leimkühler *et al.*, 2017; Moukadiri *et al.*, 2013). MiaA modifies the adenine at position 37 (Aubee *et al.*, 2017). In addition to these strains Δ*rpoS* and Δ*hns* were also investigated. For RpoS was reported that it interacts with the TusA protein (Yamashino *et al.*, 1998). H-NS is a DNA-binding protein and a global regulator (Picker and Wing, 2016). Its amount is increased when the TusA protein is absent (Dahl *et al.*, 2013). It coils the DNA in a different way so that some parts of

the DNA are more accessible for transcription factors and improve the transcription process. Referring to these gene deletion strains the growth and morphology analysis were shown in the next two figures (Figures 48 – 49).

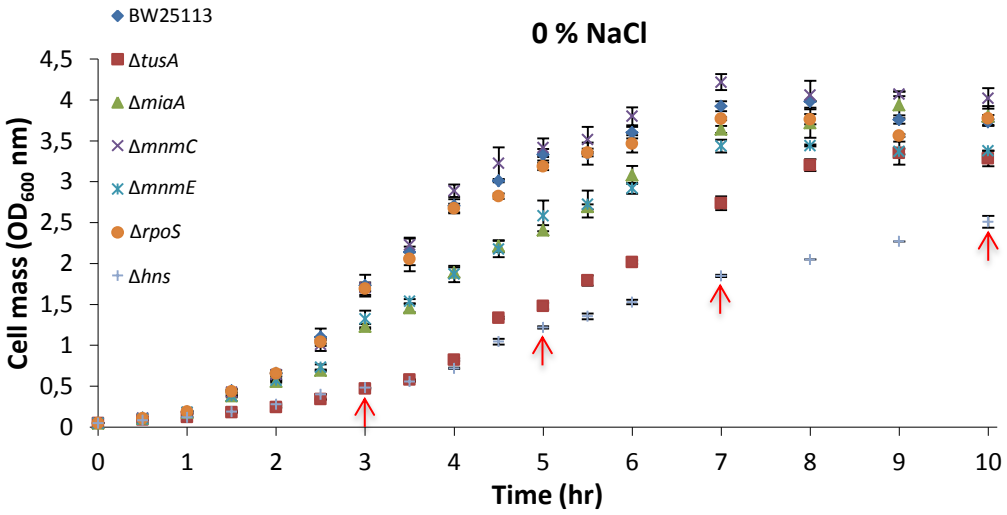

Figure 48: Growth curves of BW25113, Δ*tusA*, Δ*miaA*, Δ*mnmC*, Δ*mnmE*, Δ*rpoS* and Δ*hns*.

Cells of all strains were grown in 50 ml cultures of LB-0% NaCl at 37 °C, 180 rpm for 10 h. The increasing cell density was recorded in the first six hours every 30 min and later every hour by measuring the optical density at 600 nm (OD_{600}). The start OD_{600} was 0.05. Red arrows indicate the time at which 2 ml cells were collected for microscopy studies.

Δ*mnmC* and Δ*rpoS* cells showed no growth defect. Their growth was at the same level as WT (Figure 48). Δ*miaA* and Δ*mnmE* cells represented a slightly decreased growth than WT but were still higher than Δ*tusA*. Δ*hns* cells grew the slowest.

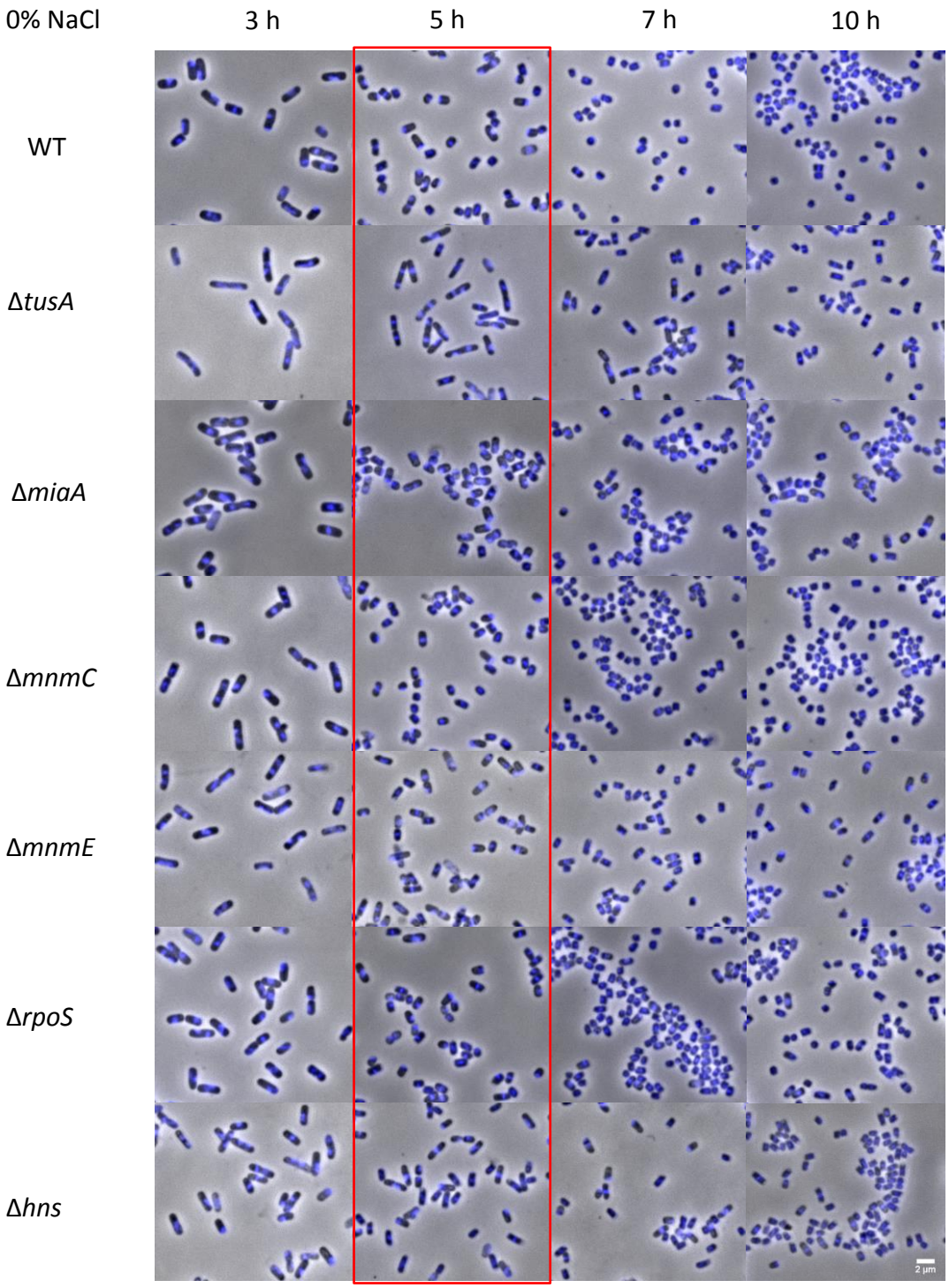

Figure 49: Cell morphology analysis of WT, Δ*tusA*, Δ*miaA*, Δ*mnmC*, Δ*mnmE*, Δ*rpoS* and Δ*hns*.

WT (upper panel), Δ*tusA* (second panel), Δ*miaA* (third panel), Δ*mnmC* (fourth panel), Δ*mnmE* (fifth panel), Δ*rpoS* (sixth panel) and Δ*hns* (lower panel) cells were grown in LB-0% NaCl and 2ml cells were analyzed at 3 h, 5 h, 7 h and 10 h after inoculation. DNA is stained with DAPI 1:1000 and has a blue fluorescence. The morphology of the cells was observed by fluorescence microscopy. The red frame highlights the different cell morphology. Scale bars: 2 µm.

All strains except Δ*tusA* revealed rod-shaped cells like WT (Figure 46). The difference between rod-shaped and filamentous cells was more clearly visible in the exponential phase (Figure 49, 3 h and 5 h).

A further control experiment was performed to confirm that the cell division defect of mnm^{5}s^{2}U34 tRNA thiolation strains was caused by a defective tRNA thiolation and not by another factor. Therefore, overexpression of the *suf* operon was used. The SufS protein is encoded by the *suf* operon (*sufABCDSE*) and is a homologous protein of IscS and is expressed under stress conditions. It is a cysteine desulfurase and mobilizes sulfur. Furthermore, it can complement the defective Fe-S cluster biosynthesis in the Δ*iscS* strain (Bühning *et al.*, 2017). The gene deletion strains of the tRNA thiolation pathway have no defect in Fe-S cluster biosynthesis (Bühning *et al.*, 2017). The effect of the *suf* operon overexpression was tested on WT (DE3), Δ*tusA* (DE3) and Δ*iscS* (DE3) cell growth to exclude that filamentous growth of mnm^{5}s^{2}U34 tRNA thiolation deletion strains was not caused by the defect of Fe-S cluster biosynthesis. All strains were transformed with a pACYCDuet-1 plasmid cloned with the *suf* operon. As controls were used same strains were transformed with the respective empty plasmid.

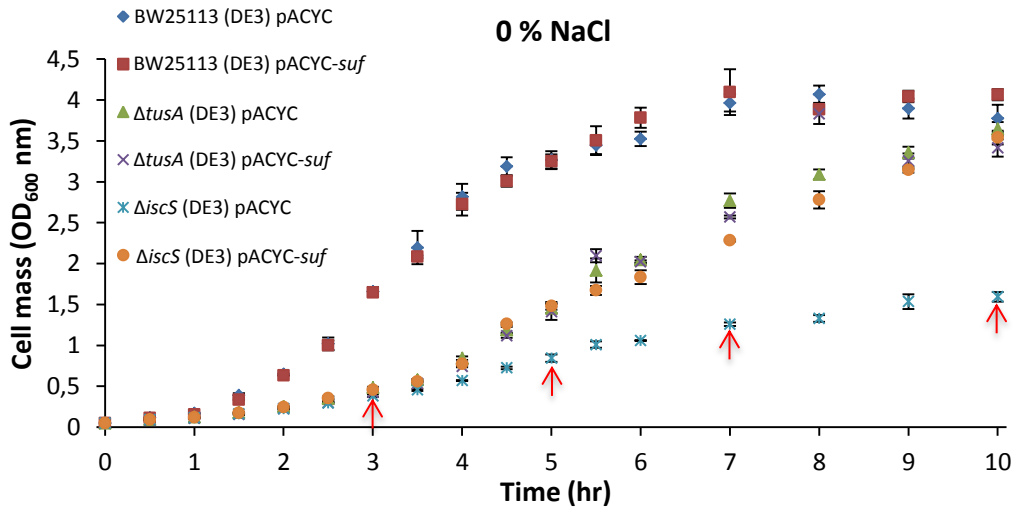

Figure 50: Effect of *suf* operon overexpression on growth of BW25113 (DE3), Δ*tusA* (DE3) and Δ*iscS* (DE3).

BW25113 (DE3), Δ*tusA* (DE3) and Δ*iscS* (DE3) strains were transformed with pACYCDuet-1-*suf* for *suf* operon overexpression or with the corresponding empty pACYCDuet-1 vector. Cells were grown in 50 ml cultures of LB-0% NaCl at 37 °C, 180 rpm for 10 h. Cell density was recorded by measuring OD_{600}. The

start OD_{600} was 0.05. Red arrows indicate the time at which 2 ml cells were collected for microscopy studies.

The expression of *suf* operon had no influence on WT (DE3) and Δ*tusA* (DE3) growth which is shown in Figure 50. The *suf* operon overexpressing cells and their control showed the same growth. But the Δ*iscS* (DE3) showed another phenotype. The control Δ*iscS* (DE3) cells grew worse than Δ*tusA* (DE3) (Figure 50, Δ*iscS* (DE3) pACYC). In contrast to this, the *suf* operon expression led to a higher growth of Δ*iscS* (DE3) (Figure 50, Δ*iscS* (DE3) pACYC-*suf*). The growth defect of Δ*iscS* (DE3) cells was complemented to the level of Δ*tusA* (DE3).

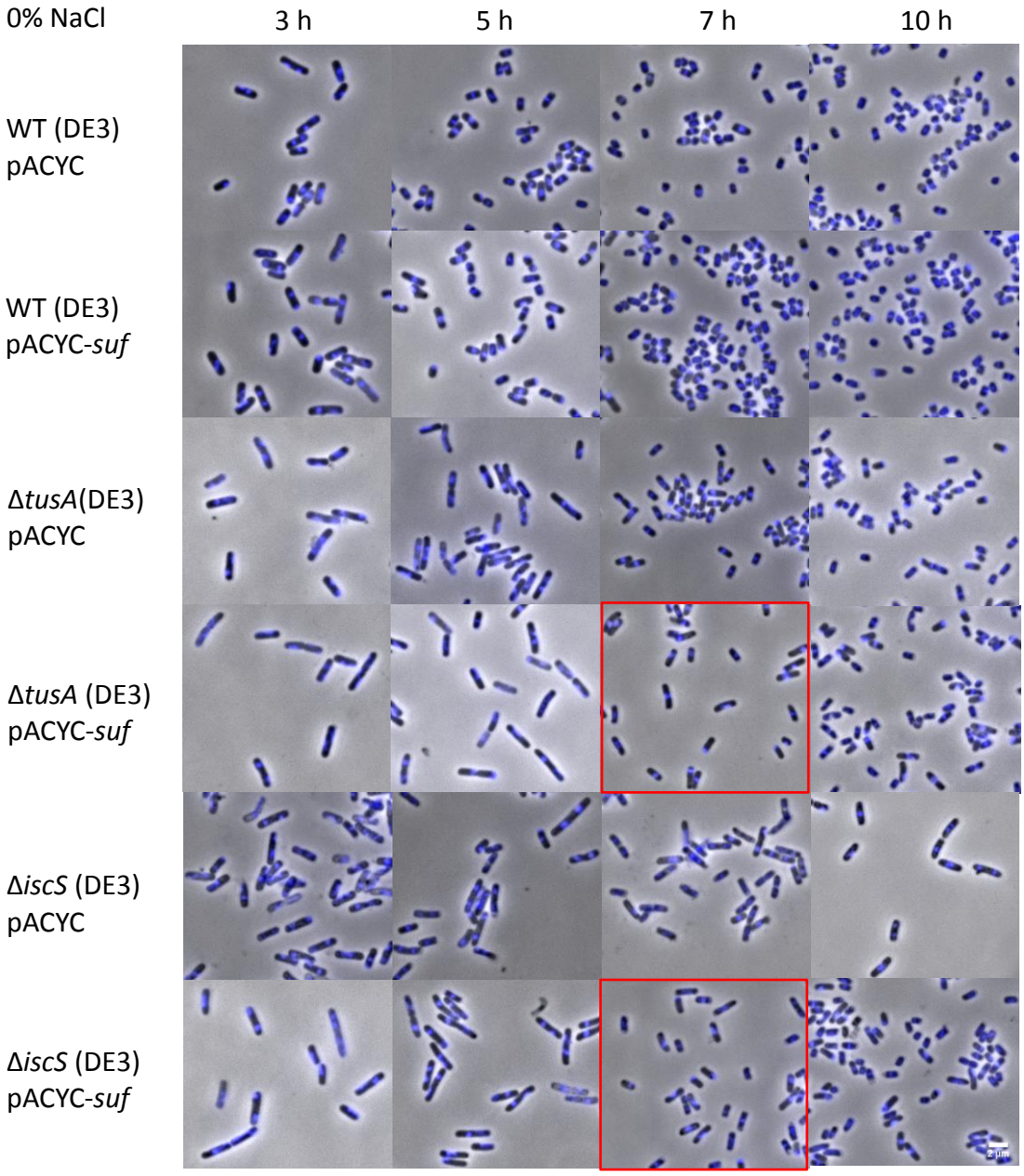

Figure 51: Effect of *suf* operon overexpression on BW25113 (DE3), Δ*tusA* (DE3) and Δ*iscS* (DE3) cell morphology.

WT (DE3), Δ*tusA* (DE3) and Δ*iscS* (DE3) were grown in LB-0% NaCl and samples (2ml) were analyzed at 3 h, 5 h, 7 h, and 10 h after inoculation. WT (DE3) cells with empty pACYCDuet-1 (upper panel), with the *suf* operon expression (second panel), Δ*tusA* cells with empty pACYCDuet-1 (third panel) and with the *suf* operon expression (fourth panel), Δ*iscS* cells with empty pACYCDuet-1 (fifth panel) and with the *suf* operon expression (sixth panel). DNA is stained with DAPI 1:1000 and has a blue fluorescence. The red frames highlight the similar shortened cell shape of Δ*tusA* (DE3) and Δ*iscS* (DE3) by the *suf* operon expression in contrast to control Δ*iscS* (DE3). Scale bars: 2 μm.

The microscopy analysis of WT (DE3) and Δ*tusA* (DE3) cell morphology is shown in Figure 51. WT (DE3) and Δ*tusA* cells with the *suf* operon overexpression depicted the same morphology as their respective controls. WT (DE3) cells were short and rod-shaped (Figure 51, upper and second panel). Δ*tusA* (DE3) cells were long, filamentous in the exponential phase and short, rod-shaped in the stationary phase compared to WT (DE3) (Figure 51, third and fourth panel). The noticeable observation in this assay was that the *suf* operon expression in Δ*iscS* (DE3) revealed the same shortened cell shape in the stationary phase as Δ*tusA* (DE3) (Figure 51, sixth panel 7 h, red frames). The respective Δ*iscS* (DE3) control cells were longer at the same time (Figure 51, fifth panel 7 h). This shortening of cell length by *suf* operon overexpression in Δ*iscS* (DE3) emphasizes on the morphological level that the growth defect was complemented to Δ*tusA* (DE3) level. So, the *suf* operon overexpression complemented only the part of the growth defect which was caused by a defect in Fe-S cluster biosynthesis in Δ*iscS* (DE3). The remaining growth defect compared to WT cells was only caused by a defective mnm^5s^2U34 tRNA thiolation. Both results, growth behavior (Figure 50) and morphological phenotype (Figure 51), confirmed the idea that the growth and cell division defect was caused by a defect in mnm^5s^2U34 tRNA thiolation since the *suf* operon overexpression did not affect the growth of the Δ*tusA* (DE3). Compared to WT (DE3), Δ*tusA* (DE3) strain still grew slowly and formed filaments. The *suf* operon overexpression was only a control and complements only the defect in Fe-S cluster biosynthesis, which occurs in Δ*iscS* (DE3) due to the absence the of IscS protein. So using this as a control supported to highlight that the growth and cell division defect of *tusA*-deficient cells was based only on a defect in mnm^5s^2U34 tRNA thiolation.

To confirm this result also on the protein level an immunoblot was carried out for the detection of the SufS protein. Cells of WT, Δ*tusA,* Δ*sufS* and Δ*iscU* were cultivated in 50 ml cultures of LB-0% NaCl at 37 °C, 180 rpm for 5 h. They were harvested, sonicated and the protein concentration of the supernatant was determined by Bradford. 50 µg protein of every supernatant sample was loaded on 12% SDS-Gel and the protein bands were blotted on a nitrocellulose membrane via western blot.

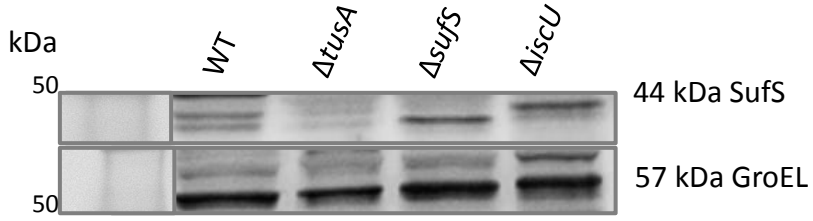

Figure 52: Detection of cellular SufS amount in BW25113 (WT), Δ*tusA*, Δ*sufS*, Δ*iscU*.

Cells of WT, Δ*tusA,* Δ*sufS* and Δ*iscU* were cultivated in 50 ml cultures of LB-0% NaCl at 37 °C, 180 rpm for 5 h. After 5 h cells were harvested, sonicated and the protein concentration of the supernatant was determined by Bradford. 50 µg protein of every supernatant sample was loaded on the SDS-Gel (12%) and then transferred on a nitrocellulose membrane. The Prestained Protein Molecular Weight Marker (Fermentas, 20 kDa – 120 kDa) was used for size determination. Blots were incubated with α-SufS (chicken) antibody 1:2000 diluted at 4 °C, ON and with α-GroEL (rabbit, abcam) antibody 1:10000 diluted at 4°C, ON. The detection of α-SufS antibody was done using α-chicken POD-conjugated secondary antibody (goat, abcam) 1:5000 diluted and for α-GroEL antibody, by α-rabbit POD-conjugated secondary antibody (goat, Sigma) 1:10000 diluted for 1 h at RT. The protein bands were detectable via chemiluminescence. SufS is visible at 44 and GroEL 57 kDa. Δ*tusA* strain contained no SufS protein whereas SufS was present in WT and Δ*iscU* (in Δ*iscU* is the cellular SufS amount increased).

Figure 52 shows the result of cellular SufS protein amount detection in WT, Δ*tusA*, Δ*sufS* and Δ*iscU* cells. WT strain showed two close bands, in which the upper protein band is around 44 kDa for the SufS protein. This SufS protein band was absent in Δ*tusA*, whereas, in the Δ*iscU* strain, SufS was slightly higher than WT. Thus, the absence of SufS protein in Δ*tusA* strengthened the idea that the growth and cell division defect was based on a defect in mnm^5s^2U34 tRNA thiolation. Since the Fe-S cluster biosynthesis is working properly in the Δ*tusA* strain it contained no SufS protein. Moreover, Δ*iscU* had a defect in Fe-S cluster biosynthesis which explained the higher SufS amount to compensate for the defect. As loading control, the GroEL protein was detected at 57 kDa which is almost similar in all tested strains (Figure 52).

4.9 Complementation of Δ*tusA* growth defect by RpoS overexpression

A further interesting candidate was RpoS, which interacts with TusA since it was reported that the deletion of the *tusA* gene affects the stability of RpoS (Yamashino *et al.*, 1998; Aubee *et al.*, 2017). To check this WT and Δ*tusA* cells were transformed with the empty pACYCDuet-1 plasmid and with pACYCDuet-1-*rpoS*. It was aimed to test whether the expression of *rpoS* can complement the growth defect and filaments of Δ*tusA* cells.

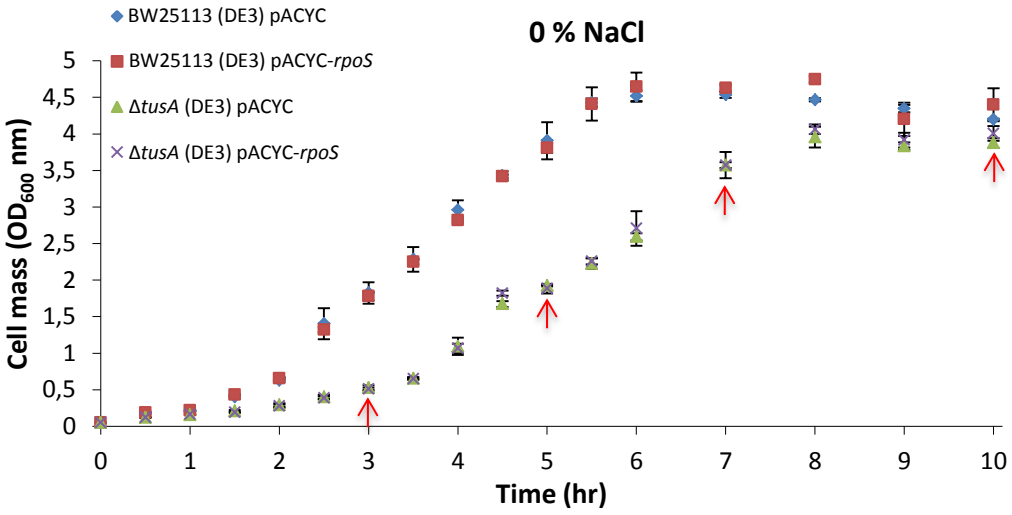

Figure 53: Effect of RpoS overexpression on growth of BW25113 (DE3) and Δ*tusA* (DE3).

BW25113 (DE3) and Δ*tusA* (DE3) strains were transformed with pACYCDuet-1-*rpoS* for RpoS overexpression or with the corresponding empty pACYCDuet-1 vector. Cells were grown in 50 ml cultures of LB-0% NaCl at 37 °C, 180 rpm for 10 h. Cell mass was observed by measuring OD_{600}. The start OD_{600} was 0.05. Red arrows indicate the time to which 2 ml cells were collected for microscopy studies.

Both strains, WT (DE3) and Δ*tusA* (DE3), displayed the same growth with and without RpoS overexpression (Figure 53).

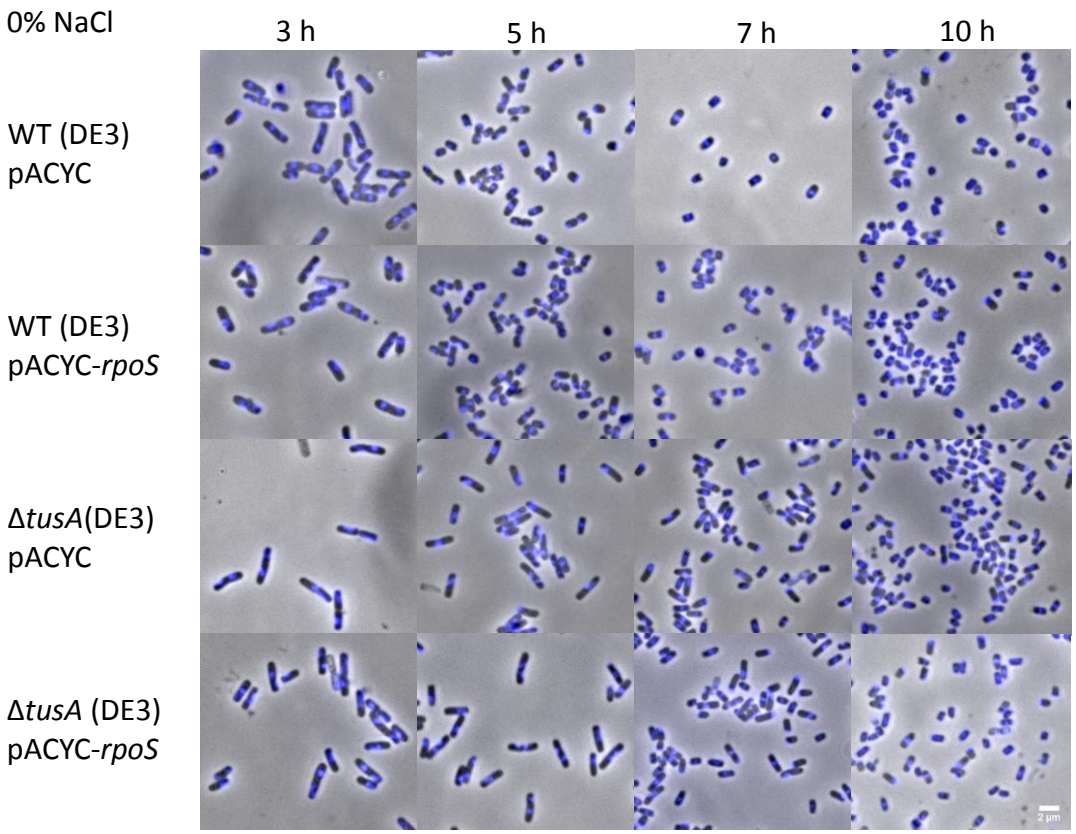

Figure 54: Effect of RpoS overexpression on BW25113 (DE3) and Δ*tusA* (DE3) cell morphology.

WT (DE3) and Δ*tusA* (DE3) were grown in LB-0% NaCl and samples (2ml) were analyzed at 3 h, 5 h, 7 h and 10 h after inoculation. WT (DE3) cells with empty pACYCDuet-1 (first panel), with *rpoS* expression (second panel), Δ*tusA* (DE3) cells with empty pACYCDuet-1 (third panel), with *rpoS* expression (fourth panel). DNA is stained with DAPI 1:1000 and has a blue fluorescence. Scale bars: 2 µm.

The cell morphology analysis confirmed the results of the recorded growth curves (Figure 54). WT (DE3) cells with and without RpoS overexpression had the typical *E. coli* short rod shape. For Δ*tusA* (DE3) cells and RpoS expressing Δ*tusA* (DE3) cells were also determined the same cell morphology. They have both longer filamentous cells than WT (DE3). The results indicated that the RpoS overexpression could not complement the growth defect of Δ*tusA* cells.

4.10 Detection of cellular FtsZ amount in BW25113 and Δ*tusA*

After finding an obvious, visible cell division defect of the pure Δ*tusA* strain, which is very clearly visible at 5 h of growth (they grew as filaments and were longer than the WT cells at the same time (Figure 41, third and first panel)), it seemed very important to investigate the cellular FtsZ amount. Since the cell division problem was caused by a defect in the FtsZ assembly, which is the main contractile force for cell division. In addition, the amount of FtsZ changes during cell growth since it should be first produced until the cells reach the division step (Weart and Levin, 2003). Therefore, it was important to analyze the amount of FtsZ protein and how it changes during growth in different strains. For this purpose, the FtsZ amount was examined in Δ*tusA* and WT strains at 5 h of growth (since the morphological difference in the pure strains was clearly visible at that time), to determine whether there was a difference between WT and Δ*tusA* strains. The expectation was that there was a difference, which led to the filaments of Δ*tusA* strain already without overexpression of FtsZ protein. The detection of the cellular FtsZ amount was performed via an immunoblot (Figure 55).

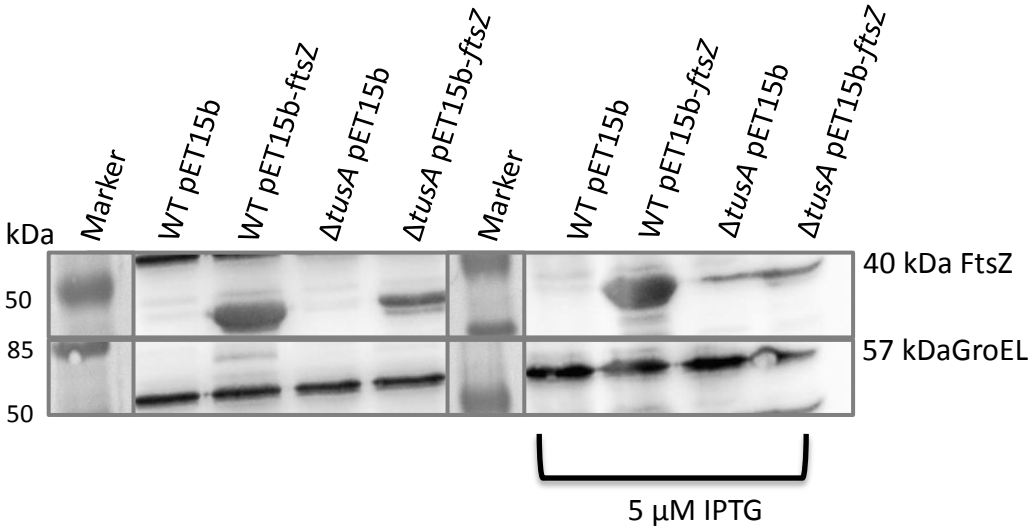

Figure 55: Detection of cellular amount of FtsZ in WT (DE3) and Δ*tusA* (DE3) with and without induction of FtsZ overexpression.

BW25113 (WT) (DE3) and Δ*tusA* (DE3) strains were transformed with pET15b-*ftsZ* or the corresponding empty pET15b vector. Cells of both strains were cultivated in 50 ml cultures of LB-0% NaCl at 37 °C, 180 rpm for 5 h. The first four samples (left to right) show FtsZ overexpression without IPTG and the last four samples with 5 µM IPTG. WT (DE3) cells with empty pET15b (second lane), with *ftsZ* overexpression (third lane), Δ*tusA* (DE3) cell with empty pET15b (fourth lane) and with *ftsZ* overexpression (fifth lane).

After 5 h cells were harvested, sonicated and the protein concentration of the supernatant was determined by Bradford. 50 µg protein of every supernatant sample was loaded on the SDS-Gel (12%) and then transferred on a PVDF membrane. The first and sixth lanes show the Prestained Protein Molecular Weight Marker (Fermentas, 20 kDa – 120 kDa) which was used for size determination. Blots were incubated with the α-FtsZ (rabbit) antibody 1:20000 diluted at RT, 1 h and with α-GroEL (rabbit, abcam) antibody 1:10000 diluted at 4 °C, ON. The detection of both antibodies was done using α-rabbit POD-conjugated secondary antibody (goat, Sigma) 1:5000 diluted for 1 h at RT. The protein bands were detectable via chemiluminescence. FtsZ is visible at 40 kDa and GroEL at 57 kDa. In both strains, cellular FtsZ is only detectable via overexpression from a plasmid (independently of whether the expression was on a basal level or with IPTG induction). At 5 h the cellular FtsZ amount is not enough to detect it over basal expression.

The detection of FtsZ in WT (DE3) and Δ*tusA* (DE3) via immunodetection was shown in Figure 55. The first four samples show the presence of the FtsZ protein in WT (DE3) and Δ*tusA* (DE3) mutant without IPTG and the last four with IPTG. The GroEL protein is visible at 57 kDa, which is the loading control for this experiment. The GroEL protein is produced in every protein expression as a housekeeping protein always in the same amount in every strain. So it was possible to detect FtsZ around 40 kDa if it was overexpressed from a plasmid in WT (DE3) and Δ*tusA* (DE3) mutant (Figure 55, WT and Δ*tusA* pET15b-*ftsZ*). The band for FtsZ in WT (DE3) was stronger than in Δ*tusA* (DE3) mutant which indicated that the amount of FtsZ in WT (DE3) is higher than in the *tusA* (DE3) deleted strain (since it was loaded with the same protein amount of every sample - 50 µg). However, the expression of FtsZ on at the basal level showed no band for FtsZ (Figure 55, WT and Δ*tusA* pET15b), which indicated insufficient FtsZ amount. Since no FtsZ band was already detectable for the WT (DE3) strain as a control. The expression with IPTG did not affect the FtsZ amount in both strains, as it was visible at the intensity of the FtsZ band. It was similar to the one without IPTG. Thus, due to the high FtsZ level, FtsZ was only visible in cells with overexpression.

Based on this result that WT (DE3) showed no band for FtsZ, further growth times were used in addition to 5 h to detect the FtsZ at basal expression level (Figure 56).

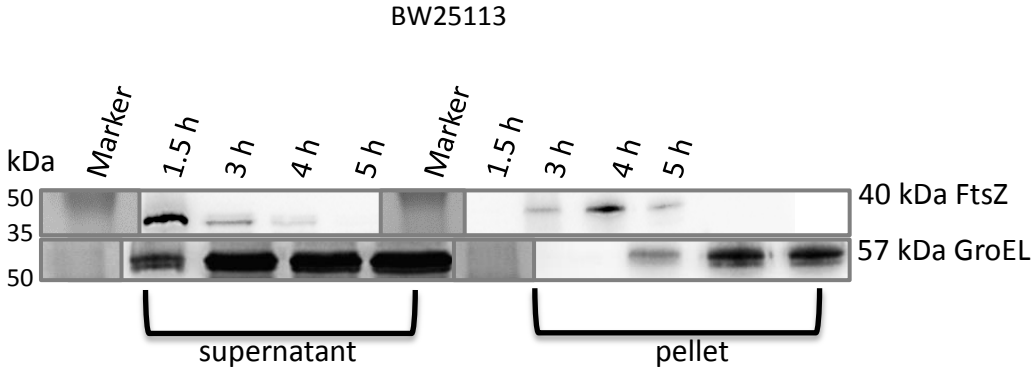

Figure 56: Analysis of cellular FtsZ amount in BW25113 (WT).

BW25113 (WT) cells were cultivated in 50 ml cultures of LB-0% NaCl at 37 °C, 180 rpm for 5 h. The first four samples (left to right) belong to the supernatant and the last four samples to the pellet. WT at 1.5 h of growth (second lane), at 3 h (third lane), 4 h (fourth lane) and at 5 h (fifth lane). The pellet samples were only loaded exemplary. After 5 h cells were harvested, sonicated and the protein concentration of the supernatant was determined by Bradford. 50 µg protein of every supernatant sample was loaded on the SDS-Gel (12%) and then transferred on a PVDF membrane. The first and sixth lanes show the Prestained Protein Molecular Weight Marker (Fermentas, 20 kDa – 120 kDa) which was used for size determination. Blots were incubated with α-FtsZ (rabbit) antibody 1:20000 diluted at RT, 1 h and with α-GroEL (rabbit, abcam) antibody 1:10000 diluted at 4 °C, ON. The detection of both antibodies was done using α-rabbit POD-conjugated secondary antibody (goat, Sigma) 1:10000 diluted for 1 h at RT. The protein bands were detectable via chemiluminescence. FtsZ is visible at 40 kDa and GroEL at 57 kDa. WT revealed high FtsZ concentration at the onset of growth (1,5 h) which disappeared until 5 h.

Figure 56 visualizes the result of the FtsZ detection in the WT strain at different time points. During the cultivation of WT cell samples were analyzed not only at 5 h. Further time points were 1.5 h, 3 h and 4 h. A strong FtsZ signal was detected at around 1.5 h in the supernatant which disappeared with the increasing growth time. So this confirmed the previous result (Figure 55) that in WT FtsZ was not present at 5 h. And also, at 1.5 h where the FtsZ Signal was strong in the supernatant, there is no FtsZ in the pellet (Figure 56). But the FtsZ signal increased until 4 h of growth and dropped again at 5 h. The FtsZ signal in the pellet at 4 h indicated that the FtsZ was associated with the membrane. The GroEL signal at the onset of the growth was not much since it is a chaperone that has to be first produced. And the signal for GroEL is stronger in the supernatant than in the pellet as expected (because it is a cytoplasmic protein).

Subsequently, the same conditions were applied for the *tusA* mutant strain (Figure 57) with the aim to see a difference in the FtsZ signal between the *tusA* mutant and WT.

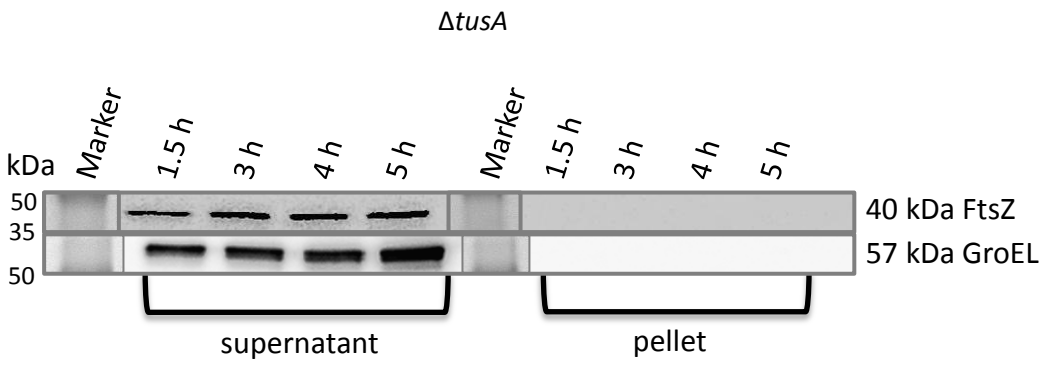

Figure 57: Analysis of cellular FtsZ amount in Δ*tusA*.

Δ*tusA* cells were cultivated in 50 ml cultures of LB-0% NaCl at 37 °C, 180 rpm for 5 h. The first four samples (left to right) belong to the supernatant and the last four samples to the pellet. Δ*tusA* at 1.5 h of growth (second lane), at 3 h (third lane), 4 h (fourth lane) and at 5 h (fifth lane). The pellet samples were only loaded exemplary. After 5 h cells were harvested, sonicated and the protein concentration of the supernatant was determined by Bradford. 50 µg protein of every supernatant sample was loaded on the SDS-Gel (12%) and transferred on a PVDF membrane. The first and sixth lanes show the Prestained Protein Molecular Weight Marker (Fermentas, 20 kDa – 120 kDa) which was used for size determination. Blots were incubated with α-FtsZ (rabbit) antibody 1:20000 diluted at RT, 1 h and with α-GroEL (rabbit, abcam) antibody 1:10000 diluted at 4 °C, ON. The detection of both antibodies was done using α-rabbit POD-conjugated secondary antibody (goat, Sigma) 1:10000 diluted for 1 h at RT. The protein bands were detectable via chemiluminescence. FtsZ is visible at 40 kDa and GroEL at 57 kDa. Δ*tusA* displayed the opposite result to that of WT. In Δ*tusA* the cellular FtsZ was less at the onset of growth (1,5 h) and increased until 5 h.

As can be seen from Figure 57, in the *tusA* mutant FtsZ was detectable in the supernatant at all selected time points (Figure 57). The FtsZ amount was less at 1.5 h than at the other 3 h, 4 h and 5 h after growth start whereas the amount in the last 3 samples is the same. For the pellet of the same samples, no FtsZ protein band was visible. So the result of the *tusA* mutant was contrary to that of the WT (Figure 57) since in WT was the highest FtsZ amount at 1.5 h (in the supernatant and the pellet at 4 h). WT strain revealed decreasing FtsZ amount until 5 h and Δ*tusA* increasing FtsZ amount in the supernatant. The amount of GroEL in the *tusA* mutant (Figure 57) was lower than in WT but the increase from the onset of growth to 5 h was as in WT. At 1.5 h, less GroEL was present since it should be first produced and then it increases (Figure 57).

4.11 Detection of cellular FtsZ amount in different *E. coli* strains

All deletion strains of the mnm^{5}s^{2}U34 tRNA thiolation pathway demonstrated the same growth and cell division defect as the Δ*tusA* strain. They grew slowly and had filamentous cell morphology. To emphasize that the cell division defect of all deletion strains involved in mnm^{5}s^{2}U34 tRNA modification affects the FtsZ concentration, the cellular FtsZ amount was detected by immunodetection (Figure 58).

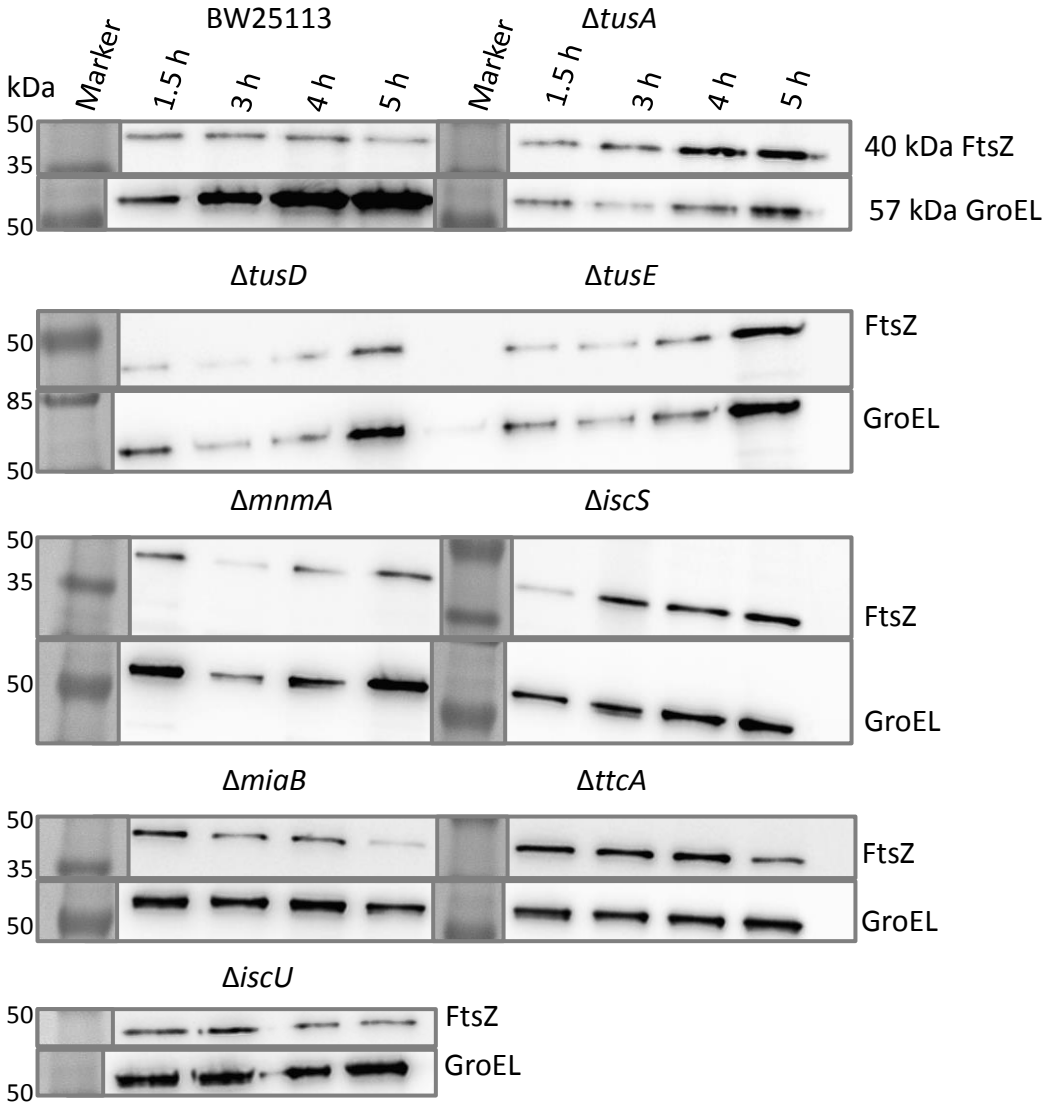

Figure 58: Detection of cellular FtsZ amount in gene deletion strains involved in mnm^{5}s^{2}U34 tRNA thiolation.

WT and Δ*miaB,* Δ*ttcA,* Δ*iscU* are controls for non-tRNA thiolation strains. BW25113 (WT), Δ*tusA*, Δ*tusD,* Δ*tusE,* Δ*mnmA,* Δ*iscS,* Δ*miaB,* Δ*ttcA* and Δ*iscU* cells were cultivated in 50 ml cultures of LB-0% NaCl at 37 °C, 180 rpm for 5 h. After 5 h of cultivation cells were harvested, sonicated and the protein concentration

of the supernatant was determined by Bradford. 50 µg protein of every supernatant sample was loaded on the SDS-Gel (12%) and transferred on a PVDF membrane. The first and sixth lanes show the Prestained Protein Molecular Weight Marker (Fermentas, 20 kDa – 120 kDa) which was used for size determination. Blots were incubated with α-FtsZ (rabbit) antibody 1:20000 diluted at RT, 1 h and with α-GroEL (rabbit, abcam) antibody 1:10000 diluted at 4 °C, ON. The detection of both antibodies was done using α- rabbit POD-conjugated secondary antibody (goat, Sigma) 1:10000 diluted for 1 h at RT. The protein bands were detectable via chemiluminescence. FtsZ is visible at 40 kDa and GroEL at 57 kDa. Deletion strains for mnm^5s^2U34 tRNA thiolation showed increasing cellular FtsZ amount at the late exponential phase (at 5 h) instead of WT which revealed high FtsZ concentration at the onset of growth (1.5 h). Low FtsZ amounts are responsible for not separating cells of deletion strains.

Figure 58 shows the result of the FtsZ immunodetection detection in deletion strains of mnm^5s^2U34 tRNA deletion strains. WT, Δ*miaB*, Δ*ttcA* and Δ*iscU* were used as control strains. The concentration of FtsZ decreased in WT until 5 h. Contrary to the WT, the FtsZ concentration in Δ*tusA* increased until 5 h. The Δ*tusD* and Δ*tusE* strains show the same tendency of the increasing FtsZ amount. But the amount in Δ*tusD* at 3 h and 4 h were a bit less than at 1.5 h. Both strains exhibited slightly decreased FtsZ amounts as Δ*tusA* (Figure 58, second blot). Only Δ*tusE* had at 5 h the same FtsZ amount as in Δ*tusA*. The Δ*mnmA* and Δ*iscS* strains shared also the same increase of FtsZ concentration until 5 h whereas the amount at 3 h and 4 h in Δ*mnmA* was less compared to Δ*tusA* (Figure 58, third blot). In Δ*iscS* the FtsZ amount was slightly higher at 5 h than in Δ*tusA* visible. The control strains Δ*miaB,* Δ*ttcA and* Δ*iscU* are not involved in mnm^5s^2U34 tRNA thiolation but in Fe-S cluster biosynthesis. This made them to the controls for the deletion strains of mnm^5s^2U34 tRNA thiolation in this assay. Δ*miaB* and Δ*ttcA* displayed the same FtsZ amount as the WT, it decreased until 5 h (Figure 58, fourth blot). The FtsZ amount in Δ*miaB* at 3 h was a bit less than at 4 h. In Δ*ttcA* was the FtsZ concentration a bit higher until 4 h as the WT. The last control strain was the Δ*iscU*, which also revealed the decreasing FtsZ amount until 5 h like the WT strain (Figure 58, last blot). The GroEL signal in WT got higher with the increasing growth time (Figure 58, first blot). The *tusA* mutant presented also this increase of GroEL signal until 5 h but its amount was less than that of the WT. Moreover, this decreased GroEL signal in Δ*tusA* reflected its retarded growth and as a result, its growth defect compared to WT. All the other deletion strains of mnm^5s^2U34 tRNA thiolation (Δ*tusD,* Δ*tusE,* Δ*mnmA*) displayed the same result as Δ*tusA*. The GroEL signal rose until 5 h. Only in Δ*mnmA* was the GroEL signal weaker at 3 h than at 1.5 h. So the control strains Δ*miaB,* Δ*ttcA* and Δ*iscU* represented nearly constant GroEL amount until 5 h during the growth. Only in Δ*miaB* was the GroEL amount at 5 h slightly decreased compared to its previous time points.

4.12 Detection of cellular Fis amount in BW25113 and Δ*tusA*

Another protein in this study for immunoblot investigation was the Fis protein with a length of 98 aa. It is a small DNA-binding protein, which activates the transcription of genes and has many regulatory functions. Fis can regulate the transcription of genes directly or indirectly, e.g. it influences the activity of RNA polymerase and controls the DNA supercoiling level in the cell (Cho *et al.*, 2008). Its amount is high in the exponential phase (high regulation) and decreases in the stationary phase (no regulation) (Azam *et al.*, 1999). Furthermore, it has an impact on FtsZ and therefore also on cell division which would explain the filamentation (Logan, 2006). The filamentation as a result of Fis overexpression led to the idea of whether Δ*tusA* filaments in the exponential phase were produced due to high Fis amounts.

To investigate this idea the difference in cellular Fis protein was detected in WT and Δ*tusA* strains.

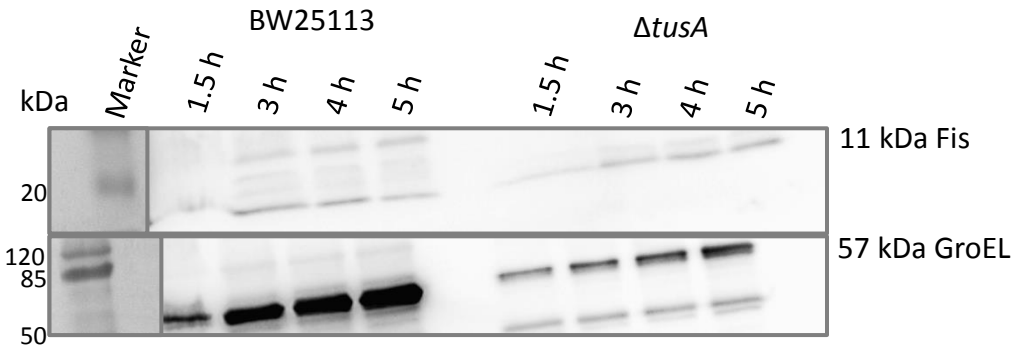

Figure 59: Detection of cellular Fis amount in BW25113 (WT) and Δ*tusA*.

WT and Δ*tusA* cells were cultivated in 50 ml cultures of LB-0% NaCl at 37 °C, 180 rpm for 5 h. The first four samples (left to right) belong to the supernatant of BW25113 and the last four samples of Δ*tusA*. BW25113 at 1.5 h of growth (second lane), at 3 h (third lane), 4 h (fourth lane) and at 5 h (fifth lane), Δ*tusA* at 1.5 h of growth (seventh lane), at 3 h (eighth lane), 4 h (ninth lane) and at 5 h (tenth lane). After 5 h of cultivation cells were harvested, sonicated and the protein concentration of the supernatant was determined by Bradford. 50 µg protein of every supernatant sample was loaded on the SDS-Gel (12%) and transferred on a PVDF membrane. The first and sixth lanes show the Prestained Protein Molecular Weight Marker (Fermentas, 20 kDa – 120 kDa) which was used for size determination. Blots were incubated with α-Fis (rabbit) antibody 1:10000 diluted at 4 °C, ON and with α-GroEL (rabbit, abcam) antibody 1:10000 diluted at 4 °C, ON. The detection of both antibodies was done using α-rabbit POD-conjugated secondary antibody (goat, Sigma) 1:10000 diluted for 1 h at RT. The protein bands were detectable via chemiluminescence. Fis is visible at 11 kDa and GroEL at 57 kDa. WT showed decreasing cellular Fis amount until 5 h and Δ*tusA* increasing Fis concentration.

As expected, the cellular Fis protein amount displayed differences between WT and Δ*tusA* (Figure 59). In WT the amount decreased until 5 h (Fis protein band at 3 h and 4 h is stronger than at 5 h) which was visible at 11 kDa. In contrast to the WT, the *tusA* mutant represented an increasing amount of Fis until 5 h (Figure 59). This result confirmed that the Fis concentration is high in the exponential phase and decreased in the stationary phase. Due to the fast growth WT strain reached earlier the stationary phase than the *tusA* mutant and therefore revealed decreased Fis amount at 5 h. The Δ*tusA* strain was still in the exponential phase, which explained the clearly visible Fis band at 5 h. The *tusA* mutant grew slower because of the defective tRNA thiolation. As a control protein, GroEL was detected, which showed a higher concentration in WT than in the mutant (Figure 59). In both cases, the increasing amount of GroEL was clearly visible from the onset of growth to 5 h.

In the next step for the Fis protein, a higher separation was carried out since Fis is a very small protein of 11 kDa. SDS-Gel of 15% was used for SDS-PAGE and the same samples were used as for 12% Gel (Figure 59). In both cases, a clear band was detectable for the Fis protein at 11 kDa which was not anymore at the same level as the gel border (Figure 60).

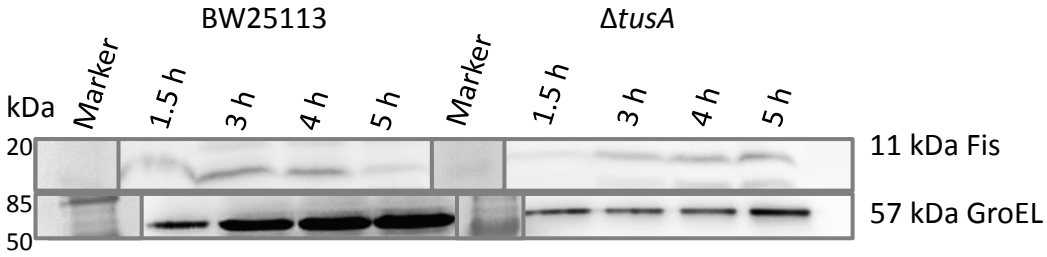

Figure 60: Detection of cellular Fis amount in BW25113 (WT) and Δ*tusA* in 15% SDS-Gel.

WT and Δ*tusA* cells were cultivated in 50 ml cultures of LB-0% NaCl at 37 °C, 180 rpm for 5 h. The first four samples (left to right) belong to the supernatant of BW25113 and the last four samples of Δ*tusA*. BW25113 at 1.5 h of growth (second lane), at 3 h (third lane), 4 h (fourth lane) and at 5 h (fifth lane), Δ*tusA* at 1.5 h of growth (seventh lane), at 3 h (eighth lane), 4 h (ninth lane) and at 5 h (tenth lane). After 5 h of cultivation cells were harvested, sonicated and the protein concentration of the supernatant was determined by Bradford. 50 µg protein of every supernatant sample was loaded on the SDS-Gel (15%) and transferred on a PVDF membrane. The first and sixth lanes show the Prestained Protein Molecular Weight Marker (Fermentas, 20 kDa – 120 kDa) which was used for size determination. Blots were incubated with α-Fis (rabbit) antibody 1:10000 diluted at 4 °C, ON and with α-GroEL (rabbit, abcam) antibody 1:10000 diluted at 4 °C, ON. The detection of both antibodies was done using α-rabbit POD-conjugated secondary antibody (goat, Sigma) 1:10000 diluted for 1 h at RT. The protein bands were detectable via chemiluminescence. Fis is visible at 11 kDa and GroEL at 57 kDa. The same results of Figure 59 were confirmed by the higher separation with 15% SDS-Gel: WT revealed decreasing cellular Fis amount until 5 h and Δ*tusA* increasing Fis concentration. The Fis protein band is higher than the running front.

In WT the amount of Fis decreased until 5 h and in Δ*tusA* it increased (Figure 60). Furthermore, this blot which arose from the gel with a higher acrylamide concentration (15%) confirmed a higher separation of the samples. The Fis band was higher than the gel border (Figure 60). The control protein GroEL showed that the blots were successful.

4.13 Detection of cellular Fis amount in different *E. coli* strains

As already described TusA was originally identified in a Δ*hns* background when screening for genes affecting cellular RpoS levels during the exponential phase (Yamashino *et al.*, 1998). The importance of Fis arises from the fact that it regulates the expression of *hns* and from this, there is a possible link of Fis to TusA. The amount of Fis is high in the exponential phase and decreases in the stationary phase (Azam *et al.*, 1999). Moreover, Fis is involved in cell division (Logan, 2006) and probably has a relation to FtsZ. So Fis could have an effect on cell division defect and therefore the filamentation of Δ*tusA* cells. Thus it appeared to be interesting and important to investigate the content of Fis in Δ*tusA* strain and its change during cell growth. In an immunoblot assay, the cellular Fis amount was analyzed including Δ*tusA* and all deletion strains involved in the mnm^5s^2U34 tRNA thiolation pathway (by using the same blots of FtsZ (Figure 58)) since all these strains show the same growth and cell division defect as Δ*tusA* strain (see chapter 4.7 Figure 44 and 45). The following Figure 61 shows the result of this Fis detection.

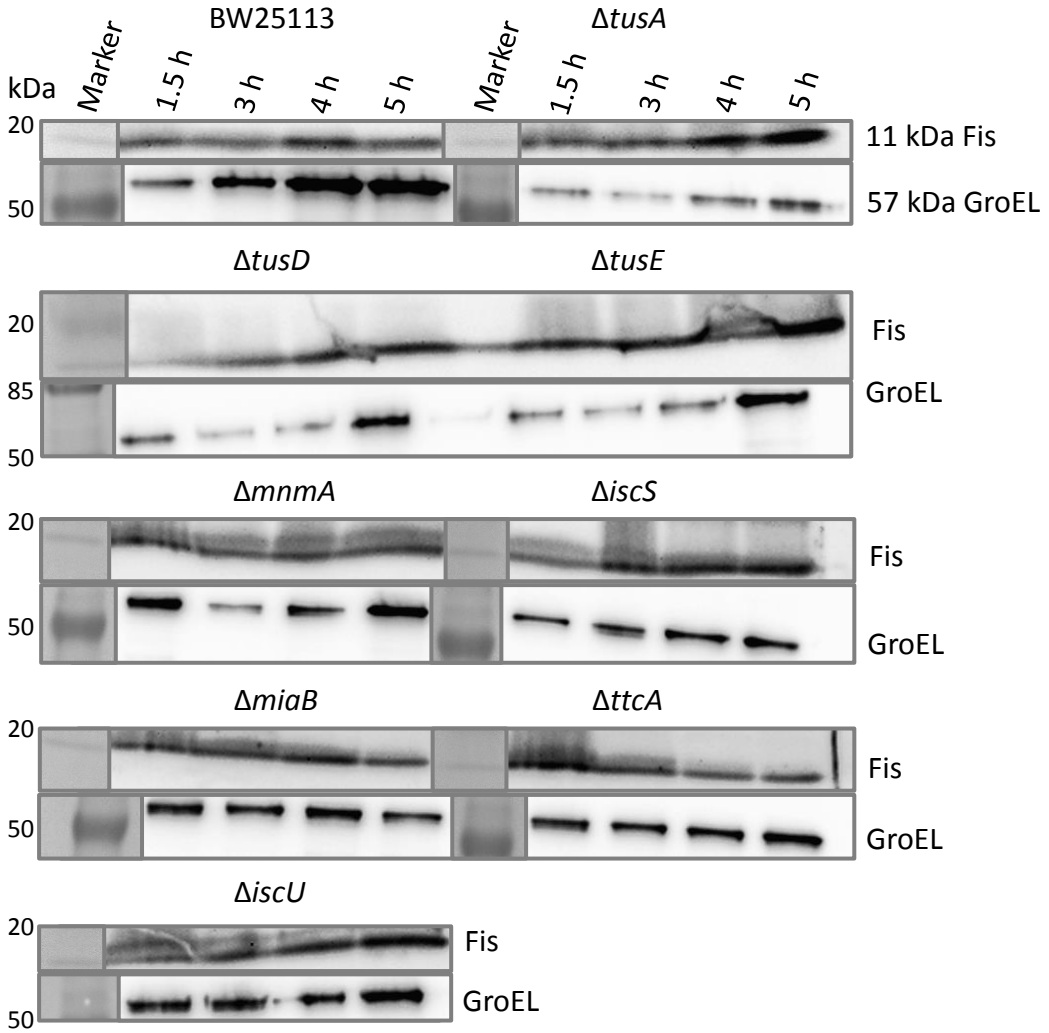

Figure 61: Detection of cellular Fis amount in gene deletion strains involved in mnm^{5}s^{2}U34 tRNA thiolation.

WT and Δ*miaB,* Δ*ttcA,* Δ*iscU* are controls for non-tRNA thiolation strains. BW25113 (WT), Δ*tusA*, Δ*tusD,* Δ*tusE,* Δ*mnmA,* Δ*iscS,* Δ*miaB,* Δ*ttcA* and Δ*iscU* cells were cultivated in 50 ml cultures of LB-0% NaCl at 37 °C, 180 rpm for 5 h. After 5 h of cultivation cells were harvested, sonicated and the protein concentration of the supernatant was determined by Bradford. 50 µg protein of every supernatant sample was loaded on the SDS-Gel (12%) and transferred on a PVDF membrane. The first and sixth lanes show the Prestained Protein Molecular Weight Marker (Fermentas, 20 kDa – 120 kDa) which was used for size determination. Blots were incubated with α-Fis (rabbit) antibody 1:10000 diluted at 4 °C, ON and with α-GroEL (rabbit, abcam) antibody 1:10000 diluted at 4 °C, ON. The labeling of both antibodies was done by α-rabbit POD-conjugated secondary antibody (goat, Sigma) 1:10000 diluted for 1 h at RT. The protein bands were detectable via chemiluminescence. Fis is visible at 11 kDa and GroEL at 57 kDa. Deletion strains for mnm^{5}s^{2}U34 tRNA thiolation showed increasing cellular Fis amount at the late exponential phase (at 5 h) instead of WT which revealed high Fis concentration until 4 h and subsequent decrease. High Fis concentration is probably responsible for filamentation.

The Fis concentration in WT increased until 4 h and at 5 h the decrease already started (Figure 61). In Δ*tusA* the Fis amount appeared to increase until 5 h after growth initiation

(Figure 61, first blot). This confirmed the previously reported different Fis amounts during the different growth phases (Cho *et al.*, 2008). Therefore the Fis concentration in WT decreased after reaching the stationary phase. In contrast to this Δ*tusA* grew slower which meant it was at 5 h in the exponential phase (which explained the still increasing Fis amount). The same result of increasing Fis concentration was visible in Δ*tusD,* Δ*tusE,* Δ*mnmA and* Δ*iscS* (Figure 61, second and third blot). Δ*mnmA* had a slightly decreased Fis amount compared to the other mnm^5s^2U34 tRNA thiolation deletion strains, which was especially visible at 5 h. Fis amounts in Δ*miaB* rose until 4 h and dropped at 5 h as WT (Figure 61, fourth blot). For Δ*ttcA* there was not a clear reduction of Fis concentration at 5 h detectable. It looked that the Fis amount was more constant to 5 h of growth. The last control Δ*iscU* presented a rising Fis amount until 5 h (Figure 61, last blot).

In a further assay, the amount of Fis was tested in the stationary phase in addition to the exponential phase. The hypothesis was whether there was a correlation between the reported low Fis amount in the stationary phase (Cho *et al.*, 2008) and the shortening of the Δ*tusA* filaments. For this analysis, the immunoblotting method (as described in Figure 61) was used again to detect the cellular Fis content in deletion strains of the mnm^5s^2U34 tRNA thiolation pathway. The difference from the previous immunoblotting (Figure 61) was that this time the measurement was continued until 10 h of growth (stationary phase) instead of only until 5 h (exponential growth). The results for cellular Fis concentration of mnm^5s^2U34 tRNA thiolation pathway deletion strains are shown in Figure 62.

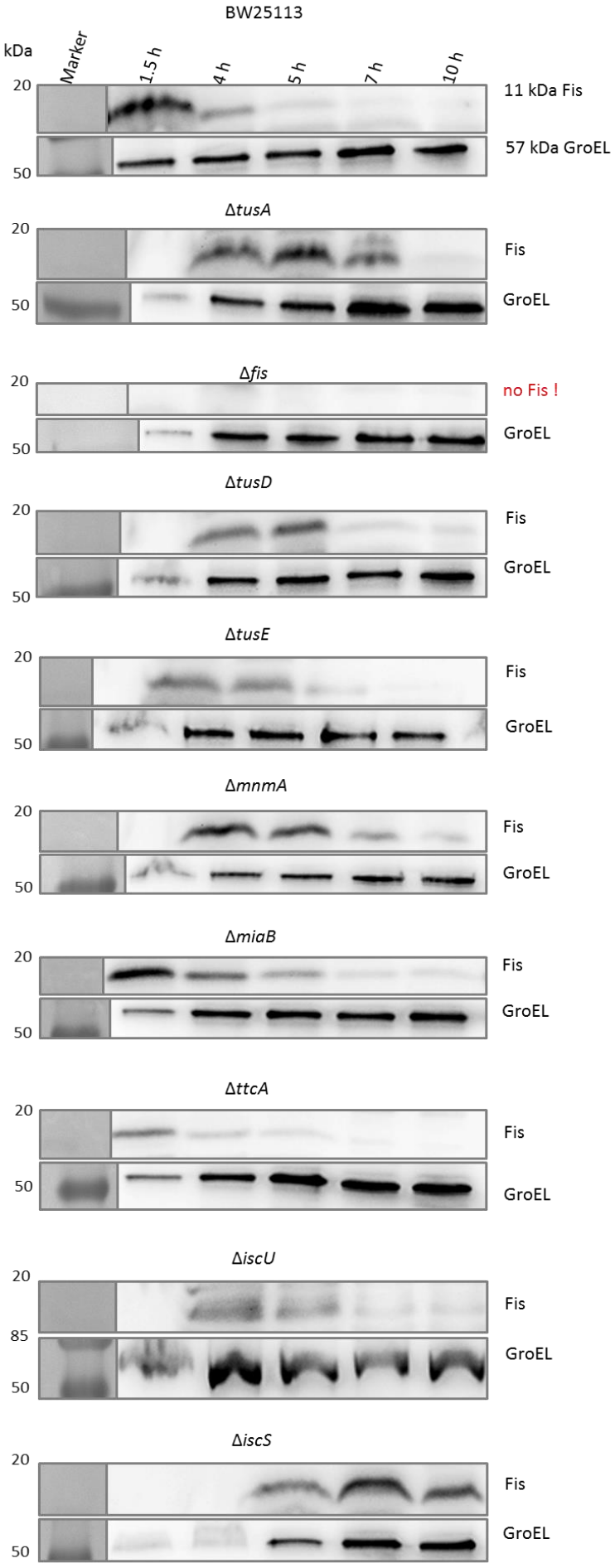
BW25113
kDa
Marker
1.5 h
4 h
5 h
7 h
10 h
20
50
11 kDa Fis
57 kDa GroEL
ΔtusA
Fis
GroEL
Δfis
no Fis !
GroEL
ΔtusD
Fis
GroEL
ΔtusE
Fis
GroEL
ΔmnmA
Fis
GroEL
ΔmiaB
Fis
GroEL
ΔttcA
Fis
GroEL
ΔiscU
85
Fis
GroEL
ΔiscS
Fis
GroEL

Figure 62: Detection of cellular Fis amount in gene deletion strains involved in mnm^{5}s^{2}U34 tRNA thiolation in exponential and stationary phase.

WT and Δ*miaB,* Δ*ttcA,* Δ*iscU* are controls for non-tRNA thiolation strains. BW25113 (WT), Δ*tusA*, Δ*tusD,* Δ*tusE,* Δ*mnmA,* Δ*iscS,* Δ*miaB,* Δ*ttcA* and Δ*iscU* cells were cultivated in 50 ml cultures of LB-0% NaCl at 37 °C, 180 rpm for 10 h. After 10 h cells were harvested, sonicated and the protein concentration of the supernatant was determined by Bradford. 50 µg protein of every supernatant sample was loaded on the SDS-Gel (15%) and transferred on a PVDF membrane. The first lane shows the Prestained Protein Molecular Weight Marker (Fermentas, 20 kDa – 120 kDa) which was used for size determination. Blots were incubated with α-Fis (rabbit) antibody 1:10000 diluted at 4 °C, ON and with α-GroEL (rabbit, abcam) antibody 1:10000 diluted at 4 °C, ON. The labeling of both antibodies was done by α-rabbit POD-conjugated secondary antibody (goat, Sigma) 1:10000 diluted for 1 h at RT. The protein bands were detectable via chemiluminescence. Fis is visible at 11 kDa and GroEL at 57 kDa. WT and non-tRNA thiolation strains had the same high Fis amount at 1.5 h and subsequent decrease and complete disappearing until 10 h. All mutants of the mnm^{5}s^{2}U34 tRNA thiolation pathway showed the same increasing Fis concentration until 5 h and subsequent decrease.

The investigation of Fis amount in the exponential and stationary phase is presented in Figure 62. Fis concentration was high in WT at 1.5 h, dropped slightly at 4 h and started to decrease from 5 h until it completely disappeared at 10 h (Figure 62, first blot). In Δ*tusA,* there was no Fis protein at 1.5 h, indicating the protein expression was still at the beginning. Subsequently, it rose until 5 h and from 7 h it started to decrease until it completely disappeared at 10 h (Figure 62, second blot). In Δ*fis,* no Fis protein existed (as expected) which confirms the deletion of the *fis* gene for this strain (Figure 62, third blot). Δ*tusD*, Δ*tusE* and Δ*mnmA* contained no Fis protein at 1.5 h as Δ*tusA* strain. Fis concentration rose then until 5 h and from 7 h it decreased until it completely disappeared at 10 h (Figure 62, fourth, fifth and sixth blot). Thus they showed the same result as the Δ*tusA.* In Δ*miaB* and Δ*ttcA* the Fis amount was high at the onset of growth and decreased continuously until 10 h and disappeared completely (Figure 62, seventh and eighth blot). The Δ*iscU* strain displayed no Fis protein at 1.5 h (as Δ*tusA*), which then increased until 4 h and decreased from 5 h until it completely disappeared at 10 h (Figure 62, ninth blot). For the Δ*iscS* was no Fis protein detectable at 1.5 h and 4 h since the protein expression was still at the beginning and the growth was slower than the Δ*tusA* strain (Figure 62, tenth blot). Then it increased until 7 h and from 10 h it started to decrease. So the growth of Δ*iscS* strain was shifted to one phase or time point compared to Δ*tusA*. The GroEL concentration increased in WT to 7 h and then decreased. Δ*tusA* showed continuously increasing GroEL amounts until 10 h. For Δ*fis*, Δ*tusD*, Δ*tusE*, Δ*mnmA* and Δ*iscS* were also detected continuously rising GroEL amounts until 10 h as

in Δ*tusA*. Δ*miaB* and Δ*ttcA* revealed GroEL amounts that rose to 4 h or 5 h and stayed then nearly constant. In Δ*iscU* it was also nearly constant from 4 h on.

WT and deletion strains not involved in the mnm^5s^2U34 tRNA thiolation pathway had the same high Fis amount at 1.5 h and subsequent decrease and complete disappearing until 10 h. All mutants of the mnm^5s^2U34 tRNA thiolation pathway showed the same increasing Fis concentration until 5 h and subsequent decrease. These results indicated a link between the Fis protein and the growth defect of mnm^5s^2U34 tRNA thiolation proteins.

4.14 Translation efficiencies in different *E. coli* strains

As already reported (Ishii *et al.,* 2000) and shown in the result section (4.1.) the gene deletion of the TusA protein has an effect on cell growth and morphology since the cells had a retarded growth and show filaments as cell shape. Since the role of TusA is to transfer the sulfur for thiolation of U34 at the wobble position in tRNA which occurs in tRNAs that decode for lysine, glutamine and glutamate (Björk *et al.*, 2007). As this thiomodification of U34 has the important function to enable more efficient ribosome binding and averts frameshifting during the translation of proteins (Ashraf *et al.,* 1999; Yokoyama *et al.*, 1985; Moukadiri *et al.*, 2013), it was relevant to analyze whether *tusA* deletion has a further effect on the translational level. Because the absence of TusA would mean a lack of U34 thiomodification and that in turn a poorer translation. Therefore the effect of tusA deletion on translation was investigated by measuring the translation efficiency.

Moreover, the deletion of the TusA protein led to further changes in the cell except for the filamentous growth. If the TusA protein was deleted the expression of some genes was increased or decreased (Dahl *et al.*, 2013). Among these are also the *rpoS* and *fur* genes. Thereby the expression of the *rpoS* gene is increased and that of the *fur* gene is decreased. The *rpoS* gene encodes for the sigma factor σ^S, also called RpoS, which is induced in stress situations. It enhances the expression of several genes in the stationary phase (Yamashino *et al.*, 1998). The *fur* gene encodes the FUR (ferric uptake regulator) protein that positively regulates iron usage and iron storage in the cell (Masse and Gottesmann, 2002).

Additionally, as already mentioned the Fis protein appeared to have some regulatory impact on filamentous growth and thus on Δ*tusA* filaments in the exponential phase or on FtsZ cell division. Therefore, the Fis protein was one further potential candidate to analyze its influence on the Δ*tusA* strain. So the influence of Fis, Fur and RpoS proteins should be analyzed in the Δ*tusA* strain. The following image 63 shows the richness of lysine, glutamate and glutamine in Fis, Fur and RpoS protein sequences which enhances the possibility that their translation could be affected in case of the absence of thiomodification of U34 at wobble position in tRNA.

Fis:

MFEQRVNSDVLTVSTVNSQDQVTQKPLRDSVKQALKNYFAQLNGQDVNDLYELVLAEVEQPLL
DMVMQYTRGNQTRAALMMGINRGTLRKKLKKYGMN **98**

Fur:

MTDNNTALKKAGLKVTLPRLKILEVLQEPDNHHVSAEDLYKRLIDMGEEIGLATVYRVLNQFDDAG
IVTRHNFEGGKSVFELTQQHHHDHLICLDCGKVIEFSDDSIEARQREIAAKHGIRLTNHSLYLYGHC
AEGDCREDEHAHEGK **148**

RpoS:

MSQNTLKVHDLNEDAEFDENGVEVFDEKALVEQEPSDNDLAEEELLSQGATQRVLDATQLYLGEI
GYSPLLTAEEEVYFARRALRGDVASRRRMIESNLRLVVKIARRYGNRGLALLDLIEEGNLGLIRAVEK
FDPERGFRFSTYATWWIRQTIERAIMNQTRTIRLPIHIVKELNVYLRTARELSHKLDHEPSAEEIAEQ
LDKPVDDVSRMLRLNERITSVDTPLGGDSEKALLDILADEKENGPEDTTQDDDMKQSIVKWLFELN
AKQREVLARRFGLLGYEAATLEDVGREIGLTRERVRQIQVEGLRRLREILQTQGLNIEALFRE **330**

Figure 63: Amino acid sequences of Fis, Fur and RpoS proteins as proof for lysine, glutamate- and glutamine-richness

Shown are the amino acid sequences of Fis, Fur and RpoS proteins. Based on the sequences it is clearly visible how many lysines, glutamates and glutamines all of these three proteins include. Lysine is highlighted by green color, glutamate by purple and glutamine by yellow. K= Lysine (7x in Fis; 9x in Fur; 12x RpoS), E= Glutamate (4x in Fis; 14x in Fur; 41x RpoS), Q= Glutamine (10x in Fis; 4x in Fur; 15x RpoS). Protein sequences are from https://ecocyc.org/.

To test the expression of *rpoS*, *fur* and *fis* genes at the translation level, fusion protein constructs were synthesized (by GeneArt, Regensburg, Germany), where each of these genes was fused C-terminally to EGFP protein. These constructs are visualized in the following figure (Figure 64).

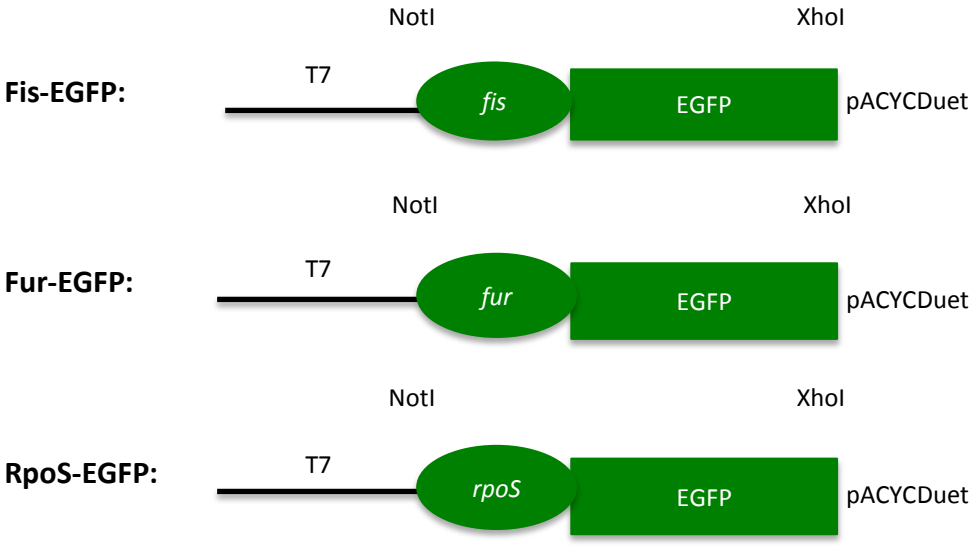

Figure 64: Synthetic gene constructs of Fis-, Fur-, RpoS-EGFP for flow cytometry

Schematic image of fusion protein constructs for detection of EGFP reporter protein by flow cytometry. All three genes *fis*, *fur* and *rpoS* are fused to the EGFP gene without stopping codon in the pACYCDuet-1 vector. The total fusion construct is cloned with NotI and XhoI restriction sites.

Fis, *fur* and *rpoS* gene sequences are fused to EGFP without any stop codon in between. The fusion was cloned in the pACYCDuet-1 expression vector with NotI (forward) and XhoI (reverse) restriction sites (Figure 64). The function of the EGFP was to act as a reporter protein if the *rpoS*, *fur* or *fis* gene expression was induced. And the level of the translation can be determined by measuring the EGFP fluorescence.

In this way, it appeared to be possible to create translation profiling for the Δ*tusA* strain and determined the difference to the respective WT strain. Due to the growth and cell division defect that occurred in deletion strains of mnm^{5}s^{2}U34 tRNA thiolation, it was assumed that tRNA thiolation and there out the frameshifts were slowed down. To explore the effect of mnm^{5}s^{2}U34 tRNA modifications on the translation efficiency of selected genes, EGFP fusion proteins were analyzed by flow cytometry. The method of flow cytometry measurement was learned in the group of Dr. Katrin Messerschmidt at the University of Potsdam and then carried out in collaboration and using their equipment.

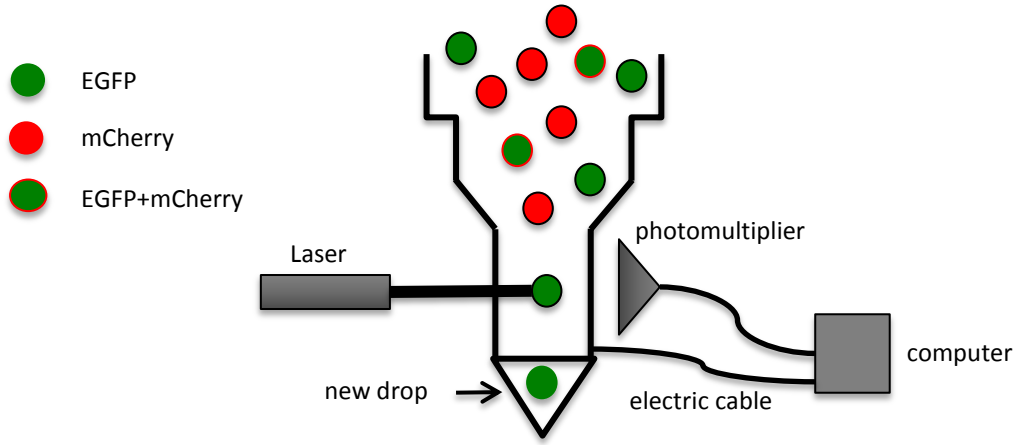

Figure 65: Scheme of flow cytometry.

Shown is the principle of flow cytometry. The suspension contains EGFP and mCherry-expressing cells which are detected individually by laser. EGFP expressed in the cells was excited with light of 488 nm and the mCherry with 587 nm. The fluorescence signal is enhanced via the photomultiplier and emission of EGFP is detected at 507 nm and of mCherry at 610 nm.

Figure 65 images the principle of flow cytometry. The cells are flowing through the channel. The fluorescence of the protein is excited within the cell by the laser light and enhanced by a photomultiplier for better detection. At this point, it is possible to measure the different fluorescence signals and simultaneously count the cell number. In this study, 10000 cells were measured for each sample. EGFP and mCherry were used as fluorescence proteins. EGFP expressed in the cells was excited at 488 nm and the mCherry at 587 nm. The fluorescence signal of EGFP was detected at 507 nm and of mCherry at 610 nm.

First of all the translation efficiency of Fis-EGFP was analyzed in WT (DE3) and gene deletion strains involved in the mnm^5s^2U34 tRNA thiolation pathway (Figure 66 -68).

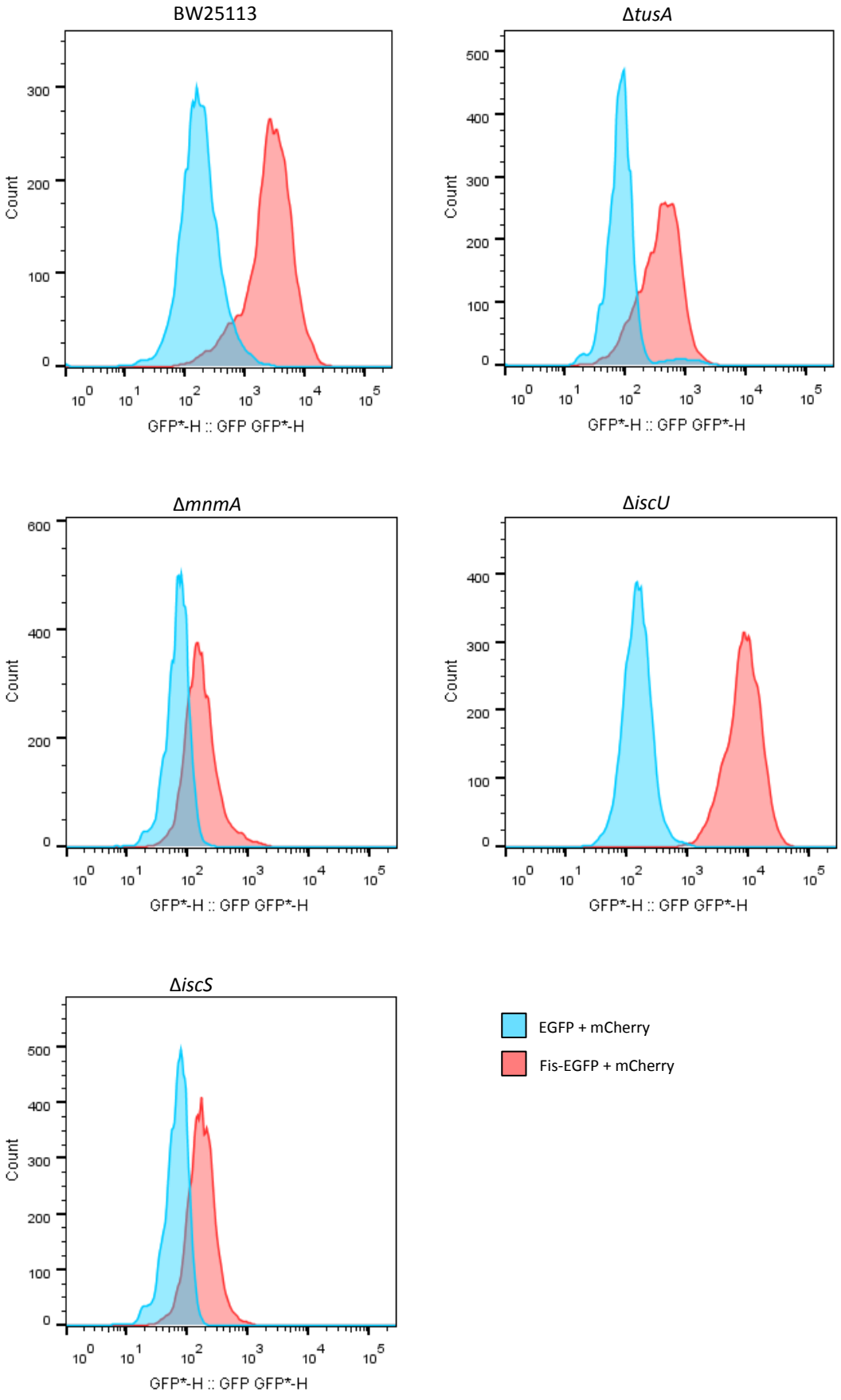
BW25113
ΔtusA
ΔmnmA
ΔiscU
ΔiscS
Count
GFP*-H :: GFP GFP*-H
EGFP + mCherry
Fis-EGFP + mCherry

Figure 66: Flow cytometry histograms of the fluorescence recorded from Fis-EGFP fusion (GFP channel) expressed in deletion strains of genes involved in mnm^{5}s^{2}U34 tRNA thiolation.

Translation efficiency of lysine-, glutamate- and glutamine-rich protein Fis was analyzed in BW25113 WT (DE3) and tRNA thiolation-deficient strains.

BW25113 (WT) (DE3), Δ*tusA* (DE3), Δ*mnmA* (DE3), Δ*iscU* (DE3) and Δ*iscS* (DE3) strains were transformed with *fis*-EGFP-pACYCDuet-1 (for Fis-EGFP overexpression) and mCherry-pCDFDuet-1 (as an internal control for translation) or with the corresponding empty EGFP-pACYCDuet-1 + mCherry-pCDFDuet-1 vector. Cells were grown in 50 ml cultures of LB-0% NaCl at 37 °C, 180 rpm for 5 h. Protein overexpression was induced with 100 µM IPTG. The cell count for each sample was set to 10^8 cells/ml for flow cytometry. Each sample was detected for EGFP and mCherry fluorescence signal. In total 10000 cells were measured for each sample with a flow rate of 1. Shown is the GFP channel; Fis-EGFP signal of the Fis-EGFP + mCherry sample (red) and the EGFP signal of the EGFP + mCherry sample (blue). X-axis shows the fluorescence intensity (the more right the higher the signal) and the y-Axis the cell number. The translation efficiency of Fis-EGFP was lowest in all mnm^{5}s^{2}U34 tRNA thiolation-deficient strains.

WT (DE3), Δ*tusA* (DE3), Δ*mnmA* (DE3), Δ*iscU* (DE3) and Δ*iscS* (DE3) strains were transformed with *fis*-EGFP-pACYCDuet-1 (for Fis-EGFP overexpression) and mCherry-pCDFDuet-1. The mCherry acted as an internal control for translation. So, one cell contained the EGFP fusion protein construct (or corresponding empty EGFP-pACYCDuet-1) and the mCherry-pCDFDuet-1. The EGFP fluorescence signal as a reporter gene was changing in relation to the Fis protein translation. Figure 66 shows the Fis-EGFP signal in the GFP channel (red). The corresponding control EGFP fluorescence signal represents the blue-colored peak. The fluorescence intensity is imaged on the x-axis and the more right the higher is the fluorescence signal. WT (DE3) displayed a positive signal via high Fis-EGFP expression. The fluorescence was around 10^3 - 10^4 detectable with a narrow peak in the upper part which indicated a homogenous population expressing almost the same amount of Fis-EGFP. The lower part of the Fis-EGFP peak was a bit wider and therefore presented a heterologous population that contained cells expressing less and more Fis-EGFP. In WT (DE3) around 270 cells of 10000 expressed Fis-EGFP fusion protein. The control EGFP fluorescence signal exhibited a distinct weaker signal at 10^2 than that of Fis-EGFP. Approximately 290 cells out of 10000 produced the control EGFP protein. Δ*tusA* (DE3) depicted a Fis-EGFP fluorescence around 10^2 – 10^3 which is clearly weaker than the Fis-EGFP signal in WT (DE3). The lower Fis-EGFP signal in Δ*tusA* (DE3) was caused by slow growth and thereby also lower translation of proteins. Around 265 cells of 10000 expressed Fis-EGFP. A shift to the control EGFP peak is clearly visible but lower than that of WT (DE3). Δ*mnmA* (DE3) and Δ*iscS* (DE3) had similar Fis-EGFP fluorescence signals to Δ*tusA* (DE3) around 10^2 – 10^3 whereas the signal is a bit more shifted to 10^2. Consequently, Δ*mnmA* (DE3) and Δ*iscS* (DE3) signals were clearly lower than WT (DE3). In Δ*mnmA* (DE3)

around 375 cells expressed Fis-EGFP and in Δ*iscS* (DE3) were these 400 cells. The shift in both strains to their respective control EGFP peak was slightly lower than in Δ*tusA* (DE3) and bigger in WT (DE3). In both strains, 500 cells produced the control EGFP protein. The last measured deletions strain was the Δ*iscU* (DE3) which was one further control (except the WT (DE3) strain) since it is not involved in mnm^5s^2U34 tRNA thiolation. Δ*iscU* (DE3) showed a clear strong Fis-EGFP positive fluorescence signal at 10^4 which was slightly shifted to the higher fluorescence intensity than in WT (DE3). Around 320 cells produced Fis-EGFP in Δ*iscU* (DE3). The control EGFP signal in Δ*iscU* (DE3) was distinctly lower at 10^2 than the Fis-EGFP signal and approximately 390 cells expressed this control EGFP.

The shift from Fis-EGFP to EGFP in WT (DE3) was significantly bigger than in Δ*tusA* (DE3) and the other mnm^5s^2U34 tRNA thiolation strains. So this shift indicated differences in translation efficiency between WT (DE3) and Δ*tusA* (DE3). Due to the growth defect in Δ*tusA* (DE3), the translation of proteins was also slowed down and generally fewer proteins were expressed.

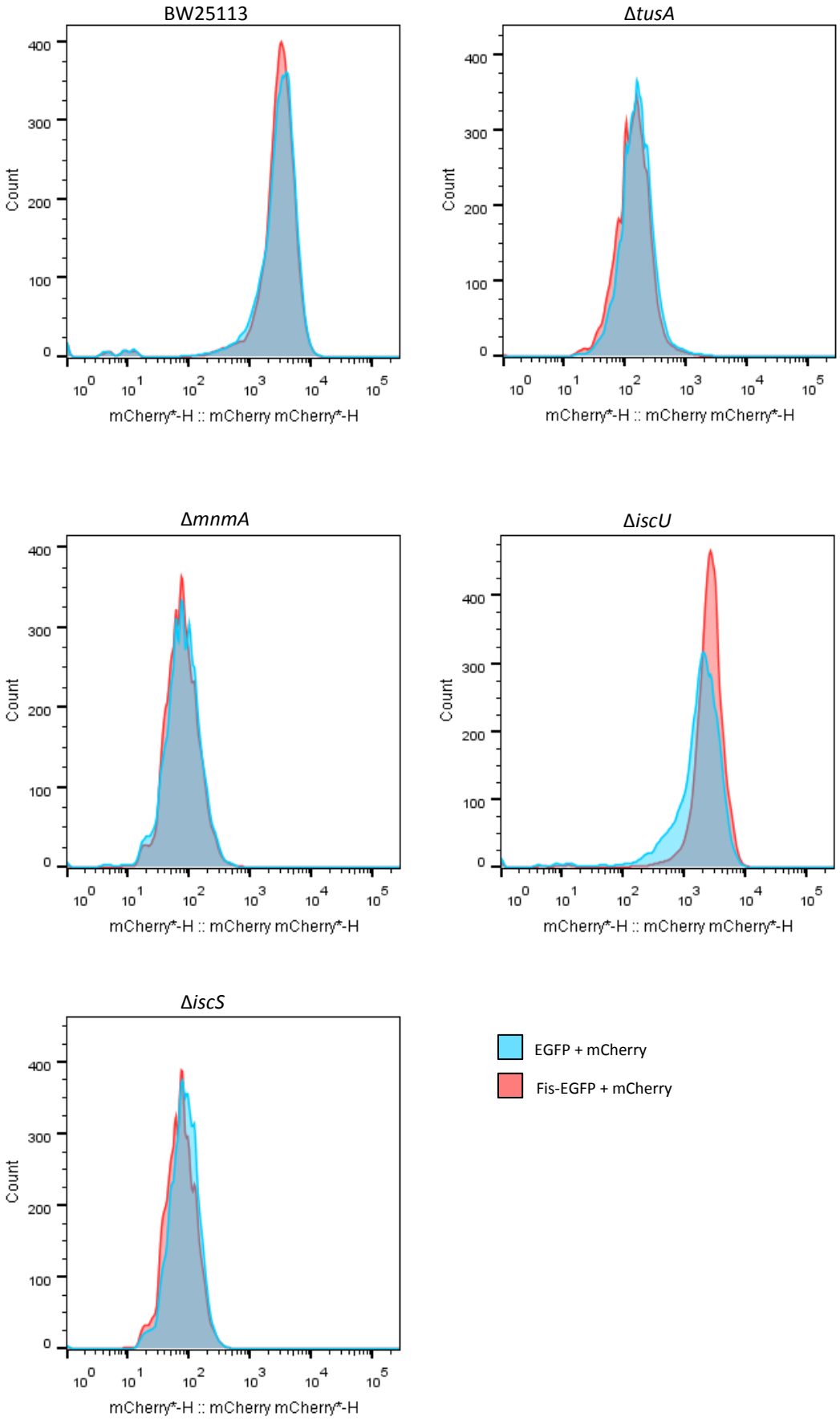
BW25113
ΔtusA
ΔmnmA
ΔiscU
ΔiscS
Count
mCherry*-H :: mCherry mCherry*-H
EGFP + mCherry
Fis-EGFP + mCherry

Figure 67: Flow cytometry histograms of the fluorescence recorded from Fis-EGFP fusion (mCherry channel) expressed in deletion strains of genes involved in mnm^{5}s^{2}U34 tRNA thiolation.

Translation efficiency of lysine-, glutamate- and glutamine-rich protein Fis was analyzed in BW25113 WT (DE3) and tRNA thiolation-deficient strains.

BW25113 (WT) (DE3), Δ*tusA* (DE3), Δ*mnmA* (DE3), Δ*iscU* (DE3) and Δ*iscS* (DE3) strains were transformed with *fis*-EGFP-pACYCDuet-1 (for Fis-EGFP overexpression) and mCherry-pCDFDuet-1 (as an internal control for translation) or with the corresponding empty EGFP-pACYCDuet-1 + mCherry-pCDFDuet-1 vector. Cells were grown in 50 ml cultures of LB-0% NaCl at 37 °C, 180 rpm for 5 h. Protein overexpression was induced with 100 µM IPTG. The cell count for each sample was set to 10^8 cells/ml for flow cytometry. Each sample was detected for EGFP and mCherry fluorescence signal. In total 10000 cells were measured for each sample with a flow rate of 1. Shown is the mCherry channel; mCherry signal of the Fis-EGFP + mCherry sample (red) and of the EGFP + mCherry sample (blue). X-axis shows the fluorescence intensity (the more right the higher the signal) and the y-Axis the cell number. The translation of internal mCherry of the Fis-EGFP sample and control was the same. As expected the translation efficiency of mCherry is lower in all mnm^{5}s^{2}U34 tRNA thiolation-deficient strains.

Nearly for all the tested strains it was possible to detect equal mCherry fluorescence (red) of Fis-EGFP samples compared to the control mCherry signal (blue) (Figure 67). WT (DE3) showed a narrow mCherry peak at 10^3 - 10^4 which completely overlapped with the control mCherry peak. This means even the cell expressed Fis-EGFP fusion protein (which showed differences to control EGFP fluorescence (Figure 66)) the mCherry signal (as internal control) was not changed compared to the corresponding control. In WT (DE3) about 400 cells expressed the mCherry protein. Δ*tusA* (DE3), Δ*mnmA* (DE3) and Δ*iscS* (DE3) revealed a mCherry fluorescence around 10^2 whereas the peaks for Δ*mnmA* (DE3) and Δ*iscS* (DE3) were slightly shifted to the left. In Δ*tusA* (DE3) 350 cells of 10000 produced mCherry protein, in Δ*mnmA* (DE3) 360 cells and in Δ*iscS* (DE3) 385 cells. All these three mnm^{5}s^{2}U34 tRNA thiolation strains had lower mCherry fluorescence than WT (DE3). Only Δ*iscU* (DE3) showed nearly the same mCherry signal at 10^3 - 10^4 as WT (DE3) since it is not involved in tRNA thiolation. Approximately 470 Δ*iscU* (DE3) cells expressed mCherry protein.

The assay confirmed that the internal mCherry control is correct because its fluorescence signal matches with the control. Thus the EGFP fluorescence was caused by the different translation efficiencies of the Fis protein in WT (DE3) and mnm^{5}s^{2}U34 tRNA thiolation deletion strains.

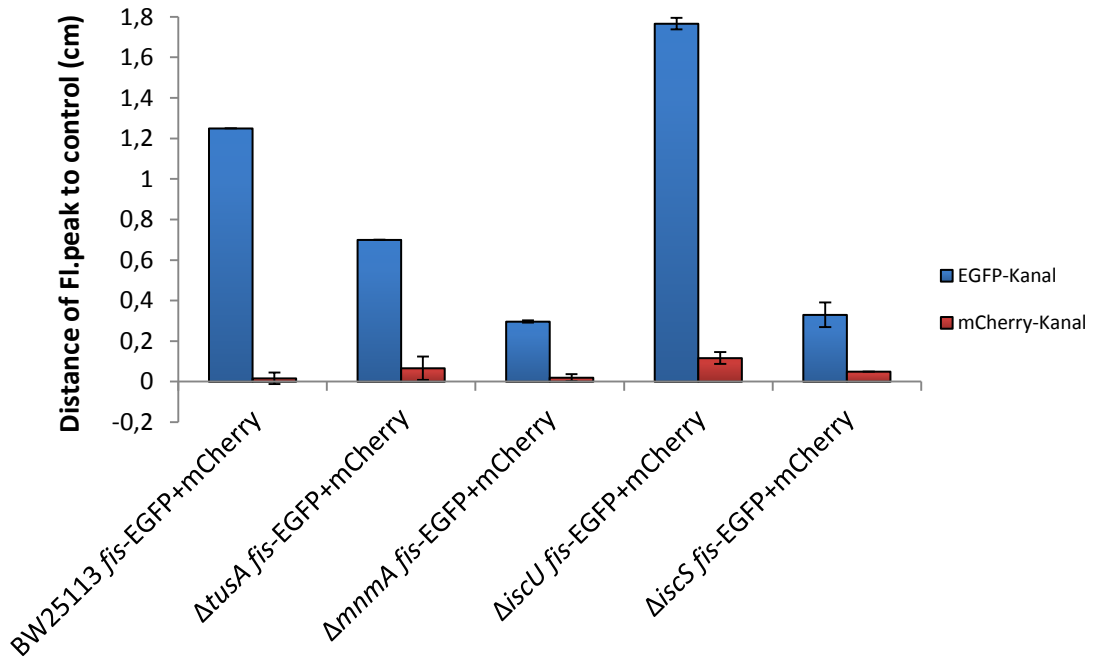

Figure 68: Fis-EGFP overexpression in deletion strains of genes involved in mnm^{5}s^{2}U34 tRNA thiolation shown in distance measurement to the control EGFP + mCherry fluorescence signal in each strain.

BW25113 (WT) (DE3), Δ*tusA* (DE3), Δ*mnmA* (DE3), Δ*iscU* (DE3) and Δ*iscS* (DE3) strains were transformed with *fis*-EGFP-pACYCDuet-1 (for Fis-EGFP overexpression) and mCherry-pCDFDuet-1 (as an internal control for translation) or with the corresponding empty EGFP-pACYCDuet-1 + mCherry-pCDFDuet-1 vector. Blue is the EGFP signal and red is the mCherry signal. From flow cytometry histograms, the distance of the Fis-EGFP peak to the EGFP control peak (in EGFP channel) or mCherry signal peak to its corresponding control peak (in mCherry channel) was measured in each sample. The translation efficiency of Fis-EGFP was lowest in all mnm^{5}s^{2}U34 tRNA thiolation-deficient strains.

Figure 68 shows the difference of Fis-EGFP fusion protein on translation level between WT (DE3) and gene deletion strains of mnm^{5}s^{2}U34 tRNA thiolation. It visualizes the shift between Fis-EGFP or mCherry fluorescence signals to their respective control peak. From flow cytometry histograms, the distance of the Fis-EGFP peak to the EGFP control peak (of triple measurements) was manually determined in each sample and the mean value was plotted against the distance. Strains of mnm^{5}s^{2}U34 tRNA thiolation exhibited the lowest shift to control in the GFP channel whereas this in Δ*tusA* (DE3) was slightly higher. Thus the expression of Fis-EGFP was almost similar in all these three tRNA thiolation strains. Δ*mnmA* (DE3) and Δ*iscS* (DE3) showed a distance of around 0.3 cm and Δ*tusA* (DE3) about 0.7 cm. WT (DE3) depicted a distance of 1.25 cm to its control which is almost the double of Δ*tusA* (DE3) value and suggested accordingly a higher translation of Fis-EGFP. Surprisingly the highest Fis-EGFP translation represented Δ*iscU* (DE3) strain with a distance of 1.76 cm. The translation efficiency was definitely lower in deletion strains of mnm^{5}s^{2}U34 tRNA thiolation.

As already explained the deletion of the TusA protein led to decreased *fur* gene expression (Dahl *et al.*, 2013) which encodes for ferric uptake protein FUR and regulates the iron usage in the cell (Masse and Gottesmann, 2002). Therefore, in the next step, the Fur-EGFP translation efficiency was analyzed in WT (DE3), Δ*tusA* (DE3), Δ*mnmA* (DE3), Δ*iscU* (DE3) and Δ*iscS* (DE3) strains (Figure 69 – 71).

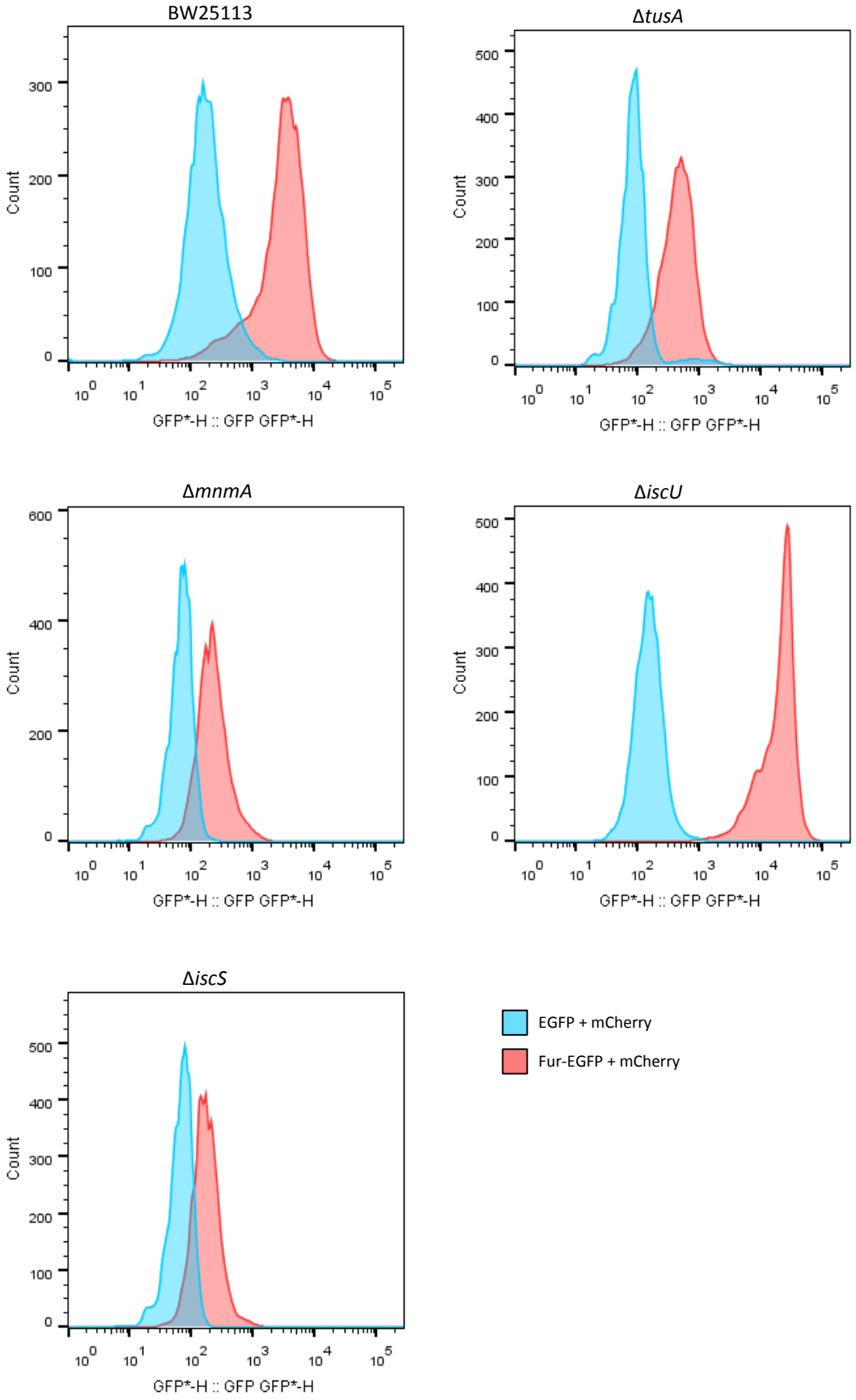

Figure 69: Flow cytometry histograms of the fluorescence recorded from Fur-EGFP fusion (GFP channel) expressed in deletion strains of genes involved in mnm^{5}s^{2}U34 tRNA thiolation.

Translation efficiency of lysine-, glutamate- and glutamine-rich protein Fur was analyzed in BW25113 WT (DE3) and tRNA thiolation-deficient strains.

BW25113 (WT) (DE3), Δ*tusA* (DE3), Δ*mnmA* (DE3), Δ*iscU* (DE3) and Δ*iscS* (DE3) strains were transformed with *fur*-EGFP-pACYCDuet-1 (for Fur-EGFP overexpression) and mCherry-pCDFDuet-1 (as an internal control for translation) or with the corresponding empty EGFP-pACYCDuet-1 + mCherry-pCDFDuet-1 vector. Cells were grown in 50 ml cultures of LB-0% NaCl at 37 °C, 180 rpm for 5 h. Protein overexpression was induced with 100 µM IPTG. The cell count for each sample was set to 10^8 cells/ml for flow cytometry. Each sample was detected for EGFP and mCherry fluorescence signal. In total 10000 cells were measured for each sample with a flow rate of 1. Shown is the GFP channel; Fur-EGFP signal of Fur-EGFP + mCherry sample (red) and the EGFP signal of EGFP + mCherry sample (blue). X-axis shows the fluorescence intensity (the more right the higher the signal) and the y-Axis the cell number. The translation efficiency of Fur-EGFP was lowest in all mnm^5s^2U34 tRNA thiolation-deficient strains.

Sample preparation and measurement procedure were the same as already described for Fis-EGFP translation. The Fur-EGFP translation was quite similar to Fis-EGFP expression in WT (DE3), Δ*tusA* (DE3), Δ*mnmA* (DE3), Δ*iscU* (DE3) and Δ*iscS* (DE3) strains (Figure 69, Fur-EGFP GFP channel). 280 cells of 10000 WT (DE3) expressed Fur-EGFP with a strong EGFP fluorescence at 10^3 – 10^4. Δ*tusA* (DE3), Δ*mnmA* (DE3) and Δ*iscU* (DE3) revealed a positive Fur-EGFP signal around 10^2 – 10^3 which was lower than that in WT (DE3). The peak of EGFP signal in Δ*mnmA* (DE3), Δ*iscU* (DE3) was a bit shifted to 10^2 as in Δ*tusA* (DE3). 310 cells out of 10000 were producing Fur-EGFP in Δ*tusA* (DE3), in Δ*mnmA* (DE3) and Δ*iscU* (DE3) this number was around 375 cells and 413 cells. A small difference depicted the Fur-EGFP expression in Δ*iscU* (DE3). Fur-EGFP fluorescence was a bit higher at 10^4 – 10^5 in Δ*iscU* (DE3) than in WT (DE3) and in Δ*iscU* (DE3) Fis-EGFP fluorescence signal (Figure 66). Approximately 490 Δ*iscU* (DE3) cells expressed Fur-EGFP.

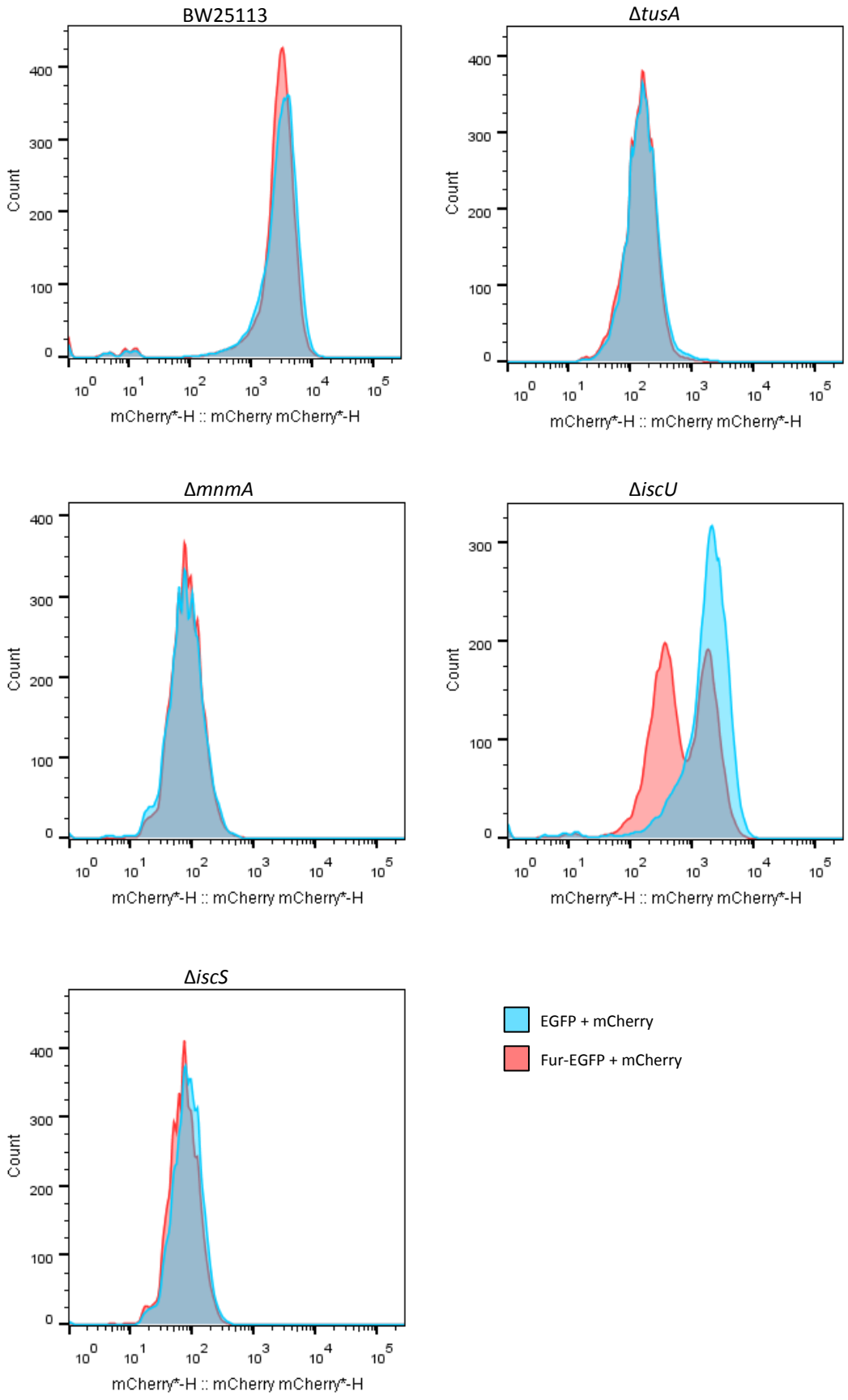

Figure 70: Flow cytometry histograms of the fluorescence recorded from Fur-EGFP fusion (mCherry channel) expressed in deletion strains of genes involved in mnm^{5}s^{2}U34 tRNA thiolation.

Translation efficiency of lysine-, glutamate- and glutamine-rich protein Fur was analyzed in BW25113 WT (DE3) and tRNA thiolation-deficient strains.

BW25113 (WT) (DE3), Δ*tusA* (DE3), Δ*mnmA* (DE3), Δ*iscU* (DE3) and Δ*iscS* (DE3) strains were transformed with *fur*-EGFP-pACYCDuet-1 (for Fur-EGFP overexpression) and mCherry-pCDFDuet-1 (as an internal control for translation) or with the corresponding empty EGFP-pACYCDuet-1 + mCherry-pCDFDuet-1 vector. Cells were grown in 50 ml cultures of LB-0% NaCl at 37 °C, 180 rpm for 5 h. Protein overexpression was induced with 100 µM IPTG. The cell count for each sample was set to 10^8 cells/ml for flow cytometry. Each sample was detected for EGFP and mCherry fluorescence signal. In total 10000 cells were measured for each sample with a flow rate of 1. Shown is the mCherry channel; mCherry signal of Fur-EGFP + mCherry sample (red) and of EGFP + mCherry sample (blue). X-axis shows the fluorescence intensity (the more right the higher the signal) and the y-Axis the cell number. The translation of internal mCherry of the Fur-EGFP sample and control was the same. As expected the translation efficiency of mCherry is lower in all mnm^5s^2U34 tRNA thiolation-deficient strains.

The internal control mCherry (Figure 70) showed also nearly the same fluorescence intensities as described for mCherry signals of Fis-EGFP samples (Figure 64). The tRNA thiolation-deficient strains displayed an overlapping mCherry signal with the control fluorescence around 10^2. WT (DE3) exhibited again the strong mCherry fluorescence at 10^3 – 10^4. Only Δ*iscU* (DE3) imaged a difference to mCherry Fis-EGFP signal. For the mCherry Fur-EGFP sample, it showed also a strong mCherry signal around 10^3 – 10^4 but it had a further peak at 10^2-10^3 (Figure 70). This double peak suggested that Δ*iscU* (DE3) contained a heterogeneous population of the cell expressing Fur-EGFP. The peak at higher fluorescence intensity represented cells expressing more mCherry and the peak at lower intensity cells with less mCherry amounts.

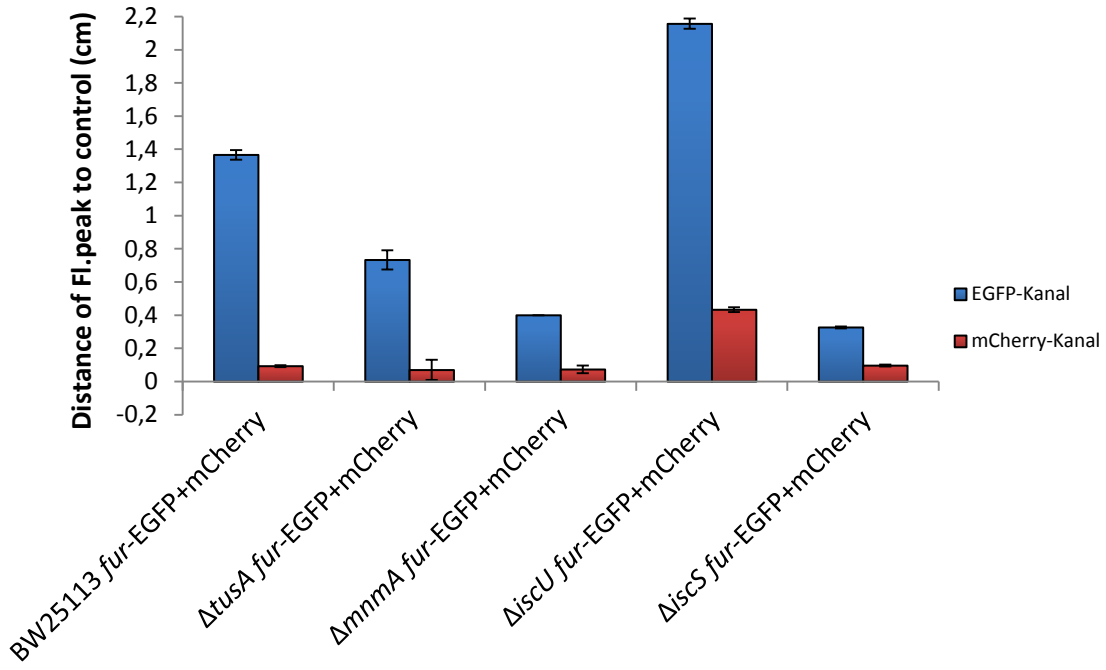

Figure 71: Fur-EGFP overexpression in deletion strains of genes involved in mnm^{5}s^{2}U34 tRNA thiolation shown in distance measurement to the control EGFP + mCherry fluorescence signal in each strain.

BW25113 (WT) (DE3), Δ*tusA* (DE3), Δ*mnmA* (DE3), Δ*iscU* (DE3) and Δ*iscS* (DE3) strains were transformed with *fur*-EGFP-pACYCDuet-1 (for Fur-EGFP overexpression) and mCherry-pCDFDuet-1 (as an internal control for translation) or with the corresponding empty EGFP-pACYCDuet-1 + mCherry-pCDFDuet-1 vector. Blue is the EGFP signal and red is the mCherry signal. From flow cytometry histograms, the distance of the Fur-EGFP peak to the EGFP control peak (in EGFP channel) or mCherry signal peak to its corresponding control peak (in mCherry channel) was measured in each sample. The translation efficiency of Fur-EGFP was lowest in all mnm^{5}s^{2}U34 tRNA thiolation-deficient strains.

Figure 71 visualizes the difference of Fur-EGFP fusion protein on the translation level between WT (DE3) and deletion strains of mnm^{5}s^{2}U34 tRNA thiolation. As already mentioned for Fis-EGFP the shift between Fis-EGFP or mCherry fluorescence signal to their respective control peak were manually determined from flow cytometry histograms. The results of Fur-EGFP resemble that of Fis-EGFP. Strains of mnm^{5}s^{2}U34 tRNA thiolation displayed the lowest shift to control in the GFP channel whereas this in Δ*tusA* (DE3) was slightly higher (Figure 71). Δ*mnmA* (DE3) and Δ*iscS* (DE3) showed a distance of around 0.4 cm and 0.3 cm and Δ*tusA* (DE3) about 0.7 cm. WT (DE3) depicted a distance of 1.36 cm. Δ*iscU* (DE3) strain represented an increased distance of 2.15 cm compared to the Fis-EGFP translation (1.76 cm). In total, the Fur-EGFP translation was nearly identical to that of Fis-EGFP in the tested strains.

As described for the Fur protein a further candidate to test was the RpoS protein since its gene expression is increased if the TusA protein is deleted (Dahl *et al.,* 2013). So the translation efficiency of RpoS-EGFP fusion was proven in WT (DE3) and tRNA thiolation-deficient strains (Figure 72 – 74).

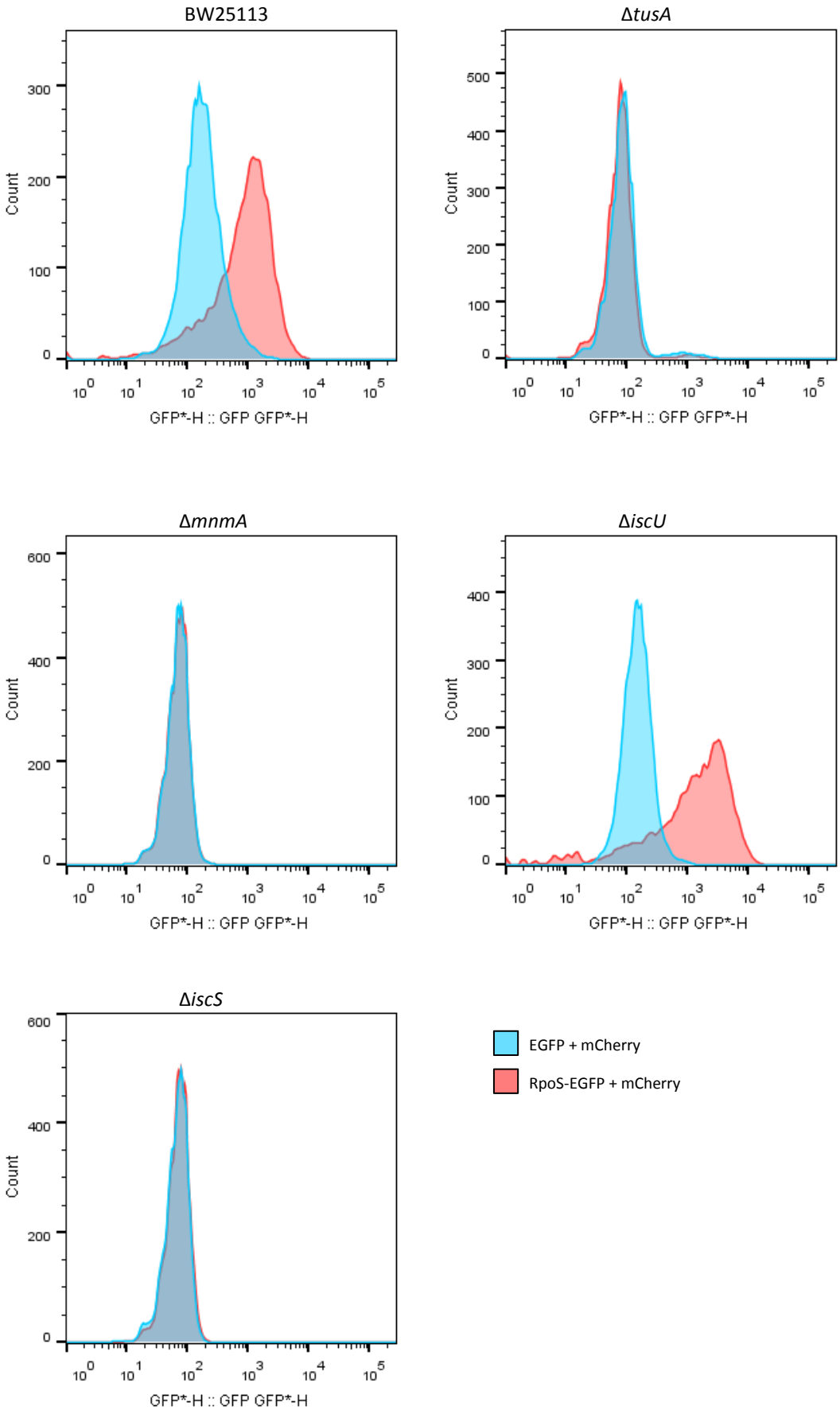
BW25113
ΔtusA
ΔmnmA
ΔiscU
ΔiscS
Count
GFP*-H :: GFP GFP*-H
EGFP + mCherry
RpoS-EGFP + mCherry

Figure 72: Flow cytometry histograms of the fluorescence recorded from RpoS-EGFP fusion (GFP channel) expressed in deletion strains of genes involved in mnm^{5}s^{2}U34 tRNA thiolation.

Translation efficiency of lysine-, glutamate- and glutamine-rich protein RpoS was analyzed in BW25113 WT (DE3) and tRNA thiolation-deficient strains.

BW25113 (WT) (DE3), Δ*tusA* (DE3), Δ*mnmA* (DE3), Δ*iscU* (DE3) and Δ*iscS* (DE3) strains were transformed with *rpoS*-EGFP-pACYCDuet-1 (for RpoS-EGFP overexpression) and mCherry-pCDFDuet-1 (as an internal control for translation) or with the corresponding empty EGFP-pACYCDuet-1 + mCherry-pCDFDuet-1 vector. Cells were grown in 50 ml cultures of LB-0% NaCl at 37 °C, 180 rpm for 5 h. Protein overexpression was induced with 100 µM IPTG. The cell count for each sample was set to 10^8 cells/ml for flow cytometry. Each sample was detected for EGFP and mCherry fluorescence signal. In total 10000 cells were measured for each sample with a flow rate of 1. Shown is the GFP channel; RpoS-EGFP signal of RpoS-EGFP + mCherry sample (red) and the EGFP signal of EGFP + mCherry sample (blue). X-axis shows the fluorescence intensity (the more right the higher the signal) and the y-Axis the cell number. The translation efficiency of RpoS-EGFP was lowest in all mnm^{5}s^{2}U34 tRNA thiolation-deficient strains. Compared to the other EGFP-fusion constructs (Fis- and Fur-EGFP) the translation of RpoS-EGFP was lower overall.

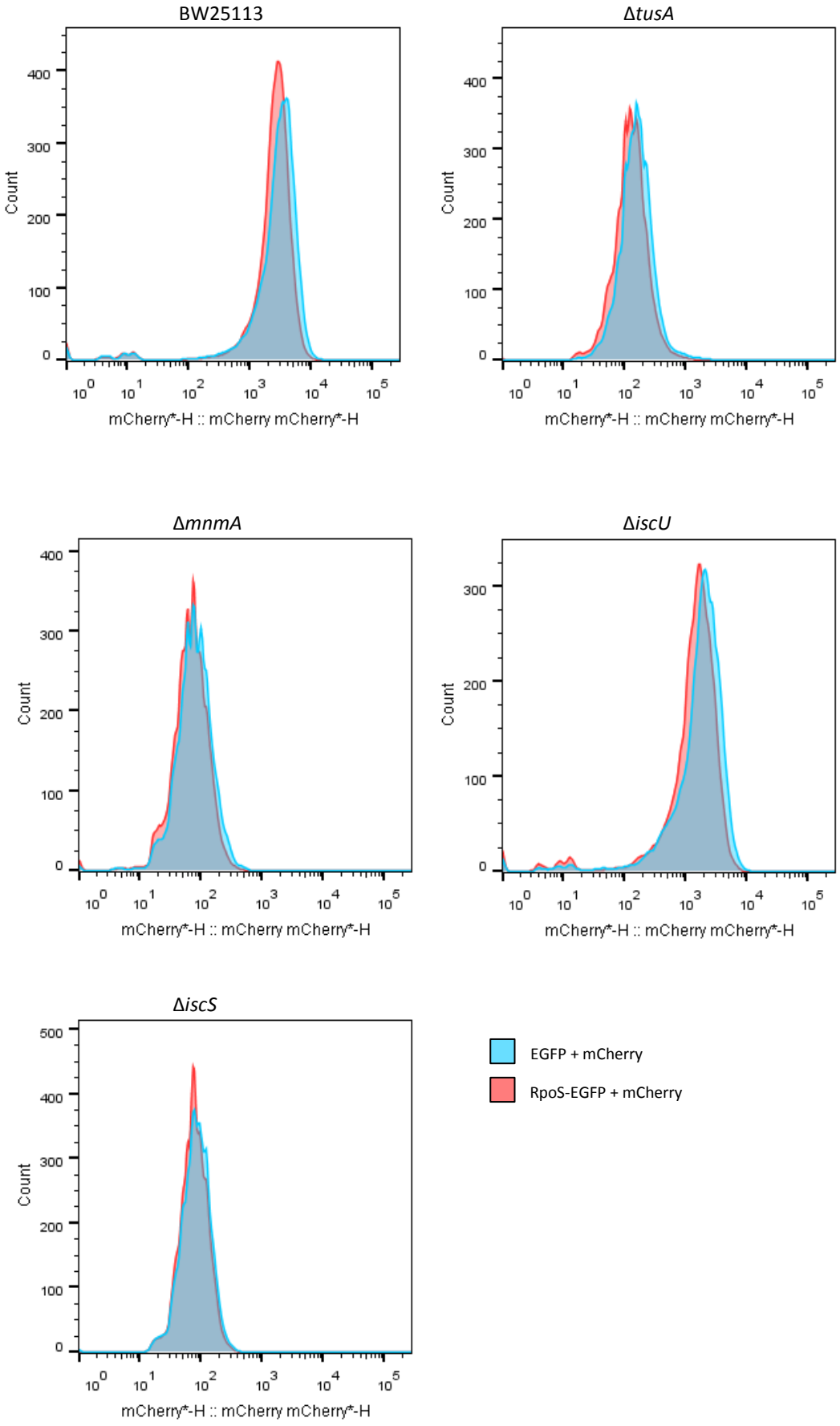
BW25113
ΔtusA
ΔmnmA
ΔiscU
ΔiscS
Count
mCherry*-H :: mCherry mCherry*-H
EGFP + mCherry
RpoS-EGFP + mCherry

Figure 73: Flow cytometry histograms of RpoS-EGFP fusion (mCherry channel) expressed in deletion strains of genes involved in mnm^{5}s^{2}U34 tRNA thiolation.

Translation efficiency of lysine-, glutamate- and glutamine-rich protein RpoS was analyzed in BW25113 WT (DE3) and tRNA thiolation-deficient strains.

BW25113 (WT) (DE3), Δ*tusA* (DE3), Δ*mnmA* (DE3), Δ*iscU* (DE3) and Δ*iscS* (DE3) strains were transformed with *rpoS*-EGFP-pACYCDuet-1 (for RpoS-EGFP overexpression) and mCherry-pCDFDuet-1 (as an internal control for translation) or with the corresponding empty EGFP-pACYCDuet-1 + mCherry-pCDFDuet-1 vector. Cells were grown in 50 ml cultures of LB-0% NaCl at 37 °C, 180 rpm for 5 h. Protein overexpression was induced with 100 µM IPTG. The cell count for each sample was set to 10^8 cells/ml for flow cytometry. Each sample was detected for EGFP and mCherry fluorescence signal. In total 10000 cells were measured for each sample with a flow rate of 1. Shown is the mCherry channel; mCherry signal of RpoS-EGFP + mCherry sample (red) and of EGFP + mCherry sample (blue). X-axis shows the fluorescence intensity (the more right the higher the signal) and the y-Axis the cell number. The translation of internal mCherry of the RpoS-EGFP sample and control was the same. As expected the translation efficiency of mCherry is lower in all mnm^{5}s^{2}U34 tRNA thiolation-deficient strains.

Expression of RpoS-EGFP in WT (DE3), Δ*tusA* (DE3), Δ*mnmA* (DE3), Δ*iscU* (DE3) and Δ*iscS* (DE3) strains led to deviating results than that of Fis- and Fur-EGFP. Figures 72 and 73 visualize the results of RpoS-EGFP translation in EGFP and mCherry channels. WT (DE3) showed a positive fluorescence signal for RpoS-EGFP (Figure 72) which was slightly decreased than Fis- and Fur-EGFP signals (Figures 66 and 69). The peak was more centered at 10^3 and 225 cells expressed RpoS-EGFP. Furthermore, the shift of the RpoS-EGFP peak to its control EGFP fluorescence peak was lower than for Fis- and Fur-EGFP. Thus, RpoS-EGFP translation was found to be lower than the other tested two fusion proteins. Strains of mnm^{5}s^{2}U34 tRNA thiolation revealed the same RpoS-EGFP fluorescence intensity as for the EGFP control fluorescence signal (Figure 72). They were completely overlapping at around 10^2. The RpoS-EGFP peak in Δ*mnmA* (DE3), Δ*iscS* (DE3) was slightly shifted to the left compared to Δ*tusA* (DE3). Moreover, Δ*tusA* (DE3) cells formed a small shoulder at 10^3 which was a hint for a small amount of the cell population expressed more RpoS-EGFP. In Δ*tusA* (DE3) 480 cells of 10000 expressed RpoS-EGFP, in Δ*mnmA* (DE3) and in Δ*iscS* (DE3) 500 cells. RpoS-EGFP signal in Δ*iscU* (DE3) was nearly the same as in WT (DE3) only slightly higher and wider starting at 10^2 - 10^4. 174 Δ*iscU* (DE3) cells of 10000 produced the RpoS-EGFP protein. Fluorescence signals of internal mCherry (Figure 73) were identical to Fis-EGFP mCherry fluorescence (Figure 67).

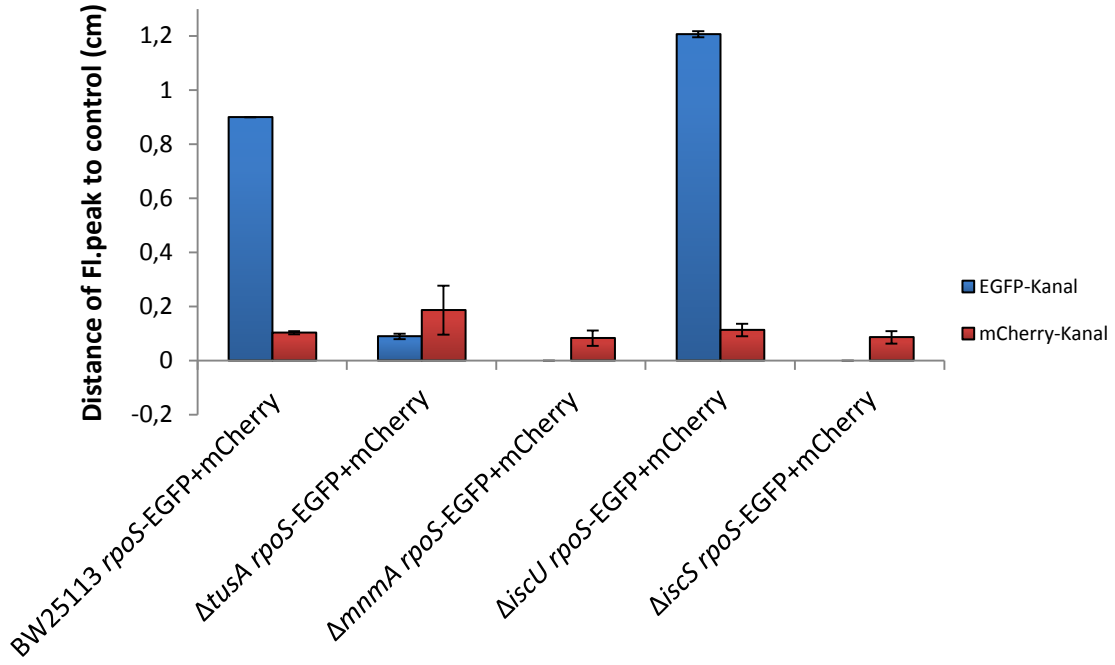

Figure 74: RpoS-EGFP overexpression in deletion strains of genes involved in mnm^{5}s^{2}U34 tRNA thiolation shown in distance measurement to the control EGFP + mCherry fluorescence signal in each strain.

BW25113 (WT) (DE3), Δ*tusA* (DE3), Δ*mnmA* (DE3), Δ*iscU* (DE3) and Δ*iscS* (DE3) strains were transformed with *rpoS*-EGFP-pACYCDuet-1 (for RpoS-EGFP overexpression) and mCherry-pCDFDuet-1 (as an internal control for translation) or with the corresponding empty EGFP-pACYCDuet-1 + mCherry-pCDFDuet-1 vector. Blue is the EGFP signal and red is the mCherry signal. From flow cytometry histograms, the distance of the RpoS-EGFP peak to the EGFP control peak (in the GFP channel) or mCherry signal peak to its corresponding control peak (in the mCherry channel) was measured in each sample. The translation efficiency of RpoS-EGFP was lowest in all mnm^{5}s^{2}U34 tRNA thiolation-deficient strains.

Figure 74 visualizes the difference of RpoS-EGFP fusion protein on the translation level between WT (DE3) and deletion strains of mnm^{5}s^{2}U34 tRNA thiolation. As previously described for histograms, RpoS-EGFP translation (Figure 74) was significantly overall lower than Fis- and Fur-EGFP expression (Figures 68 and 71). The distance of the fusion protein peak to the control peak decreased in all tested strains. But the tendency of the translation in the strains was the same as for Fis- and Fur-EGFP. Strains of mnm^{5}s^{2}U34 tRNA thiolation displayed the lowest shift to control in the GFP channel whereas this in Δ*tusA* (DE3) was slightly higher (Figure 74). Δ*mnmA* (DE3) and Δ*iscS* (DE3) expressed no RpoS-EGFP or only in very small amounts since they showed no distance to the control EGFP peak. For Δ*tusA* (DE3) the distance was only a bit higher about 0.09 cm. In WT (DE3) the shift reduced to 0.9 cm

(from 1.25 cm (Fis-EGFP) or 1.36 cm (Fur-EGFP). Δ*iscU* (DE3) pointed also a decrease from 1.76 cm (Fis-EGFP) or 2.15 cm (Fur-EGFP) to 1.2 cm. With this approach, it was figured out that if the tRNA thiolation is defective as in Δ*tusA* (DE3), Δ*mnmA* (DE3) and Δ*iscS* (DE3) then RpoS-EGFP was almost not expressed. So the defect in mnm^5s^2U34 tRNA thiolation most affected RpoS protein translation.

To have an additional control a further Fis-EGFP fusion construct was synthesized for which all amino acid codons for lysines (K), glutamates (E) and glutamines (Q) were changed to alanine. With this mutation, it was achieved to eliminate the positive effects of mnm^5s^2U34 tRNA thiolation (more efficient ribosome binding; prevention of frameshift). The new construct was called mutated Fis-EGFP (mFis-EGFP) and should be expressed in the same amount as the control EGFP. Since the mnm^5s^2U34 tRNA thiolation is defective in Δ*tusA* strain and there are no lysines, glutamates and glutamines existing anymore (which were mainly influenced by thiolation). It appeared also possible that probably the translation of mFis-EGFP in WT (DE3) and in Δ*tusA* (DE3) will be similar.

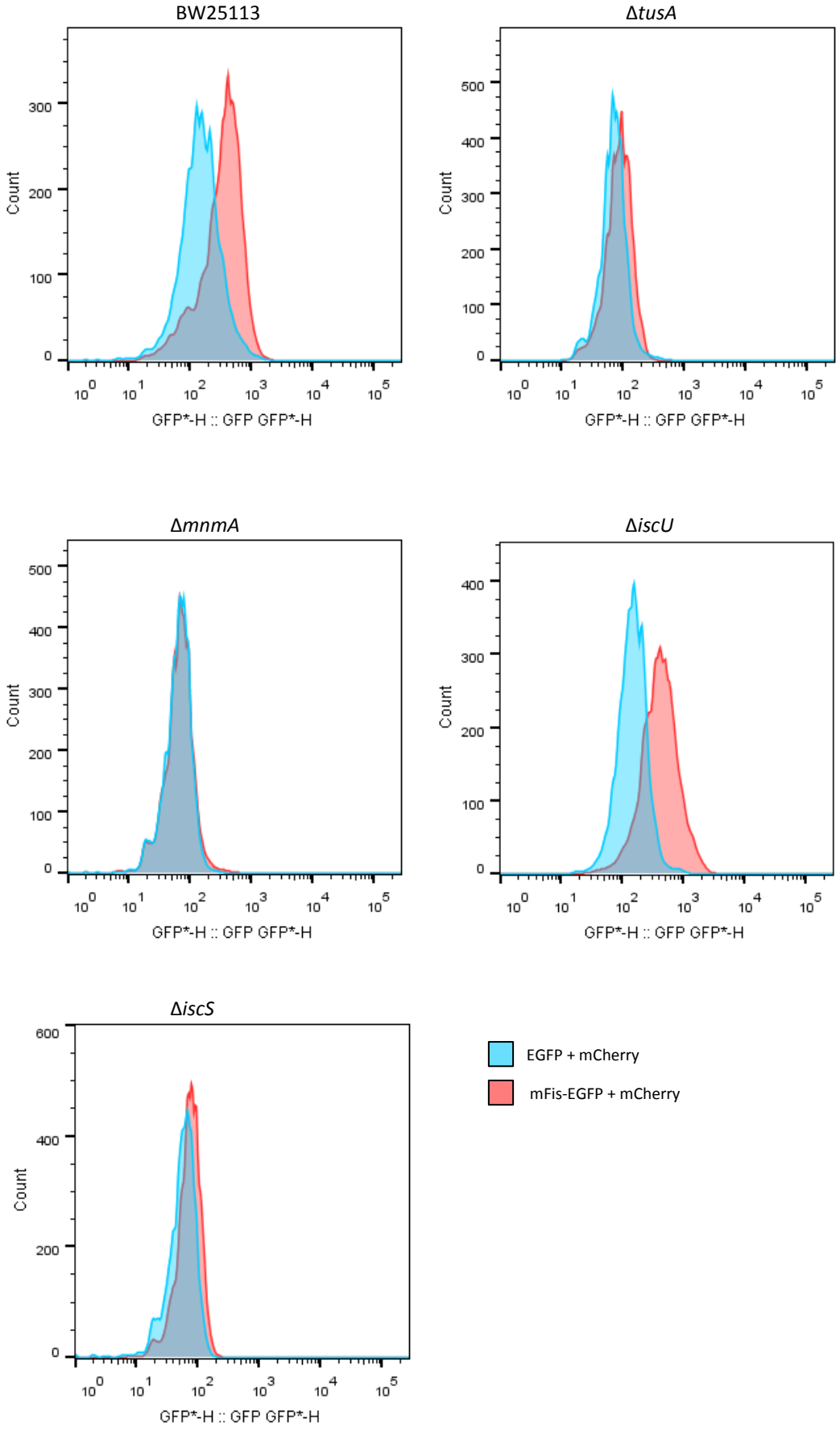
BW25113
ΔtusA
ΔmnmA
ΔiscU
ΔiscS
Count
GFP*-H :: GFP GFP*-H
EGFP + mCherry
mFis-EGFP + mCherry

Figure 75: Flow cytometry histograms of the fluorescence recorded from mutated Fis-EGFP fusion (mFis-EGFP) (GFP channel) expressed in deletion strains of genes involved in mnm^{5}s^{2}U34 tRNA thiolation.

BW25113 (WT) (DE3), Δ*tusA* (DE3), Δ*mnmA* (DE3), Δ*iscU* (DE3) and Δ*iscS* (DE3) strains were transformed with m*fis*-EGFP-pACYCDuet-1 (for mFis-EGFP overexpression) and mCherry-pCDFDuet-1 (as an internal control for translation) or with the corresponding empty EGFP-pACYCDuet-1 + mCherry-pCDFDuet-1 vector. Cells were grown in 50 ml cultures of LB-0% NaCl at 37 °C, 180 rpm for 5 h. Protein overexpression was induced with 100 µM IPTG. The cell count for each sample was set to 10^8 cells/ml for flow cytometry. Each sample was detected for EGFP and mCherry fluorescence signal. In total 10000 cells were measured for each sample with a flow rate of 1. Shown is the GFP channel; mFis-EGFP signal of mFis-EGFP + mCherry sample (red) and the EGFP signal of EGFP + mCherry sample (blue). X-axis shows the fluorescence intensity (the more right the higher the signal) and the y-Axis the cell number. The translation efficiency of mFis-EGFP was reduced in all strains compared to the not mutated Fis-EGFP fusion. The positive effect of mnm^{5}s^{2}U34 tRNA thiolation was eliminated.

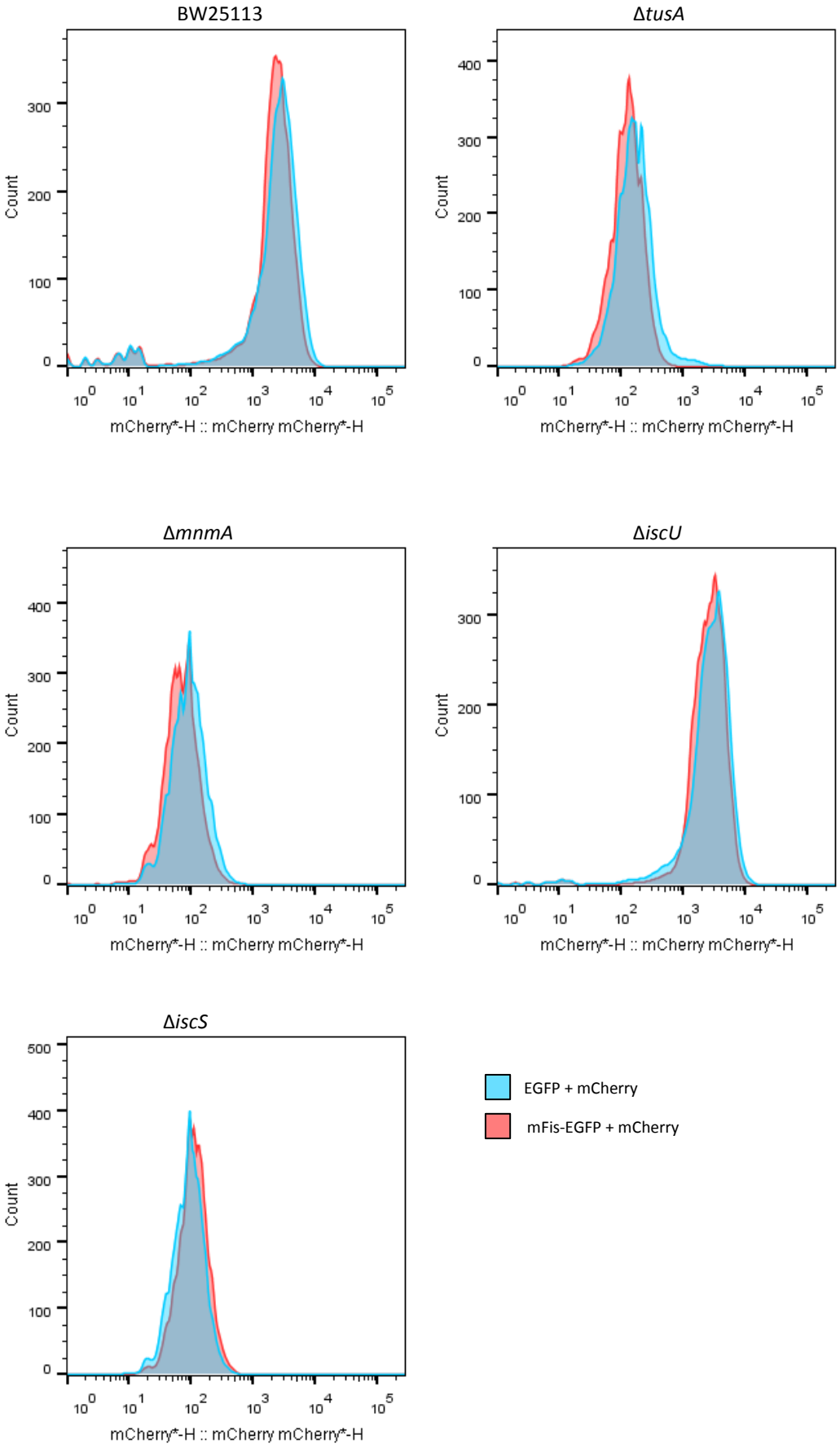
BW25113
ΔtusA
ΔmnmA
ΔiscU
ΔiscS
Count
mCherry*-H :: mCherry mCherry*-H
EGFP + mCherry
mFis-EGFP + mCherry

Figure 76: Flow cytometry histograms of the fluorescence recorded from mutated Fis-EGFP fusion (mCherry channel) expressed in deletion strains of genes involved in mnm^{5}s^{2}U34 tRNA thiolation.

BW25113 (WT) (DE3), Δ*tusA* (DE3), Δ*mnmA* (DE3), Δ*iscU* (DE3) and Δ*iscS* (DE3) strains were transformed with m*fis*-EGFP-pACYCDuet-1 (for mFis-EGFP overexpression) and mCherry-pCDFDuet-1 (as an internal control for translation) or with the corresponding empty EGFP-pACYCDuet-1 + mCherry-pCDFDuet-1 vector. Cells were grown in 50 ml cultures of LB-0% NaCl at 37 °C, 180 rpm for 5 h. Protein overexpression was induced with 100 µM IPTG. Cell mass was observed by measuring OD_{600}. The initial OD_{600} was 0.05. The cell count for each sample was set to 10^8 cells/ml for flow cytometry. Each sample was detected for EGFP and mCherry fluorescence signal. In total 10000 cells were measured for each sample with a flow rate of 1. Shown is the mCherry channel; mCherry signal of mFis-EGFP + mCherry sample (red) and of EGFP + mCherry sample (blue). X-axis shows the fluorescence intensity (the more right the higher the signal) and the y-Axis the cell number. The translation of internal mCherry of mFis-EGFP sample and control was the same. As expected the translation efficiency of mCherry is lower in all mnm^{5}s^{2}U34 tRNA thiolation-deficient strains.

Measurements of translation efficiency of mFis-EGFP are imaged in Figure 75, mFis-EGFP in the GFP channel, and 76, in the mCherry channel. WT (DE3) exhibited a positive mFis-EGFP fluorescence around 10^2 - 10^3 which is reduced compared to not mutated Fis-EGFP (Figure 67, fluorescence intensity for Fis-EGFP was between 10^3 - 10^4). So because of the mutation, the positive effect of mnm^{5}s^{2}U34 tRNA thiolation was missing which resulted in decreased mFis-EGFP translation. 340 WT (DE3) cells of 10000 expressed mFis-EGFP (Figure 75). Δ*tusA* (DE3) had a minimum translation of mFis-EGFP (10^2) compared to its corresponding control EGFP signal and it was lower than Fis-EGFP translation (10^2 – 10^3). Around 450 cells produced the mFis-EGFP. As expected the mFis-EGFP was nearly expressed in the same amount as the control EGFP which indicated a lack of lysines, glutamates and glutamines. Therefore translation efficiency decreased additionally in Δ*tusA* (DE3) strain (in addition to the consisting growth defect) by elimination of these three amino acids. Δ*mnmA* (DE3) and Δ*iscS* (DE3) displayed similar mFis-EGFP fluorescence at 10^2 whereas fluorescence in Δ*iscS* (DE3) slightly shifted to the right. Their signal intensity resembled that of Δ*tusA* (DE3). 430 cells in Δ*mnmA* (DE3) expressed mFis-EGFP and 500 cells in Δ*iscS* (DE3). A slightly stronger mFis-EGFP signal was detected in Δ*iscU* (DE3) (10^2 - 10^3) as in WT (DE3). In Δ*iscU* (DE3), the mFis-EGFP signal is minimally shifted to the right. But also for this strain was the decreased translation efficiency clearly visible as for not mutated Fis-EGFP. 310 cells of 10000 Δ*iscU* (DE3) produced mFis-EGFP fusion protein. The determination of internal mCherry fluorescence of mFis-EGFP samples (Figure 76) visualized the same intensities as for mCherry of Fis-EGFP expression.

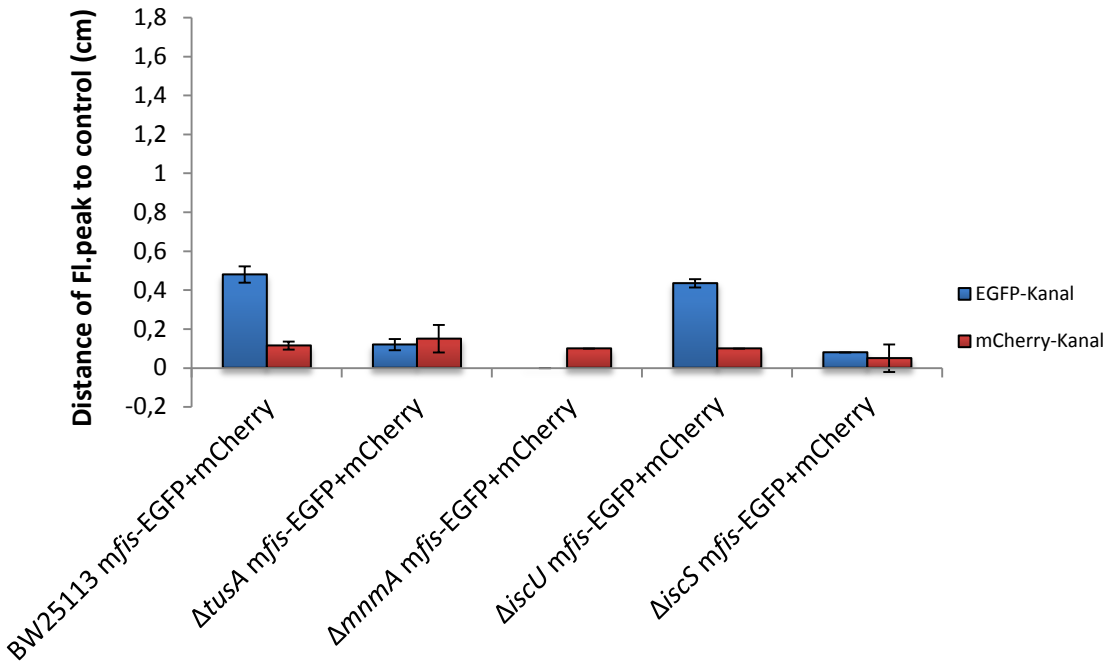

Figure 77: mutated Fis-EGFP (mFis-EGFP) overexpression in deletion strains of genes involved in mnm^{5}s^{2}U34 tRNA thiolation shown in distance measurement to the control EGFP + mCherry fluorescence signal in each strain.

BW25113 (WT) (DE3), Δ*tusA* (DE3), Δ*mnmA* (DE3), Δ*iscU* (DE3) and Δ*iscS* (DE3) strains were transformed with m*fis*-EGFP-pACYCDuet-1 (for mFis-EGFP overexpression) and mCherry-pCDFDuet-1 (as an internal control for translation) or with the corresponding empty EGFP-pACYCDuet-1 + mCherry-pCDFDuet-1 vector. Blue is the EGFP signal and red is the mCherry signal. From flow cytometry histograms, the distance of the mFis-EGFP peak to the EGFP control peak (in the GFP channel) or mCherry signal peak to its corresponding control peak (in the mCherry channel) was measured in each sample. The translation efficiency of mFis-EGFP was lowest in all mnm^{5}s^{2}U34 tRNA thiolation-deficient strains whereby the translation of mFis-EGFP was in general reduced in all strains compared to the not mutated Fis-EGFP fusion. The positive effect of mnm^{5}s^{2}U34 tRNA thiolation was eliminated.

The shown bar graph (Figure 77) represents the difference of mFis-EGFP fusion protein on translation level between WT (DE3) and gene deletion strains of mnm^{5}s^{2}U34 tRNA thiolation. All tested strains showed a reduction of translation efficiency in the case of mFis-EGFP (compared to Fis-EGFP (Figure 68)). In the GFP channel a shift of 0.12 cm was detected for Δ*tusA* (DE3) and 0.08 cm for Δ*iscS* (DE3), which were definitely higher for the not mutated Fis-EGFP protein (0.4 cm in Δ*tusA* (DE3) and 0.3 cm in Δ*iscS* (DE3)). Δ*mnmA* (DE3) mFis-EGFP showed no shift to its control EGFP peak. For the last two strains, WT (DE3) and Δ*iscU* (DE3), a higher decrease in translation efficiency was recorded. The shift of mFis-EGFP expression to the control EGFP dropped more than half to 0.48 cm (from Fis-EGFP 1.25 cm). This time

Δ*iscU* (DE3) exhibited nearly identical translation efficiency as WT (DE3) with a distance of 0.43 cm. Overall, the elimination of lysines, glutamates and glutamines resulted in reduced translation efficiency as well for mnm^5s^2U34 tRNA thiolation strains as for non-tRNA thiolation strains (control strains). Finally, these results strengthen the importance of lysines, glutamates and glutamines and the mnm^5s^2U34 tRNA thiolation for efficient protein translation.

5 Discussion

In 1998, Yamashino and colleagues discovered the YhhP enzyme, which was later renamed to TusA, the tRNA-2-thiouridine synthase (Yamashino *et al.*, 1998; Ikeuchi *et al.*, 2006). TusA is a sulfur transferase and acts as a sulfur carrier protein in tRNA thiolation for the formation of 2-thiouridine at the position 34 (wobble base) of tRNAs for lysine (Lys), glutamate (Glu) and glutamine (Gln). It binds the sulfur atom as a persulfide and transfers it to further proteins (Westley *et al*., 1983) during mnm^5s^2U tRNA modification and Moco biosynthesis (Ikeuchi *et al.*, 2006; Dahl *et al.*, 2013). This thiomodification of tRNA is important since it allows more efficient ribosome binding and averts frameshifting during the translation of proteins (Ashraf *et al.*, 1999; Yokoyama *et al.*, 1985; Moukadiri *et al.*, 2013). The absence of TusA revealed an essential role in bacterial cell physiology (Yamashino *et al.*, 1998). A *tusA* gene deletion strain showed a growth-deficient phenotype. *E. coli* cells usually grow as short rods. However, the *tusA* deleted cells were shown to grow slower than WT cells. They were long and grew as filaments during the exponential growth phase in a rich medium, and subsequently disappeared in the stationary phase. This indicated that the cells probably were not able to separate into two new cells during the growth process and therefore had a growth defect. Such a phenotype occurs only during growth in a rich medium and not in a minimal medium (Yamashino *et al.*, 1998; Ishii *et al.*, 2000). More specifically, it was already suggested that the absence of TusA protein due to the *tusA* gene deletion leads to a defect in FtsZ ring formation which results in non-dividing elongated cells (filaments) (Ishii *et al.*, 2000). This idea was confirmed by the identification of the *ftsZ* gene as a multicopy suppressor for the Δ*tusA* phenotype. Similarly, the *dksA* gene which was also discovered in the same study by Ishii *et al.* (2000) and serve as a multicopy suppressor. Both *ftsZ* and *dksA* were able to suppress the lethality of Δ*tusA* cells. They allowed the *tusA* mutant cells grow faster and have a rod cell shape like WT cells (Ishii *et al.*, 2000). However, it remained unclear how the *tusA* deletion affected the FtsZ ring formation and thus the cell separation.

As well as the initial study of Yamashino *et al.*, the report of the Ishii *et al.* described that TusA influences the stability of RpoS during the exponential growth phase. Moreover, deletion of *tusA* gene additionally impairs the translation of the RpoS protein (Aubee *et al.*, 2017). Under anaerobic conditions, deletion of the *tusA* gene results in increased *rpoS* gene

expression (Dahl *et al.*, 2013). But how the exact connection is between TusA to FtsZ, DksA and RpoS is not yet fully understood.

Therefore, this work was focused on dissecting the role of the TusA protein in cell growth and FtsZ ring assembly in *E. coli*. In the first part of this work, it was aimed to discover the reason for the filamentous growth of the *tusA* mutant strain. In particular, growth and morphological behavior were analyzed and complementation studies were performed. Moreover, it was worthwhile to know whether or not this growth-deficient phenotype was restricted to Δ*tusA* or whether or not it also affected other deletion strains. For that, several mutant strains involved in mnm^5s^2U34 tRNA modification were investigated for their growth phenotype. In the second part, since FtsZ ring formation was supposed to be defective in filaments, a possible intracellular interaction of TusA and FtsZ was examined by fluorescent (EGFP and mCherry) fusion protein expression and FRET. In the third part of this work, the cellular FtsZ concentration and its change during different growth phases were determined via immunoblotting. Not only the cellular FtsZ content seemed to be important, but also the cellular Fis amount was one of the relevant factors to be explored. The reason for this was that TusA was originally identified in a Δ*hns* background when searching for genes affecting cellular RpoS levels during the exponential phase (Yamashino *et al.*, 1998), and Fis regulates the expression of *hns*. Accordingly, a possible relationship of Fis to TusA or changes in Fis content in Δ*tusA* does not seem unimportant. Furthermore, it is remarkable that Fis is involved in cell division (Logan, 2006) and probably has a link to FtsZ. In the fourth and last part of this work, the translation efficiencies of certain proteins in *tusA* mutant and in additional gene deletion strains were studied to assess whether or not they were affected by using of unmodified U34 tRNAs of lysine, glutamate and glutamine. RpoS, Fur and Fis were counted as selected proteins for translation efficiency analysis by flow cytometry. As mentioned, TusA affects the stability and translation of RpoS (Yamashino *et al.*, 1998; Aubee *et al.*, 2017). There is a probability of a link between Fis and TusA. A deletion of the *tusA* gene revealed before that the expression of the *fur* gene is decreased (Dahl *et al.*, 2013).

5.1 TusA is important for normal cell growth and physiology in *E. coli*

First, the growth-deficient phenotype of the *tusA* mutant strain was investigated, based on the preliminary results of Ishii *et al.* (2000). For that, growth curves were recorded and cell

morphology of Δ*tusA* and the respective WT strain (BW25113) were investigated in a low-salt (0% NaCl) LB medium. The growth defect of a Δ*tusA* strain could be successfully reproduced in a low-salt LB medium. Δ*tusA* cells showed a retarded growth in the exponential phase compared to WT strain. Its growth was roughly two times slower than WT cells since in the exponential phase the cell density OD_{600} of Δ*tusA* was around 2 and for WT 4 (two times higher). Also, morphological analysis of Δ*tusA* cells confirmed the filamentous cell shape. During the exponential phase, Δ*tusA* cells were about 3 µm long, while WT cells were 1-2 µm short at the same time. The filamentous cells shortened with the transition into the stationary phase (approximately 1 µm), resembling more WT cells. So this fact highlighted that the growth defect of the *tusA* mutant strain concerning growth rate and cell morphology is obviously more pronounced during the exponential phase as also Yamashino *et al.* (1998) and Ishii *et al.* (2000) reported. Increasing the percentage of sodium chloride in LB medium (high salt – 3% NaCl) compensated for this growth defect so that the Δ*tusA* cells grew faster almost like WT cells and had short rod-shaped cell morphology. The increased amount of NaCl has probably a growth-promoting effect due to activating of cellular survival in a stress environment by RpoS. The increase of salt concentration in LB medium generates a higher osmolarity that involves some osmoregulated promoters. These promoters are induced by RpoS which acts as a regulator in stress situations (Ballesteros *et al.*, 1998). So RpoS enables the bacterial cell to adapt to the new environmental condition (the switch to high salt condition) by activating the corresponding gene expressions responsible for the adaptation process. Therefore, RpoS seemed to be necessary for the cell to distinguish, for example, the nutritional state between starvation and nutrient excess (Hengge-Aronis *et al.*, 1993).

As Ishii *et al.* (2000) postulated before, the retarded growth and filamentous cell shape indicate highly a growth and cell division defect in the Δ*tusA* strain. Probably in this Δ*tusA* mutant, there is a defect of FtsZ protein as a key protein in cell division. The microscopic investigation revealed that filamentous Δ*tusA* cells possessed multiple DNA parts that were arranged next to each other. DNA regions stained with DAPI (blue fluorescence) were clearly determined within a Δ*tusA* filament by morphological analysis. This suggested that although the DNA replication occurs correctly during cell growth, there is a defect in the step where FtsZ should act; probably either FtsZ is unable to assemble to the ring structure or the assembled ring is not able to constrict. Thus the lack of the FtsZ action due to a defect in this

process meant that the outer cell membrane was not forced to constrict and the bacterial cell cannot divide. Similar constriction problems of the bacterial cell were reported by Pogliano *et al.* (1997) and Sanchez-Gorostiaga *et al.* (2016). Consequently, Δ*tusA* cells became longer and formed filaments instead of the typical short rod shape of a bacterial cell.

To establish the ideal growth conditions for investigating the causes of the *tusA*-deficient phenotype, conditions of 0% salt were selected. For complementation studies of Δ*tusA* growth defect, the *tusA* gene was inserted into Δ*tusA* mutant on a plasmid to test whether the growth defect caused by the deletion of the *tusA* gene was reversible. Recorded growth curves of the pure WT (DE3) and Δ*tusA* (DE3) strains revealed higher growth rates in the absence of IPTG than with IPTG in a NaCl-free LB medium. In the case of TusA expression, the growth of both strains was even more increased and recorded the highest growth rate in this assay. Especially TusA expression in the Δ*tusA* (DE3) mutant exhibited a similar growth rate (OD_{600} is 3.96 at 5 h; 3.87 at 7 h) relative to the respective WT (DE3) strain (OD_{600} is 3.71 at 5 h; 4.3 at 7 h) which indicated obviously that the Δ*tusA* (DE3) growth defect was successfully complemented. In contrast, both strains showed the lowest growth in the presence of IPTG, whereas the TusA expression did not play a role. The results of the recorded growth rates were supported by the cell morphology of TusA expressing Δ*tusA* (DE3) cells, which no longer had the filamentous cell shape; they were short as WT (DE3) cells in the exponential phase. At the same time, the respective control Δ*tusA* (DE3) cells were longer. As mentioned above, this phenotype was present under IPTG-free conditions. In the presence of IPTG, cells of both strains were longer than their respective samples in the absence of IPTG. IPTG thus impairs Δ*tusA* (DE3) in addition to its pre-existing growth defect. In other words, if IPTG was not present, then complementation of the *tusA* deletion by expression of the TusA protein was successful. In turn, IPTG had a negative stress effect on the cell growth of WT (DE3) and Δ*tusA* (DE3) cells, since the cell growth was significantly decreased and aberrant morphology was observed. This suggestion that IPTG has a negative effect on cell growth is consistent with the observations of Einsfeldt *et al.* (2011) and Andersson *et al.* (1996). They reported that high levels of IPTG are toxic and significantly impair bacterial cell growth, for example, by reducing the biomass or higher expression of proteins for stress response (Einsfeldt *et al.*, 2011; Andersson *et al.*, 1996).

5.2 *In vivo* interaction studies of TusA and FtsZ in Δ*tusA* by FRET

One of the goals of this work was to detect and visualize an interaction between TusA and FtsZ. Since *tusA*-deleted cells have a cell division defect (Ishii *et al.*, 2000) and FtsZ is the main protein for the formation of the division ring at midcell during cell division (Margolin W., 2005). Thus, it appeared to be very likely that these two proteins could interact within a bacterial cell. So, if TusA and FtsZ are close together (a distance less than 10 nm (Simkova and Stanek, 2012)) within a Δ*tusA* filament, their interaction could be detected by **f**luorescence **r**esonance **e**nergy **t**ransfer (FRET). For this purpose, fluorescent fusion constructs of EGFP-TusA, mCherry-FtsZ and of EYFP-IscS (positive control later for FRET as described in Result section 4.4) were produced and their expression in WT (DE3) and Δ*tusA* (DE3) was tested individually in preparation for FRET. Nearly the same conditions were applied as above for the non-tagged proteins for growth curve studies. The expression of all three fluorescent fusion constructs in WT (DE3) was successful. Strong signals were determined for EYFP-IscS and EGFP-TusA. MCherry-FtsZ revealed a clear localization by the accumulation of red fluorescence signal at cell poles and the cell center. Two defined fluorescent points in the center of the cell meant that the FtsZ ring is still in the assembling phase, as FtsZ oscillates from one cell pole to the other during the assembly process into a rings structure until it has found its correct position in the cell center in alternation with the MinC inhibitory protein. The fact that these two red fluorescent dots showed no connection emphasized that the FtsZ protein is still assembling to a ring structure of the division machinery. During the cell growth the FtsZ ring assembly and the Min system oscillate from one cell pole to the other until nucleoid segregation is completed and the FtsZ ring can assemble at the midcell. The cell poles are occupied by MinC so that FtsZ cannot assemble at the cell poles and is therefore forced to form the Z ring at the nucleoid-free cell center (Addinall and Holland, 2002; Margolin, W., 2006). Also in WT (DE3) cells, the EGFP-TusA green fluorescence signal was spread over the whole cell, which enhances the possibility of an interaction since they are located in the same cellular region, the midcell. Moreover, the distribution of EGFP-TusA signal throughout the whole cell underlines the fact that TusA is a cytosolic protein, as also suggested by Ishii *et al.* (2000). Expression of both fusion proteins in the *tusA*-deficient strain delivered similar results as for WT (DE3). FtsZ expressing cells of the *tusA* mutant (DE3) strain showed a clearly visible signal at the cell poles, which also indicates that FtsZ is still in the assembling phase as described above for WT (DE3). Most

exciting was the cellular region of EGFP-TusA fusion protein expressed in Δ*tusA* (DE3); it again showed the EGFP signal throughout the whole cell and, in addition, a slight accumulation of the EGFP-TusA fluorescence at the cell poles, the same part of the cell as for mCherry-FtsZ. Thus, this highly suggested an interaction between TusA and FtsZ or proposed first hints for an interaction.

After establishing the cultivation conditions for expression of fusion proteins in WT (DE3) and Δ*tusA* (DE3) (induction with 15 µM IPTG instead of 5 µM to achieve higher fluorescence), interaction partners fused with different fluorescent proteins were co-expressed in WT (DE3) and *tusA* mutant (DE3). For this purpose, one *E. coli* cell contained a mCherry construct as well as EGFP-TusA or EYFP-IscS. Thus, a possible interaction between mCherry-FtsZ, mCherry-CyaY and mCherry-IscU with EGFP-TusA or EYFP-IscS was analyzed. CyaY was included in the investigation because this protein competes with the TusA protein for the binding to IscS (Leimkühler, 2014). Therefore, a possible interaction of CyaY-IscS should be tested. As already mentioned, IscU-IscS is the positive control for this approach, as their interaction has been shown previously (Shi *et al.*, 2010). A further important advance was the detection of a difference in expression and possible interaction in WT (DE3) and Δ*tusA* (DE3) cells. The co-expression of all fusion protein pairs in WT (DE3) and Δ*tusA* (DE3) was performed successfully. As already observed for the induvial expression of fusion proteins, the mCherry-FtsZ was again detectable as accumulated points within the cell. This meant that the FtsZ protein was slowly being incorporated into the ring structure but was still in the assembly phase (similar exemplary fluorescence images were shown by Monteiro *et al.*, 2018). Otherwise, the red mCherry fluorescence would have been spread over the entire *E. coli* WT (DE3) cell if no incorporation takes place. In contrast to FtsZ, the green fluorescence of the EGFP-TusA was spread more over the whole cell which emphasizes its cytosolic distribution. Consistent with expectation, the co-expression of fusion proteins with a slightly increased IPTG concentration delivered stronger fluorescence signals. This indicated that the expression of both fusion proteins (mCherry-FtsZ and EGFP-TusA) were increased and they were both expressed in the same WT (DE3) cell, since a higher the intensity of the fluorescence signal reflects an increased expression level of the fusion protein. For FRET measurement, it was important to have several cells in one and the same area expressing both proteins (to gain good statistics) and to allow for detection of FRET. Besides TusA, the dispersed red mCherry fluorescence confirmed also the cytosolic

occurrence of CyaY and IscU proteins and both proteins revealed several WT (DE3) cells co-expressing CyaY or IscU together with TusA. The cytosolic localization of CyaY and IscU was also already confirmed by Pohl *et al.* (2007) and Wachnowsky *et al.* (2016). By comparison, the co-expression of the same fusion proteins with EYFP-IscS in WT (DE3) samples were higher than with EGFP-TusA, which was detectable by the stronger and higher fluorescence signals. It is possible that the combination of mCherry and EYFP positively influence each other, leading to a higher expression of fusion proteins and thus to an increased fluorescence signal. The role as a positive control of mCherry-IscU and EYFP-IscS pair in this assay was confirmed by the simultaneous detection of mCherry and EYFP signals in the same cell. This implies most likely an *in vivo* interaction of IscS and IscU which is consistent with the report of Shi *et al.* (2010). In contrast to WT (DE3), in the *tusA* mutant (DE3) strain the interaction pair of mCherry+EGFP revealed higher fluorescence intensities and therefore increased expression levels than the EYFP-IscS samples. Due to the retarded slow growth of Δ*tusA* (DE3) strain, the overall fluorescence signals were slightly lowered than for the WT (DE3) signals. The lowered fluorescence signals would in turn reflect a reduced expression level of the fusion proteins studied. The mCherry-FtsZ sample accumulated in specific cell areas such as the cell poles and or the midcell. The other fusion proteins mCherry-CyaY, -IscU and EGFP-TusA are cytosolic (Pohl *et al.*, 2007; Wachnowsky *et al.*, 2016; Ishii *et al.*, 2000). Also, the Δ*tusA* mutant (DE3) showed more cells expressing both fusion proteins simultaneously in one area. The mCherry-FtsZ + EGFP-TusA Δ*tusA* (DE3) sample showed a vertically oriented elongated cell (about 4 µm, red arrow) in the middle of the merged image which showed the expressed FtsZ very clearly as dots more at cell poles as in midcell. Probably FtsZ oscillates during the assembly phase to find its correct position at the center of the cell (Margolin W., 2006). Co-expression of the mCherry fusion protein coincident with EYFP-IscS was reduced in Δ*tusA* (DE3), as mentioned. Nevertheless, it was possible to identify mCherry-FtsZ and mCherry-CyaY together with EYFP-IscS in some cells. For the positive control, mCherry-IscU in combination with EYFP-IscS, it was not easy to detect the fluorescence. Only in areas of clustered cells was a low fluorescence signal detectable. This could be based on the growth defect of the *tusA* mutant (DE3), which is not able to express enough fluorescent fusion proteins that their signal is detectable. This would also explain the low expression level. It was also striking that the fluorescence signals of the control cells with both fluorophores were not as strong as those of the fusion proteins in the same Δ*tusA*

(DE3) strain. That would mean that probably the fusion of proteins to the fluorophores mCherry, EGFP and EYFP increases the expression of fluorescent proteins. Especially in the *tusA* mutant (DE3), the absence of the thiomodification of $tRNA^{Lys}$, $tRNA^{Glu}$ and $tRNA^{Gln}$ most likely impairs the expression of the proteins during their translation process. In such a situation, the positive effect of mnm^5s^2U34 tRNA modification, such as efficient ribosome binding and averting of frameshift during translation, is missing (Ashraf *et al.*, 1999; Yokoyama *et al.*, 1985; Moukadiri *et al.*, 2013). The FRET measurement was performed for the co-expression of mCherry-IscU with EYFP-IscS in WT (DE3) with the application of the acceptor bleaching method. In this method, the fluorescence of the acceptor is bleached in one area and the fluorescence intensity of the donor will be increased exactly in this area when both proteins interact. Based on the microscope images, the bleaching of the acceptor mCherry-IscU appeared successful. However, only with the eye the difference between the fluorescence intensity of the donor EYFP-IscS before and after bleaching is not clearly recognizable. With the analysis of the fluorescence intensities of the FRET measurement of mCherry-IscU with EYFP-IscS in WT (DE3), a slight increase of the EYFP donor fluorescence was detectable after bleaching (around 44 sec). The calculated FRET efficiency is about 0.5% which is already very low for a positive control IscU-IscS (*in vitro* interaction of IscU-IscS reported in Raulfs *et al.*, 2008; Shi *et al.*, 2010). For a conclusion to claim to have FRET, the FRET efficiency should be above 1% (Sourjik *et al.*, 2007; set by Dr. Gabriel Malengo (MPI Marburg)). But with this method, it was not possible to detect a significant FRET signal. Maybe it was not really the right method to detect the interaction of proteins under *in vivo* conditions, because if the FRET efficiency was already so low for the positive control and even in the WT (DE3) strain, for the Δ*tusA* strain it would be probably very hard to detect any signal. As already explained in part (Growth of BW25113 and Δ*tusA*), the Δ*tusA* strain grows slower than the WT due to its growth defect, which also resulted in lower fluorescence intensities than for WT (DE3) samples. Further problems could be related to low expression levels of the fusion proteins due to the growth defect of Δ*tusA*, which could lead to low fluorescence intensities that exacerbated fluorescence and interaction detection by FRET. Furthermore, it was also not easy to find areas with simultaneous good expression levels for both donor (EGFP / EYFP) and acceptor (mCherry). In several cases, it seemed that the donor and acceptor expressions are affecting each other, so there were samples where

cells expressing donor expressed only very low acceptor or vice versa. These aspects should be considered for future investigations.

5.3 Suppression of Δ*tusA* growth deficiency and the cell division defect by FtsZ and DksA overexpression

The growth deficiency of the *tusA* mutant was shown to be reversible by the expression of selected genes (Ishii *et al.*, 2000). The multicopy suppressor genes *ftsZ* and *dksA* were identified as candidates capable of suppressing the lethality of Δ*tusA* cells in a rich LB medium. The Δ*tusA* cells can grow as fast as the WT strain, and their respective cell morphology shortens from long filaments to short rods in the exponential phase. However, the effect of deletion of the *tusA* gene on the FtsZ ring formation and thus the cell separation remains unclear (Ishii *et al.*, 2000). To elucidate the role of TusA for cell division, the Δ*tusA* growth defect should be complemented by insertion of *ftsZ* or *dksA* genes into Δ*tusA* cells. These inserted genes were expressed on a basal level (since cultivation with IPTG caused stress, see chapter 4.2). This work ascertained the opposite effect of *ftsZ* and *dksA* expression on Δ*tusA* growth defect as reported by Ishii *et al.* (2000). FtsZ was expressed in Δ*tusA* (DE3) and as a control in WT (DE3). Concerning the growth behavior, there was almost no significant difference between FtsZ-expressing WT (DE3) or Δ*tusA* (DE3) and the corresponding control samples with an empty pET15b plasmid. Even more surprising was the morphological analysis by phase contrast microscopy. The FtsZ overexpression led to longer WT (DE3) filaments compared to the control WT (DE3) cells which had the typical rod shape (around 1-2 µm). The cell length of the filaments further increased with the increasing growth time. FtsZ-expressing WT (DE3) cells were about 16 µm at exponential phase (5 h) or even longer (19 µm) in the stationary phase (7 h and 10 h). This result suggests that increased levels of cellular FtsZ leads to division problems. Such a phenomenon was also observed by Dai and Lutkenhaus (1992), where it was postulated that an appropriate ratio of FtsZ to other division components is important for a correct cell division process. It is likely that the increased FtsZ amount leads to an excessive number of FtsZ subunits, which cannot be incorporated into the ring structure and therefore results in division defect and elongation of cells. In Δ*tusA* (DE3) cells, the expression of FtsZ did not complement the growth-deficient phenotype of the *tusA* mutation. Filaments were present when FtsZ was

overexpressed in Δ*tusA* (DE3) strain, but the cells were not so long as FtsZ-expressing WT (DE3) cells. For example, a Δ*tusA* (DE3) cell length of about 8 µm was detected in the exponential phase (5h) and about 12 µm in the stationary phase (7 h and 10 h). The filaments contain many nuclei which were visible in the blue DAPI-stained DNA. But they were still within one cell that is covered by the cell membrane. So neither the growth rate nor the morphological abnormality could thus be complemented by the overexpression of FtsZ, as it was reported in Ishii *et al.* (2000). Similar findings were observed for an effect of DksA overexpression in Δ*tusA* (DE3). In contrast, DksA expression had no impact on WT (DE3) growth. Only DksA-expressing Δ*tusA* cells depicted a slightly reduced growth compared to their control. The overexpression of DksA did not affect the WT (DE3) cell morphology since the cells showed the same short cell morphology as the control WT (DE3) cells. They were about 1-2 µm, as is typical for *E. coli* cells. The result was the same for Δ*tusA* (DE3) cells. When DksA was overexpressed the cells were long, filamentous like the respective control Δ*tusA* (DE3) cells (about 4 µm in exponential phase). Thus, the cell length shortening effect of DksA expression on Δ*tusA* cells was not visible as was reported in the literature (Ishii *et al.*, 2000). So these observations suggest that there is no direct effect of DksA on Δ*tusA*. It is likely that DksA could have an indirect influence on TusA as a transcriptional regulator. Since DksA is involved in the transcription of genes during transcript elongation by binding directly to RNA polymerase (Perederina *et al.*, 2004). It also regulates the expression of the *rpoS* gene. DksA activates the *rpoS* expression and leads to increased cellular RpoS levels (Brown *et al.*, 2002), which is a further potential interaction partner of TusA (Yamashino *et al.*, 1998). Thus, such a possible relation does not exclude an effect of DksA to TusA via the RpoS protein.

5.4 Growth of deletion strains in genes involved in mnm^{5}s^{2}U34 tRNA thiolation

TusA is a sulfur carrier that is responsible for the transfer of sulfur to form 2-thiouridine at position 34 (wobble base) of tRNAs for Lys, Glu and Gln (Ikeuchi *et al.*, 2006). Since TusA is not the only enzyme involved in mnm^{5}s^{2}U34 thiomodification, further gene deletion strains of enzymes involved in this mnm^{5}s^{2}U34 tRNA thiolation pathway were investigated for their growth phenotype. The motivation here was to determine whether only the deletion of *tusA* led to the cell division defect or remaining proteins in tRNA thiolation were also responsible

for this defect. For this purpose, gene deletion strains of IscS, TusD, TusE and MnmA of mnm^{5}s^{2}U34 tRNA thiolation were examined for their cell growth and morphology.

All tested mutant strains (Δ*tusD*, Δ*tusE* and Δ*mnmA*) shared the similar slowed growth like Δ*tusA* strain (OD_{600} of all deletion strains around 2.5 and compared to them at WT 3.5 after 7 h). Only Δ*iscS* cells displayed an even more reduced growth phenotype than Δ*tusA* cells (OD_{600} of Δ*iscS* was around 1.3 at 7 h almost half less of Δ*tusA*). The growth of Δ*iscS* was so slowed down that it could not reach the WT OD_{600} in the stationary phase (OD_{600} of WT at 3.2 and of Δ*iscS* at 1.8 after 10 h). Also on a morphological level, all analyzed deletion strains of mnm^{5}s^{2}U34 tRNA modification had the same filamentous cell shape. They were longer in the exponential phase (3 h and 5 h) and shorter in the stationary phase (7 h and 10 h). Only Δ*iscS* cells were slightly longer than Δ*tusA*, Δ*tusD*, Δ*tusE* and Δ*mnmA* cells in the stationary phase, representing a more pronounced growth defect (Δ*iscS* cell were 3 µm long and Δ*tusA* cells around 1-2 µm at 7 h). Based on these results, it is obvious that the cell division defect could be due to a defect in mnm^{5}s^{2}U34 tRNA thiolation. To confirm this conclusion, as a control assay the growth behavior and morphological phenotype of mnm^{5}s^{2}U34 tRNA modification mutant strains were compared with deletions strains outside mnm^{5}s^{2}U34 tRNA modification pathway (Δ*iscU*, Δ*moaD*, Δ*thiI*, Δ*miaB*, Δ*ttcA*, Δ*sufS*). To review, IscU is involved in Fe-S cluster biosynthesis, MoaD in Moco biosynthesis, ThiI in thiamine biosynthesis (Kambampati and Lauhon, 2000) and s^{4}U8 modification, as well as MiaB in ms^{2}i^{6}adenosine and TtcA in s^{2}cytidine modifications (Leimkühler, 2014). SufS is a homologous protein of IscS and is expressed under stress conditions. Furthermore, it can complement the defective Fe-S cluster biosynthesis in the Δ*iscS* strain (Bühning *et al.*, 2017). The growth of Δ*miaB*, Δ*ttcA* and Δ*sufS* mutant strains behaved similar to WT cells. Δ*moaD* and Δ*thiI* cells showed a slightly reduced growth relative to WT cells but were still higher than Δ*tusA* cells. The slowest growth was observed for the Δ*iscU* strain. Cells of every tested strain (except Δ*iscU*) possessed similar rod-shaped cell morphology as for WT. Only Δ*iscU* cells had an intermediate cell length, which was not as short as WT cells and not as long as Δ*tusA* cells (Δ*iscU* cells were around 2 µm, Δ*tusA* 3 µm and WT 1 µm at 5 h). Δ*iscU* cells became shorter, akin to WT cells at 10 h. This approach allowed to identify the source of the growth-deficient phenotype. Mutant strains, which are not involved in mnm^{5}s^{2}U34 tRNA thiolation, displayed a typical short, rod-shaped cell morphology like WT cells (except Δ*iscU*). They had no elongated cell morphology, the filaments. Accordingly, this indicated that only strains with

gene deletions involved in mnm^5s^2U34 tRNA modification possessed a growth defect and had long, filamentous cells compared to WT. Thus the cell division defect originated from a defect in mnm^5s^2U34 tRNA thiolation and not by another tRNA modification like s^4U8 (ThiI), ms^2i^6A37 (MiaB) or s^2C32 (TtcA). That the mnm^5s^2U34 tRNA modification affects cell growth was also described by Nakai *et al.* (2019). They reported that the absence of this mnm^5s^2U34 tRNA modification impaired the leaf development and resulted in non-symmetrical leaves in *Arabidopsis thaliana*.

With the information that the cell division defect in Δ*tusA* is based on a defect in mnm^5s^2U34 tRNA thiolation obtained, it was additionally important to determine where exactly the defect in mnm^5s^2U34 tRNA thiolation lies. For this, strains of *miaA, mnmC*, *mnmE* gene deletions were tested in addition to WT and Δ*tusA*. MnmC and MnmE are responsible for different modifications of the tRNA U34 than MnmA (Leimkühler *et al.*, 2017; Moukadiri *et al.*, 2013). During the process of tRNA thiolation, MnmA transfers the sulfur to the tRNA uridine at position 34 and leads to the formation of 2-thiouridine. Further modifications are done by MnmE and MnmC proteins which depend on the substrate (glycine or ammonium). In the presence of glycine, MnmE (in complex with MnmG) produces $cmnm^5U$ (5-carboxymethylaminomethyluridine) and in the case of ammonium, the enzyme complex forms mnm^5U (5- methylaminomethyluridine). The bi-functional enzyme MnmC can convert $cmnm^5$ to nm^5U and nm^5U to the mature mnm^5U by adding a methyl group (Leimkühler *et al.*, 2017; Moukadiri *et al.*, 2013). MiaA modifies the adenine at position 37 (Aubee *et al.*, 2017). In addition, the Δ*rpoS* and Δ*hns* strains were also investigated. RpoS has been previously reported to interact with the TusA protein (Yamashino *et al.*, 1998). More specifically, TusA affects the stability and translation of RpoS (Yamashino *et al.*, 1998; Aubee *et al.*, 2017). In addition, H-NS is a DNA-binding protein and a global regulator (Picker and Wing, 2016); TusA was originally identified in a Δ*hns* background when screening for genes affecting cellular RpoS levels during the exponential phase (Yamashino *et al.*, 1998). The amount of H-NS is increased under aerobic conditions when the TusA protein is absent (Dahl *et al.*, 2013). It coils the DNA in a different way so that some parts of the DNA are more accessible for transcription factors and improves the transcription process. The growth rate of Δ*mnmC* and Δ*rpoS* exhibited no growth defect since their growth was at the same level as WT. Δ*miaA* and Δ*mnmE* cells represented a slightly reduced growth than WT but still higher than *tusA* mutant. The slowest growth was observed in Δ*hns*. Although Δ*hns* grew more

slowly, the cells of all strains except Δ*tusA* were short and rod-shaped like WT cells, and not elongated as Δ*tusA* filaments during the exponential phase. From these findings, it could be concluded that precisely a defect in mnm^5s^2U34 tRNA modification during the sulfur transfer from IscS to MnmA pathway is responsible for the growth and cell division defect of Δ*tusA* (and all gene deletions strains involved in mnm^5s^2U34 tRNA thiolation).

As described before, IscS supports the transfer of sulfur to a variety of important sulfur-containing biomolecules (Hidese *et al.*, 2011). Among these biomolecules, Fe-S clusters are the most important (Roche *et al.*, 2013). To emphasize that a defective mnm^5s^2U34 tRNA is the source of the growth-deficient phenotype of Δ*tusA*, and also to exclude another factor that could be the cause for this cell division defect, the defect in Fe-S cluster biosynthesis in Δ*iscS* was complemented by insertion of the *suf* operon (*sufABCDSE*) (Outten *et al.*, 2004). This *suf* operon (*sufABCDSE*) harbors the gene for the SufS enzyme which is a homologous protein of IscS and is expressed under stress conditions. Like IscS, SufS also mobilizes the sulfur and can complement the defective Fe-S cluster biosynthesis in the Δ*iscS* strain (Bühning *et al.*, 2017). Furthermore, the gene deletion strains of the tRNA thiolation pathway have no defect in Fe-S cluster biosynthesis (Bühning *et al.*, 2017). In addition to Δ*iscS* (DE3), the effect of *suf* operon overexpression was tested on WT (DE3) and Δ*tusA* (DE3) cell growth and morphology. The expression of the *suf* operon had no effect on WT (DE3) and Δ*tusA* (DE3) growth, but the intended result was observed for the complemented Δ*iscS* (DE3) strain. The control Δ*iscS* (DE3) grew worse than Δ*tusA* (DE3) while the *suf* operon-expressing Δ*iscS* (DE3) cells resulted in a higher growth. The growth defect of Δ*iscS* (DE3) cells could be regressed to the level of Δ*tusA* (DE3) which meant that the complemented Δ*iscS* (DE3) cells shared the same growth phenotype as strains with an impaired mnm^5s^2U34 tRNA modification. Also, the same effect was on the morphological level detectable. Δ*iscS* (DE3) cells with *suf* operon expression had the same slightly shortened cell length as Δ*tusA* (DE3) in the stationary phase (around 2 µm at 7 h). In contrast to this, control Δ*iscS* (DE3) were present as long filaments at the same growth phase (around 3 µm at 7 h). Consequently, the growth defect and filamentous cell morphology were caused by the absence of mnm^5s^2U34 tRNA modification and not the lack of Fe-S clusters, since *suf* operon overexpression did not affect the growth of the Δ*tusA* (DE3). Thus, all deletion strains involved in mnm^5s^2U34 tRNA modification (Δ*tusA*, Δ*tusD,* Δ*tusE,* Δ*mnmA and* Δ*iscS*) share

the retarded growth and elongated cell morphology that is induced by the absence of mnm^5s^2U34 tRNA thiolation. This phenomenon was confirmed by comparison to deletions strains outside the mnm^5s^2U34 tRNA thiolation (Δ*thiI*, Δ*miaB*, Δ*ttcA,* Δ*iscU*). In contrast, deletion strains with other defective tRNA modifications like s^4U8 (Δ*thiI*), ms^2i^6A37 (Δ*miaB*) or s^2C32 (Δ*ttcA*) or a defect in Fe-S cluster (Δ*iscU*) depicted no filamentous cell shape.

This conclusion could be confirmed on protein level. The SufS protein detection was investigated in WT, Δ*tusA,* Δ*sufS* and Δ*iscU* cells by immunoblotting. No SufS protein was present in Δ*tusA*, while its amount was slightly higher in Δ*iscU* than in WT. As reported in Outten *et al.* (2004) and Bühning *et al.* (2017) SufS is expressed under stress conditions, e.g. iron limitation which explains the fact for increased SufS presence in Δ*iscU*, since deletion of *iscU* disturbs the formation of Fe-S cluster which indicates a defect in Fe-S cluster biosynthesis. As a consequence to this, the cell activates its SufS expression to compensate the defect in Fe-S cluster formation, leading to an increased cellular amount of SufS. Thus, the absence of SufS protein in Δ*tusA* reinforced the idea that the growth and cell division defect was based on a defect in mnm^5s^2U34 tRNA thiolation, since the Fe-S cluster biosynthesis is working properly in Δ*tusA* strain.

5.5 Complementation of Δ*tusA* growth defect by RpoS overexpression

In the initial study by Yamashino *et al.* (1998), TusA was identified during screening for genes in Δ*hns* background that affects the cellular amount of RpoS. It was found that TusA influences the stability of RpoS during the exponential growth phase. Later it was discovered that the *tusA* gene deletion diminishes additionally the translation and stability of the RpoS protein (Aubee *et al.*, 2017) and under anaerobic conditions, it results in increased *rpoS* gene expression (Dahl *et al.*, 2013). However, the more specific details about the effect of TusA on RpoS stability, the link to FtsZ and in relation to this to the filamentous growth remained unclear. Based on this reported relationship between TusA and RpoS, the effect of RpoS overexpression on the *tusA* mutant strain was investigated by introducing the *rpoS* gene into this strain. It was aimed to test whether the expression of *rpoS* can complement the growth defect and filaments of Δ*tusA* cells. The RpoS complementation assay revealed that overexpression of RpoS had no influence on Δ*tusA* (DE3), neither on the growth rate nor on the morphological level. As RpoS-expressing Δ*tusA* (DE3) cells and their respective control Δ*tusA* (DE3) sample displayed the identical growth curve and long filaments in the

exponential phase and shortened rod-shaped cells in the stationary phase. In comparison, there was also no effect of RpoS overexpression on WT (DE3). According to these results, RpoS could not complement the growth defect of Δ*tusA* cells, at least not at the level tested. Therefore, it was assumed that the link between TusA and RpoS is directed from TusA to RpoS and not vice versa.

5.6 Detection of FtsZ levels in mnm^{5}s^{2}U34 tRNA thiolation deletion strains at different growth phases

TusA has a fundamental role in bacterial cell physiology (Yamashino *et al.*, 1998) since through a mutation of the *tusA* gene the cells grow slower than WT cells. They are long and grow as filaments during the exponential growth phase in a rich medium, deviating from the normally short rod shape of *E. coli* cells. The occurrence of such a growth defect indicates that the cells probably are not able to separate into two new cells during the growth process, suggesting that the TusA protein probably plays a role in the cytokinesis of *E. coli* cells. More specifically, absence of the TusA protein due to the *tusA* gene deletion leads to a defect in FtsZ ring formation which results in non-dividing elongated cells (filaments) (Ishii *et al.*, 2000). From this point of view, it appeared to be interesting to analyze the role of TusA on FtsZ levels by determining the cellular FtsZ amounts at different growth phases. According to the previous findings, the cell division defect of the pure Δ*tusA* strain is very clearly visible at 5 h of (Figure 41, third and first panel). Therefore, it seemed reasonable to first investigate the FtsZ levels at this time point. For the first approach, the FtsZ detection was performed with and without IPTG induction in WT (DE3) and Δ*tusA* (DE3) cells. FtsZ was visible around 40 kDa only when overexpressed from a plasmid in WT (DE3) and Δ*tusA* (DE3) mutant, with a stronger FtsZ signal in WT (DE3) than for Δ*tusA* (DE3). The strength of the signal implies the amount of FtsZ protein, which means in this case a higher cellular FtsZ amount was observed for WT (DE3) than for Δ*tusA* (DE3). IPTG had no influence since the FtsZ signal overexpressed from pET15b is the same as the FtsZ signal without IPTG induction, e.g. in WT (DE3). On the other hand, the FtsZ signal was not present when expressed at basal levels (without IPTG), indicating insufficient cellular FtsZ levels. Based on this result, further growth times (1.5 h, 3 h, 4 h) in addition to 5 h were observed to investigate the FtsZ at the basal expression level. The absence of FtsZ at 5 h of growth was also confirmed, as the

highest cellular FtsZ level in WT occurred more or less at the onset of the growth (1.5 h). This FtsZ level decreased as the growth time progressed until it finally disappeared completely in the supernatant. Interestingly, in contrast, the FtsZ concentration in the pellet increased until 4 h and decreased again after 5 h. This increased FtsZ amount in the pellet at 4 h could be an indication of the association of FtsZ to the cell membrane. During the formation of the FtsZ ring at the midcell of a bacterial cell a link of this FtsZ ring is built to the cell membrane via further proteins. Two proteins, one membrane-anchored ZipA protein and one membrane-associated FtsA protein, are binding to FtsZ. This binding stabilizes the FtsZ ring at the center of the bacterial cell and anchors it to the cell membrane (Pichoff *et al.*, 2015). GroEL (at 57 kDa) is the loading control for this assay and is produced in every protein expression as a housekeeping protein always in the same amount in every strain. At the beginning of the growth, the signal of GroEL was not strong since it is a chaperone that has to be first produced. Its signal was stronger in the supernatant than in the pellet as expected (since it is a cytoplasmic protein (Ishihama *et al.*, 2008)). The opposite result of cellular FtsZ amount was shown in the Δ*tusA* mutant. FtsZ was present at all selected time points in the supernatant. Its amount was lower at the onset of the growth (1.5 h) than at the later time points (3 h, 4 h and 5 h). The cellular FtsZ level increased at 3 h, 4 h and 5 h and appeared to remain constant. For the pellet of the same samples, no FtsZ protein band was visible. Thus, the *tusA* mutant had opposite cellular FtsZ concentrations than the WT: the amount of FtsZ decreased in WT up to 5 h and increased in the Δ*tusA* strain. Since all deletion strains of mnm^5s^2U34 tRNA modification demonstrated the same growth and cell division defect as the Δ*tusA* strain, it was important to investigate also their cellular FtsZ amount. The same trend of increasing cellular FtsZ levels as in Δ*tusA* was also shown by further deletion strains involved in the mnm^5s^2U34 tRNA modification pathway (Δ*tusD*, Δ*tusE*, Δ*mnmA* and Δ*iscS*). So the gene deletion of proteins involved in mnm^5s^2U34 modification most likely resulted in a defective mnm^5s^2U34 tRNA thiolation. This defect in mnm^5s^2U34 tRNA thiolation has an impact on FtsZ levels in the bacterial cell. As a result, the cellular FtsZ concentration is insufficient (Weart and Levin, 2003) during the exponential phase, which leads to the elongated cells being unable to divide.

5.7 Detection of Fis levels in mnm^{5}s^{2}U34 tRNA thiolation deletion strains at different growth phases

TusA was originally identified in a Δ*hns* background when screening for genes affecting cellular RpoS levels during the exponential phase (Yamashino *et al.*, 1998). Fis regulates the expression of *hns*, resulting in a possible relationship of Fis to TusA, whereby changes of Fis content in Δ*tusA* seem to be important. Furthermore, Fis is involved in cell division (Logan, 2006) and probably has a link to FtsZ. So Fis could have an effect on cell division defect and therefore the filamentation of Δ*tusA* cells. Since filaments were not reported only for Δ*ftsZ* strain, but also for cells with a defect in Fis (Ishii *et al.*, 2000; Lioy *et al.*, 2018). Based on these aspects, the cellular FtsZ concentration in *tusA*-deficient cells was analyzed in different growth phases.

In WT, the cellular Fis amount decreased up to 5 hours after growth. In contrast to WT, the Fis concentration in Δ*tusA* increased up to 5 hours. This result agrees with the report of Azam *et al.* (1999), according to which the Fis concentration was high in the exponential phase and decreased in the stationary phase. Due to the retarded growth of Δ*tusA*, the Fis concentration is still high at 5 h, as Δ*tusA* is still in the exponential phase. Since the WT grows faster, it reaches the stationary phase earlier than the Δ*tusA* and therefore revealed a lower Fis amount at 5 h. Since all deletion strains of mnm^{5}s^{2}U34 tRNA modification demonstrated the same growth and cell division defect as the Δ*tusA* strain, their cellular Fis amount was analyzed. The examination of Fis concentration during the exponential phase revealed similar results as for the cellular FtsZ amount. The controls of this assay (WT, Δ*miaB* and Δ*ttcA*) showed an increase in the amount of Fis up to 4 h, and at 5 h the decrease already started. Therefore the Fis concentration decreased after reaching the stationary phase. The last control Δ*iscU* showed slightly different from the other three controls an increasing Fis amount up to 5 h. All mnm^{5}s^{2}U34 tRNA modification deletion strains (Δ*tusA,* Δ*tusD,* Δ*tusE,* Δ*mnmA* and Δ*iscS*) had still increasing cellular Fis concentration up to 5 h, as they were still in the exponential phase due to their retarded growth. This also confirmed the previously reported different Fis amounts during the different growth phases (Cho *et al.*, 2008). In addition to the analysis of Fis in the exponential phase, the cellular Fis amount was tested in the stationary phase (growth up to 10 h). In all control strains (WT, Δ*miaB*, Δ*ttcA* and Δ*iscU*), Fis concentration was high in the exponential phase (up to 1.5 h or 4 h) and

declined with the entry into the stationary phase (4 h or 5 h) until it disappeared completely (10 h). Deletion strains of mnm^{5}s^{2}U34 tRNA thiolation (Δ*tusA,* Δ*tusD,* Δ*tusE,* Δ*mnmA* and Δ*iscS*) contained no Fis at the onset of the growth (1.5 h or 4 h (Δ*iscS*)). Then their Fis amount increased during the exponential phase (5 h or 7 h (Δ*iscS*)) and dropped with the transition to the stationary phase (7 h or 10 h (Δ*iscS*)). Fis disappeared completely (10 h) except in Δ*iscS*, which is due to its slowed growth over more or less one phase behind the Δ*tusA* strain. *ΔiscS* strain growth was shifted to one phase or time point compared to Δ*tusA*. So these results indicated a link between Fis protein and growth defect of mnm^{5}s^{2}U34 tRNA thiolation proteins. In total, all tested deletion strains of mnm^{5}s^{2}U34 tRNA modification showed high cellular FtsZ and Fis levels in the exponential phase, shifting to the later growth phases. This shift reflected a slowed growth, whereby the deletion strains reached later the exponential phase. In conclusion, it can be stated that the growth and cell division defect and thus the formation of filaments is most likely caused by changes in the cellular FtsZ and Fis concentrations. The drastic changes in cellular Fis levels during the different growth phases underline its role as a major regulatory protein for bacterial cell physiology (Cho *et al.*, 2008).

5.8 Translation efficiencies in deletion strains involved in mnm^{5}s^{2}U34 tRNA modification

Following the new information that the absence of mnm^{5}s^{2}U34 tRNA modifications affects the growth most strongly in terms of cell division and filament formation, it was interesting to analyze any effects on the translational level. Since TusA is missing due to the *tusA* gene deletion, it could influence the translation of proteins by using the unmodified U34 tRNAs of lysine, glutamate and glutamine. Moreover, this thiomodification of U34 has the important function to enable more efficient ribosome binding, it averts frameshifting during the translation of proteins (Ashraf *et al.*, 1999; Yokoyama *et al.*, 1985; Moukadiri *et al.*, 2013). Genes affected by the *tusA* deletion were therefore selected for translation analysis. Among these were the *rpoS* and *fur* genes, since the expression of the *rpoS* gene is increased and that of the *fur* gene is decreased (Dahl *et al.*, 2013). The *rpoS* gene encodes for the sigma factor σ^S, also called RpoS, which is induced in stress situations. It enhances the expression of several genes in the stationary phase (Yamashino *et al.*, 1998). The stability and

translation of RpoS are affected by TusA (Yamashino *et al.*, 1998; Aubee *et al.*, 2017). The *fur* gene encodes the FUR (ferric uptake regulator) protein that positively regulates iron usage and iron storage in the cell (Masse and Gottesmann, 2002). In addition, TusA was originally identified in a Δ*hns* background during screening for genes affecting cellular RpoS levels during the exponential phase (Yamashino *et al.*, 1998). Fis regulates the expression of *hns* (Yamashino *et al.*, 1998) and influences cell division and filamentation of Δ*tusA* cells through changes in its concentration. Moreover, Fis inversely regulates the *rpoS* expression by acting as a repressor (Brown *et al.*, 2002; Hirsch and Elliott, 2002; Hirsch and Elliott, 2005 (RpoS and Fis); McLeod *et al.*, 2000). As the last aspect, these three proteins contain many lysines, glutamates and glutamines, which make their translation more vulnerable due to the absence of thiomodification of U34 at the wobble position in tRNA. Therefore, the translation efficiencies of Fis, Fur and RpoS proteins were investigated in strains with impaired mnm^5s^2U34 tRNA modification.

As estimated, the translation of Fis was impaired in the deletion strains involved in mnm^5s^2U34 tRNA modification (Δ*tusA* (DE3), Δ*mnmA* (DE3) and Δ*iscS* (DE3)). Since the fluorescence intensity of EGFP and its shift to the control EGFP peak were lowered in strains of mnm^5s^2U34 tRNA modification relative to control strains (WT (DE3) and Δ*iscU* (DE3) (since it is not involved in mnm^5s^2U34 tRNA thiolation)). This reduction of Fis translation is due to the absence of the thiomodification of U34 in the tRNA, resulting in poorer translation of proteins. Furthermore, this result confirms the importance of mnm^5s^2U34 tRNA modification for an efficient ribosome binding and correct reading frame (Ashraf *et al.*, 1999; Yokoyama *et al.*, 1985; Moukadiri *et al.*, 2013).

The Fur-EGFP translation was similar to the Fis-EGFP expression. Deletion strains of mnm^5s^2U34 tRNA modification revealed reduced Fur-EGFP translation levels than the controls. A small difference depicted the Fur-EGFP expression in Δ*iscU* (DE3). Fur-EGFP fluorescence was slightly increased than in WT (DE3) and in Δ*iscU* (DE3) Fis-EGFP fluorescence signal. This could be probably related to a defect in Fe-S cluster biosynthesis. Since IscU is the scaffold protein on which the Fe-S cluster formation occurs (Marinoni *et al.*, 2012) that is absent in the Δ*iscU* strain. As mentioned, Fur is the ferric uptake regulator protein that binds the Fe in the cell if the Fe amount is enough. With this Fe-binding by Fur, the cell can adjust the cellular Fe metabolism (Bagg and Neilands, 1987). A defect in Fe-S

cluster assembly due to the deletion of *iscU* thus presumably leads to an iron-rich environment. This would lead to the induction of Fur expression to regulate the iron usage and iron storage in the cell, as already described by Masse and Gottesmann (2002). Finally, such a scenario would explain the increase of Fur translation in Δ*iscU* (DE3) strain compared to WT (DE3). In total, the Fur-EGFP translation was nearly identical to that of Fis-EGFP in the tested strains.

The translation efficiency of RpoS-EGFP in mnm^5s^2U34 tRNA modification-deficient strains and controls showed more divergent results than for those of Fis- and Fur-EGFP. Already in WT (DE3), the translation of RpoS-EGFP was lowered relative to the translation of the other two fusion proteins tested (Fis- and Fur-EGFP). Strains of mnm^5s^2U34 tRNA thiolation revealed an overlapping RpoS-EGFP fluorescence intensity with the EGFP control fluorescence signal (Figure 72). This indicated that RpoS-EGFP was almost not expressed. Thus, the absence of mnm^5s^2U34 tRNA thiolation most affected RpoS-EGFP translation efficiency.

An additional new construct of Fis-EGFP fusion was produced to confirm the positive effects of the thiomodification of mnm^5s^2U34. For this purpose, all amino acid codons for lysines (K), glutamates (E) and glutamines (Q) were mutated to alanine. The new construct was named mutated Fis-EGFP (mFis-EGFP). Already in the control strains (WT (DE3) and Δ*iscU*) the double impairment of mFis-EGFP translation was clearly detectable. The mFis-EGFP fusion construct was expressed but to a lesser extent (mFis-EGFP fluorescence around 10^2 - 10^3) compared to the non-mutated Fis-EGFP version (Figure 67, fluorescence intensity for Fis-EGFP was between 10^3 – 10^4). So, due to the mutation, the positive effect of mnm^5s^2U34 tRNA thiolation in WT (DE3) was absent, resulting in a decreased mFis-EGFP translation. Deletion strains involved in mnm^5s^2U34 tRNA modification displayed minimum translation of mFis-EGFP compared to its corresponding control EGFP signal. Also in these strains, the mFis-EGFP translation was lower than the Fis-EGFP translation. As expected, the mFis-EGFP was almost expressed to the same extent as the control EGFP, indicating a deficiency of lysines, glutamates and glutamines. Thus, the translation efficiency is decreased in mnm^5s^2U34 tRNA modification-impaired strains in addition to their existing growth and cell division defect due to the elimination of these three amino acids. Since the thiomodification of mnm^5s^2U34 mainly affects lysines, glutamates and glutamines. Finally, these results confirm and reinforce the importance of lysines, glutamates and glutamines and the

mnm^5s^2U34 tRNA thiolation for efficient protein translation. Thus, this valuable information verifies that the translation of *fur*, *fis* and *rpoS* is regulated by mnm^5s^2U34 tRNA modifications, which is growth phase-dependent.

Another aspect could be considered for future analyses: since mnm^5s^2U34 thiolation affects the protein translation by enabling more efficient ribosome binding and averting frameshifting (Ashraf *et al.*, 1999; Yokoyama *et al.*, 1985; Moukadiri *et al.*, 2013), a defect during this process leads to slowed FtsZ expression (as also shown in this work for *fis*, *fur* and *rpoS* by translation efficiency investigations). This would explain the insufficient FtsZ levels in deletions strains of mnm^5s^2U34 modification during the exponential phase. It does not seem unlikely since the protein sequence of FtsZ exhibits many lysines (17x K), glutamates (26x E) and glutamines (14x Q). In the future, this aspect could be investigated to clarify whether the translation of FtsZ is affected by the absence of thiomodification of U34 at the wobble position in tRNA.

It is also important to mention here that in one of the initial reports (Ishii *et al.*, 2000) the cell division defect or the filamentous phenotype was complemented by overexpression of DksA in Δ*tusA* strain. Interestingly, DksA is involved in the expression of *fis* and *rpoS* genes. It activates the *rpoS* expression and results in an increased level of RpoS (Brown *et al.*, 2002; Hirsch *et al.*, 2002). On the other hand, DksA impairs the transcription of Fis by reducing the lifetime of the RNA polymerase-*fis*-promoter complex (Mallik *et al.*, 2006). Together with the findings of this work, it seems possible that TusA is subject to a more complex regulatory network. Therefore, overexpression of *dksA* could complement the filamentous phenotype of the *tusA* mutant by activating and increasing the *rpoS* expression. At the same time, the transcription of *fis* is repressed, whereby the induction of transcription of *rpoS* leads to higher cellular RpoS concentrations. This in turn could compensate for the impaired RpoS translation efficiency in Δ*tusA* caused by the absence of TusA, and thus the lack of mnm^5s^2U34 tRNA thiolation. Moreover, RpoS is involved in the regulation of *ftsZ* expression in the stationary phase (Majdalani *et al.*, 2002; Ballesteros *et al.*, 1998). Normally, the housekeeping σ^{70} is responsible for the expression of *ftsZ*. However, upon entry into the stationary phase, RpoS takes over the role and induces the *ftsZ* expression from a second promotor site (Ballesteros *et al.*, 1998; Sitnikov *et al.*, 1996). As a conclusion, the deletion of the *tusA* gene disrupted a complex regulatory network within the bacterial cell. This

disruption is most influenced by the decreased translation of Fis and RpoS, caused by the absence of mnm^{5}s^{2}U34 tRNA modifications (Figure 78).

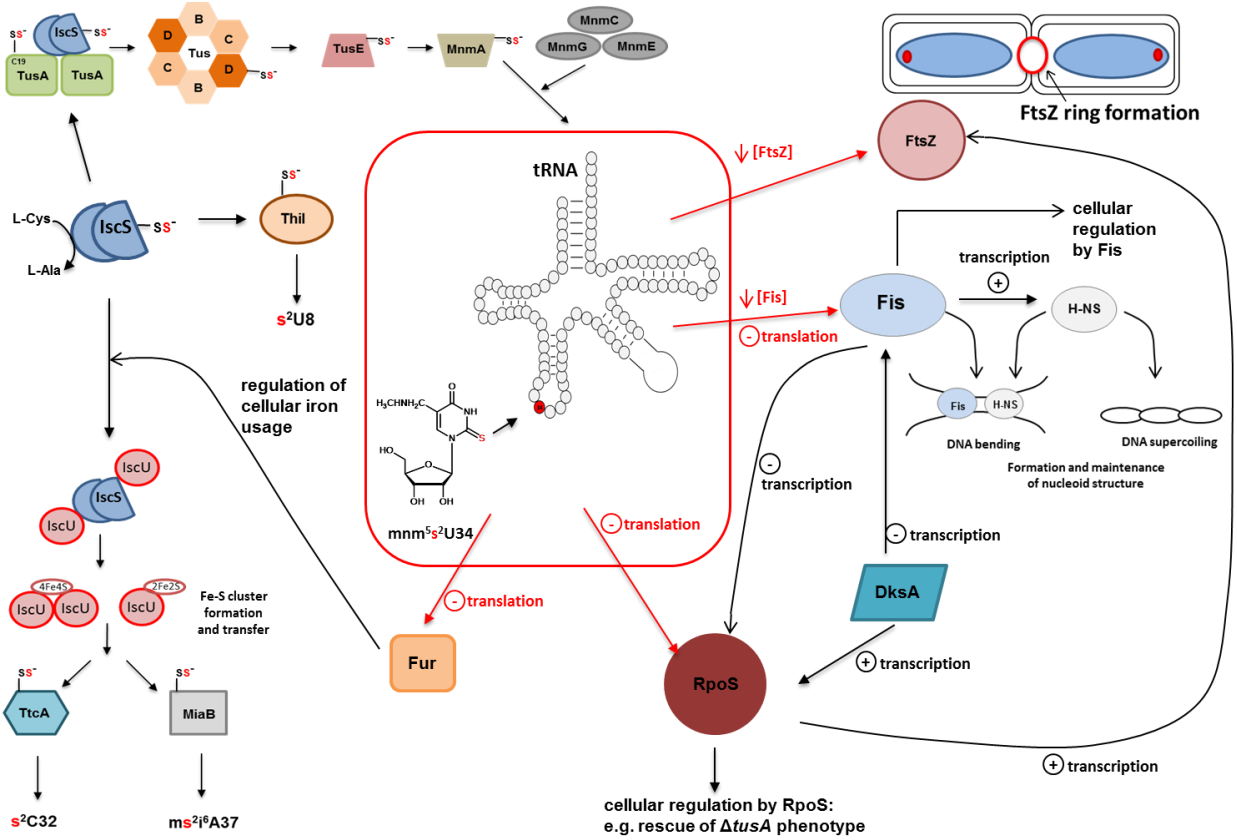

Figure 78: Model of cellular connection of TusA, cell division, RpoS and Fis regulatory network.

Based on the results obtained in this work, it was possible to create a model that visualizes the connection between tRNA thiolation, cell division and regulatory networks through RpoS and Fis. The essential sulfur is mobilized by IscS cysteine desulfurase and transfers it to further sulfur-containing biomolecules. One of the important sulfur-containing biomolecules are Fe-S clusters and thiolated tRNAs. The formation of thionucleosides occurs in two different ways: the Fe-S cluster independent and dependent pathway. The Fe-S cluster independent-pathways are catalyzed by TusA and ThiI protein. TusA accelerates the sulfur transfer for the formation of mnm^{5}s^{2}U34 and ThiI for s^{4}U8 synthesis. TtcA and MiaB require a Fe-S cluster which is assembled first on the IscU scaffold protein. TtcA transfers the sulfur to tRNA for the synthesis of s^{2}C32 and MiaB for ms^{2}i^{6}A37 formation. For both pathways, the sulfur is provided by the IscS protein. The importance of the tRNA modification with sulfur is that the translation efficiency proceeds more accurately. The absence of TusA and thus of the mnm^{5}s^{2}U34 modification affects several cellular targets, in particular the translation efficiency of proteins. Among these, RpoS is one of the targets which is most affected by the absence of mnm^{5}s^{2}U34 modification. Its translation efficiency is drastically reduced. RpoS has the role of a master regulator that is involved in the positive regulation of the expression of many genes. FtsZ and Fis are two of those proteins which are regulated by RpoS (Ballesteros *et al.*, 1998; Lu *et al.*, 2016). FtsZ is the main protein in the cell division process. For cell division, the FtsZ protein assembles in the center of the cell and forms a ring structure (FtsZ ring). Together with additional proteins, the contraction of this Z ring leads to the constriction of the outer membrane and cell division. Fis is the **f**actor for **i**nversion **s**timulation that acts as a global regulator during transcription and is involved in the transcription regulation of genes. It binds to the DNA together with H-NS and further proteins to form the nucleoid structure. Fis and H-NS act together to bend the DNA. Furthermore, the transcription of Fis and RpoS proteins are regulated by DksA. Another candidate affected in its translation efficiency is the Fur protein. Fur translation is decreased due to the absence of mnm^{5}s^{2}U34 modification and thus non-efficient protein translation. Fur is the **f**erric **u**ptake **r**egulator and is responsible for the regulation of iron usage in bacterial cells. Most likely the reduced Fur translation could impair the Fe-S cluster biosynthesis network.

Conclusively, the absence of TusA and thereby of the mnm^{5}s^{2}U34 modification disrupts the RpoS and Fis cellular network which influences the cellular FtsZ level in the early exponential phase. Finally, the reduced FtsZ concentration leads to elongated, filamentous *E. coli* cells, which are unable to divide. ↓: reduction; [ ]: concentration; +: activation; - repression; black arrows: already reported information in literature; red arrows: results encompassing this work.

So the absence of TusA and therefore of the mnm^{5}s^{2}U34 modification affects several cellular targets, in particular the translation efficiency of proteins. RpoS is one of the targets which is strongly influenced by the absence of mnm^{5}s^{2}U34 modification. Its translation efficiency is drastically reduced. RpoS has a role as a master regulator that is involved in the positive regulation of 268 gene expressions. So a reduction in RpoS translation would therefore bring about significant alterations within the cell (Dong *et al.*, 2008; Weber *et al.*, 2005). A further candidate affected by this absence of thiomodification of the U34 tRNA is the Fis protein. Fis, the **f**actor for **i**nversion **s**timulation, acts as a global regulator during transcription and is involved in transcription regulation of 21 % of genes in *E. coli* (Travers and Muskhelishvili, 2005; Cho *et al.*, 2008). It is able to activate or repress the transcription of affected genes (Kahramanoglou *et al.*, 2010). In addition, Fis binds to the DNA together with H-NS for nucleoid structure organization (Cho *et al.*, 2008). Moreover, Fis is together with HNS, HU, IHF and DPS one of the major components of the bacterial nucleoid (Dame, 2005). So, the reduced translation efficiency of Fis would most likely influence the nucleoid structure in the bacterial cell. The formation and maintenance of nucleoid structure could be impaired due to reduced Fis levels. Furthermore, Fur, the **f**erric **u**ptake **r**egulator, is also affected in its translation efficiency. Fur translation is decreased due to the absence of mnm^{5}s^{2}U34 modification and thus non-efficient protein translation. Fur is responsible for the regulation of iron usage in bacterial cells (Masse and Gottesmann, 2002). Most likely the reduced Fur translation could impair the Fe-S cluster biosynthesis network. Conclusively, the absence of TusA and thereby of the mnm^{5}s^{2}U34 modification disrupts the RpoS and Fis cellular network which influences the cellular FtsZ level in the early exponential phase. Finally, the reduced FtsZ concentration leads to elongated, filamentous *E. coli* cells, which are unable to divide. So starting from retarded growth and cell division defect, the lack of mnm^{5}s^{2}U34 tRNA modification and decreased translation of RpoS and Fis appear to have various effects within the bacterial cell. Finally, changes in the translation level of important cellular proteins with regulatory roles that are influenced by the thiomodification of tRNA, can lead to significant alterations in the cellular regulatory network.

5.9 Further investigations

In this study, the role of TusA for cell functionality and FtsZ ring assembly in *E. coli* cells was dissected. Based on previous analyses, it has been reported that deletion of the *tusA* gene leads to retarded growth and elongated cell shape. Concerning that such a phenotype deviates from typical WT growth (e.g. faster growth and rod-shaped cells), it was assumed that Δ*tusA* strain has a cell division defect. Since FtsZ is the main protein in the cell division process, it was suggested that a step in FtsZ ring formation is defective in the Δ*tusA* filaments. Therefore, the *tusA* mutant cells cannot divide and become longer and form filaments. This problem was investigated by recording of growth curves of *tusA*-deficient cells, analyzing the cell morphology and complementing this deficiency by expressing selected genes. This work determined that cell division defect is caused due to the absence of the thiomodification at the wobble base U34 of tRNA Lys, Glu and Gln. All deletion strains of this mnm^5s^2U34 tRNA modification pathway shared the same *tusA*-deficient phenotype. Microscopic morphology analysis revealed that elongated cells contain several nuclei but are covered by one cell membrane. In addition, the expression of the mCherry-FtsZ fusion protein and investigation by fluorescence microscopy showed that FtsZ is located at the cell poles and cell center in Δ*tusA* filaments. This confirmed that FtsZ is not fully formed to perform cell division. It is still in the assembly phase, oscillating from one cell pole to the other until it finds its correct position at cell center and forms the Z ring structure for the cell membrane constriction. First evidence for an intracellular interaction of TusA and FtsZ was shown by co-expression and co-localization of EGFP-TusA and mCherry-FtsZ by fluorescence microscopy *in vivo*. To highlight this possible interaction, FRET measurements were performed. However, it was not possible to detect a significant FRET signal. One of the possible problems was that the FRET efficiency was already so low in the positive control and even in the WT (DE3) strain. Therefore, it would be probably very hard for the Δ*tusA* strain to detect any signal. As Δ*tusA* strain grows slower than the WT due to its growth defect, which also resulted in lower fluorescence intensities than in WT (DE3) samples. Another problem could be the low expression levels of fusion proteins due to the growth defect of Δ*tusA*, which led to low fluorescence intensities that exacerbate the fluorescence and interaction detection by FRET. Furthermore, it was very difficult to find areas with simultaneous good expression levels for both donor (EGFP / EYFP) and acceptor (mCherry). In several cases, it appeared that donor and acceptor expressions are affecting each other,

since there were samples in which cells expressing the donor expressed only very low acceptor or vice versa. These aspects should be analyzed in future studies. The co-expression of fusion proteins in Δ*tusA* could be optimized for higher fluorescence intensities. Additionally, if donor and acceptor expressions are still affecting each other, it could be considered to change the combinations donor and acceptor fluorophores. Furthermore in this work, during the investigations of the translation efficiencies of lysine-, glutamine- and glutamate-rich proteins Fis, Fur and RpoS by flow cytometry, it was determined that their translation efficiencies were significantly reduced in deletion strains of mnm^5s^2U34 tRNA modification. Due to the absence of mnm^5s^2U34 tRNA modification, the translation process was slowed down, resulting in poorer translation of proteins. To further investigate translation efficiency, FtsZ should be also analyzed in detail. As was shown for Fis, Fur and RpoS, the translation of FtsZ in Δ*tusA* strain might be also affected due to the absence of mnm^5s^2U34 tRNA thiolation. Since the protein sequence of FtsZ exhibits many lysines (17x K), glutamates (26x E) and glutamines (14x Q). This aspect could be investigated to clarify whether the translation of FtsZ is affected by the absence of thiomodification of U34 at the wobble position in tRNA. If this is the case, which seems very likely regarding the findings of this work, it would also explain the insufficient FtsZ levels in deletion strains of mnm^5s^2U34 modification.

6 Zusammenfassung

In dieser Arbeit wurde die Rolle des TusA-Proteins für die Zellfunktionalität und FtsZ-Ringbildung in *Escherichia coli* untersucht. Bei TusA handelt es sich um die tRNA-2-Thiouridine-Synthase, die als Schwefeltransferase bei der tRNA-Thiolierung zur Bildung von 2-Thiouridin an der Position 34 (Wobble-Base) von $tRNA^{Lys}$, $tRNA^{Glu}$ und $tRNA^{Gln}$ dient. Dieses Protein bindet das Schwefelatom als Persulfid und überträgt dieses bei der mnm^5s^2U tRNA-Modifikation an der Wobble-Position und der Molybdän-Cofaktor (Moco)-Biosynthese auf weitere Proteine. Durch diese Thiomodifikation der tRNA wird eine effizientere Bindung des Ribosoms erreicht und zudem eine Verschiebung des Leserasters während der Proteintranslation verhindert. Frühere Studien haben eine essenzielle Rolle für TusA in der bakteriellen Zellphysiologie gezeigt: die Deletion des *tusA*-Gens führte zu einem verlangsamten Wachstum und filamentösen (fadenförmigen) Zellen als WT-Zellen während der exponentiellen Wachstumsphase in einem reichhaltigen Medium. In der stationären Phase waren diese Filamente hingegen nicht mehr zu beobachten, was auf einen Defekt während der Zellteilung hindeutete. Ziel dieser Arbeit war es daher die Rolle des TusA-Proteins für die Zellfunktionalität und FtsZ-Ringbildung zu analysieren.

Im Rahmen der vorliegenden Doktorarbeit wurde die Ursache für das filamentöse Wachstum der *tusA*-Mutante untersucht. Dafür wurden Wachstums- und Morphologieanalysen durchgeführt. Die Δ*tusA*-Zellen zeigten im Vergleich zum WT-Stamm ein verzögertes Wachstum in der exponentiellen Phase. Die filamentöse Zellform der Δ*tusA*-Zellen wurde ebenfalls durch die Analyse der Zellmorphologie bestätigt. Demnach deutete das Wachstums- und Zellteilungsproblem von Δ*tusA* auf einen Defekt des FtsZ-Proteins hin, das eine Schlüsselrolle bei der Zellteilung besitzt. Anhand von mikroskopischen Untersuchungen konnte gezeigt werden, dass die filamentöse Δ*tusA*-Zellen mehrere nebeneinander angeordnete DNA-Abschnitte besaßen. Dies ließ die Vermutung zu, dass trotz korrekt verlaufender DNA-Replikation, ein Defekt in dem Schritt, in dem FtsZ einsetzen sollte, vorliegt. Folglich scheint FtsZ sich nicht zur Ringstruktur anordnen zu können. Denkbar wäre auch, dass der zusammengesetzte Ring nicht in der Lage ist zu kontrahieren. Alle getesteten Mutantenstämme (Δ*tusD*, Δ*tusE* und Δ*mnmA*), die an der mnm^5s^2U34-Modifikation beteiligt sind, zeigten ein ähnlich verzögertes Wachstum und eine ähnliche filamentöse Zellform wie der Δ*tusA*-Stamm. Somit ist der Zellteilungsdefekt auf einen Defekt in der mnm^5s^2U34-tRNA-Thiolierung zurückzuführen.

Des Weiteren wurde eine mögliche intrazelluläre Interaktion von TusA und FtsZ anhand der Expression von fluoreszierender (EGFP und mCherry) Fusionsproteine und FRET-Analysen überprüft, da die Bildung des FtsZ-Rings in den Filamenten defekt zu sein scheint. Für FtsZ-exprimierende *tusA* (DE3)-Zellen wurden rote mCherry-Signale an den Zellpolen detektiert, was auf das sich noch assemblierende FtsZ hindeutete. Interessanterweise war die zelluläre Region des EGFP-TusA Signals, das in Δ*tusA* (DE3) exprimiert wurde, überlappend mit dem von mCherry-FtsZ. Das EGFP-Signal zeigte eine Verteilung über die gesamte Zelle, wobei noch zusätzlich eine leichte Akkumulation der EGFP-TusA-Fluoreszenz an den Zellpolen (wie bei mCherry-FtsZ) festgestellt wurde. Somit deutet dies auf eine Interaktion zwischen TusA und FtsZ hin.

Zusätzlich wurden die FtsZ- und Fis-Konzentrationen und deren Änderung während der unterschiedlichen Wachstumsphasen anhand von Immunoblot-Analysen ermittelt. Alle getesteten Deletionsstämme der mnm^5s^2U34-tRNA-Modifikation zeigten hohe zelluläre FtsZ- und Fis-Mengen in der exponentiellen Phase, die in die späteren Wachstumsphasen verschoben sind. Diese Verschiebung spiegelt das verlangsamte Wachstum wider, wodurch die Deletionsstämme später die exponentielle Phase erreichen. Demzufolge ist anzunehmen, dass der Wachstums- und Zellteilungsdefekt und daraus die Bildung von Filamenten durch Veränderungen der zellulären FtsZ- und Fis-Konzentrationen verursacht werden.

Abschließend wurde in dieser Arbeit mittels Durchflusszytometrie die Translationseffizienz bestimmter Proteine (RpoS, Fur, Fis und mFis) in Δ*tusA* und zusätzlichen Gendeletionsstämmen untersucht. Insbesondere sollte gezeigt werden, ob die Translation der Proteine durch die Verwendung von unmodifizierten U34-tRNAs für Lys, Glu und Gln beeinträchtigt wird. Somit ist die Translationseffizienz in den Stämmen mit beeinträchtigter mnm^5s^2U34-tRNA-Modifikation verringert, was zusätzlich zu ihren bereits bestehenden Wachstums- und Zellteilungsdefekten aufgrund der Eliminierung dieser drei Aminosäuren hinzukommt. Damit bestätigen und verstärken diese Ergebnisse die Bedeutung von Lys, Glu und Gln und der mnm^5s^2U34 tRNA-Thiolierung für eine effiziente Proteintranslation. Sie belegen auch, dass die Translation von *fur*, *fis* und *rpoS* durch die mnm^5s^2U34-tRNA-Modifikation reguliert wird, welche wachstumsphasenabhängig ist.

Im Résumé zeigen die Ergebnisse dieser Forschungsarbeit neue Funktionen des TusA-Proteins für die Funktionalität und Physiologie von Bakterienzellen. Durch die Deletion des *tusA*-Gens wurde ein komplexes regulatorisches Netzwerk innerhalb der Zelle gestört, das vor allem durch die verringerte Translation von Fis und RpoS beeinflusst wird (die durch das Fehlen der mnm^5s^2U34-tRNA-Modifikation verursacht wird). Die Unterbrechung des zellulären RpoS- und Fis-Netzwerks beeinflusst wiederum die zelluläre FtsZ-Menge in der frühen exponentiellen Phase. Schließlich führt diese Verringerung der FtsZ-Konzentration zu filamentösen *E. coli*-Zellen, die sich nicht mehr teilen können.

7 References

Beinert H. (2000a). A tribute to sulfur. Eur J Biochem. 267(18):5657-64.
doi: 10.1046/j.1432-1327.2000.01637.

Kessler D. (2006). Enzymatic activation of sulfur for incorporation into biomolecules in prokaryotes. FEMS Microbiol Rev. 30(6):825-40.
doi: 10.1111/j.1574-6976.2006.00036.x. PMID: 17064282.

Mueller EG. (2006). Trafficking in persulfides: delivering sulfur in biosynthetic pathways. Nat Chem Biol. 2(4):185-94.
doi: 10.1038/nchembio779.

Zheng L, Cash VL, Flint DH, Dean DR. (1998). Assembly of iron-sulfur clusters. Identification of an iscSUA- hscBA-fdx gene cluster from Azotobacter vinelandii. J Biol Chem. 273(21):13264-72.
doi: 10.1074/jbc.273.21.13264.

Johnson DC, Dean DR, Smith AD, Johnson MK. Structure, function, and formation of biological iron-sulfur clusters. (2005). Annu Rev Biochem. 74:247-81.
doi: 10.1146/annurev.biochem.74.082803.133518.

Agar, J. N., Krebs, C., Frazzon, J., Huynh, B. H., Dean, D. R., and Johnson, M. K. (2000). IscU as a scaffold for iron-sulfur cluster biosynthesis: sequential assembly of [2Fe-2S] and [4Fe-4S] clusters in IscU. Biochemistry 39, 7856–7862.

Agar JN, Krebs C, Frazzon J, Huynh BH, Dean DR, Johnson MK. (2000). IscU as a scaffold for iron-sulfur cluster biosynthesis: sequential assembly of [2Fe-2S] and [4Fe-4S] clusters in IscU. Biochemistry. 39(27):7856-62.
doi: 10.1021/bi000931n.

Kato S, Mihara H, Kurihara T, Takahashi Y, Tokumoto U, Yoshimura T, Esaki N. (2002). Cys-328 of IscS and Cys-63 of IscU are the sites of disulfide bridge formation in a covalently bound IscS/IscU complex: implications for the mechanism of iron-sulfur cluster assembly. Proc Natl Acad Sci U S A. 99(9):5948-52.
doi: 10.1073/pnas.082123599.

Shi R, Proteau A, Villarroya M, Moukadiri I, Zhang L, Trempe JF, Matte A, Armengod ME, Cygler M. (2010). Structural basis for Fe-S cluster assembly and tRNA thiolation mediated by IscS protein-protein interactions. PLoS Biol. 8(4):e1000354.
doi: 10.1371/journal.pbio.1000354.

Mettert EL, Kiley PJ. (2015). How Is Fe-S Cluster Formation Regulated? Annu Rev Microbiol. 69:505-26.
doi: 10.1146/annurev-micro-091014-104457.

Roche B, Aussel L, Ezraty B, Mandin P, Py B, Barras F. (2013). Iron/sulfur proteins biogenesis in prokaryotes: formation, regulation and diversity. Biochim Biophys Acta. 1827(3):455-69.
doi: 10.1016/j.bbabio.2012.12.010.

Schwartz CJ, Giel JL, Patschkowski T, Luther C, Ruzicka FJ, Beinert H, Kiley PJ. (2001). IscR, an Fe-S cluster-containing transcription factor, represses expression of *Escherichia coli* genes encoding Fe-S cluster assembly proteins. Proc Natl Acad Sci U S A. 98(26):14895-900.
doi: 10.1073/pnas.251550898.

Marinoni EN, de Oliveira JS, Nicolet Y, Raulfs EC, Amara P, Dean DR, Fontecilla-Camps JC. (2012). $(IscS\text{-}IscU)_2$ complex structures provide insights into Fe_2S_2 biogenesis and transfer. Angew Chem Int Ed Engl. 51(22):5439-42.
doi: 10.1002/anie.201201708.

Chandramouli K, Unciuleac MC, Naik S, Dean DR, Huynh BH, Johnson MK. (2007). Formation and properties of [4Fe-4S] clusters on the IscU scaffold protein. Biochemistry. 46(23):6804-11. doi: 10.1021/bi6026659.

Ollagnier-de-Choudens S, Sanakis Y, Fontecave M. (2004). SufA/IscA: reactivity studies of a class of scaffold proteins involved in [Fe-S] cluster assembly. J Biol Inorg Chem. 9(7):828-38. doi: 10.1007/s00775-004-0581-9.

Kim JH, Tonelli M, Frederick RO, Chow DC, Markley JL. (2012). Specialized Hsp70 chaperone (HscA) binds preferentially to the disordered form, whereas J-protein (HscB) binds preferentially to the structured form of the iron-sulfur cluster scaffold protein (IscU). J Biol Chem. 287(37):31406-13. doi: 10.1074/jbc.M112.352617.

Hoff KG, Silberg JJ, Vickery LE. (2000). Interaction of the iron-sulfur cluster assembly protein IscU with the Hsc66/Hsc20 molecular chaperone system of *Escherichia coli*. Proc Natl Acad Sci U S A. 97(14):7790-5. doi: 10.1073/pnas.130201997.

Silberg JJ, Hoff KG, Tapley TL, Vickery LE. The Fe/S assembly protein IscU behaves as a substrate for the molecular chaperone Hsc66 from *Escherichia coli*. (2001). J Biol Chem. 276(3):1696-700. doi: 10.1074/jbc.M009542200.

Chandramouli K, Johnson MK. (2006). HscA and HscB stimulate [2Fe-2S] cluster transfer from IscU to apoferredoxin in an ATP-dependent reaction. Biochemistry. 45(37):11087-95. doi: 10.1021/bi061237w.

Unciuleac MC, Chandramouli K, Naik S, Mayer S, Huynh BH, Johnson MK, Dean DR. (2007). In vitro activation of apo-aconitase using a [4Fe-4S] cluster-loaded form of the IscU [Fe-S] cluster scaffolding protein. Biochemistry. 46(23):6812-21. doi: 10.1021/bi6026665.

Shakamuri P, Zhang B, Johnson MK. (2012). Monothiol glutaredoxins function in storing and transporting [Fe_2S_2] clusters assembled on IscU scaffold proteins. J Am Chem Soc. 134(37):15213-6. doi: 10.1021/ja306061x.

Roche B, Huguenot A, Barras F, Py B. (2015). The iron-binding CyaY and IscX proteins assist the ISC-catalyzed Fe-S biogenesis in *Escherichia coli*. Mol Microbiol. 95(4):605-23. doi: 10.1111/mmi.12888.

Blanc B, Gerez C, Ollagnier de Choudens S. (2015). Assembly of Fe/S proteins in bacterial systems: Biochemistry of the bacterial ISC system. Biochim Biophys Acta. 1853(6):1436-47. doi: 10.1016/j.bbamcr.2014.12.009.

Hidese R, Mihara H, Esaki N. (2011). Bacterial cysteine desulfurases: versatile key players in biosynthetic pathways of sulfur-containing biofactors. Appl Microbiol Biotechnol. 91(1):47-61. doi: 10.1007/s00253-011-3336-x.

Ikeuchi Y, Shigi N, Kato J, Nishimura A, Suzuki T. (2006). Mechanistic insights into sulfur relay by multiple sulfur mediators involved in thiouridine biosynthesis at tRNA wobble positions. Mol Cell. 21(1):97-108. doi: 10.1016/j.molcel.2005.11.001.

Dahl JU, Radon C, Bühning M, Nimtz M, Leichert LI, Denis Y, Jourlin-Castelli C, Iobbi-Nivol C, Méjean V, Leimkühler S. (2013). The sulfur carrier protein TusA has a pleiotropic role in *Escherichia coli* that also affects molybdenum cofactor biosynthesis. J Biol Chem. 288(8):5426-42. doi: 10.1074/jbc.M112.431569.

Dai Y, Outten FW. (2012). The *E. coli* SufS-SufE sulfur transfer system is more resistant to oxidative stress than IscS-IscU. FEBS Lett. 586(22):4016-22.
doi: 10.1016/j.febslet.2012.10.001.

Outten FW, Djaman O, Storz G. (2004). A *suf* operon requirement for Fe-S cluster assembly during iron starvation in *Escherichia coli*. Mol Microbiol. 52(3):861-72.
doi: 10.1111/j.1365-2958.2004.04025.x.

Jang S, Imlay JA. (2010). Hydrogen peroxide inactivates the *Escherichia coli* Isc iron-sulphur assembly system, and OxyR induces the Suf system to compensate. Mol Microbiol. 78(6):1448-67.
doi: 10.1111/j.1365-2958.2010.07418.x.

Mihara H, Esaki N. (2002). Bacterial cysteine desulfurases: their function and mechanisms. Appl Microbiol Biotechnol. 60(1-2):12-23.
doi: 10.1007/s00253-002-1107-4.

Loiseau L, Ollagnier-de-Choudens S, Nachin L, Fontecave M, Barras F. (2003). Biogenesis of Fe-S cluster by the bacterial Suf system: SufS and SufE form a new type of cysteine desulfurase. J Biol Chem. 278(40):38352-9.
doi: 10.1074/jbc.M305953200.

Bagg A, Neilands JB. (1987). Ferric uptake regulation protein acts as a repressor, employing iron (II) as a cofactor to bind the operator of an iron transport operon in Escherichia coli. Biochemistry. 26(17):5471-7.
doi: 10.1021/bi00391a039.

Massé E, Gottesman S. (2002). A small RNA regulates the expression of genes involved in iron metabolism in *Escherichia coli*. Proc Natl Acad Sci U S A. 99(7):4620-5.
doi: 10.1073/pnas.032066599.

Massé E, Escorcia FE, Gottesman S. (2003). Coupled degradation of a small regulatory RNA and its mRNA targets in *Escherichia coli*. Genes Dev. 17(19):2374-83.
doi: 10.1101/gad.1127103.

Moll I, Afonyushkin T, Vytvytska O, Kaberdin VR, Bläsi U. (2003). Coincident Hfq binding and RNase E cleavage sites on mRNA and small regulatory RNAs. RNA. 9(11):1308-14.
doi: 10.1261/rna.5850703.

Westley J, Adler H, Westley L, Nishida C. (1983). The sulfurtransferases. Fundam Appl Toxicol. 3(5):377-82.
doi: 10.1016/s0272-0590(83)80008-6.

Yamashino T, Isomura M, Ueguchi C, Mizuno T. (1998). The *yhhP* gene encoding a small ubiquitous protein is fundamental for normal cell growth of Escherichia coli. J Bacteriol. 180(8):2257-61.
doi: 10.1128/JB.180.8.2257-2261.1998.

Ashraf SS, Sochacka E, Cain R, Guenther R, Malkiewicz A, Agris PF. (1999). Single atom modification (O-->S) of tRNA confers ribosome binding. RNA. 5(2):188-94.
doi: 10.1017/s1355838299981529.

Yokoyama S, Watanabe T, Murao K, Ishikura H, Yamaizumi Z, Nishimura S, Miyazawa T. (1985). Molecular mechanism of codon recognition by tRNA species with modified uridine in the first position of the anticodon. Proc Natl Acad Sci U S A. 82(15):4905-9.
doi: 10.1073/pnas.82.15.4905.

Moukadiri I, Garzón MJ, Björk GR, Armengod ME. (2013). The output of the tRNA modification pathways controlled by the *Escherichia coli* MnmEG and MnmC enzymes depends on the growth conditions and the tRNA species. Nucleic Acids Res. 42(4):2602-23.
doi: 10.1093/nar/gkt1228.

Kambampati R, Lauhon CT. (2003). MnmA and IscS are required for *in vitro* 2-thiouridine biosynthesis in *Escherichia coli*. Biochemistry. 42(4):1109-17.
doi: 10.1021/bi026536+.

Yokoyama S, Yamaizumi Z, Nishimura S, Miyazawa T. (1979). ^{1}H NMR studies on the conformational characteristics of 2-thiopyrimidine nucleotides found in transfer RNAs. Nucleic Acids Res. 6(7):2611-26.
doi: 10.1093/nar/6.7.2611.

Durant PC, Bajji AC, Sundaram M, Kumar RK, Davis DR. (2005). Structural effects of hypermodified nucleosides in the *Escherichia coli* and human tRNA^{Lys} anticodon loop: the effect of nucleosides s^2U, mcm^5U, mcm^5s^2U, mnm^5s^2U, t^6A, and ms^2t^6A. Biochemistry. 44(22):8078-89.
doi: 10.1021/bi050343f. PMID: 15924427.

Rodriguez-Hernandez A, Spears JL, Gaston KW, Limbach PA, Gamper H, Hou YM, Kaiser R, Agris PF, Perona JJ. (2013). Structural and mechanistic basis for enhanced translational efficiency by 2-thiouridine at the tRNA anticodon wobble position. J Mol Biol. 425(20):3888-906.
doi: 10.1016/j.jmb.2013.05.018.

Shigi N. (2014). Biosynthesis and functions of sulfur modifications in tRNA. Front Genet. 5:67.
doi: 10.3389/fgene.2014.00067.

Kambampati R, Lauhon CT. (2000). Evidence for the transfer of sulfane sulfur from IscS to ThiI during the *in vitro* biosynthesis of 4-thiouridine in *Escherichia coli* tRNA. J Biol Chem. 275(15):10727-30.
doi: 10.1074/jbc.275.15.10727.

Hernández HL, Pierrel F, Elleingand E, García-Serres R, Huynh BH, Johnson MK, Fontecave M, Atta M. (2007). MiaB, a bifunctional radical-S-adenosylmethionine enzyme involved in the thiolation and methylation of tRNA, contains two essential [4Fe-4S] clusters. Biochemistry. 46(17):5140-7.
doi: 10.1021/bi7000449.

Gutzke G, Fischer B, Mendel RR, Schwarz G. (2001). Thiocarboxylation of molybdopterin synthase provides evidence for the mechanism of dithiolene formation in metal-binding pterins. J Biol Chem. 276(39):36268-74.
doi: 10.1074/jbc.M105321200.

Rudolph MJ, Wuebbens MM, Rajagopalan KV, Schindelin H. (2001). Crystal structure of molybdopterin synthase and its evolutionary relationship to ubiquitin activation. Nat Struct Biol. 8(1):42-6.
doi: 10.1038/83034.

Leimkühler S. (2014). The biosynthesis of the Molybdenum Cofactor in *Escherichia coli* and its connection to FeS cluster assembly and the thiolation of tRNA. Advances in Biology. Vol. 2014, Article ID 808569, 21 pages.
doi.org/10.1155/2014/808569

Neumann M, Mittelstädt G, Seduk F, Iobbi-Nivol C, Leimkühler S. (2009). MocA is a specific cytidylyltransferase involved in molybdopterin cytosine dinucleotide biosynthesis in *Escherichia coli*. J Biol Chem. 284(33):21891-21898.
doi: 10.1074/jbc.M109.008565.

Hilton JC, Rajagopalan KV. (1996). Identification of the molybdenum cofactor of dimethyl sulfoxide reductase from *Rhodobacter sphaeroides* f. sp. *denitrificans* as bis(molybdopterin guanine dinucleotide)molybdenum. Arch Biochem Biophys. 325(1):139-43.
doi: 10.1006/abbi.1996.0017.

Ishii Y, Yamada H, Yamashino T, Ohashi K, Katoh E, Shindo H, Yamazaki T, Mizuno T. (2000). Deletion of the *yhhP* gene results in filamentous cell morphology in *Escherichia coli*. Biosci Biotechnol Biochem. 64(4):799-807.
doi: 10.1271/bbb.64.799.

Katoh E, Hatta T, Shindo H, Ishii Y, Yamada H, Mizuno T, Yamazaki T. (2000). High precision NMR structure of YhhP, a novel *Escherichia coli* protein implicated in cell division. J Mol Biol. 304(2):219-29.
doi: 10.1006/jmbi.2000.4170.

Perederina A, Svetlov V, Vassylyeva MN, Tahirov TH, Yokoyama S, Artsimovitch I, Vassylyev DG. (2004). Regulation through the secondary channel--structural framework for ppGpp-DksA synergism during transcription. Cell. 118(3):297-309.
doi: 10.1016/j.cell.2004.06.030.

Brown L, Gentry D, Elliott T, Cashel M. (2002). DksA affects ppGpp induction of RpoS at a translational level. J Bacteriol. 184(16):4455-65.
doi: 10.1128/JB.184.16.4455-4465.2002.

Aubee JI, Olu M, Thompson KM. (2017). TrmL and TusA are necessary for *rpoS* and MiaA is required for *hfq* expression in *Escherichia coli*. Biomolecules. 7(2):39.
doi: 10.3390/biom7020039.

Maciag A, Peano C, Pietrelli A, Egli T, De Bellis G, Landini P. (2011). In vitro transcription profiling of the σ^S subunit of bacterial RNA polymerase: re-definition of the σ^S regulon and identification of σ^S-specific promoter sequence elements. Nucleic Acids Res. 39(13):5338-55.
doi: 10.1093/nar/gkr129.

Hengge-Aronis R. (1993). Survival of hunger and stress: the role of *rpoS* in early stationary phase gene regulation in *E. coli*. Cell. 72(2):165-8.
doi: 10.1016/0092-8674(93)90655-a.

Vaughan S, Wickstead B, Gull K, Addinall SG. (2004). Molecular evolution of FtsZ protein sequences encoded within the genomes of archaea, bacteria, and eukaryota. J Mol Evol. 58(1):19-29.
doi: 10.1007/s00239-003-2523-5.

Margolin W. (2005). FtsZ and the division of prokaryotic cells and organelles. Nat Rev Mol Cell Biol. 6(11):862-71.
doi: 10.1038/nrm1745.

Haeusser DP, Rowlett VW, Margolin W. (2015). A mutation in *Escherichia coli ftsZ* bypasses the requirement for the essential division gene *zipA* and confers resistance to FtsZ assembly inhibitors by stabilizing protofilament bundling. Mol Microbiol. 97(5):988-1005.
doi: 10.1111/mmi.13081.

Mukherjee A, Lutkenhaus J. (1994). Guanine nucleotide-dependent assembly of FtsZ into filaments. J Bacteriol. 176(9):2754-8.
doi: 10.1128/jb.176.9.2754-2758.1994.

Pichoff S, Du S, Lutkenhaus J. (2015). The bypass of ZipA by overexpression of FtsN requires a previously unknown conserved FtsN motif essential for FtsA-FtsN interaction supporting a model in which FtsA monomers recruit late cell division proteins to the Z ring. Mol Microbiol. 95(6):971-87.
doi: 10.1111/mmi.12907.

Tsang MJ, Bernhardt TG. (2015). A role for the FtsQLB complex in cytokinetic ring activation revealed by an *ftsL* allele that accelerates division. Mol Microbiol. 95(6):925-44.
doi: 10.1111/mmi.12905.

Norris V, Woldringh C, Mileykovskaya E. (2004). A hypothesis to explain division site selection in *Escherichia coli* by combining nucleoid occlusion and Min. FEBS Lett. 561(1-3):3-10.
doi: 10.1016/S0014-5793(04)00135-8.

Margolin W. (2006). Bacterial division: another way to box in the ring. Curr Biol. 16(20):R881-4.
doi: 10.1016/j.cub.2006.09.025.

Sun Q, Margolin W. (2004). Effects of perturbing nucleoid structure on nucleoid occlusion-mediated toporegulation of FtsZ ring assembly. J Bacteriol. 186(12):3951-9.
doi: 10.1128/JB.186.12.3951-3959.2004.

Addinall SG, Holland B. (2002). The tubulin ancestor, FtsZ, draughtsman, designer and driving force for bacterial cytokinesis. J Mol Biol. 318(2):219-36.
doi: 10.1016/S0022-2836(02)00024-4.

Travers A, Muskhelishvili G. (2005). DNA supercoiling - a global transcriptional regulator for enterobacterial growth? Nat Rev Microbiol. 3(2):157-69.
doi: 10.1038/nrmicro1088. PMID: 15685225.

Cho BK, Knight EM, Barrett CL, Palsson BØ. (2008). Genome-wide analysis of Fis binding in *Escherichia coli* indicates a causative role for A-/AT-tracts. Genome Res. 18(6):900-10.
doi: 10.1101/gr.070276.107.

Kahramanoglou C, Seshasayee AS, Prieto AI, Ibberson D, Schmidt S, Zimmermann J, Benes V, Fraser GM, Luscombe NM. (2010). Direct and indirect effects of H-NS and Fis on global gene expression control in *Escherichia coli*. Nucleic Acids Res. 39(6):2073-91.
doi: 10.1093/nar/gkq934.

Dame RT. (2005). The role of nucleoid-associated proteins in the organization and compaction of bacterial chromatin. Mol Microbiol. 56(4):858-70.
doi: 10.1111/j.1365-2958.2005.04598.x.

Bradley MD, Beach MB, de Koning APJ, Pratt TS, Osuna R. (2007). Effects of Fis on *Escherichia coli* gene expression during different growth stages. Microbiology (Reading). 153(Pt 9):2922-2940.
doi: 10.1099/mic.0.2007/008565-0.

Ali Azam T, Iwata A, Nishimura A, Ueda S, Ishihama A. (1999). Growth phase-dependent variation in protein composition of the *Escherichia coli* nucleoid. J Bacteriol. 181(20):6361-70.
doi: 10.1128/JB.181.20.6361-6370.1999.

Schneider R, Travers A, Muskhelishvili G. (1997). Fis modulates growth phase-dependent topological transitions of DNA in *Escherichia coli*. Mol Microbiol. 26(3):519-30.
doi: 10.1046/j.1365-2958.1997.5951971.x.

Hirsch M, Elliott T. (2002). Role of ppGpp in *rpoS* stationary-phase regulation in *Escherichia coli*. J Bacteriol. 184(18):5077-87.
doi: 10.1128/JB.184.18.5077-5087.2002.

Hirsch M, Elliott T. (2005). Stationary-phase regulation of RpoS translation in Escherichia coli. J Bacteriol. 187(21):7204-13.
doi: 10.1128/JB.187.21.7204-7213.2005.

Hirsch M, Elliott T. (2005). Fis regulates transcriptional induction of RpoS in *Salmonella enterica*. J Bacteriol. 187(5):1568-80.
doi: 10.1128/JB.187.5.1568-1580.2005.

McLeod SM, Xu J, Johnson RC. (2000). Coactivation of the RpoS-dependent proP P2 promoter by fis and cyclic AMP receptor protein. J Bacteriol. 182(15):4180-7.
doi: 10.1128/JB.182.15.4180-4187.2000.

Schneider R, Travers A, Muskhelishvili G. (2000). The expression of the *Escherichia coli fis* gene is strongly dependent on the superhelical density of DNA. Mol Microbiol. 38(1):167-75.
doi: 10.1046/j.1365-2958.2000.02129.x.

Logan DC. (2006). Plant mitochondrial dynamics. Biochim Biophys Acta. 1763(5-6):430-41.
doi: 10.1016/j.bbamcr.2006.01.003.

Lioy VS, Cournac A, Marbouty M, Duigou S, Mozziconacci J, Espéli O, Boccard F, Koszul R. (2018). Multiscale structuring of the *E. coli* Chromosome by nucleoid-associated and condensin proteins. Cell. 172(4):771-783.e18.
doi: 10.1016/j.cell.2017.12.027.

Mallik P, Paul BJ, Rutherford ST, Gourse RL, Osuna R. (2006). DksA is required for growth phase-dependent regulation, growth rate-dependent control, and stringent control of *fis* expression in *Escherichia coli*. J Bacteriol. 188(16):5775-82.
doi: 10.1128/JB.00276-06.

Dame RT, Wyman C, Goosen N. (2000). H-NS mediated compaction of DNA visualised by atomic force microscopy. Nucleic Acids Res. 28(18):3504-10.
doi: 10.1093/nar/28.18.3504.

Falconi M, Brandi A, La Teana A, Gualerzi CO, Pon CL. (1996). Antagonistic involvement of Fis and H-NS proteins in the transcriptional control of *hns* expression. Mol Microbiol. 19(5):965-75.
doi: 10.1046/j.1365-2958.1996.436961.x.

Chib S, Mahadevan S. (2012). Involvement of the global regulator H-NS in the survival of *Escherichia coli* in stationary phase. J Bacteriol. 194(19):5285-93.
doi: 10.1128/JB.00840-12.

Atlung T, Ingmer H. (1997). H-NS: a modulator of environmentally regulated gene expression. Mol Microbiol. 24(1):7-17.
doi: 10.1046/j.1365-2958.1997.3151679.x.

Paul BJ, Ross W, Gaal T, Gourse RL. (2004). rRNA transcription in *Escherichia coli*. Annu Rev Genet. 38:749-70.
doi: 10.1146/annurev.genet.38.072902.091347.

Travers A, Muskhelishvili G. (1998). DNA microloops and microdomains: a general mechanism for transcription activation by torsional transmission. J Mol Biol. 279(5):1027-43.
doi: 10.1006/jmbi.1998.1834.

Finkel SE, Johnson RC. (1992). The Fis protein: it's not just for DNA inversion anymore. Mol Microbiol. 6(22):3257-65.
doi: 10.1111/j.1365-2958.1992.tb02193.x.

Skoko D, Yoo D, Bai H, Schnurr B, Yan J, McLeod SM, Marko JF, Johnson RC. (2006). Mechanism of chromosome compaction and looping by the *Escherichia coli* nucleoid protein Fis. J Mol Biol. 364(4):777-98.
doi: 10.1016/j.jmb.2006.09.043.

Hanahan D. (1983). Studies on transformation of *Escherichia coli* with plasmids. J Mol Biol. 166(4):557-80.
doi: 10.1016/s0022-2836(83)80284-8.

Baba T, Ara T, Hasegawa M, Takai Y, Okumura Y, Baba M, Datsenko KA, Tomita M, Wanner BL, Mori H. (2006). Construction of *Escherichia coli* K-12 in-frame, single-gene knockout mutants: the Keio collection. Mol Syst Biol. 2:2006.0008.
doi: 10.1038/msb4100050.

Bühning M, Valleriani A, Leimkühler S. (2017). The Role of SufS Is Restricted to Fe-S Cluster Biosynthesis in *Escherichia coli*. Biochemistry. 56(14):1987-2000.
doi: 10.1021/acs.biochem.7b00040.

Hänzelmann P, Schindelin H. (2004). Crystal structure of the S-adenosylmethionine-dependent enzyme MoaA and its implications for molybdenum cofactor deficiency in humans. Proc Natl Acad Sci U S A. 101(35):12870-5. doi: 10.1073/pnas.0404624101.

Hiraga S, Niki H, Ogura T, Ichinose C, Mori H, Ezaki B, Jaffé A. (1989). Chromosome partitioning in *Escherichia coli*: novel mutants producing anucleate cells. J Bacteriol. 171(3):1496-505. doi: 10.1128/jb.171.3.1496-1505.1989.

Laemmli UK. (1970). Cleavage of structural proteins during the assembly of the head of bacteriophage T4. Nature. 227(5259):680-5. doi: 10.1038/227680a0.

Simková E, Staněk D. (2012). Probing nucleic acid interactions and pre-mRNA splicing by Förster Resonance Energy Transfer (FRET) microscopy. Int J Mol Sci. 13(11):14929-45. doi: 10.3390/ijms131114929.

Raulfs EC, O'Carroll IP, Dos Santos PC, Unciuleac MC, Dean DR. (2008). *In vivo* iron-sulfur cluster formation. Proc Natl Acad Sci U S A. 105(25):8591-6. doi: 10.1073/pnas.0803173105.

Leimkühler S, Bühning M, Beilschmidt L. (2017). Shared Sulfur Mobilization Routes for tRNA Thiolation and Molybdenum Cofactor Biosynthesis in Prokaryotes and Eukaryotes. Biomolecules. 7(1):5. doi: 10.3390/biom7010005.

Weart RB, Levin PA. (2003). Growth rate-dependent regulation of medial FtsZ ring formation. J Bacteriol. 185(9):2826-34. doi: 10.1128/JB.185.9.2826-2834.2003.

Björk GR, Huang B, Persson OP, Byström AS. (2007). A conserved modified wobble nucleoside (mcm^5s^2U) in lysyl-tRNA is required for viability in yeast. RNA. 13(8):1245-55. doi: 10.1261/rna.558707.

Ballesteros M, Kusano S, Ishihama A, Vicente M. (1998). The *ftsQ1p* gearbox promoter of *Escherichia coli* is a major sigma S-dependent promoter in the *ddlB-ftsA* region. Mol Microbiol. 30(2):419-30. doi: 10.1046/j.1365-2958.1998.01077.x.

Hengge-Aronis R, Lange R, Henneberg N, Fischer D. (1993). Osmotic regulation of *rpoS*- dependent genes in *Escherichia coli*. J Bacteriol. 175(1):259-65. doi: 10.1128/jb.175.1.259-265.1993.

Pogliano J, Pogliano K, Weiss DS, Losick R, Beckwith J. (1997). Inactivation of FtsI inhibits constriction of the FtsZ cytokinetic ring and delays the assembly of FtsZ rings at potential division sites. Proc Natl Acad Sci U S A. 94(2):559-64. doi: 10.1073/pnas.94.2.559.

Sánchez-Gorostiaga A, Palacios P, Martínez-Arteaga R, Sánchez M, Casanova M, Vicente M. (2016). Life without Division: Physiology of *Escherichia coli* FtsZ-Deprived Filaments. mBio. 7(5):e01620-16. doi: 10.1128/mBio.01620-16.

Einsfeldt K, Severo Júnior JB, Corrêa Argondizzo AP, Medeiros MA, Alves TL, Almeida RV, Larentis AL. (2011). Cloning and expression of protease ClpP from Streptococcus pneumoniae in *Escherichia coli*: study of the influence of kanamycin and IPTG concentration on cell growth, recombinant protein production and plasmid stability. Vaccine. 29(41):7136-43. doi: 10.1016/j.vaccine.2011.05.073.

Andersson L, Yang S, Neubauer P, Enfors SO. (1996). Impact of plasmid presence and induction on cellular responses in fed batch cultures of *Escherichia coli*. J Biotechnol. 46(3):255-63.

doi: 10.1016/0168-1656(96)00004-1.

Monteiro JM, Pereira AR, Reichmann NT, Saraiva BM, Fernandes PB, Veiga H, Tavares AC, Santos M, Ferreira MT, Macário V, VanNieuwenhze MS, Filipe SR, Pinho MG. (2018). Peptidoglycan synthesis drives an FtsZ-treadmilling-independent step of cytokinesis. Nature. 554(7693):528-532.
doi: 10.1038/nature25506.

Pohl T, Walter J, Stolpe S, Soufo JH, Grauman PL, Friedrich T. (2007). Effects of the deletion of the *Escherichia coli* frataxin homologue CyaY on the respiratory NADH:ubiquinone oxidoreductase.
BMC Biochem. 8:13.
doi: 10.1186/1471-2091-8-13.

Wachnowsky C, Fidai I, Cowan JA. (2016). Cytosolic iron-sulfur cluster transfer-a proposed kinetic pathway for reconstitution of glutaredoxin 3. FEBS Lett. 590(24):4531-4540.
doi: 10.1002/1873-3468.12491.

Sourjik V, Vaknin A, Shimizu TS, Berg HC. (2007). *In vivo* measurement by FRET of pathway activity in bacterial chemotaxis. Methods Enzymol. 423:365-91.
doi: 10.1016/S0076-6879(07)23017-4.

Picker MA, Wing HJ. (2016). H-NS, Its Family Members and Their Regulation of Virulence Genes in Shigella Species. Genes (Basel). 7(12):112.
doi: 10.3390/genes7120112.

Ishihama Y, Schmidt T, Rappsilber J, Mann M, Hartl FU, Kerner MJ, Frishman D. (2008). Protein abundance profiling of the *Escherichia coli* cytosol. BMC Genomics. 9:102.
doi: 10.1186/1471-2164-9-102.

Majdalani N, Hernandez D, Gottesman S. (2002). Regulation and mode of action of the second small RNA activator of RpoS translation, RprA. Mol Microbiol. 46(3):813-26.
doi: 10.1046/j.1365-2958.2002.03203.x.

Sitnikov DM, Schineller JB, Baldwin TO. (1996). Control of cell division in *Escherichia coli*: regulation of transcription of *ftsQA* involves both *rpoS* and SdiA-mediated autoinduction. Proc Natl Acad Sci U S A. 93(1):336-41.
doi: 10.1073/pnas.93.1.336.

Lu P, Wang Y, Zhang Y, Hu Y, Thompson KM, Chen S. (2016). RpoS-dependent sRNA RgsA regulates Fis and AcpP in *Pseudomonas aeruginosa*. Mol Microbiol. 102(2):244-259.
doi: 10.1111/mmi.13458.

Dong T, Kirchhof MG, Schellhorn HE. (2008). RpoS regulation of gene expression during exponential growth of *Escherichia coli* K12. Mol Genet Genomics. 279(3):267-77.
doi: 10.1007/s00438-007-0311-4.

Weber H, Polen T, Heuveling J, Wendisch VF, Hengge R. (2005). Genome-wide analysis of the general stress response network in *Escherichia coli*: sigmaS-dependent genes, promoters, and sigma factor selectivity. J Bacteriol. 187(5):1591-603.
doi: 10.1128/JB.187.5.1591-1603.2005.

Acknowledgements

Meinen größten Dank möchte an Prof. Dr. Silke Leimkühler aussprechen. Sie hat mich während meiner wissenschaftlichen Karriere fortlaufend unterstützt und mich und diese Arbeit mit Ihren Ideen und Herangehensweisen bereichert. Des Weiteren hat Sie mir die Chance gegeben an diesem Projekt zu arbeiten, mich wissenschaftlich weiterzuentwickeln und einen Teil Ihres Teams zu sein. Ich weiß Ihre Unterstützung sehr zu schätzen.

Prof. Dr. Ralph Gräf und PD Dr. Christiane Dahl möchte ich mich herzlich für die Begutachtung meiner Arbeit bedanken.

Außerdem möchte ich mich bei Angelika Lehmann und Jasmin Kurtzke für jegliche Unterstützung im Labor danken. Für das hilfreiche und anstrengende Korrekturlesen möchte ich auch meinen ganz großen Dank an Benjamin Duffus, Muhammad Abrar Hasnat, Hemant Kumar und meiner ehemaligen Kommilitonin und sehr gute Freundin Nadine Radomski äußern. Besonders danke ich Mariam Esmaeeli Moghaddam, Muhammad Abrar Hasnat und Arkadiusz Zupok für die kompetenten fachliche Austausche und die freundliche Arbeitsatmosphäre im gemeinsamen Büro. Hiermit möchte ich mich auch bei allen Mitgliedern der Arbeitsgruppe Molekulare Enzymologie und Analytische Biochemie für die gemeinsame Zeit bedanken. Der DFG danke ich für die finanzielle Unterstützung meiner Arbeit.

Ganz herzlich danke ich natürlich meinem Ehemann, meiner kleinen Tochter, meiner Mutter, meinem Vater und meinem Bruder für die ganz große fortwährende Unterstützung zu jeder Zeit, damit ich meine Arbeit erfolgreich absolvieren kann.

Affirmation

Hiermit erkläre ich, Tugba Yildiz, dass ich die vorliegende Dissertation an keiner anderen Hochschule eingereicht sowie selbstständig und ohne unerlaubte Hilfsmittel angefertigt habe und von mir keine anderen als die angegebenen Quellen und Hilfsmittel verwendet wurden.

Berlin, den 06.06.2023

Ort, Datum

Unterschrift Tugba Yildiz